Study of the liquefaction of geo-materials taking into account the unsaturation

Khai Hoan Tran

Normandie Université

THESE

Pour obtenir le diplôme de doctorat

Spécialité GENIE CIVIL

Préparée au sein de « Laboratoire Ondes et Milieux Complexes CNRS UMR 6294 »

Study of the liquefaction of geo-materials taking into account the unsaturation
Etude de la liquéfaction des géomatériaux avec prise en compte de la non saturation

Présentée et soutenue par
Khai Hoan TRAN

Thèse soutenue publiquement le 10 Décembre 2020 devant le jury composé de		
M. Pierre BREUL	Professeur à l'Université Clermont Auvergne	Rapporteur
Mme Arezou MODARESSI	Professeur à CentraleSupélec	Rapporteur
Mme Mahdia HATTAB	Professeur à l'Université de Lorraine	Examinateur
M. Jean-Marie FLEUREAU	Professeur à CentraleSupélec	Examinateur
M. Jean-François HEITZ	Dr, Directeur de projets, SETEC	Examinateur
M. Saber IMANZADEH	Maître de conférences à l'INSA ROUEN Normandie	Co-encadrant
Mme Hanene SOULI	Maître de conférences HDR à ENISE	Co-directeur de thèse
M. Said TAIBI	Professeur à l'Université du Havre Normandie	Directeur de thèse

Thèse dirigée par Said TAIBI, Laboratoire LOMC CNRS UMR 6294

UNIVERSITÉ LE HAVRE NORMANDIE

ED PSIME

LABORATOIRE ONDES et MILIEUX COMPLEXES

ACKNOWLEDGEMENT

I would like to express my deep appreciation to my supervisor, Professor Said TAIBI, for his supervision and guidance during the past three years. His encouragement in research work and daily life is really great motivation for me to complete this research.

I would like to extend my sincere thanks to my co-supervisor, Dr. Saber IMANZADEH; co-director of my thesis, Hanène SOULI, for their valuable ideas and enthusiastic advice. Their contribution plays an important role in this project.

I would like to express the special thanks to the jury members: Professors Pierre BREUL, Arezou MODARESSI, Mahdia HATTAB, Jean-Marie FLEUREAU and Dr. Jean-François HEITZ for their willing review valuable and helpful suggestions to improve my thesis.

I want to thank the technical staffs, Mr. Claude HOUSSIN and Mr. Mathieu BEAUJARD, who helped me a lot in troubleshooting the problems relating to the experimental apparatus.

I would also like to thank professors Innocent MUTABAZI, Abdelghani SAOUAB, François MARIN, Anne PANTET for helping and encouraging me in the process of working at the laboratory.

I am forever grateful to my friends for making my time here unforgettable with great memories and sincere friendship.

Finally, I want to thank my wife, my daughter, and my parents for their unconditional love and support during the past three years.

TABLE OF CONTENTS

ACKNOWLEDGEMENT i
SUMMARY vii
LIST OF FIGURES ix
LIST OF TABLES xvi
LIST OF SYMBOLS xvii

GENERAL INTRODUCTION 1

CHAPTER 1: UNSATURATED SOIL MECHANICS FUNDAMENTALS 4
I.1. General of unsaturated soils 4
I.1.1. Constituents of soil and saturation states 4
I.1.2. Field visualization of degree of saturation 6
I.1.2.1. Distribution of unsaturated soils on Earth's surface 6
I.1.2.2. Distribution of unsaturated soils with depth. 7
I.2. Solubility of air in water 9
I.2.1. Ideal gas law and Boyler's law 9
I.2.2. Henry's law 9
I.2.3. Coefficient of diffusion 10
I.2.4. Skempton's parameters A and B 11
I.3. Suction in soils 12
I.3.1. Capillary Phenomenon 12
I.3.2. Suction in soils. 13
I.3.3. Degree of water saturation 15
I.3.4. Soil drying and wetting curves 16
I.4. Stress state variables 19
I.4.1. Concept of effective stress in the case of totally saturated or totally dry soil 19
I.4.2. Stress state variables in the case of partially saturated soil 20
I.4.2.1. Generalized effective stress concept. 21
I.4.2.2. Capillary stress model 23
I.4.2.3. Independent stress variables 25
I.5. Conclusions 29

CHAPTER 2: LIQUEFACTION PHENOMENON – LITERATURE REVIEW 30
II.1. Liquefaction phenomenon 30
II.1.1. Experience of liquefaction 30
II.1.2. Concept of liquefaction 32
II.1.3. Mechanical behavior of soil 34
II.1.3.1. Characteristic state 34
II.1.3.2. Critical state 37
II.1.4. Static liquefaction phenomenon 37
II.1.4.1. Demonstration of the phenomenon in the laboratory: introduction by the concept of the flow structure 37
II.1.4.2. Different types of behavior of sand subjected to an undrained monotonic shear 38
II.1.5. Cyclic liquefaction and cyclic mobility phenomenon 41
II.1.5.1. Drained behavior under cyclic loading. 41
II.1.5.2. Liquefaction under undrained cyclic loading 42
II.1.5.3. Case of cyclic mobility 43
II.1.5.4. Case of cyclic liquefaction 46
II.1.6. Factors influencing the liquefaction of soil under cyclic loading 49
II.1.6.1. Influence of relative density 49
II.1.6.2. Influence of initial static shear stress. 50
II.1.6.3. Influence of the over consolidation 51
II.1.6.4. Influence of the stress history 52
II.1.6.5. Influence of sample reconstitution method 53
II.1.6.6. Influence of the fines content 55
II.1.6.7. Influence of the failure criterion 55
II.1.6.8. Influence of the certain experimental parameters 56
II.1.6.9. Influence of saturation degree 56
II.1.7. Liquefaction assessment 57
II.1.7.1. Liquefaction assessment procedures overview 57
II.1.7.2. Pore pressure prediction 58
II.1.8. Regulatory context 59
II.1.9. Conclusions 63
II.2. Effect of the degree of saturation on liquefaction phenomenon 64
II.2.1. Context 64
II.2.2. Some observations on the liquefaction potential of partially saturated soils 64
II.2.3. Studies of liquefaction on unsaturated soils 66

II.3. Conclusions 84

CHAPTER 3: MATERIALS AND METHODS 86
III.1 Introduction 86
III.2 Material, apparatus 86
III.2.1. Material – RF Hostun sand 86
III.2.2. Dynamic triaxial system 88
III.2.2.1. Apparatus overview 88
III.2.2.2. Axial loading and frequency calculation 90
III.2.2.3. Back pressure control system and pore water pressure transducer 91
III.2.2.4. Cell pressure control system 92
III.2.2.5. De-air water supply system 93
III.2.2.6. Porous stone and permeable paper 93
III.2.2.7. Axial strain measurement 94
III.3 Test procedure 95
III.3.1. Sample preparation by the wet tamping method 95
III.3.2. Sample saturation and Skempton's parameter B measurement 98
III.3.3. Sample consolidation 99
III.3.4. Deviator cyclic loading 100
III.3.4.1. Load parameters 100
III.3.4.2. First group: Cyclic loading with constant CSR 102
III.3.4.3. Second group: Cyclic loading with stepping CSR 102
III.3.5. Monotonic loading after liquefaction 103
III.3.5.1. Compressed monotonic loading 103
III.3.5.2. Closed loop monotonic loading 104
III.3.6. Sample removal after the tests 104
III.3.7. The measurement of the sample volume changes during the tests 106
III.3.8. Block diagrams for the test procedure 109
III.3.8.1. Tests with constant CSR cyclic loading 109
III.3.8.2. Tests with stepping CSR cyclic loading 110
III.4 Conclusions 111

CHAPTER 4: EFFECT OF UNSATURATION ON LIQUEFACTION POTENTIAL-Cyclic Loading with Constant CSR 113
IV.1. Introduction 113

IV.2. Liquefaction potential and residual strength of saturated sand 113
IV.2.1. Liquefaction potential of saturated sand 113
IV.2.1.1. Test program 113
IV.2.1.2. Results 114
IV.2.2. Residual strength after liquefaction of saturated sand 126
IV.2.2.1. Test program 126
IV.2.2.2. Results 127
IV.2.3. Test parameter variation during the saturated test 129
IV.3. Liquefaction potential and residual strength of unsaturated sand. 130
IV.3.1. Liquefaction potential of unsaturated sand 130
IV.3.1.1. Test program 130
IV.3.1.2. Results 132
IV.3.1.2.1.Samples with saturation near 95 %: Liquefaction of soil due to the increase of pore water pressure and the excess development of axial strain 132
IV.3.1.2.2.Samples with saturation near 86 %: Liquefaction of soil due to the excess development of axial strain 141
IV.3.2. Residual strength after liquefaction 149
IV.3.2.1. Test program 149
IV.3.2.2. Results 150
IV.3.3. Test parameters variation during the unsaturated test 152
IV.4. Effect of saturation degree on the liquefaction potential of sand 154
IV.5. Volumetric strain at the liquefaction state 156
IV.6. Conclusions 159

CHAPTER 5: EFFECT OF UNSATURATION ON LIQUEFACTION POTENTIAL-Cyclic Loading with Stepping CSR 161
V.1. Introduction 161
V.2. Undrained behavior of RF Hostun sand 162
V.2.1. Test program 162
V.2.2. Results 162
V.3. Saturated sand: Liquefaction potential and residual strength 164
V.3.1. Liquefaction potential 164
V.3.1.1. Test program 164
V.3.1.2. Results 165
V.3.2. Residual strength after liquefaction 171
V.3.2.1. Test program 171

V.3.2.2. Results 171
V.4. Unsaturated sand: Liquefaction potential and residual strength 176
V.4.1. Liquefaction potential 176
V.4.1.1. Test program 176
V.4.1.2. Results 177
4.1.2.1. Instability and liquefaction evidence 177
4.1.2.2. The results of the first load case: CSR=0.15 180
4.1.2.3. Behavior of soil under the highest CSR loading (the last load case) 184
V.4.2. Residual strength after liquefaction of unsaturated sand 193
V.4.2.1. Test program 193
V.4.2.2. Results 194
V.5. Test parameters variation during the tests. 195
V.6. Discussion on the effect of saturation degree on the liquefaction and residual strength of unsaturated sand. 199
V.7. Conclusions 203

GENERAL CONCLUSIONS AND PERSPECTIVES 205
VI.1. General conclusions 205
VI.2. Perspectives. 207

REFERENCES 209
APPENDIX: VARIATION OF PARAMETERS DURING THE TEST -with constant CSR cyclic loading- 221

SUMMARY

In the last few years, many studies have focused on the behavior of unsaturated sands subjected to dynamic loading and there is a consensus that soil with a saturation degree lower than 100% can be liquefied. Despite some achievements, much remains unclear about the behavior of unsaturated soil, there are still issues that need to be clarified such as: (i) the behavior before and after the main shock and the effect of foreshocks on the liquefaction potential; (ii) the effect of the saturation degree on the CSR (cyclic stress ratio); (iii) in the case of dense soils, what is the effect of unsaturation on the CSR-number of cycles relationship to reach liquefaction? This research work tries to provide some answers to these questions.

Two groups of tests were carried out by triaxial dynamic apparatus to survey the sand behavior when subjected to cyclic loading as well as the residual strength after liquefaction under monotonic loading. All the samples were prepared by the wet tamping method. The vacuum method was used to control the saturation degree of the samples. Then, the Skempton parameter B was used to evaluate the saturation degree of the samples. After that, sample consolidation and cyclic loading were conducted step by step.

- In the first group of tests, all samples at different levels of saturation degree were subjected to the cyclic loading with constant cyclic stress ratio (CSR) until liquefaction. The cyclic stress ratio varies between tests; however, is constant in each test.
- In the second group of tests, all samples with a different saturation degree subjected to a stepping CSR loading process. The initial amplitude of the deviator stress was the same for all tests; however, it increased to a higher level after each one hundred cycles of loading. This increase repeated until liquefaction. This loading protocol allows relating to the effect of foreshocks in earthquakes to the liquefaction behavior of soil caused by the main shock.

After cyclic loading, to study the residual strength of soil after liquefaction, the pore water pressure increment due to liquefaction was dissipated and then the samples were compressed or stretched monotonically in drained condition.

The results of cyclic loading process show that the liquefaction susceptibility is directly proportional to the sample saturation degree. The relationship between cyclic stress ratio and the Skempton's parameter is highlighted. The results of the monotonic loading show that the strength of sand recuperates when the pore water pressure dissipates after liquefaction.

Besides, the experimental protocol established in this study has handled well the main challenges of the unsaturated soil liquefaction test. The main parameters of tests including void ratio, saturation degree, and sample volume change which can be measured or calculated for each stage of the tests help understand the liquefaction of unsaturated soil more obviously.

LIST OF FIGURES

Figure 1.1 Phase diagram showing the relationship between volume and weight of gas, fluid, and solid phases in soil. 5

Figure 1.2 Saturation states and different existences of water in voids of soil (Dysli 1997) 6

Figure 1.3 Extremely arid, arid, and semiarid areas of the world (GNUEACR 2013). 7

Figure 1.4 Subdivisions of unsaturated soil zone (vadose zone) based depth, local, and regional basis (in Fredlund et al. 2012) 8

Figure 1.5 Molecule of water on the air – water interface (Delage et al. 2000) 12

Figure 1.6 Capillary rises in a tube (Delage et al. 2000) 13

Figure 1.7 Capillary tubes showing the air – water interfaces at different radii of curvature (from Janse and Demsey 1980) 15

Figure 1.8 The form of air bubbles changes when the saturation decreases (a) air bubble not wetting solid surface; (b) both fluids in contact with solid surfaces (Zienkiewicz et al. 1999) 16

Figure 1.9 Soil water characteristic curve for sandy soil, silty soil and clayey soil (Fredlund and Xing 1994) 17

Figure 1.10 Soil water characteristic curve of sandy soil (Bian 2007) 18

Figure 1.11 Suction versus water content on drying, wetting paths for Hostun sand (Biarez et al. 1989) 19

Figure 1.12 Different approaches to solve an unsaturated soil problem (Taibi et al. 2013) 20

Figure 1.13 Schema for the capillary stress model (Taibi et al. 2008; 2013) 24

Figure 1.14 Extended Mohr-Coulomb failure envelop for unsaturated soils. (Fredlund et al. 1978) 26

Figure 1.15 Relationship between preconsolidation stresses p_0 and p_0^* - compression curve for saturated and unsaturated soil Alonso et al. (1990). 28

Figure 1.16 Three – dimensional view of the yield surfaces in (*p,q,s*) stress space (Alonso et al. 1990). 28

Figure 2.1 Examples of liquefaction damages during earthquakes 31

Figure 2.2 Dilatant and contractant volumetric tendencies of soils subjected to shear loading. 34

Figure 2.3 Concept of contractancy and dilatancy. 34

Figure 2.4 Definition of characteristic state 35

Figure 2.5 Characteristic criterion divides the contracting area of the material 36

Figure 2.6 Effect of saturation degree on the characteristic line (He 2013) 36

Figure 2.7 The definition of critical state 37

Figure 2.8 Monotonic loading response of dense (D_r = 100%) and the loose (D_r = 38%) speciments of sacramento River sand in drainded triaxial compression tests, as

shown in graphs (a) and (b) respectively (Lee and Seed 1967 in Idriss and Boulanger 2008) 39

Figure 2.9 Typical behaviors of dense sand under undrained triaxial compression tests. 40

Figure 2.10 Typical behavior of medium sand under undrained triaxial compression tests. 40

Figure 2.11 Typical behaviors of loose sand under undrained triaxial compression tests. 41

Figure 2.12 Void ratio versus cyclic shear displacement, showing the densification of a sand specimen with successive cycles of drained simple shear loading (Youd 1972). 42

Figure 2.13 Cyclic mobility of RF Hostun sand (Benahmed 2001) 44

Figure 2.14 Initiation of the cyclic mobility of dense Hostun RF sand (Benahmed 2001) 45

Figure 2.15 Deviator stress versus mean effective stress in cyclic mobility phenomenon (Canou et al. 2000) 46

Figure 2.16 Cyclic liquefaction behavior of soil (Castro 1969) 47

Figure 2.17 Initiation of cyclic liquefaction (Vaid et al. 1989). 47

Figure 2.18 Comparison between monotonic and cyclic behavior for the same initial conditions and different cyclic amplitudes for Hostun sand (contracting case); $\sigma c' = 200$ kPa 49

Figure 2.19 Influence of the void index on the cyclic shear strength (Lee and Seed, 1967). 50

Figure 2.20 Influence of the density index on the number of cycles triggering cyclic liquefaction of Hostun RF sand (Benahmed 2001). 50

Figure 2.21 Effect of initial static stress on the cyclic stress ratio causing several levels of deformation in ten cycles (Vaid and Chern, 1983). 51

Figure 2.22 Effect of over consolidation on the characteristics of liquefaction 52

Figure 2.23 Effect of the history of shear stresses on liquefaction characteristics. (a) Seed et al. (1977), (b) Tokimatsu and Hosaka (1986). 53

Figure 2.24 The microscopic image of the sample prepared by different methods to highlight the different granular structures (a) by wet tamping method (b) water sedimentation (c) dry deposition (Benahmed et al. 2007) 53

Figure 2.25 Influence of the deposition method using several manufacturing methods. .. 54

Figure 2.26 Influence of the failure criterion on the stress conditions inducing the failure (Lee and Seed 1967). 55

Figure 2.27 Influence of certain experimental parameters on cyclic resistance (Tatsuoka et al. 1986) 56

Figure 2.28 Influence of saturation degree on the cyclic shear strength. (a) Martin et al. (1978); (b) Xia and Hu (1991) (B: Skempton's coefficient). 57

Figure 2.29 Pore pressure generation models for cyclic stress-controlled tests (Seed et al. 1975) 59

Figure 2.30 Pore pressure generation models strain-controlled cyclic triaxial tests (Dobry et al. 1982 after Chang et al. 2007) 59

Figure 2.31 Map of earthquake risk in France. Old map on the left and new map on the right. 60

Figure 2.32 Map of earthquake risk following Vietnamese standard..... 62

Figure 2.33 Typical pore water pressure increment versus the number of cycles for low B and high B samples (Sherif et al. 1977) 66

Figure 2.34 Degree of saturation effect on laboratory tests results of liquefaction resistance of Ottawa sand (Sherif et al. 1977)..... 67

Figure 2.35 The number of cycles to reach 5% of axial deformation as a function of the Skempton's coefficient (Chaney 1978)..... 68

Figure 2.36 Effects of degree of saturation on liquefaction characteristics of sand (Yoshimi 1989)..... 69

Figure 2.37 Effect of the un-saturation to liquefaction resistance ratio of Toyoura sand (Yoshimi 1989)..... 69

Figure 2.38 The behavior of soil under cyclic loading (Yoshimi 1989). 70

Figure 2.39 Effect of saturation degree on the liquefaction resistance of sand (Xia and Hu 1991)..... 70

Figure 2.40 Effect of back pressure on the liquefaction resistance of unsaturated sand (Xia and Hu 1991)..... 71

Figure 2.41 Appearance of gas pocket inside the tailing sand (Fourie et al. 2001) 72

Figure 2.42 Relationship between hypothetical volumetric strain and liquefaction resistance of partially saturated sand normalized with that of fully saturated sand (Okamura and Soga 2006)..... 72

Figure 2.43 Effect of initial pore pressure on the relationship between cyclic stress ratio and number of cycles (Okamura and Soga 2006) 73

Figure 2.44 Time history of axial strain during cyclic loading process (Unno et al. 2008) 73

Figure 2.45 Time history of pore air pressure and pore-water pressure (Unno et al. 2008) 74

Figure 2.46 Time history of effective stress reduction ratio for Toyoura sand samples having relative density of 26% (Unno et al. 2008)..... 75

Figure2.47 Time history of effective stress reduction ratio for Toyoura sand samples having relative density of 60% (Unno et al. 2008)..... 76

Figure 2.48 Liquefaction prediction of the test result using Toyoura sand at Dr = 60% (Unno et al. 2008)..... 77

Figure 2.49 Results of monotonic tri-axial test carried out on Toyoura sand at deferent initial saturation degrees (Kamata et al. 2007)..... 78

Figure 2.50 Behavior of unsaturated silty sand subjected to cyclic loading (Tsukamoto et al. 2014)..... 78

Figure 2.51 Plots of volumetric strain observed at 5% of double axial strain against intial degree of saturation S_{ri} for Inagi sand (Tsukamoto et al. 2014)..... 79

Figure 2.52 Effect of Skempton' parameter B on the first cycles of soil behavior under cyclic loading (Arab et al. 2016) 80

Figure 2.53 Influence of saturation degree on the cyclic undrained response of the Hostun Rf sand (Arab et al. 2016) 81

Figure 2.54 Cyclic triaxial test and model simulation results for the samples having a saturation degree of 63% (Mase et al. 2019) 81

Figure 3.1 RF Hostun sand 87

Figure 3.2 RF Hostun sand at different scales 87

Figure 3.3 Comparison of the grain size distribution of Hostun RF sands to other liquefiable sands (Iwasaki 1986) 88

Figure 3.4 Triaxial dynamic testing apparatus 89

Figure 3.5 Schema of the triaxial dynamic testing apparatus 90

Figure 3.6 Diagram for loading frequency calculation. 91

Figure 3.7 Cell pressure controller Pneumatic APC 92

Figure 3.8 De-aired water system 93

Figure 3.9 Porous stone with two layers of permeable paper. 94

Figure 3.10 LVDT transducer 95

Figure 3.11 Mixing the dry sand with the water to have the mixture having 8% of water content. 96

Figure 3.12 Sample compaction in wet tamping method 97

Figure 3.13 Sample preparation by wet tamping method 97

Figure 3.14 The variation of controlled pore-water pressure and cell pressure during sample full saturation process 99

Figure 3.15 Cell pressure and back pressure variations during Skempton's parameter B measurement and sample consolidation process of saturated tests. 100

Figure 3.16 Cell pressure and back pressure variations during Skempton's parameter B measurement and sample consolidation process of unsaturated tests. 100

Figure 3.17 Constant CSR cyclic deviator stress 102

Figure 3.18 Stepping CSR cyclic loading 103

Figure 3.19 Axial strain variation for the sample monotonic loading after being liquefied by constant CSR cyclic loading 103

Figure 3.20 Axial strain variation for the sample monotonic loading after being liquefied by stepping CSR cyclic loading 104

Figure 3.21 Sample saturation to measure the saturation degree 106

Figure 3.22 Sample removal 106

Figure 3.23 Sample volume changes from the consolidation to the end of the tests 107

Figure 3.24 Using balance to measure the sample volume change during cyclic loading. 108

Figure 3.25 Procedure for the saturated tests subjected to constant CSR cyclic loading 109

Figure 3.26 Procedure for the unsaturated tests subjected to the constant CSR cyclic loading 109

Figure 3.27 Procedure for the saturated tests subjected to stepping CSR cyclic loading 110

Figure 3.28 Procedure for the unsaturated tests subjected to stepping CSR cyclic loading 111

Figure 4.1 Deviator stress versus number of cycles for saturated tests. 115

Figure 4.2 Pore water pressure versus number of cycles for saturated tests. 117

Figure 4.3 Axial strain versus number of cycles for saturated tests. 118

Figure 4.4 Pore water pressure versus number of cycles for saturated tests. 119

Figure 4.5 Normalized Excess pore water pressure ratio ru versus number of cycles for saturated tests. 120

Figure 4.6 Mean effective stress versus deviator stress for saturated tests. 123

Figure 4.7 Axial strain versus deviator stress for saturated tests. 125

Figure 4.8 Axial strain versus pore water pressure for saturated tests. 126

Figure 4.14 Deviator stress versus number of cycles for the samples with saturation degree of approximately 95%. 133

Figure 4.15 Pore water pressure versus number of cycles for the samples with saturation degree of approximately 95%. 135

Figure 4.16 Axial strain versus number of cycles for the samples with saturation degree of approximately 95%. 136

Figure 4.17 Effective confining stress versus number of cycles for the samples with saturation degree of approximately 95%. 137

Figure 4.18 Normalized excess pore water pressure versus number of cycles for the samples with saturation degree of approximately 95%. 138

Figure 4.19 Deviator stress versus mean effective stress for the samples with saturation degree of approximately 95%. 139

Figure 4.20 Deviator stress versus axial strain for the samples with saturation degree of approximately 95%. 140

Figure 4.21 Pore water pressure versus axial strain for the samples with saturation degree of approximately 95%. 141

Figure 4.22 Deviator stress versus number of cycles for the samples with saturation degree of approximately 86 %. 142

Figure 4.23 Pore water pressure increment versus number of cycles for the samples with saturation degree of approximately 86%. 143

Figure 4.24 Axial strain versus number of cycles for the samples with saturation degree of approximately 86%. 144

Figure 4.25 Effective confining stress versus number of cycles for the samples with saturation degree of approximately 86%. 145

Figure 4.26 Normalized excess pore water pressure versus number of cycles for the samples with saturation degree of approximately 86%. 146

Figure 4.27 Deviator stress versus mean effective stress for the samples with saturation degree of approximately 86%. 147

Figure 4.28 Stress – strain path for the samples with saturation degree of approximately 86%. 148

Figure 4.29 Deviator stress versus pore water pressure for the samples with saturation degree of approximately 86%. 149

Figure 4.30. Deviator stress versus mean effective stress for unsaturated test CUI2 + MT2 151

Figure 4.31 Void ratio versus axial strain for monotonic unsaturated test MT2. 151

Figure 4.32. Sample volumetric strain versus axial strain for monotonic unsaturated test MT2. 152

Figure 4.33 Deviator stress versus axial strain for monotonic unsaturated test MT2. 152

Figure 4.34 Saturation degree and void ratio changes during the unsaturated test CUI2+MT2 154

Figure 4.35 Influence of saturation degree on the liquefaction potential of Hostun Rf sand 155

Figure 4.36 Influence of Skempton's coefficient (saturation degree) on the cyclic undrained response of the Hostun Rf sand. 156

Figure 4.37 Volumetric strain at liquefaction state versus the degree of saturation 157

Figure 4.38 Void ratio change in relationship with the initial saturation degree. 158

Figure 4.39 Sample volumetric strain prediction in relationship with saturation degree (Unno et al. 2008) 159

Figure 5.1 Undrained behavior of RF Hostun sand at a relative density of 83% under the compressed monotonic loading 164

Figure 5.2 Deviator stress in a function of number of cycles for the saturated stepping CSR test. 166

Figure 5.3 Axial strain versus deviator stress for the saturated stepping CSR test. 166

Figure 5.4 (a) Pore water pressure in function of number of cycles and (b) effective confining stress in function of number of cycles for the saturated stepping CSR test. 167

Figure 5.5 Normalized pore water pressure increment r_u for the saturated stepping CSR test. 168

Figure 5.6 Axial strain versus number of cycle for the saturated stepping CSR test. 169

Figure 5.7 Axial strain versus pore water pressure for the saturated stepping CSR test... 169

Figure 5.8 Deviator stress versus mean effective stress for the saturated stepping CSR test. 170

Figure 5.9 The axial strain variation of the monotonic loading after liquefaction 172

Figure 5.10 Deviator stress in a function of axial strain of the saturated monotonic loading test after liquefaction 172

Figure 5.11 Void ratio in a function of axial strain of the saturated monotonic loading test after liquefaction 173
Figure 5.12 Void ratio in a function of effective mean stress of the saturated monotonic loading test after liquefaction 174
Figure 5.13 Deviator stress versus effective mean stress of the saturated monotonic loading test after liquefaction 175
Figure 5.14 Different drained behaviors of (Coarse) Hostun sand (Biarez & Hicher, 1994) 176
Figure 5.15 Pore water pressure and axial strain in a function of number of cycles for the samples with different saturation degree subjected to stepping CSR cyclic loading 179
Figure 5.16. Deviator stress during the first load case of stepping CSR tests 180
Figure 5.17 Stress – strain path of the first load case of stepping CSR tests 181
Figure 5.18 Pore water pressure increment during the first load case of stepping CSR tests 182
Figure 5.19 Axial strain versus pore water pressure during the first load case of the stepping CSR tests 183
Figure 5.20 Stress path during the first load case of the stepping CSR tests 184
Figure 5.22 Pore-water pressure increment of the last load case for stepping CSR test. 188
Figure 5.23 Pore-water pressure increment during the last load case – stepping CSR tests. 190
Figure 5.24 Relationship between deviator tress and effective mean stress during the last load case – stepping CSR tests. 193
Figure 5.25 Residual behavior after liquefaction 195
Figure 5.26 Summary of the saturation degree change and void ratio change of test CUST 4 with B of 0.6 197
Figure 5.27 Sample volume change measured by two independent methods (test CUST 4) 198
Figure 5.28. Sample volumetric strain during stepping CSR unsaturated test measured by two independent methods (test CUST 4) 198
Figure 5.29 Void ratio change during the stepping CSR unsaturated test (test CUST 4) 199
Figure 5.30 Deviator stress and number of cycles in function of B value. 200
Figure 5.31 Test path in the relationship between CSR and numbers of cycles 201
Figure 5.32 Relationship between CSR and numbers of cycles in comparison to the results of Arab et al. (2016) 202
Figure 5.33 Pore-water pressure increments versus the number of cycles 203

LIST OF TABLES

Table 1.1. Terminology commonly used to describe degrees of saturation in field and laboratory (Fredland et al. 2012)..... 8

Table 1.2. Partial Pressure, Henry's Law Constant, and Molar Concentration of Major Air Components in Water at 25^0C and 1 bar Total Pressure..... 10

Table 1.3. Coefficient of diffusion for certain gases in water under different temperatures (Kohn 1965 in Fredlund et al 2013)..... 11

Table 1.4. Different expressions of the Bishop χ parameter (Taibi et al. 2013) 23

Table 3.1. The parameters of RF Hostun sand. (Fargeix 1986)..... 88

Table 4.1. Summary of the test series 113

Table 4.2. Series 1: tests on the full saturated samples. 114

Table 4.3. The friction angle of Hostun sand in literature. 124

Table 4.4. Residual strength tests on the fully saturated samples. 127

Table 4.5. Variation of parameters during saturated test CS1 + MT1. 130

Table 4.6. Series of tests on the samples with saturation near 95 %..... 131

Table 4.7. Series of tests on the samples with saturation near 86 %..... 131

Table 4.9. Variation of parameters during the unsaturated test CUI1+MT2. 153

Table 5.1. Series of stepping CSR tests. 162

Table 5.2. Test program for undrained behavior of Hostun sand. 162

Table 5.3. The test series on saturated samples subjected to the stepping CSR cyclic loading..... 165

Table 5.4. Test program for residual strength after liquefaction of saturated sand..... 171

Table 5.5. Series of tests subjected to stepping CSR cyclic loading..... 177

Table 5.6. Monotonic tests after liquefaction..... 193

Table 5.7. The variations of the parameters during the tests..... 197

LIST OF SYMBOLS

D_r	Relative density
e	Void ratio
e_{max}	Maximum void ratio
e_{min}	Minimum void ratio
ε_a	Axial strain
ε_v	Volumetric strain
f	cyclic loading frequency
N_{liq}	Number of cycles causing liquefaction
N_c	Number of cycles
p'	Effective mean stress
q	Deviator stress
r_u	Normalized excess pore water pressure
S	Suction
S_r	Saturation degree
u	Pore water pressure
V_a	Volume of air
V_s	Volume of soil particles
V_t	Total volume of sample
V_v	Volume of void
V_w	Volume of water
σ_3	Cell pressure

GENERAL INTRODUCTION

Soil liquefaction is a phenomenon known for a long time and has caused many damages over the world. The severe damage due to liquefaction in the Indonesian earthquake in 2018 shows that until now, it is still a great danger for human safety. This phenomenon is usually related to saturated granular soils and is due to the increase of pore water pressure resulting in the decrease of effective confining stress. Generally, liquefaction can be classified into three types: flow liquefaction, cyclic liquefaction, and cyclic mobility. The two first types relate to the loose soils and the last one relates to the liquefaction of dense soils. The most accepted criterion for liquefaction in laboratory tests is that the sample is liquefied if one of the following conditions appears: i) pore water pressure increases to cell pressure leading to the loss of effective confining stress; ii) axial strain in one cycle reaches 5%.

Many studies have focused on the liquefaction of saturated soils and it has been clearly understood (Castro 1969; Seed et al. 1982, etc.); however, recent studies have shown that liquefaction can be observed not only on saturated soil but also on unsaturated sandy soils. Tsukamoto et al. (2014) showed that the air bubbles can be found at 5m below the groundwater table, it means that most of the building structures could be based on unsaturated soil layers. The theoretical study of Martin et al. (1978) predicted the effect of saturation degree on the cyclic liquefaction resistance of sands. Whereby, the unsaturated sands can be liquefied and a small change of saturation can cause a significant change in the cyclic stress ratio causing liquefaction. This finding has been confirmed by the laboratory results (Yoshimi et al. 1989; Unno et al. 2008; Tran et al. 2018a,b; Tran et al. 2019a,b). Della et al. (2011) demonstrated that the dilatancy and the contractancy of soils change when the Skempton's pore pressure coefficient B decreases; however, the influence is not the same for all soils. It depends on the soil type, initial density and confining pressure. Arab et al. (2016) studied the liquefaction of unsaturated RF Hostun sand according to the value of Skempton's coefficient B. They showed that the saturation degree affects soil behavior characteristics including initial stiffness, shear strength, cyclic shear strength, and the sample deformation during cyclic loading. Vernay (2018) and Vernay et al. (2019) investigated the effect of suction, pore fluid compressibility and saturation degree on the unstable behavior of Fontainebleau sand samples using cyclic triaxial tests. The experiments carried out in three zones of saturation demonstrate that the soil can liquefy even if it is not initially fully saturated. Tsukamoto

(2018) performed laboratory triaxial tests to exam the undrained shear strength and liquefaction cyclic resistance of silty sands. The tests are also conducted separately in the three phases of full saturation, partial saturation, and unsaturation to highlight the influence of saturation on the liquefaction triggering and occurrence of liquefaction-induced flow slides. Mase et al. (2019) studied the cyclic shear strength behavior of sand using the cyclic triaxial test on undisturbed specimens. In this study, the excess pore pressure ratio, hysteresis loop, and effective stress path were investigated.

The studies on the liquefaction of unsaturated soil recently have achieved some results and it is clear that liquefaction can be observed not only in saturated soil but also in unsaturated sandy soils. However, much remains unclear about the behavior of unsaturated soil, there are still issues that need to be clarified such as:

- The behavior before and after the main shock and the effect of foreshocks on the liquefaction potential;
- The effect of the saturation degree on the CSR (cyclic stress ratio)
- In the case of dense soils, what is the effect of unsaturation on the CSR-number of cycles relationship to reach liquefaction?

Besides, the complexity in the experimental protocol for the unsaturated liquefaction tests is also a big challenge to the popularity of this experiment. Thus, not much data related to this experiment have been published in the literature.

Due to the lack of the database in the research on unsaturated soils, the calculation of liquefaction the soil in practice is still inadequate. Most standards only mention the liquefaction of saturated soils. The unsaturated soil is neglected or considered as non-liquefiable. This viewpoint conflicts with the results of the laboratory test and the observations carried out on site.

From this observation, in this study, two groups of tests were carried out to provide some answers to these questions.

- In the first group of tests, the cyclic loading with constant cyclic stress ratio (CSR) was applied to the samples. The cyclic stress ratio varies between tests; however, is constant in each test. The saturation degree of the samples decreases from 100% to 87%.

- In the second groups of tests, the cyclic loading with stepping CSR was applied to the samples with a saturation degree in the vicinity of the full saturation state (from 98% to 100%). The initial amplitude of the deviator stress was the same for all tests; however, it increased to a higher level after each one hundred cycles of loading. This increase repeated until liquefaction. This loading protocol allows relating the effect of foreshocks in earthquakes to the liquefaction behavior of soil. All tests were followed by the monotonic loading to study the residual strength after liquefaction.

There are six chapters presented in this study. The content of each chapter is summarized below:

- Chapter 1 outlines some basic fundamentals of unsaturated soil mechanics that are different from full saturated soils.
- Chapter 2 gives a brief statement of the studies on the liquefaction of soil in literature and the results of recent studies on liquefaction unsaturated soils. In this chapter, some most basic concepts depicting soil liquefaction are also mentioned.
- Chapter 3 presents the triaxial apparatus used in this study. The test protocol and the technique used for each step of test. This chapter also gives some experience when performing the liquefaction test with the triaxial dynamic system.
- Chapter 4 studies the effect of saturation degree on the liquefaction potential of soil subjected to cyclic loading with constant cyclic stress ratio (CSR).
- Chapter 5 studies the effect of saturation degree on the liquefaction potential of soil subjected to cyclic loading with CSR increase after each one hundred cycles.
- Conclusions and perspectives are to summary the results of the study and suggest some future work.
- The tables presenting the change of parameters during the tests are presented in Appendix.

CHAPTER 1: UNSATURATED SOIL MECHANICS FUNDAMENTALS

I.1. General of unsaturated soils

I.1.1. Constituents of soil and saturation states

In geotechnical engineering, soils are considered as complex materials. They are generally three phase materials including: rock or mineral particles collectively called soil particles, water, and air. The voids of a soil, the spaces in between soil particles, are filled with water or air or both the water and air. The water and air existing in pores of soils affect significantly to their behavior and will be mentioned later in this chapter.

The volume of the soil is calculated based on the volume of the various components according to equation 1.1:

$$V = V_v + V_s = (V_a + V_W) + V_s \quad \text{(Eq. 1.1)}$$

where$V$ is the total volume of a soil; V_v is the volume of the voids (pores); V_s is the volume of the solid phase; V_a is the volume of the gas in the voids; V_W is the volume of the liquid in the voids;

The weight of the soil is calculated based on the mass of the various components according to equation 1.2:

$$W = W_v + W_s = (W_a + W_w) + W_s \quad \text{(Eq. 1.2)}$$

whereas, W is the total weight of a soil; W_v is the weight of the voids (pores); W_s is the weight of the solid phase; W_a is the weight of the gas in the voids; W_W is the weight of the liquid in the voids.

Because the weight of air is very small and it can be negligible, equation 1.2 becomes:

$$W = W_v + W_s = W_w + W_s \quad \text{(Eq. 1.3)}$$

The mass-volume and weight-volume relations can be visualized very conveniently through the use of phase diagrams, in which the three phases of a soil as being segregated are depicted. For example, Figure 1.1 shows a similar phase diagram relating to the volume and weight of the three phases.

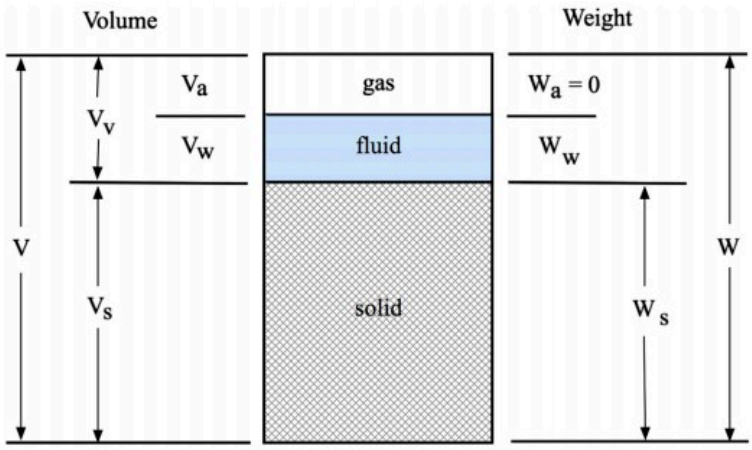

Figure 1.1 Phase diagram showing the relationship between volume and weight of gas, fluid, and solid phases in soil.

We consider a soil specimen with volume V in which the void occupies a volume V_v and the soil grain occupies a volume V_s, (Figure 1.1). The void is filled by both air with volume V_a and water with volumeV_W. If the void is occupied only by the air ($V_v = V_a$, $V_w = 0$), the soil is totally dry; If the void is totally occupied by water ($V_v = V_w$, $V_a = 0$), the soil is full saturated. Between the two special mentioned cases, the soil is partially saturated, or unsaturated. For the pore-gas, when the influence of temperature is important, it should be divided into two parts: dry air and water vapor (Loret et al. 2000; Khalili et al. 2001; Coussy 2004; Jia 2006). However, in this study, the isothermal condition is assumed; pore air is used to indicate the mixture including the dry air and water vapor. The translation between the liquid water and the water vapor is also neglected.

A parameter usually used to assess the saturation of soils is saturation degree. This parameter is defined as the ratio of pore-water volume to total volume of the voids. It allows distinguishing the soils from the full saturated state to the complete dry state. When the water saturation is less than 100% and greater than zero, it is partially saturated. If the water saturation reaches 0%, the soil is dry and if the saturation degree is 100%, the soil is full saturated. In the other words, all the soils could be considered as unsaturated soils, while dry and saturated soils are two special cases of partially saturated soils. The saturation degree of soils affects the behavior of soil due to the different existence of water in voids of a soil which can be observed through figure 1.2.

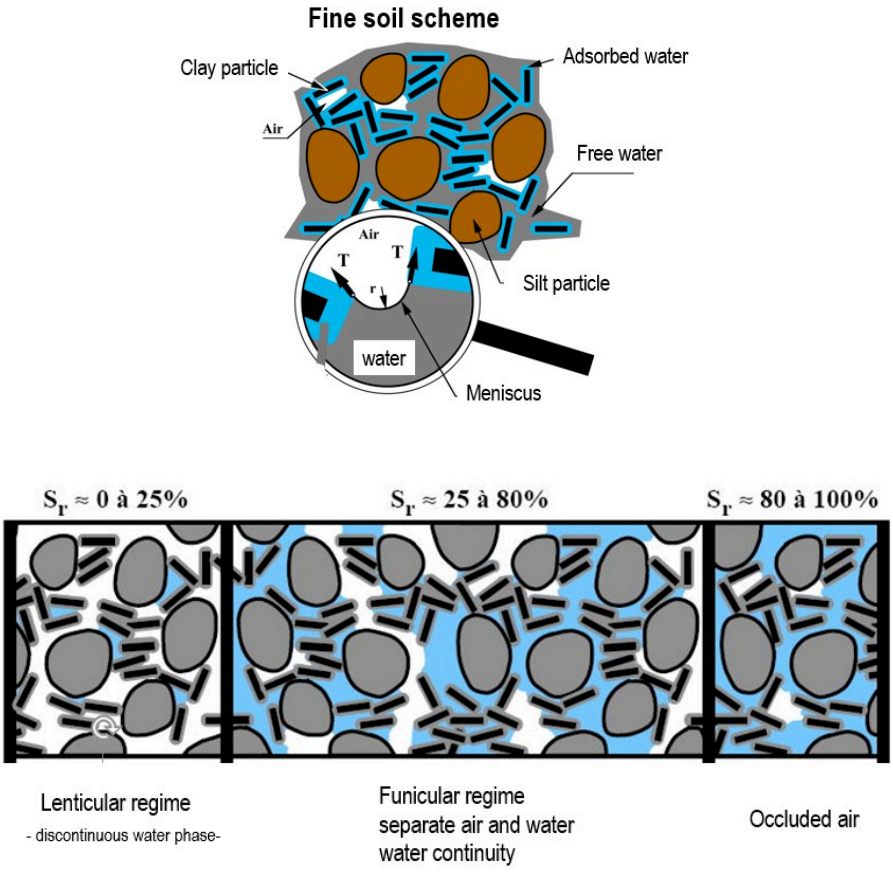

Figure 1.2 Saturation states and different existences of water in voids of soil (Dysli 1997)

I.1.2. Field visualization of degree of saturation

I.1.2.1.Distribution of unsaturated soils on Earth's surface

Unsaturated soils present over a large part of the globe due to climatic and geological conditions. The majority of unsaturated soil formations are located in arid to semi-arid regions on the surface of the earth (Figure 1.3). A study conducted by Fredlund (1996) shows that these areas cover 60% of the countries on the surface of the earth with 60% of the world population. Artificial constructions such as embankments or dames consisting of their unsaturated soil layers and vegetation also play a role in the water variations within these soils (Richards et al. 1983; Ravina 1983). Furthermore, it is now clear that the strong climate changes that we are witnessing at the global scale will generate an even stronger generalization of these unsaturated zones (Ng and Menzies 2007; Gens 2010). Partial saturation of the soil can also cause major damage linking to accidental situations, such as severe droughts in the 1990s and 1991 in France. Recent problems, such as the diffusion of pollutants in soils, or the storage of radioactive waste constitute new challenges which are directly linked to the properties of unsaturated soils (Nazaroff 1992; Fredlund 1996).

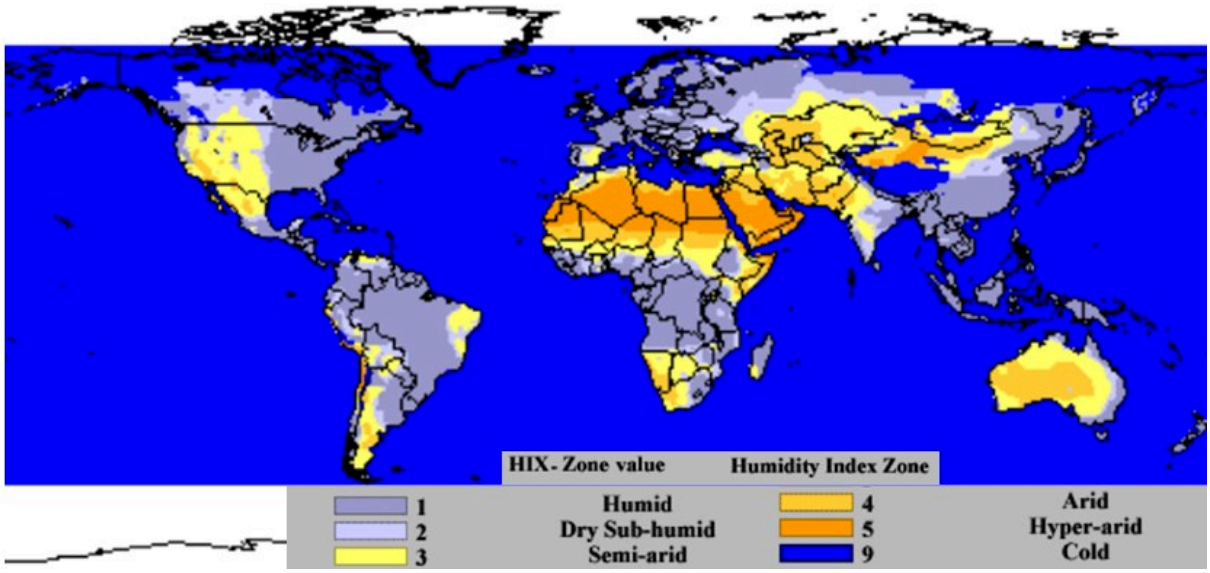

Figure 1.3 Extremely arid, arid, and semiarid areas of the world (GNUEACR 2013).

I.1.2.2.Distribution of unsaturated soils with depth.

In general, the state of saturation depends on the deep of the soil layer and the climatic conditions on the world's surface. Thornthwaite (1948) supposed that it is possible for climatic classification based on the average annual moisture calculated by subtracting the precipitation fluxing at the ground surface for the evaporation. The ground surface climate can affect significantly the level to the groundwater table and therefore the thickness of the unsaturated soil domain. Based on the depth of the soil layer, the ground can be classified into different areas: the soil layers between the ground surface and the water table have a saturation degree from zero to lower than 100% hence they are considered unsaturated soils. In this zone, the pore water pressures can vary from zero at the water table to the maximum of 1,000,000 kPa under dry soil conditions (Croney et al. 1958). Fredlund et al. (2012) showed a classification for unsaturated soil areas (figure 1.4). Above the water table, the soil is generally unsaturated. This zone can be divided into three "sub-zones". Immediately above the level of the groundwater table, the capillary zone, the degree of saturation is between 90% and 100%. The thickness of this capillary zone can be between 1m to 10 m above the water table, depending on climatic conditions and the type of soil. In this zone, water fills most of the voids and the air phase can be considered discontinuous. Above the capillary zone is the two-phase zone, for which the degree of saturation is generally between 15% and 90%. In this area, air and water are two distinct phases and the air phase and water phase in this area are continuous. The top zone is the dry zone. In this area, the saturation degree is between zero and 15%. The water phase is discontinuous and air fills almost voids.

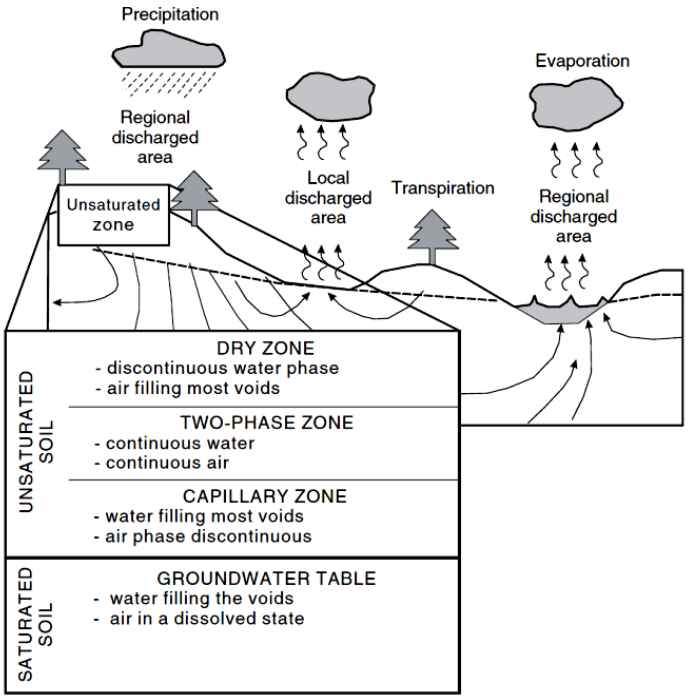

Figure 1.4 Subdivisions of unsaturated soil zone (vadose zone) based depth, local, and regional basis (in Fredlund et al. 2012)

With the soil layer under the water table, Fredlund et al. (2012) classified it as saturated soils; however, in his classification, the saturated soils are the soils with saturation around 100% as being shown in table 1.1. It means that it is possible for the air bubbles appearance under the water table. In another study, Tsukamoto et al. (2014) showed that the air bubbles can be found at 5m below the groundwater table. It means that many of the building structures could be perhaps based on unsaturated soil layers. This shows the need to study the effect of the unsaturation on the liquefaction behavior of soil.

Table 1.1. Terminology commonly used to describe degrees of saturation in field and laboratory (Fredlund et al. 2012)

Degree of Saturation, S, %	Field Description	Laboratory Description
~100	Saturated	Saturated
~90–100	Capillary zone	Boundary effect zone
~15–90	Two-phase zone	Transition zone
~15–0	Dry zone	Residual zone

I.2. Solubility of air in water

I.2.1. Ideal gas law and Boyler's law

As mention in the part I.1, in unsaturated soils, air and water mainly exist as separate phases. Nevertheless, a part of air may exist in the water phase as solute. In tri-axial tests, this solubility of air in water is used to saturate the sample. There are some fundamental questions associated with the sample saturation process needed to be clarified: (1) how much air can be dissolved in water? (2) How much is the rate of air to dissolve into the water? In the tri-axial tests, it can be considered that the temperature during the experimental process is constant and under this condition, the volume of dissolved air in water essentially depends on air or water pressures. This can be demonstrated using the ideal gas law, Boyler's law, and Henry's law.

With sand, it can be considered that the temperature is constant and under this condition, the behavior of dry and moist air following the ideal gas law can be written as in equation 1.4:

$$\overline{u_a}V_a = \frac{M_a}{\omega_a}RT \qquad \text{(Eq. 1.4)}$$

where $\overline{u_a}$: absolute air pressure (kPa), V_a: volume of air (m^3), M_a: mass of air (kg); ω_a: molecular mass of air (kg/mol), R: universal gas constant; has the value of 8.314 J/(K·mol), and T: absolute temperature (K).

In a closed system, the right – hand side of equation 1.4 is constant for a gas and this equation can be written as Boyler's law (Equation 1.5):

$$\overline{u_{a1}}V_{a1} = \overline{u_{a2}}V_{a2} = constant \qquad \text{(Eq. 1.5)}$$

where $\overline{u_{a1}}$ and V_{a1} are the absolute pressure and volume of air, respectively, at condition 1. $\overline{u_{a2}}$ and V_{a2} are the absolute pressure and volume of air, respectively, at condition 2.

I.2.2. Henry's law

Air and water exist in soil in two different phases, however under height pressure, the air dissolve into water. After some time, this process stops when an equilibrium condition between the pressure in the free air and the dissolved air is reached.

Henry's law states that the molar mass of a dissolved gas in a given volume of liquid is proportional to the partial pressure of the gas in the gas phase at equilibrium, that is,

$$\frac{M_i/\omega_i}{V_l} = K_{H_i}.\mu_i \qquad \text{Eq. 1.6}$$

where M_i is the mass of the gas i (kg), ω_i is the molecular mass of gas i (kg/ mol), V_l is the volume of liquid (L), μ_i is the partial pressure of gas i (bar) and K_{H_i} is the Henry's law constant for the dissolution of gas i in that particular liquid. Henry's law constant is commonly expressed in units of mass concentration per unit pressure, typically M/bar (mol.L^{-1}.bar^{-1}, where 1 bar = 100 kPa). The larger the value of K_H, the more soluble the gas and vice versa. The value of K_H and M are shown in table 1.2 for three gases.

Table1.2. Partial Pressure, Henry's Law Constant, and Molar Concentration of Major Air Components in Water at 25^{0}C and 1 bar Total Pressure (Lu and Likos2004)

Gas	Partial pressure u_i (bar)	Henry's Law Constant KH (M/bar)	Molar concentration (M)
O_2	0.2095	1.26 x 10^{-3}	0.2646 x 10^{-3}
N_2	0.7808	6.40 x 10^{-4}	4.9920 x 10^{-4}
CO_2	0.0003	3.39 x 10^{-2}	0.0011 x 10^{-2}

However, the application of Henry's law to the case of unsaturated soil is not easy. In unsaturated soil, air exists as air bubbles entrapped in the soil skeleton. Therefore, the air pressure is much different from the pore water pressure. In practice, the Henry's law can be only used to approximate the pore water pressure needed to saturate completely the sample. The amount of air that can be dissolved in water is referred to as its solubility. Henry's law mentions the mass of air can dissolve into water, but the mass of air going into or coming out of pore water at a time also depends on the test duration and the rate of solution is referred to as its diffusivity.

In the case of tri-axial tests, where the samples are usually saturated by increasing pore water pressure, it can be seen that this process takes some time to finish. In addition, because this process takes place slowly, it should be noted that during the experiment, the saturation of the sample can change significantly if the test time is long enough.

I.2.3. Coefficient of diffusion

The diffusion coefficient of gas indicates how fast the gas dissolves into another substance, pore water in this case. The higher the diffusivity is the faster the air dissolves into the water.

Diffusivity is mentioned in Fick's law and numerous other equations of physical chemistry. The diffusion coefficient of gas into water depends on the pressure, the temperature, the gas, and some other parameters. The diffusion coefficient increases when the pressure goes up. The value of the diffusion coefficient of some gases is presented in table 1.3.

Table 1.3 Coefficient of diffusion for certain gases in water under different temperatures (Kohn 1965 in Fredlund et al 2012).

Gas	Temperature, t^0 (°C)	Coefficient of Diffusion, D (m^2/s)
CO_2	20	1.7×10^{-9}
N_2	22	2.0×10^{-9}
H_2	21	5.2×10^{-9}
O_2	25	2.92×10^{-9}

I.2.4. Skempton's parameters A and B

To link the variations in pore pressures associated with variations in total stresses in soils, two parameters defined by Skempton (Skempton 1954) are used. The two parameters called Skempton coefficients, A and B and the relationship is shown by equation 1.7:

$$\Delta u_w = B[\Delta\sigma_3 + A(\Delta\sigma_1 - \Delta\sigma_3)] \qquad \text{(Eq. 1.7)}$$

Where A and B are the Skempton coefficients and $\Delta\sigma_1$ and $\Delta\sigma_3$ are the variations of the major and minor total principal stresses. These coefficients are applied in a variety of geotechnical experiments. They have, for example, been used in studies of the stability of earthworks (Bishop 1954).

One of the common uses of these coefficients is to assess the saturation of triaxial samples in isotropic pressure condition. With this condition, the second term of the equation ($A(\Delta\sigma_1 - \Delta\sigma_3)$) equals to zero and the equation 1.7 becomes simple in practical measurement. This is the reason why this coefficient is used widely in the context of the triaxial test. The evaluation of the saturation of a sample is quantified by the Skempton coefficient B, which can then be simplified in the case of isotropic pressure condition as equation 1.8:

$$B = \frac{\Delta u_w}{\Delta\sigma_3} \qquad \text{(Eq. 1.8)}$$

Where $\Delta\sigma_3$ and Δu_w are the imposed increment of isotropic confining stress and the resulting measured increment of pore water pressure, respectively.

A number of studies have demonstrated that the Skempton's parameter B links to the saturation degree. The theoretical and experimental studies (Lade and Hernadez 1977; Xia and Hu 1991; Yoshimi et al. 1989; Arab et al. 2016; Vernay et al. 2019) have shown that the value of B reaches the maximum value (varying from 0.8 to 0.96 depending on the type of the soil) when the sample is full saturated.

In the remainder of this manuscript, the term "Skempton coefficient" will refer to the Skempton's pore water B parameter.

I.3. Suction in soils

I.3.1. Capillary Phenomenon

When a fluid contacts to the surface of other material, the molecules on the interface of the fluid are subjected to some forces. One group of forces is the bonding forces between the molecules on the surface and other molecules inside the fluid. The other is the forces between these surface molecules with the molecules of other material. For example, the molecule in figure 1.5 below is subjected two groups of forces and the imbalance between them causes a phenomenon called surface-tension. It is also responsible for the shape of liquid droplets. In case there is not any other load, including gravity, drops of all liquids are spherical according to Laplace's law.

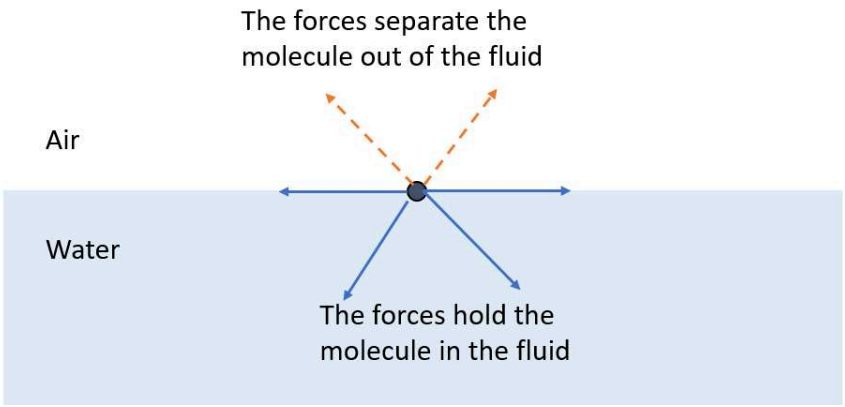

Figure 1.5 Molecule of water on the air – water interface (Delage et al. 2000)

In the system of soil particles, this behavior leads to the phenomenon of capillarity. The pore between soils particles can be described as capillary tubes (figure 1.6). A tube with a small radius r is immersed in a container filled with water. Due to the surface tension, the water level inside the tube is higher than that outside the pipe.

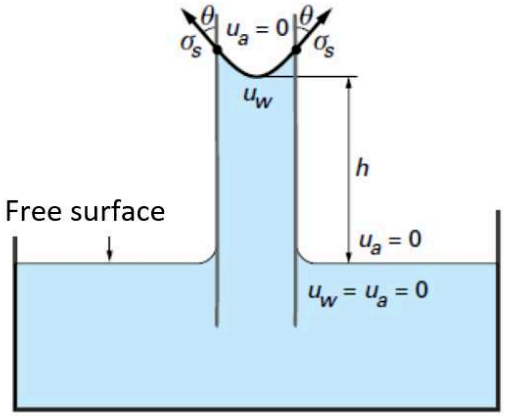

Figure 1.6 Capillary rises in a tube (Delage et al. 2000)

The difference between the pressure at the free surface of the liquid u_a and the pressure at the surface of the water column u_w is given by the Jurin's law (equation 1.9):

$$u_a - u_w = \frac{2.\sigma_s.cos\theta}{r} \qquad \text{(Eq. 1.9)}$$

Where σ_s is the surface tension (N/m); θ is the contact angle of the liquid on the tube wall (in degree); r is the radius of the tube (m). u_a is the air pressure and u_w is the water pressure on the bending interface in the tube (Pa). From this equation, it can be seen clearly that the capillary depends on the materials and the radius of the tube. The smaller the tube radius is, the higher the fluid increase.

I.3.2. Suction in soils.

In the early 1900s, there were many studies focusing on the theoretical concept of soil suction (Buckingham 1907; Corey et al. 1967). However, the results of these researches mainly supported for developing the soil-water-plant system. Until 1965, (Aitchison 1965), the definition of soil suction has been provided in a thermodynamic context and has become accepted concepts in geotechnical engineering (Krahn et al. 1972; Wray 1984). In this definition, the total suction of soils (Ψ) includes two components, namely, matrix suction

$(u_a - u_w)$ and osmotic suction (π) (equation 1.10). The definition of total suction, matrix suction, and osmotic suction are shown below (Aitchison 1965).

Matrix or capillary component of free energy, in suction terms, is the equivalent suction derived from the measurement of the partial pressure of the water vapor in equilibrium with the soil water, relative to the partial pressure of the water vapor in equilibrium with a solution identical in composition with the soil water.

Osmotic (or solute) component of free energy-in suction terms, it is the equivalent suction derived from the measurement of the partial pressure of the water vapor in equilibrium with a solution identical in composition with the soil water, relative to the partial pressure of water vapor in equilibrium with free pure water.

Total suction or free energy of the soil water-in suction terms, it is the equivalent suction derived from the measurement of the partial pressure of the water vapor in equilibrium with a solution identical in composition with the soil water, relative to the partial pressure of water vapor in equilibrium with free pure water.

$$\Psi = (u_a - u_w) + \pi \qquad \text{(Eq. 10)}$$

Where, $(u_a - u_w)$ is matrix suction (kPa); u_a is pore-air pressure (kPa); u_w is pore-water pressure (kPa).

From the above definitions, it can be seen that the matrix suction mainly arises from the water in the pore, and the osmotic suction is due to the chemical forces. In this study, the osmotic suction will be neglected hence the matrix suction and the total suction are the same (equation 1.11).

$$\text{Matric suction} = \text{total suction} = \text{suction s} = (u_a - u_w) \qquad \text{(Eq. 1.11)}$$

The soil suction can be used to explain the characteristics of unsaturated soils that affect soil behaviors. The joints formed between the contact points of soil particles are subjected to soil suction and they create a connected force between the soil particles, which bonds them in a temporary way. Thus soil suction can enhance the stability of soil structures. As discussed the soil below and above the water table could be also partially saturated. In these unsaturated zones, the water phase can be continuous or discontinuous. Pore-pressure in depths below the water table is normally positive and the pore-water in the capillary zone above the water table is negative. The attraction in the capillary, as discussed, exerts on the water is termed “soil

suction". Similar to the high of the fluid column discussed in the part 1.4.1 the largeness of the attractive force that soil above the water table influence the water depends on the size of the voids. The smaller the void, the higher the water column is in the void. This conclusion can be demonstrated clearly through the experiment of Jansse and Demsey (1980) presented in figure 1.7. In this figure, the radius of the tube was varied to simulate the void in different types of soil.

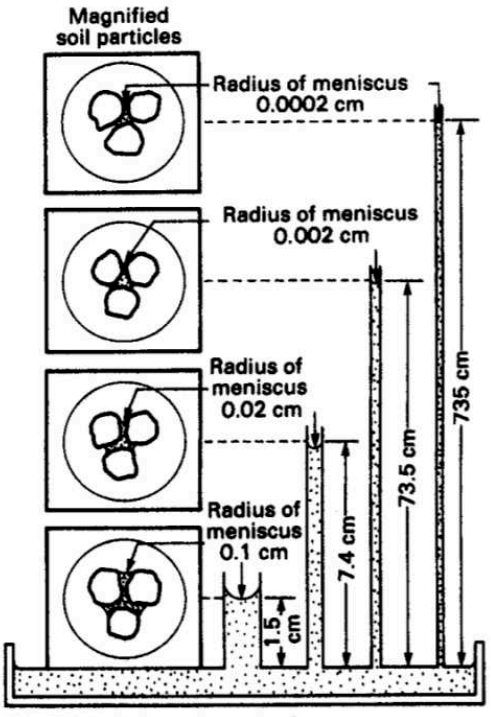

Figure 1.7 Capillary tubes showing the air – water interfaces at different radii of curvature (from Jansse and Demsey 1980)

I.3.3. Degree of water saturation

The change of saturation degree affects the microstructures of the air phase and water phase in the pores of the soils. There are three types of air phase as described below (Wroth et al., 1985):

-The gas phase is continuous and menisci of liquid adhere to most grain boundaries. This type is found in soils with low degrees of water saturation

-At higher degrees of water saturation, the liquid phase and gas phase are both continuous.

-When the degree of water saturation increased further, the liquid phase is continuous and the gas phase becomes discontinuous. The gas exists as bubbles embed in the pore water.

Sheng (1999) showed that both water and air phase are continuous if the water saturation varies between about 50% and 90% for clay, 30% and 80% for sand. With sand, when the water saturation is higher than 80%, the gas presents as air bubbles in the void with different contact types (Figure 1.8). This change in air bubbles shape can affect the calculation of pore water pressure mentioned after.

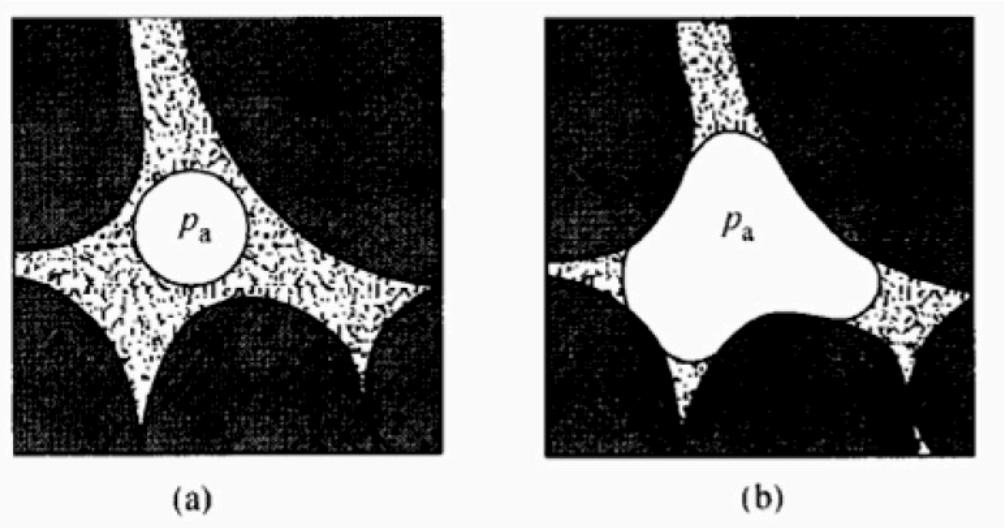

Figure 1.8 The form of air bubbles changes when the saturation decreases (a) air bubble not wetting solid surface; (b) both fluids in contact with solid surfaces (Zienkiewicz et al. 1999)

I.3.4. Soil drying and wetting curves

The soil-water characteristic curve (SWCC) describes the relationship between the gravimetric water content, w, or volumetric water content, θ, or degree of saturation, Sr, and the negative porewater pressure or the suction. Due to the difficulty in the determination of the saturation degree of undisturbed soil directly, SWCC can be used as a tool in the determination of the degree of saturation or water content changes. Figure 1.9 present typically the soil-water characteristic curves for different kinds of soils including sand, silt, and clay. Generally, with a given water saturation degree, soil suction increases when the soil particle size decreases. Significant suction can be found in fine-grained materials over a wide range of water content. While for sandy soils, when the water saturation exceeds 40%, the matrix suction is so small that it can be neglected.

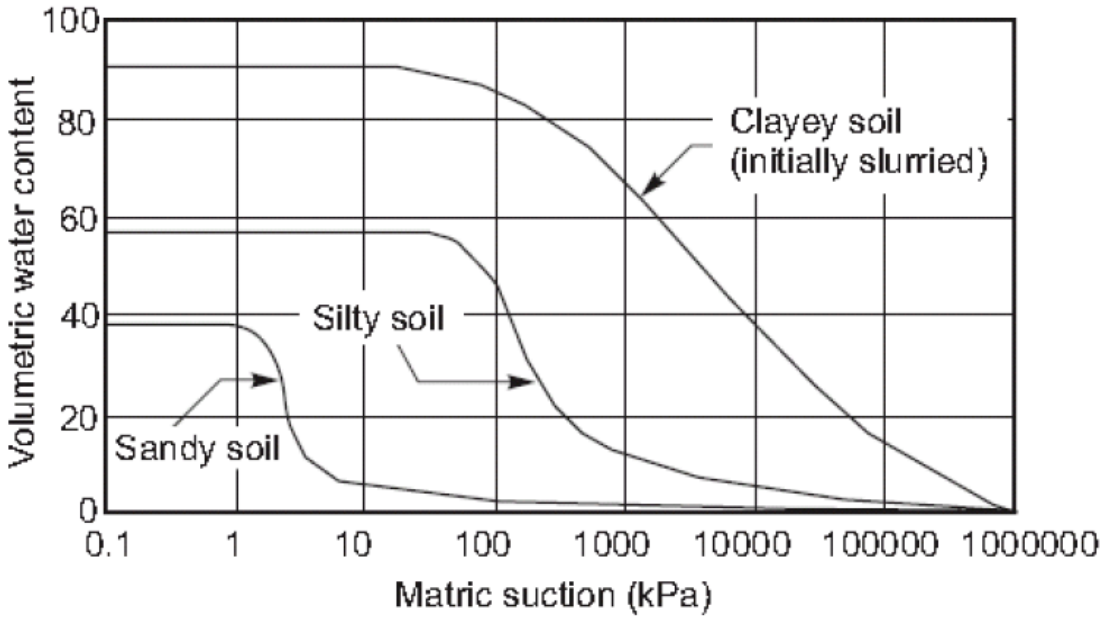

Figure 1.9 Soil water characteristic curve for sandy soil, silty soil and clayey soil (Fredlund and Xing 1994)

While although the SWCC's are useful for characterizing the properties of the test soils in general; however, in some cases, these properties may not be effective to the soil in a near saturation state. It can be predicted that the difference between the pore gas pressure and pore liquid pressure in soil depends on the size of bubbles produced in the soil. From the Young-Laplace equation, the pressure difference between the gas inside of a spherical bubble and the surrounding liquid depends on the dimensions of the gas bubbles and the surface tension of the gas-liquid interface. The pressure is proportional to bubble sizes for a given gas and liquid. For air and pure water at the temperature of 25°C, the differential pressures between the inside and outside of the bubble are 0.3 kPa for a bubble 1 mm in diameter, 3 kPa for a bubble 0.1 mm in diameter, and 30 kPa for a bubble 0.01 mm in diameter. However, this difference does not result in any matrix suction, because of the very small size of bubbles in the soil at a nearly saturated state. It means that the pressure differential between the gas and liquid phase would not act on the soil skeleton.

The soil-water characteristic curve for Hostun sand has been measured (Bian 2007) and plotted in comparison to that of Toyoura sand measured by Kamata et al. (2007) highlighted in red cube and that of residual sand suggested by Matsushi et al. (2006) (pink line, Figure 10). The results show that the soil suction is very small while the water saturation degree varies in a wide range: suction remains lower than 5kPa when the degree of water saturation

exceeds 40%. Because this value is so small, it is difficult to use in clarification the saturation of soil at the state near full saturation.

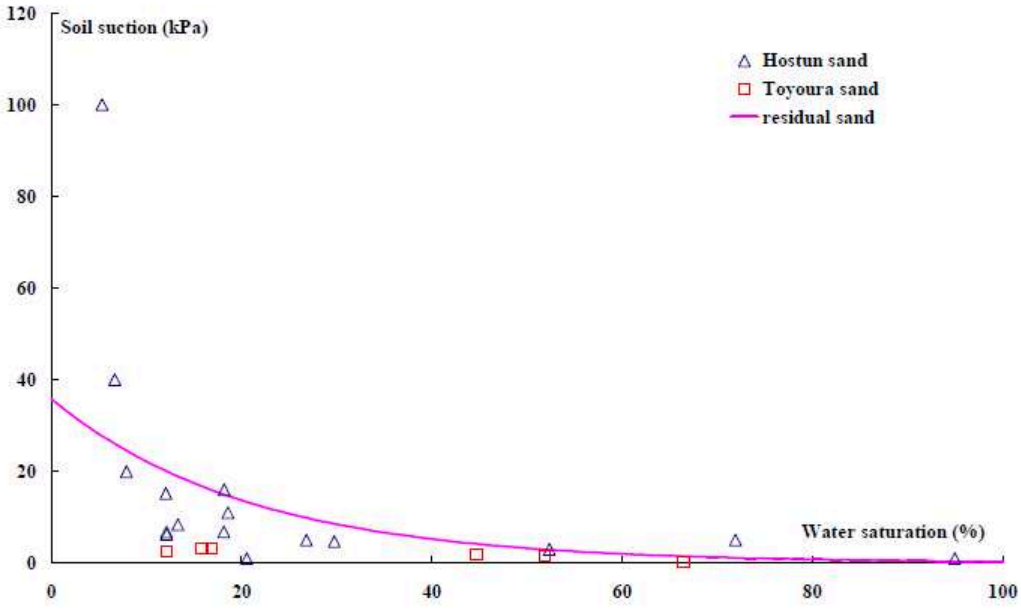

Figure 1.10 Soil water characteristic curve of sandy soil (Bian 2007)

Saturation change in soils due to climate factors such as drying–wetting cycles and associated changes in the groundwater table level may result in the change of mechanical behaviour of soil. The key driving parameter associated with these changes is the suction. It is now clear that the suction in soil does not depend only on the water content or saturation degree but also on the whether the soil is on drying or wetting paths (Fleureau et al. 1993b). This relationship also allows determining the associated changes in void ratio versus suction simultaneously along with the SWCC. The variation in the suction $s = u_a - u_w$ of the material versus its moisture content can be obtained using several devices (Biarez et al. 1989): Tensiometers and tensiometric plates for suction lower than 30 kPa, and filter papers and Richard's pressure membrane cells for pressures between 50 and 1000 kPa. The paths followed by the samples are drying-wetting paths: along wetting paths, the samples, initially dry, are prepared in the measurement cell by letting the particles fall from a height of approximately 50 cm; the water content is measured once the equilibrium of the sample is reached under the applied suction. Along drying paths, the same protocol was used with initially saturated samples. The results are shown in figure 1.11. The pF, defined as pF=log s (s: suction in cm), is plotted versus water content for both the drying and wetting paths. It must be noted that the hysteresis

between the wetting and the drying paths is very limited. The curves are in general agreement with other results obtained on similar materials.

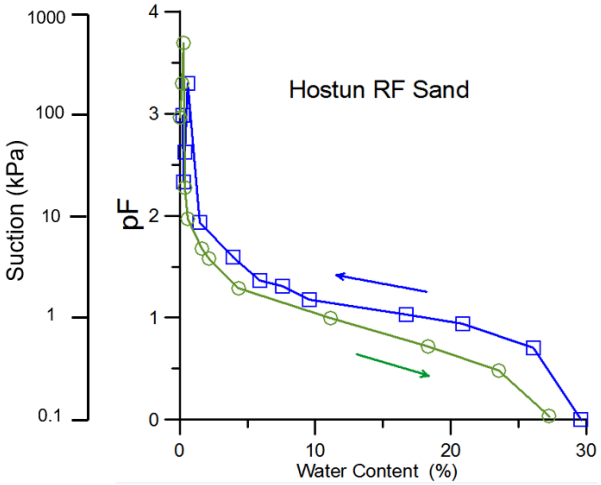

Figure 1.11 Suction versus water content on drying, wetting paths for Hostun sand (Biarez et al. 1989)

I.4. Stress state variables

I.4.1. Concept of effective stress in the case of totally saturated or totally dry soil

The concept of effective stress was introduced by Terzaghi, in which the compressive stresses in saturated soil is contributed by two parts which have different mechanical effects. The first part corresponds to the pressure in the water contained in the pore of the soil. This part is called the neutral pressure u_w. When u_w is positive, it is often called pore pressure.

The second part is called effective stress σ'. This part is the stress impact on the soil skeleton; hence, that produces measurable effects, such as densification, or an increase in shear strength.

The total stress is therefore written as the sum of the two parts constituting it (Equation 1.12):

$$\sigma = \sigma' + u_w \qquad \text{(Eq. 1.12)}$$

Terzaghi's assumption is only applied in two cases: either the soil is completely saturated, or it is completely dry. In case the soil is completely dry, the pore water pressure can be considered equal to zero or atmospheric pressure (Nuth and Laloui 2008).

I.4.2. Stress state variables in the case of partially saturated soil

The state of stress in unsaturated soil is basically different from the state of stress in saturated soil. In saturated soils, there are only two-phase systems: soil particles and water occupying entirely the volume of the pore. Similarly, in the dry soils, there are two phases: solids and gas only. However, in unsaturated soils, there are three-phase systems including solids (soil particles), liquid (pore water), and gas (pore air). The state of stress acting at the particle-particle contacts is impacted by other factors besides the pore water pressure, for example the pore air, surface tension, etc. This difference causes the impossibility for application of Terzaghi's assumption for unsaturated and therefore some methods have been proposed to satisfy this gap.

Many researchers have tried to extend the concept of the effective stress from saturated soils to unsaturated soils. During the 1960s this was the subject of intense discussion. Since this first approach was not entirely satisfactory, other authors have proposed another approach based on the use of two independent stress variables.

Figure 1.12 (Taibi et al 2013) summarizes the different approaches to solve an unsaturated soil problem.

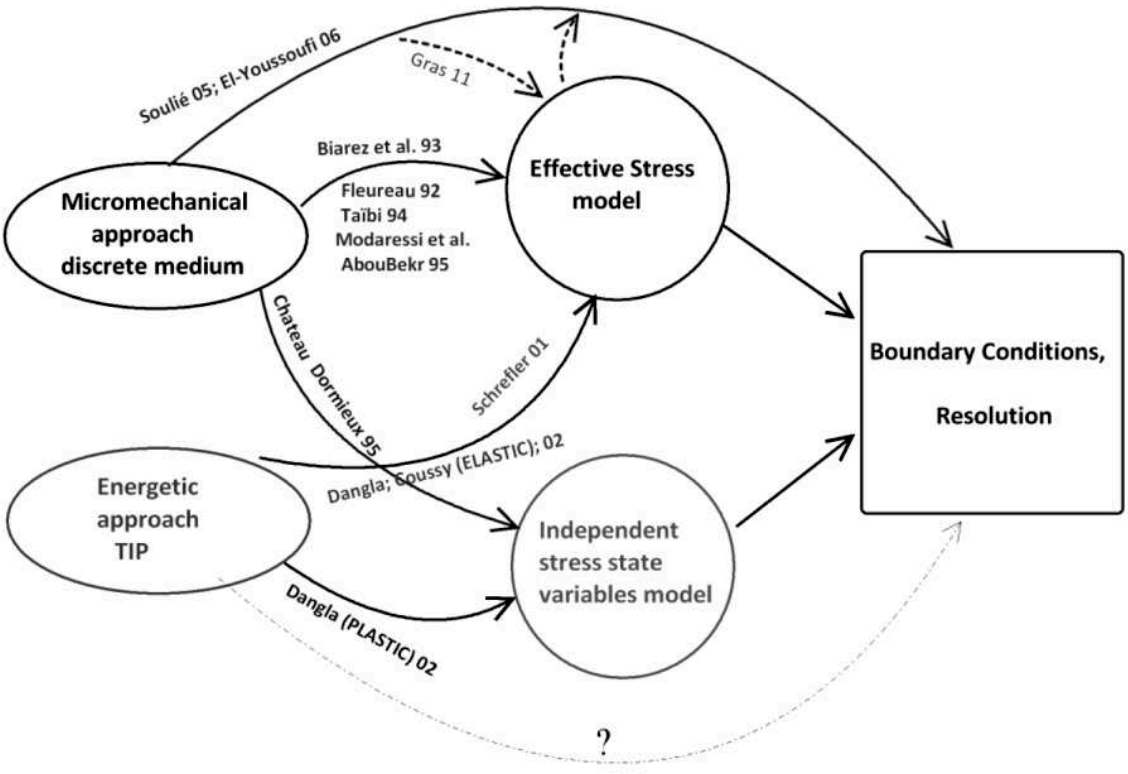

Figure 1.12 Different approaches to solve an unsaturated soil problem (Taibi et al. 2013)

I.4.2.1.Generalized effective stress concept.

For saturated soil, effective stress is the difference between the total stress and pore water pressure. In other words, effective stress is the portion of total stress putting on the soil skeleton. Because the soil is saturated, the effective stress can be calculated at any point of soil as long as the total stress and pore water pressure are known.

For unsaturated soil, two additional factors are taken into the account: the stress acting through the air phase (i.e., the pore air pressure, u_a) and the difference between the pore air pressure and the pore water pressure, or matrix suction. The extension of Terzaghi's classic effective stress equation for unsaturated soil was proposed by Bishop (1959) as follows (Equation 1.13):

$$\sigma' = (\sigma - u_a) + \chi(u_a - u_w) \qquad \text{(Eq 1.13)}$$

Where $(\sigma - u_a)$ is the net normal stress, the difference between pore air pressure and pore water pressure ($u_a - u_w$) is matrix suction. The effective stress parameter χ is a material variable which varies between zero and unity depending on the saturation state of soil. χ is equal to zero when the soil is completely dry, χ is unity when the soil is in full saturated state and the equation reduces to Tezaghi's equation for saturated soil (Equation 1.13).

Bishop and Donald (1961) presented results of triaxial tests in which the pressures u_a and u_w were controlled, thus allowing them to determine a relationship between χ and the degree of saturation S_r. After that, for simplicity of the calculation, many authors capture χ based on strong dependency on the degree of saturation (Equation 14). Nevertheless, this expression shows some limitations particularly in the evaluation of volumetric behavior.

$$\chi = \chi(Sr) \qquad \text{(Eq 1.14)}$$

Indeed, other experimental verifications have highlighted that the concept of enlarged effective stress as initially proposed by Bishop does not make it possible to represent certain volume behaviors of unsaturated soils. Delage and Cui (Delage and Cui 2001), for example, perform an oedometer collapse test on samples of unsaturated Picardy loess with constant water content (non-zero suction). They showed that during the rewetting of the samples, under constant stress, a collapse is observed, resulting in a reduction in the void ratio. During the collapse, the suction $(u_a - u_w)$ decreases towards zero, according to the expression of Bishop

(equation 1.13), the effective stress reduces and results in an increase of void ratio. There are therefore limits in the representation of Bishop.

Jennings and Burland (Jennings and Burland 1962) also carried out an experimental study to highlight the limitations of the concept of effective stress for unsaturated soils. They showed that the value of χ depends on the stress path in space $(\sigma - u_a;\ u_a - u_w)$, consequences induced by the hysteresis of the water retention curve. They also showed that the value of depends on the type of performed test. They explained these observations by the fact that the changes in granular structure are different depending on whether a variation in suction or a variation in external stress is applied.

In 1963, Bishop and Blight (Bishop and Blight 1963) re-evaluated the use of a one-strain equation of effective stress. They observed that the same variation in suction does not always lead to the same variation in effective stress. They also suggested representing data from laboratory collapse tests as a function of two independent stress variables, this leads to the transition to the use of an expression with two independent variables (Ng and Menzies 2007).

A number of studies (Bolzon 1996; Dangla 2002) have demonstrated that irreversible strains, such as those in collapse, can be correctly described by a generalized effective stress concept relating to an elasto-plastic law in which a yield surface function of capillary pressure is integrated. From this point of view, the effective stress concept is still an efficient means to describe in qualitative and quantitative ways the unified mechanical behavior of soils for both saturated and unsaturated states, and the new model of χ has been build up by some studies (table 1.4)

Another recent approach used to characterize the behavior of polyphasic granular media is the macroscopic phenomenological, homogenization, and discrete elements methods (DEM). This method extends the effective stress tensor concept to unsaturated soils, with a hypothesis, that the unsaturated soil is a poro-elastic material, in other words, the behavior of the solid constituent is reversible elastic. From this point of view, Coussy and Dangla (2002) used energy approach to exhibit that the effective properties derived from the analysis at the microscopic scale could be combined to the relations deduced from thermodynamics to interpret the effects of the pore pressure and the scale effects. Dangla (2002) also extended the energy approach to the elastoplasticity behavior in unsaturated soils by idealizing the capillary pressure – degree of saturation relation and decomposing the degree of saturation into a reversible part and a non-reversible part.

Table 1.4. Different expressions of the Bishop χ parameter (Taibi et al. 2013)

Expression of χ	Definition of the parameters	Authors
$\chi = S^w$	S^w : degree of saturation in water	Hassanizadeh & Gray (1980) Lewis & Shrefler (1987) Bolzon & Schrefler (1995) Bolzon *et al.* (1996) Hutter *et al.* (1999) Wheeler *et al.* (2003)
$\chi = 1 \quad \text{for } s < s_e$ $\chi = \dfrac{s_e + \dfrac{a_e}{s - s_e + a_e}(s - s_e)}{s} \quad \text{for } s \geq s_e$	s : suction (kPa) s_e : air entry suction a_e : parameter function of the soil	Kohgo *et al.* 1993
$\chi = S^w\left(2 - S^w\right)$	S^w : degree of saturation in water	Gudehus (1995)
$\chi = \begin{cases} 1 & \text{for } \dfrac{s}{s_e} \leq 1 \\ \left(\dfrac{s}{s_e}\right)^{-0,55} & \text{for } 1 \leq \dfrac{s}{s_e} \leq 12 \end{cases}$	s : suction (kPa) s_e : air entry suction	Khalili & Khabbaz (1998) Loret & Khalili (2000) Loret & Khalili (2002)
$\psi = \begin{cases} 1 & \text{for } \dfrac{s}{s_e} \leq 1 \\ 0{,}45\chi & \text{for } 1 \leq \dfrac{s}{s_e} \leq 25 \\ 0 & \text{for } \dfrac{s}{s_e} \succ 25 \end{cases}$	s : suction (kPa) s_e : air entry suction $\psi = \dfrac{d(\chi s)}{ds}$	Khalili *et al.* 2004
$\chi = \begin{cases} 1 & \text{for } \dfrac{s}{s_e} \leq 1 \\ \left(\dfrac{s}{s_e}\right)^{-0,55} & \text{for } 1 \leq \dfrac{s}{s_e} \leq 25 \\ 25^{0,45}\left(\dfrac{s}{s_e}\right)^{-1} & \text{for } \dfrac{s}{s_e} \succ 25 \end{cases}$	s : suction (kPa) s_e : air entry suction	Russel & Khalili (2006)
$\chi = S^w$ $\dfrac{e}{e_s} = 1 - a\left[1 - \exp(b\xi)\right]$	$e(p')$: void ratio (isotropic compression test under controlled suction) e_s (p') : void ration (isotropic saturated test) $\xi = f(s)\left(1 - S^w\right)$ a=0,369 ; b=1,419 $f(s)$: suction function	Gallipoli *et al.* (2003)
$\chi = \dfrac{1}{s + a}$	s : suction a : parameter	Sun *et al.* (2003)
$\chi = S^w \quad or \quad \chi = \sqrt{S^w}$		Sheng *et al.* (2003)

With the same approach, a thermodynamic definition of the effective stress notion in porous media was suggested by Gray and Schrefler (2001). In their macroscopic approach, the microscopic boundary conditions, eg the liquid-solid interfaces, are also taken into account.

I.4.2.2.Capillary stress model

Using a microstructural model, Taibi et al. (2008; 2013), proposed a new definition of generalized effective stress for unsaturated granular media. The model is based on a medium composed of elastic spherical isodiametral particles.

When the water phase is discontinuous, water forms torical menisci at the points of contact between particles (Figure 1.13). The air phase is continuous and its pressure plays a role, as does the water pressure, in the creation of the capillary strength; the water pressure inside the meniscus is negative with respect to that of the air ($u_w<u_a$). In this case, the intergranular forces due to water are perpendicular to the tangent planes at the contact points between the particles and therefore do not produce any rearrangement of the particles or variation involume.However,theseforcesplayanimportantroleinthestrengthofthe material.Fromapracticalpointofview,suchconditionsareobservedforwater contents below the shrinkage limit.

When the air phase is discontinuous, air forms isolated bubbles inside the pores. The water phase is continuous and completely wets the solid particles. Since no contact occurs between air and the solid particles, water pressure does not play any role in the strength of the material. However, the presence of air bubbles in the pore fluid makes it more compressible.

The passage from a discontinuous to a continuous medium is made by considering regular arrangements of particles. In a representative elementary volume (REV), the "capillary" stress in a direction is expressed as:

$$\sigma'_{cap} = \frac{\sum F_i}{S_{REV}} \qquad \text{Eq. 1.15}$$

where $\sum F_i$ is the sum of the capillary forces acting in this direction and S_{REV}, the cross-section of the REV normal to that direction.

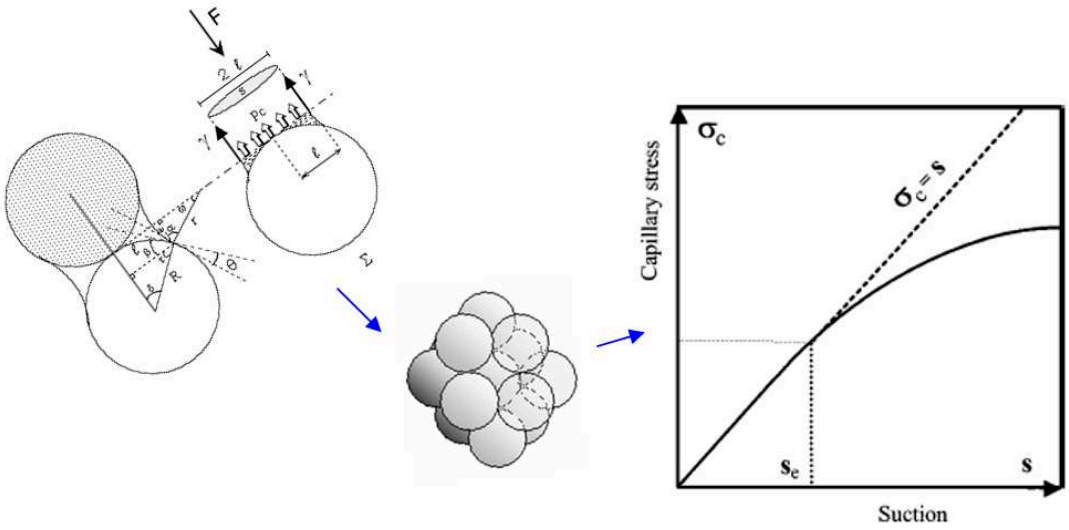

Figure 1.13 Schema for the capillary stress model (Taibi et al. 2008; 2013)

In general, the solid skeleton is submitted to an intergranular (or effective) stress, which is the sum of the total stress and the capillary stress due to capillary pressure:

$$\sigma' = \sigma + \sigma'_{cap} \qquad \text{Eq. 1.16}$$

I.4.2.3. Independent stress variables

Coleman (1962) proposed using the net normal stress $\sigma - u_a$ and matrix suction $u_a - u_w$ as two stress variables for unsaturated soil to describe stress-strain relations. This perspective was clarified by further work by Bishop and Blight (1963). They demonstrated some benefits in using net normal stress and matrix suction as stress state variables. Fredlund and Morgenstern (1977) approached from both experimental and theoretical views and proposed the use of net normal stress and matrix suction as two independent stress state variables for unsaturated soil. To depict the stress-strain relations, it is possible to use any two of three stress variables: $\sigma - u_a$and$\sigma - u_w$, $u_a - u_w$ and $\sigma - u_w$ or $u_a - u_w$ and $\sigma - u_a$.

Over the past decades, many conducted studies have demonstrated and support for Fredlund and Morgenstern's (1977) independent stress state variable approach. However, it remains a highly active area of research for identifying the most appropriate stress state variables for unsaturated soil.

In the attempt to build up the concept of two stress state variables for unsaturated soil, Fredlund and his colleagues in 1978 (Fredlund et al. 1978) proposed equation 1.17. This equation has the same form to the Mohr-Coulomb criterion for saturated soils; however, the shear strength of unsaturated soil is a function of the two stress variables, net stress, and suction.

$$\tau_{ff} = c' + (\sigma_f - u_a)_f tan\emptyset' + (\sigma_a - u_w)_f . \tan \emptyset^b \qquad \text{(Eq. 1.17)}$$

Where

c' = intercept of the "extended" Mohr-Coulomb failure envelope on the shear stress axis where the net normal stress and the matrix suction at failure are equal to zero; it is also referred to as "effective cohesion"

$(\sigma_f - u_a)_f$ = net normal stress state on the failure plane at failure

u_{af} = pore-air pressure on the failure plane at failure

$\emptyset'$ = angle of internal friction associated with the net normal stress state variable, $(\sigma_f - u_a)_f$

$(\sigma_a - u_w)_f$ = matrix suction on the failure plane at failure

$\emptyset^b$ = angle indicating the rate of increase in shear strength relative to the matrix suction, $(\sigma_a - u_w)_f$

The Mohr circles corresponding to failure conditions for an unsaturated soil can be plotted in a three-dimensional coordinate system, as presented in figure 1.14. The three-dimensional plot has the shear stress, τ, as the target function and the two stress state variables, $\sigma - u_a$, and $\sigma_a - u_w$ as horizontal axes. The frontal plane, where the matrix suction is zero, figures a saturated soil. On the frontal plane, the $(\sigma - u_a)$ axis can be replaced by the $(\sigma - u_w)$ axis because the pore-air pressure becomes equal to the pore-water pressure at saturation.

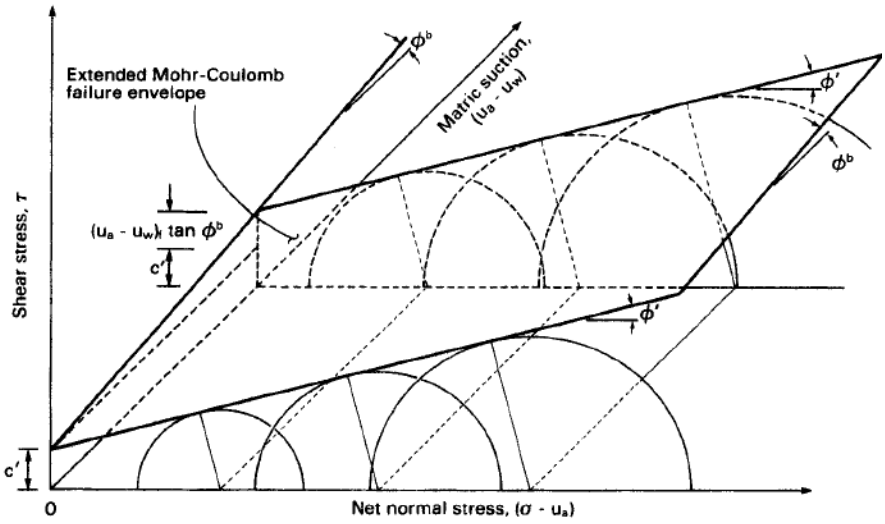

Figure 1.14 Extended Mohr-Coulomb failure envelop for unsaturated soils. (Fredlund et al. 1978)

Alonso et al. (1990) summarized the main behavior of unsaturated soil presented below.

- In unsaturated soils, suction contributes to stiffening the soil against external loading.

- In an open structure soil, under a given confining stress, a reduction in suction (wetting) may result in a volumetric collapse of soil structure. The amount of collapse goes up with the intensity of the confining stress for a certain range of confining stress. However, when the confining stress goes up, the amount of collapse may reach a

maximum, after that it decreases. The confining stress corresponding to the maximum collapse depends on initial conditions.

- On the wetting process, partially saturated soil can either expand or collapse depending on the confining stress low or high enough.

- However, suction controlled experiments have shown that, during the wetting process, a reversal in volumetric behavior may also occur. In fact, when the suction reduces from a relatively high initial value, the potentially collapsible microstructures have been experienced first expansion and then a compressive strain.

- The volumetric behavior of partially saturated soils in the wetting process depends not only on the initial and final stress and suction values but on the particular path (loading path or suction path) followed from the initial to the final state.

- Changes in suction may induce irreversible volumetric deformations. This behavior may be investigated by subjecting samples of soil to drying-wetting cycles.

From these observations, Alonso et al (1990) shown that each of the previous models covers only limited aspects of the stress-strain response of unsaturated soil. They suggested an elastoplastic hardening model in which the excess of total stress over air pressure and the water pressure deficiency (or suction) was used two independent stress variables (Equation 1.18). With this model, the stiffness changes of the soil induced by suction changes are accounted. This model also reproduces the irreversible response of the soil against stress and suction reversals, supplies the conditions for collapsibility, and connects the amount of collapse to the stiffness changes of the soil caused by changes in suction.

$$N(s) - \lambda(s) \ln \frac{P_0}{P^c} + k \ln \frac{P_0}{P_0^*} + k_s \ln \frac{S+P_{at}}{P_{at}} = N(0) - \lambda(0) \ln \frac{P_0^*}{P^c} \qquad \text{(Eq. 1.18)}$$

One can observe that the relationship between stress p and suction s is represented as a function of two reference stress values (P_0^*, P^c) and some soil parameters ($N(s)$, $\lambda(s)$, k, k_s,). These parameters are shown in figure 1.15.

This model, as they assumed, gives a simple simulation of swelling, but is impossible to approximate the behavior of strongly expansive soils. Due to this limitation, it is useful for partially saturated soils with plasticity form moderate to low, such as sandy clays, clayey sands and silts, and granular soils. The figure 1.16 presents the three – dimensional view of the yield surfaces in (p,q,s) stress space.

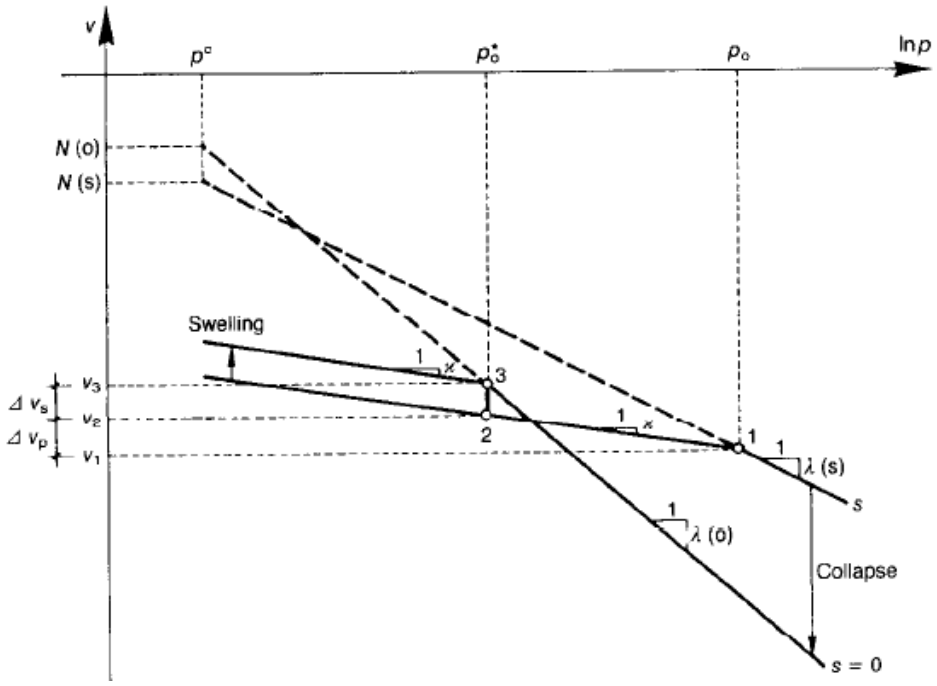

Figure 1.15Relationship between preconsolidation stresses p_0 and p_0^* - compression curve for saturated and unsaturated soil (Alonso et al. 1990).

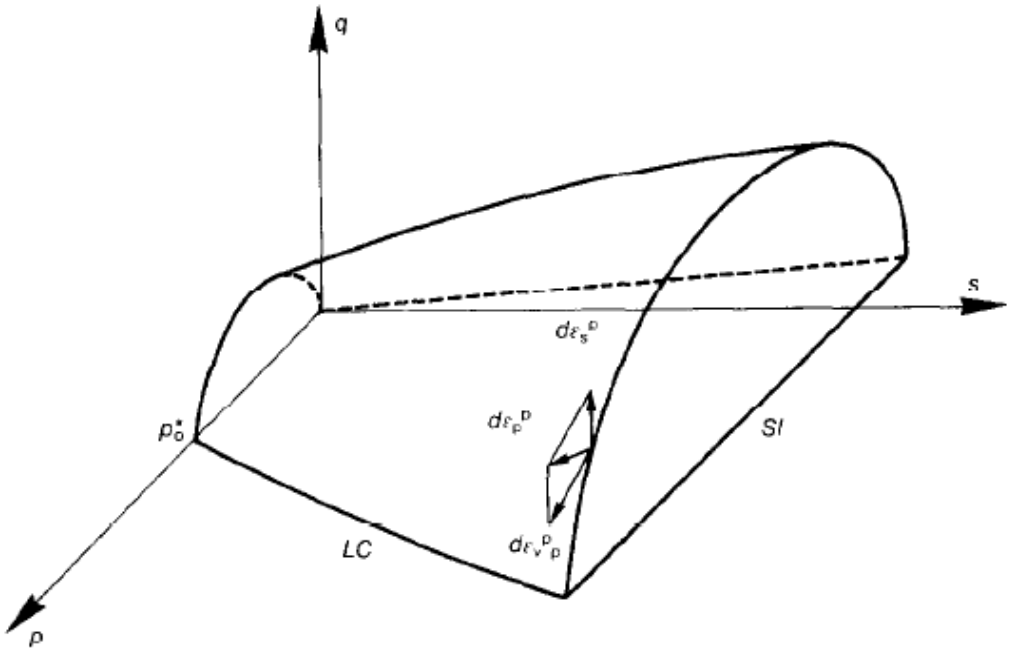

Figure 1.16 Three – dimensional view of the yield surfaces in (*p,q,s*) stress space (Alonso et al. 1990).

I.5. Conclusions

From the literature review, it can be seen that unsaturated soil occupies a large portion of the earth's surface. The appearance of air bubbles in the pore of unsaturated soil makes it constituted from three elements: solid as soil skeleton, liquid as pore water, and gaseous as pore air. Thus, there is a big difference in the behavior of unsaturated soil compared to that of saturated soil. The understanding of concepts, for example, suction, Skempton's parameter B, and the air-water interaction, etc., is necessary when studying the behavior of unsaturated soil.

In order to explain more exactly the behavior of unsaturated soil, computational models have been proposed. Accordingly, a series of factors influencing the behavior of unsaturated soils other than saturated soils should be taken into calculation including the analysis in the microscope scale.

CHAPTER 2: LIQUEFACTION PHENOMENON – LITERATURE REVIEW

II.1. Liquefaction phenomenon

II.1.1. Experience of liquefaction

Soil liquefaction is a phenomenon which has been known for a long period of time and caused a lot of damages over the world. This phenomenon is usually related to saturated incoherent soils due to the increase of pore water pressure resulting in the decrease of effective stress. From the liquefaction specification in Jefferies and Been (2016), it can be seen that the liquefaction can be induced by some reasons: The static loading; earthquake motion, vibration instruments, the vibration caused by wind, ice movement, etc. The following examples of liquefaction disasters give a feel for the subject, circumstances, and consequences of the soil liquefaction during the earthquakes.

A reason that has been attributed to relate to several dam failures, landslides, soil settlements, and other failures in geotechnical structures is static liquefaction. Liquefaction can induce destruction of land and structures according to four main modes: landslide or mudslides, lateral flow, soil oscillation and loss of bearing capacity. A typical example of this is the failure of Fort Peck Dam. This dam was constructed by the hydraulic fill method with four electrically operated dredges assembled at the site. The material is river sands and fine grained alluvial soils. The dam was damaged by a large slide occurring in its upstream shell near the end of construction in 1938 (Figure 2.1a)

The second example is the liquefaction induced by dynamic loading in the earthquake in Niigata in 1964 (Figure 2.1b) which played an important role to raise awareness amongst geotechnical engineers of earthquake-induced liquefactions and its severe consequences. Since then, there have been some more examples of liquefaction induced by earthquakes listed here as San Fernando Valley (1971), Haicheng (1975), Tangshan (1976), Imperial Valley (1979), Armenia (1988), Loma Prieto (1989) and Turkey (1999). Recently, during the earthquake in 2011 in Japan, soil liquefaction occurred and resulted in damages to many houses and buildings. Tamari et al. (2011) showed that, in some areas, the sand boiling, a characteristic of liquefaction, occurred during the main shock first and expanded during the aftershocks; however, in some areas, there was no liquefaction during the main shock but the aftershocks.

Another observation of liquefaction is the post-earthquake liquefaction as being seen in the collapse of Lower San Fernando Dam in 1971 (Figure 2.1c). There were not any failures

during the earthquake; however, the upstream slope of the Dam in California failed about a minute after. It has been explained as a result of pore water pressures generated during the earthquake but no relation to any earthquake-related inertial forces. Furthermore, earthquakes can be followed by a tsunami as the case of Japan earthquake 2011 (Figure 2.1d) which severely damaged the Japanese Fukushima Daiichi power plant.

a) Fort Peck Dam – USA 1938

b) Niigata – Japan 1964

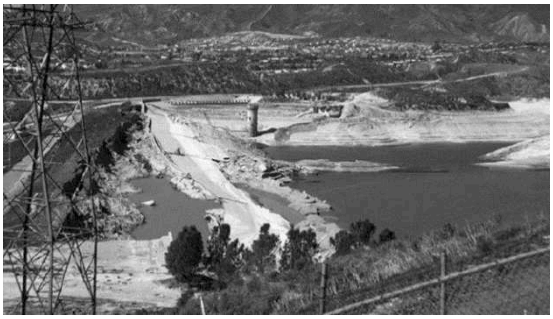

c) Lower San Fernando Dam- USA 1971

d) Japan earthquake 2011

Figure 2.1Examples of liquefaction damages during earthquakes

Besides the mentioned liquefactions above, it is noted that the liquefaction caused by many other reasons as high cycle loading in the case of Molikpaq in Gulf's caisson in Canada in 1985; vibration machines as the case of road embankment in Michigan in 1990.

From the history of this disaster, it can be seen that the liquefaction phenomenon occurs with various causes and in different circumstances. Therefore, the study of this phenomenon is necessary, especially, for countries in the ring of earthquakes. With the case of Vietnam, the country is not located on the seismic belt. However, earthquakes, foreshocks, and aftershocks with a magnitude between 4 and 6 Richter have been recorded recently. In addition to that, due to the heavy annual precipitation, the high water table, and the loose alluvial geology of

the plains, the risks of soil liquefaction should not be neglected. With France, the assessment of facilities at risk of liquefaction was carried out. Especially, as early as 2000, after the aftermath of the exceptional storm in December 1999 and the partial flooding of the Blayais power plant that ensued, ASN (French Nuclear Safety Authority) asked EDF (French Electricity company) to take immediate protective measures against this risk of external flooding and has initiated a process to reassess it for all nuclear power plants. Among the structures to be checked with regard to the seismic risk, are the embankment protection dikes and the risk of liquefaction.

II.1.2. Concept of liquefaction

Soil liquefaction and related ground failures are observed in many cases as revealed in the previous part; however, as it is most usually noted in large earthquakes. Jefferies (2016) stated that there are some definitions of liquefaction; however, none of them satisfy all requirements when applied in particular cases. In general usage, liquefaction refers to the loss of strength in cohesionless soils in both saturated and unsaturated state due to the build-up of pore water pressures during dynamic loading or static loading. In other words, the liquefaction can be described as the definition of Sladen et al. (1985):

"Liquefaction is a phenomenon wherein a mass of soil loses a large percentage of its shear resistance, when subjected to monotonic, cyclic, or shock loading, and flows in a manner resembling a liquid until the shear stresses acting on the mass are as low as the reduced shear resistance."

Accompanying to this definition, there have been some more definitions for the liquefaction phenomenon; however, they still seem to be the subject of a continuing debate within the geotechnical profession. While some researchers have suggested that liquefaction and cyclic mobility should be carefully distinguished (Castro and Poulos 1977), "liquefaction" is commonly used to depict all failure mechanisms resulting from the build-up of pore water pressures during shear loading of soils.

In 1985, the National Research Council's Committee on Earthquake Engineering (NRCCE 1985) gave a broad definition which does not mention the increase in pore water pressure as a requirement for the liquefaction: "All phenomenon giving rise to a loss of shearing resistance or the development of excessive strains as a result of transient or repeated disturbance of saturated cohesionless soils".

Relating the mechanisms of ground failure, Robertson (1994) and Robertson et al. (1994); Robertson and Fear (1996) proposed a fairly complete classification system to define "soil liquefaction". Following this, the liquefaction can be summarized as:

1) Flow liquefaction, used for the undrained flow of a saturated, contractive soil when the static shear stress exceeds the residual strength of the soil. Failure may be triggered by cyclic or monotonic shear loading. This behavior is also called static liquefaction or true liquefaction.

(2) Cyclic softening, used to describe large deformations occurring during cyclic shear due to pore pressure build-up in soils that would tend to dilate in undrained, monotonic shear. Cyclic softening, in which deformations do not continue after cyclic loading ceases, can be further classified as:

• Cyclic liquefaction, which occurs when cyclic shear stresses exceed the initial, static shear stress to produce a stress reversal. A condition of zero effective stress may be achieved during which large deformations may occur.

• Cyclic mobility, in which cyclic loads do not yield a shear stress reversal and a condition of zero effective stress does not develop. Deformations accumulate in each cycle of shear stress.

The stress reversal in this definition is understood as the loss of the shear strength. According to this classification, in cyclic mobility, soil strength does not decrease and condition of zero effective stress is reached only at some moments during the loading process. The zero effective stress does not develop continuously until the failure of the soil but the deformation accumulated in each cycle of shear stress.

The most accepted criterion for liquefaction in laboratory tests is that the sample is liquefied if one of the following conditions appears (Seed and Lee 1966; Ishihara 1993): i) pore water pressure increases to cell pressure leading to the loss of effective confining stress; ii) axial strain in one cycle reaches 5%.

In this study, liquefaction is generally considered as the sudden loss of the soil shear resistance accompanied by the increase of the pore water pressure. It includes three types: static liquefaction, cyclic liquefaction, and cyclic mobility. The two first types relate to the loose soils and the last one relates to the liquefaction of dense soils.

II.1.3. Mechanical behavior of soil

II.1.3.1. Characteristic state

When subjected to shear loading, the soil volumetric behavior has some types as presented in figure 2.2. Contractancy is a characteristic of soil relating to the decrease in volume of the soil when subjected to shearing. The reason for this phenomenon is the densification mechanism of the soil granular stack due to slippage and rolling between grains caused by the applied stress. Conversely, dilatancy is the state when the soil increases its volume due to shearing. This phenomenon can be explained through a mechanism of untangling and expansion of the granular stack (Figure 2.3). Based on these two volumetric behaviors, soil state is clarified into two types: the soils in a loose state corresponding to contract tendency when shearing and the soils in a dense state corresponding to dilatancy or both contractancy and dilatancy appear during the shearing process.

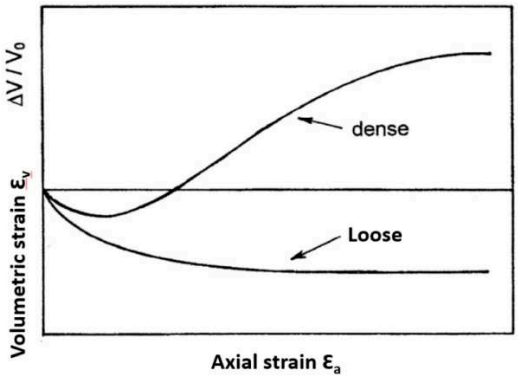

Figure 2.2Dilatant and contractant volumetric tendencies of soils subjected to shear loading.

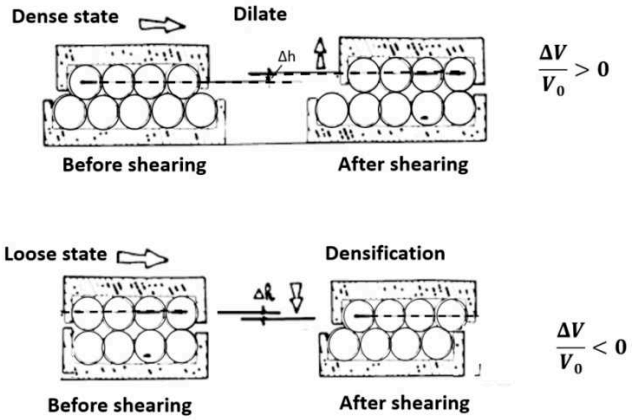

Figure 2.3 Concept of contractancy and dilatancy.

In undrained conditions, on saturated sand, the volume of the sample remains constant. Thus, at the beginning of loading, an increase in pore water pressure is observed, then, for dense sands, the rate of generation of the pore water pressures decreases when the deviator stress increases and vanishes (zero) to become negative. These phases of positive and negative generations of pore water pressures correspond to the phases of contractancy and dilatancy of the material in drained shear. This stress level defines a threshold in the volumetric behavior of a granular soil that Luong (1978) and Habib and Luong (1978) have called Characteristic State (Figure 2.4). It also called phase transformation.

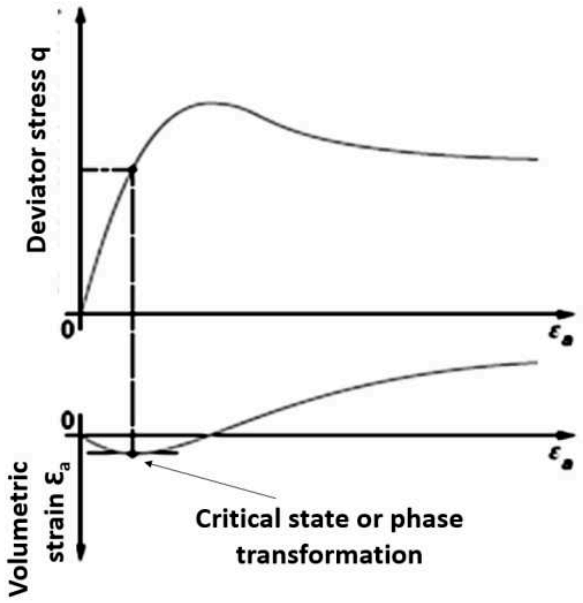

Figure 2.4 Definition of characteristic state

The characteristic state separates two types of rheological behavior of the sand (Figure 2.5): contractancy in the sub-characteristic domain, limited in the plane (p, q) by two characteristics lines, and dilatancy in the upper characteristic domain up to the limit of rupture defined by the rupture limit lines. In the case of loose sands, the characteristic lines are identical with the failure lines and the characteristic state merges with the critical state which is present in part II.1.3.2 of this chapter.

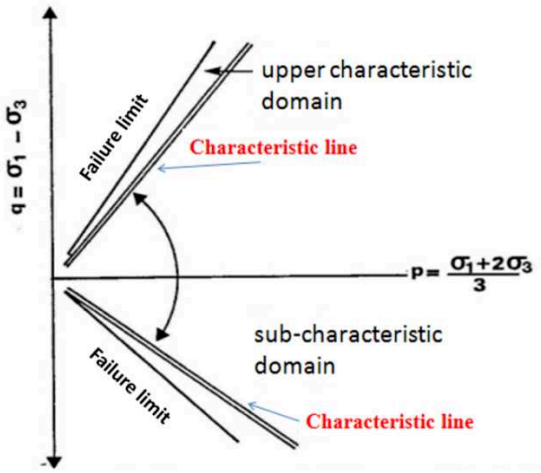

Figure 2.5 Characteristic criterion divides the contracting area of the material

Some authors carried out the triaxial tests on unsaturated soils and the results show that there seems to be no effect of saturation degree on the slope of characteristic lines when it is plotted in plane of effective mean stress versus deviator stress (Figure 2.6).

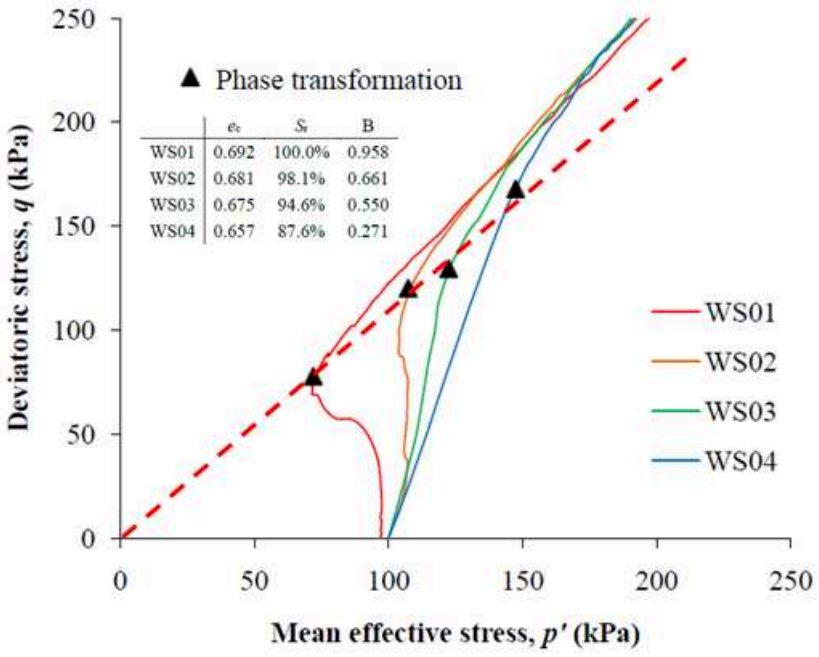

Figure 2.6 Effect of saturation degree on the characteristic line (He 2013)

II.1.3.2. Critical state

Another state observed on the behavior of sandy soil subjected to shear loading is that the volume keeps constant under no change shear stress regardless the increase of strain. This state is usually described as critical state. Following the state of art in Jefferies and Been (2016) the critical state was defined by Roscoe et al. (1958) and formalized by Poulus (1981) as: 'the steady state of deformation for any mass of particles is that state in which the mass is continuously deforming at constant volume, constant normal effective stress, constant shear stress, and constant velocity'. The definition and roll of critical state to the behavior soil in both drained condition (line AB) and undrained condition (line AC) can be seen through the figure 2.7 below.

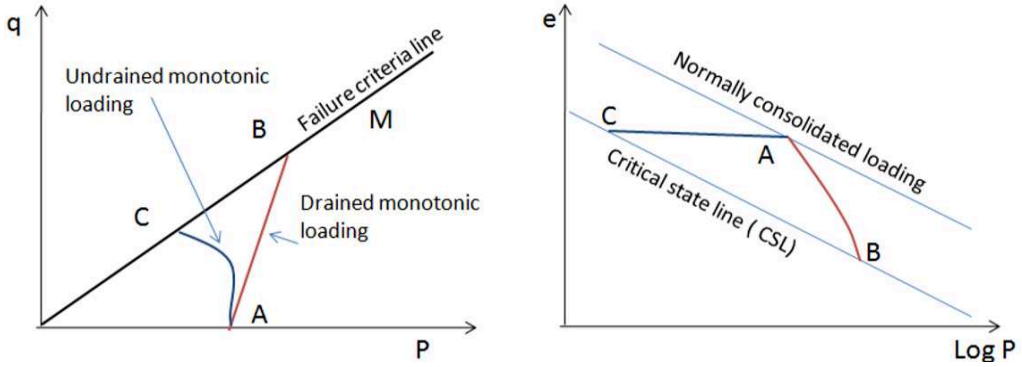

Figure 2.7 The definition of critical state

II.1.4. Static liquefaction phenomenon

II.1.4.1. Demonstration of the phenomenon in the laboratory: introduction by the concept of the flow structure

The dramatic rupture of Fort Peck Dam in 1938 in Montana while being under construction leaded to some knowledge of liquefaction. The observers showed that the flow took place over a period of 3 minutes, during which the upstream part of the dam moved 400 meters, corresponding to huge mass of transported sand. The inducement of this structure can be explained as Casagrande in the concept of flow structure. When the sand flows, each grain is rotated relative to its neighbors, so that all of the grains then offer minimal friction resistance.

The following assumptions are used in this concept of flow structure:

- It spreads within the material by chain reactions;

- It only exists during the flow

- When the flow stops, the grains re-arrange and find a static structure which, once the water has been drained, will be slightly denser than the initial structure.

The proposal of Casagrande was verified by the laboratory results of Castro (Castro 1969). Series of undrained monotonic triaxial tests on sand samples undergoing different stress-strain histories were carried out. These tests allowed highlighting the flow structure and also make it possible to identify parameters that have an influence on the development of this flow structure within the granular material. The results of tests leaded him to highlight the existence of a particular structure, developing within the granular material when the latter is subjected to shear stress in undrained conditions. The characteristics of this flow structure include a very low level of residual shear stress, the development of significant deformations. This flow structure, which does not depend on the initial conditions and is observable in large deformations, has also been observed by Verdugo and Ishihara (Verdugo and Ishihara 1996).

II.1.4.2. Different types of behavior of sand subjected to an undrained monotonic shear

There are three types of volumetric behavior observed when shearing the soils. These behaviors affect the resistance strength, stress-strain curve, and other factors of soil.

- The dilating tendency behavior: this tendency is observed on the dense sand sample. When subjected to shear load, there is a very short phase of contracting, after that, the soil dilates resulting in the increase of void ratio. If the test is in undrained condition, this stage corresponds to the decrease of pore water pressure and there is no static liquefaction observed.
- The contracting tendency behavior: The volume of sand tends to decrease when subjected to monotonic loading. This type of behavior is observed in the sands in loose state. The contracting tendency results in the decrease of sample volume in drained condition tests or increase of pore water pressure in un-drained condition tests. Due to this increase of pore water pressure, the effective stress goes down and the sample can be fallen in a very low resistance state. The sudden loss of shear resistance strength and the rapid development of large deformations exhibit the characteristics of failure by liquefaction in nature

- The constant volume tendency behavior: The volume of the sample does not change when subjected to monotonic shear loading. During this stage, it can be seen a stability in sample volume in drained tests or pore water pressure in undrained tests.

The appearance of these three states above is strongly dependent on the sand's relative density (D_r), effective confining stress, stress history, mode of deposition, and several other factors (Figure 2.8). In this figure, P_a is the atmospheric pressure, σ_3' is the effective confining stress used to consolidate the sample before shearing. $\sigma_1'$is the effective deviator stress.

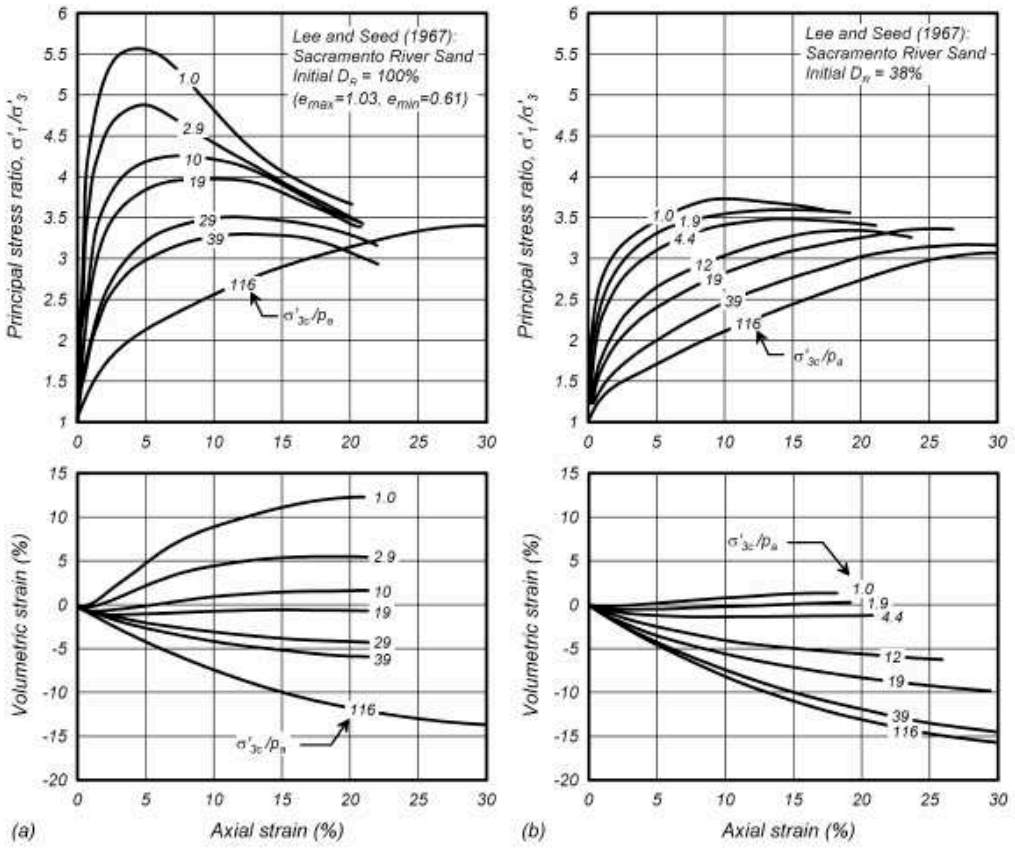

Figure 2.8 Monotonic loading response of dense (D_r = 100%) and the loose (D_r = 38%) speciments of sacramento River sand in drainded triaxial compression tests, as shown in graphs (a) and (b) respectively (Lee and Seed 1967 in Idriss and Boulanger 2008)

During sample shear loading, it can be observed one or all volumetric behaviors during the development of axial strain. From the literature review, He (2013) exhibited five patterns of undrained responses that are usually observed in laboratory testing of sand by triaxial compression apparatus. Figure 2.9 shows the dilative behavior corresponding to the sample having high relative density. Figure (a) depicts the behavior of a very dense sample. The mean

effective stress increases to the critical state (CS). In figure (b), firstly the mean effective stress shows a decreasing tendency; however, then the stress path reverses to an increasing trend in p' along with critical state line, giving a turning point on the stress-strain curve. This point corresponding to the characteristic state (Luong 1978) mentioned in part II.1.3.1 of this manuscript. This turning point is also defined as the phase transformation (PT) point by Ishihara et al. (1975).

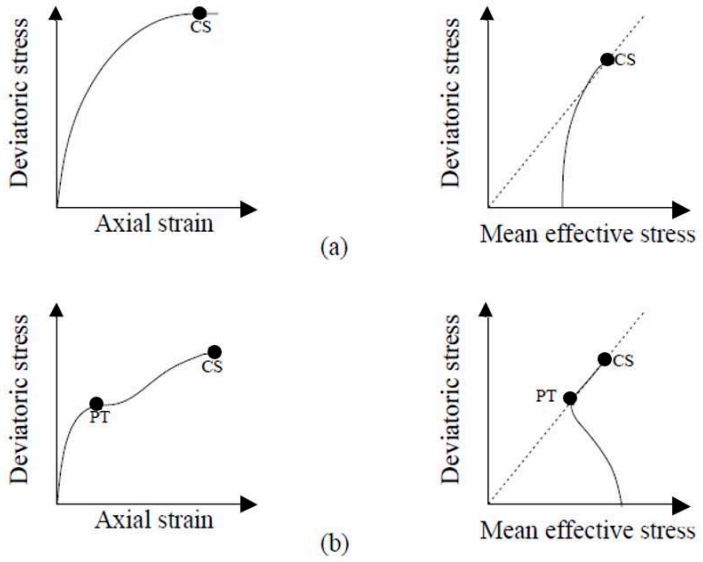

Figure 2.9 Typical behaviors of dense sand under undrained triaxial compression tests.

Figure 2.10 shows the behavior of sample with medium relative density. In this figure, the deviator stress undergoes a short contractive stage after peak deviator stress and then turning again to show a dilative manner. Alarcon-Guzman et al. (1988) defined the lowest turning point as the quasi-steady state (QSS).

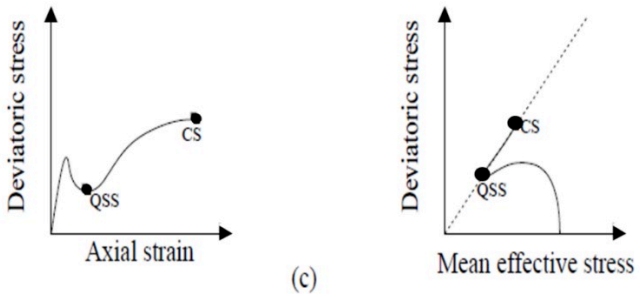

Figure 2.10 Typical behavior of medium sand under undrained triaxial compression tests.

The behavior of loose sand is presented in figure 2.11. There is an appearance of the contractive behavior before the final critical state. In figure a, the deviator stress decreases but not equals to zero in the end. Figure (b) displays the behavior of the lowest relative density samples. The deviator stress first increases a little and then decreases to zero, indicating a complete liquefaction condition. It is necessary to mention that: (1) although critical states are exhibited on all five figures, in real triaxial undrained tests, the critical state may not be observed because of the development of non-homogeneous deformation, such as shear band for relatively dense sand and necking in extension tests; (2) Normal triaxial tests should proceed to an axial strain of 20%, but this strain level may not be enough to bring the sand to a critical state.

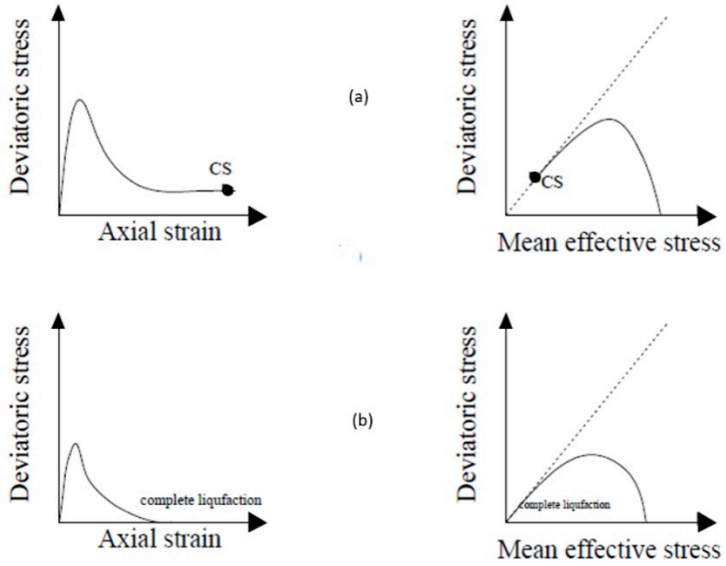

Figure 2.11 Typical behaviors of loose sand under undrained triaxial compression tests.

II.1.5. Cyclic liquefaction and cyclic mobility phenomenon

As mentioned in part I.2, in this study, two concepts cyclic liquefaction and cyclic mobility are used to describe the behavior of sand due to the pore water pressure increase during undrained cyclic loading.

II.1.5.1. Drained behavior under cyclic loading.

The reversals of shear stress in drained cyclic loading can cause the compaction of sand over a wide range of relative densities. This is why vibration is effective in compacting dry sand samples to have a high relative density.

Figure 2.12 shows the progressive densification of a sand specimen subjected to strain-controlled, drained, and cyclic loading carried out by Youd (1972). The specimen underwent alternating cycles of contraction and dilation, with an accumulation of contractive strains. It can be seen that the initial shear loading made the specimen contract from point A to point B, after that, further shear loading caused increasing dilation from point B to point C. From point C to point D the void ratio decreases due to the increase of shear stress. After passing point D, the void ratio increases again and peak at point E. This repetition continues with the decreasing void ratio change after each cycle.

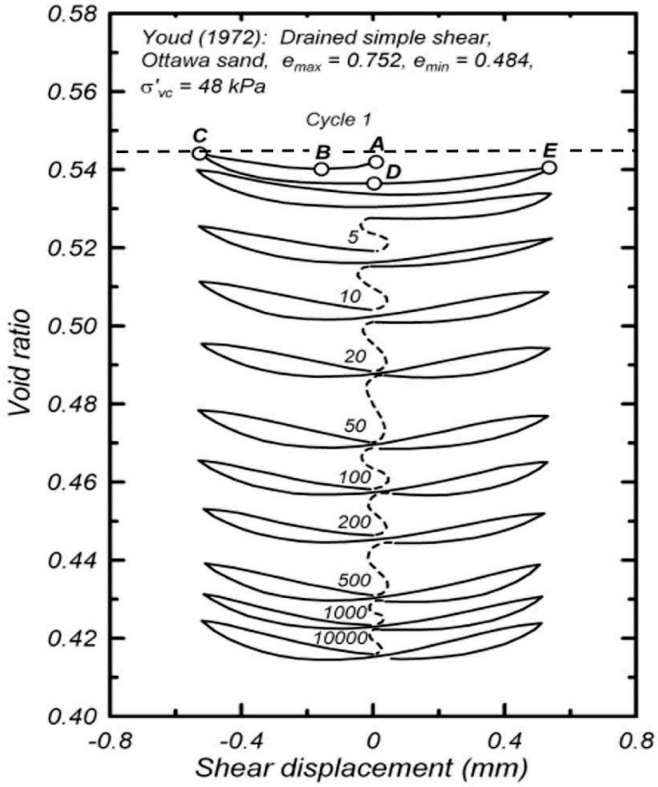

Figure 2.12Void ratio versus cyclic shear displacement, showing the densification of a sand specimen with successive cycles of drained simple shear loading (Youd 1972).

II.1.5.2. Liquefaction under undrained cyclic loading

In 1996, Verdugo and Ishihara (Verdugo and Ishihara 1996) described the difference between liquefaction and cyclic mobility although this dissimilarity had been recognized much sooner. Cyclic liquefaction is, on the one hand, characterized by a rapid increase in pore water pressure followed by a sudden loss of resistance to a residual value. On the other hand, cyclic mobility corresponds to an undrained cyclic response during which the soil does not undergo

a loss of resistance but observes a softening behavior and accumulated axial strain which are mainly due to the increase in pore water pressure under cyclic loading.

II.1.5.3. Case of cyclic mobility

In undrained cyclic loading tests of saturated specimens, the sand matrix or skeleton cannot contract under the cyclic loads; however, the tendency of contraction or dilation results in the change of pore water pressure. Cyclic mobility corresponds to the characteristic response of sands which are in a moderately dense to a very dense state under a cyclic load. It is characterized by the accumulation of significant deformations and not by a significant loss of shear strength unlike liquefaction (Benahmed 2001). Canou and his colleagues have worked a lot on the definition and characterization of cyclic mobility, in order to distinguish it from true liquefaction. Canou et al. (2000) describe in detail the characteristics of cyclic mobility as below.

From the cyclic behavior of RF Hostun sand described in figure 2.13, it can be seen that the typical cyclic mobility includes two phases:

The first phase is characterized by:

- An almost zero axial deformation, without accumulation, indicating an apparent stabilization of the material. The evolution of the axial deformation as a function of the number of cycles is shown in figure 2.13c

- At the same time, Figure 2.13b presents the continuous evolution of the pore water pressure as a function of the number of cycles. In this period, there is only one peak for each cycle.

- Finally, the stress path presented in figure 2.13a shows the apparently stable behavior over the first 40 cycles.

The second different phase prolongs in the last 20 cycles and characterized by:

- The modification of the mechanism for generating excessive pore water pressure, with a “two peak” regime per cycle;

- The rapid accumulation of deformation with large amplitudes due to the increase of pore water pressure and the decrease of effective stress.

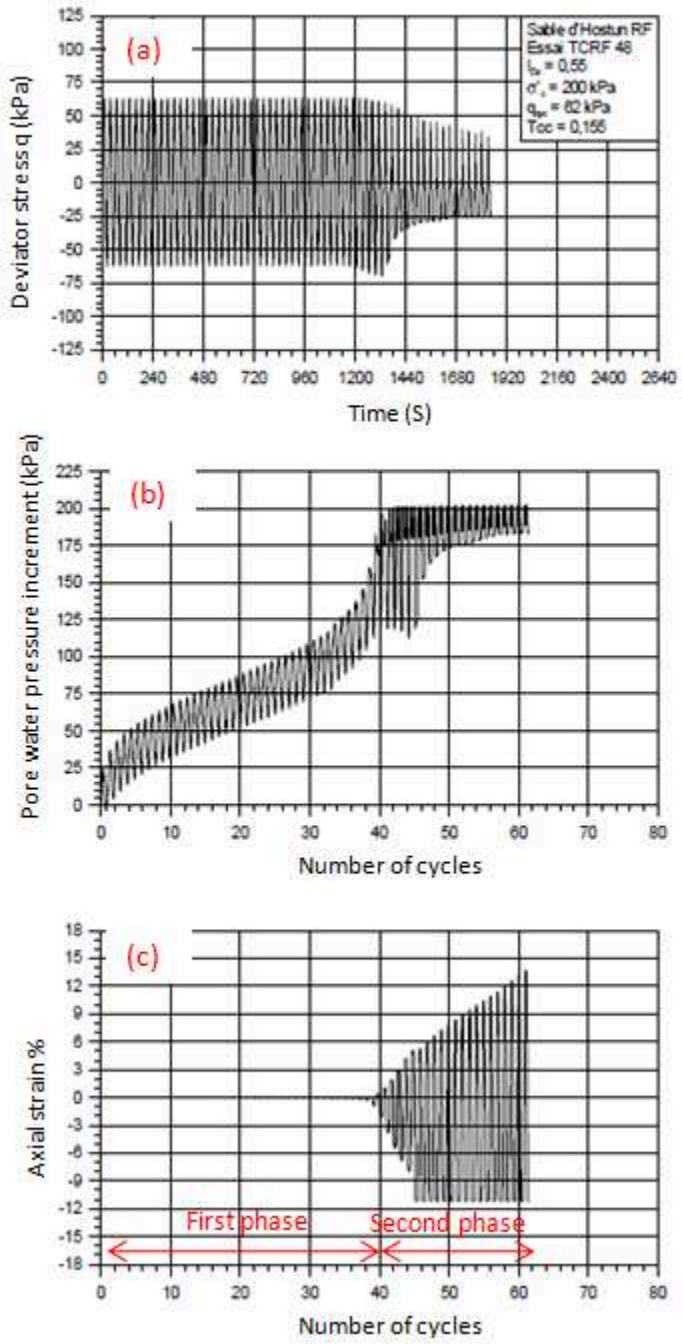

Figure 2.13 Cyclic mobility of RF Hostun sand (Benahmed 2001)

When studying more closely the change in pore water pressure in the second stage, it can be seen that for each cycle, when the axial strain varies from zero to its upper amplitude values, there are two peaks appearing in the plane of pore water pressure increment versus the number of cycles. This characteristic is shown clearly in figure 2.14 below. The two-peak behavior appears after the cycle 40th. This behavior is only observed when the pore water

pressure passes corresponding to the first time the tress path passes the characteristic lines in q-p' plane.

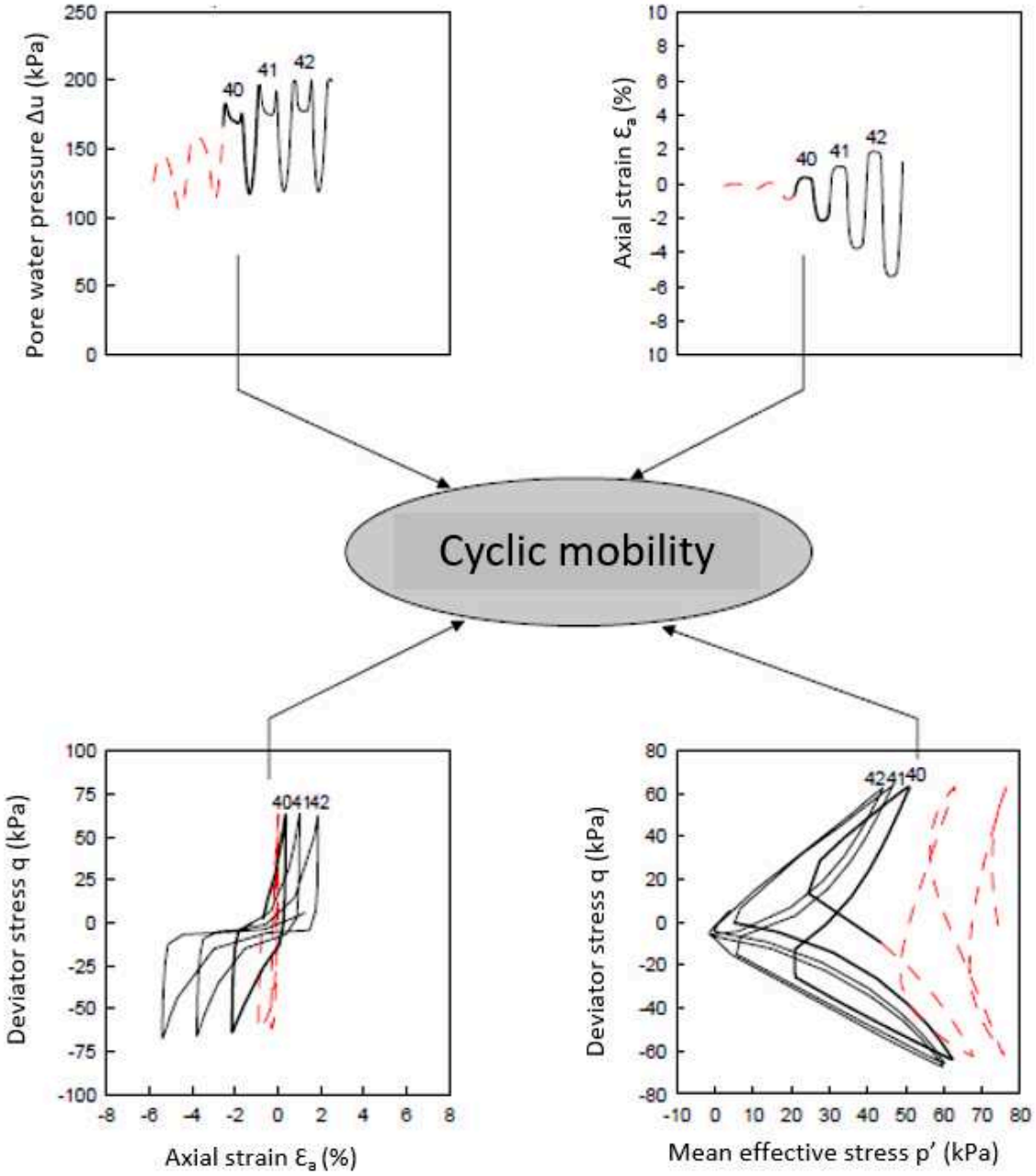

Figure 2.14 Initiation of the cyclic mobility of dense Hostun RF sand (Benahmed 2001)

When the second stage appears, the material shows significant dilatantcy and contractancy behavior under loading in each cycle. These phases of strong contracting lead to the inducing of strong pore water pressure increment and a rapid movement of the stress path towards the failure lines. The triggering of instability corresponds to the moment when the stress path touches the characteristic threshold for the first time. The accumulation of large deformations

is mainly done when the stress value passes zero. This mechanism of accumulation of deformations relating to a state of zero stress is also reported by Vaid and Sivathayalan (Vaid and Sivathayalan 2000). The state that the stress path first reaches the state of zero stressesis called the initial liquefaction (Seed 1979; Vaid and Sivathayalan 2000). During the next loading cycles, the alternation of dilatant and contract behaviors causes stress fluctuating around the zero-stress state. This is one of the most characteristic features of cyclic mobility. The material resistance falls to zero temporarily at some points; however, the axial strain develops very rapidly leading to the collapse of soil (Figure 2.15).

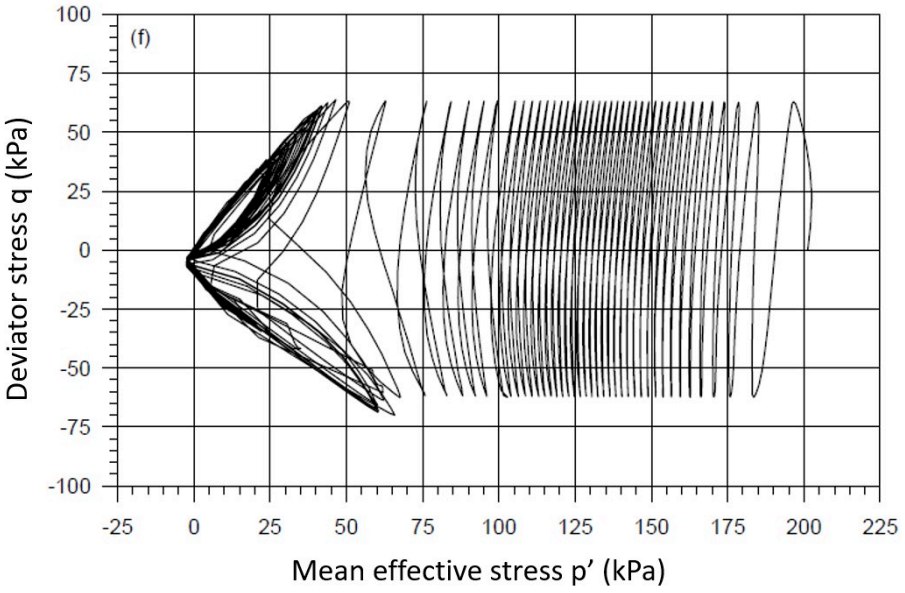

Figure 2.15 Deviator stress versus mean effective stress in cyclic mobility phenomenon (Canou et al. 2000)

II.1.5.4. Case of cyclic liquefaction

The phenomenon of cyclic liquefaction was demonstrated in the laboratory for the first time by Castro (1969) (Cited by Benahmed 2001). In which, the results of undrained cyclic tests for which the liquefaction phenomenon developed in a manner similar to that observed under undrained monotonic loading was presented. One of these results is clearly illustrated in Figure 2.16. On the curve of the deviator stress as a function of the axial deformation, during cycle 11, there is a sudden fall in the shear strength with the very sharp development of large deformations (25% in 0.3 s). At the end of the test, the residual strength levels off at a very low value. This cycle is called critical cycles. After that, the pore water pressure increases rapidly until approaching the value of the consolidation stress. The path of effective stresses

in the plane (q, p') moves to the left. The contracting characteristics of the loose sand shown during the critical cycle behavior are similar to the phenomenon of static liquefaction.

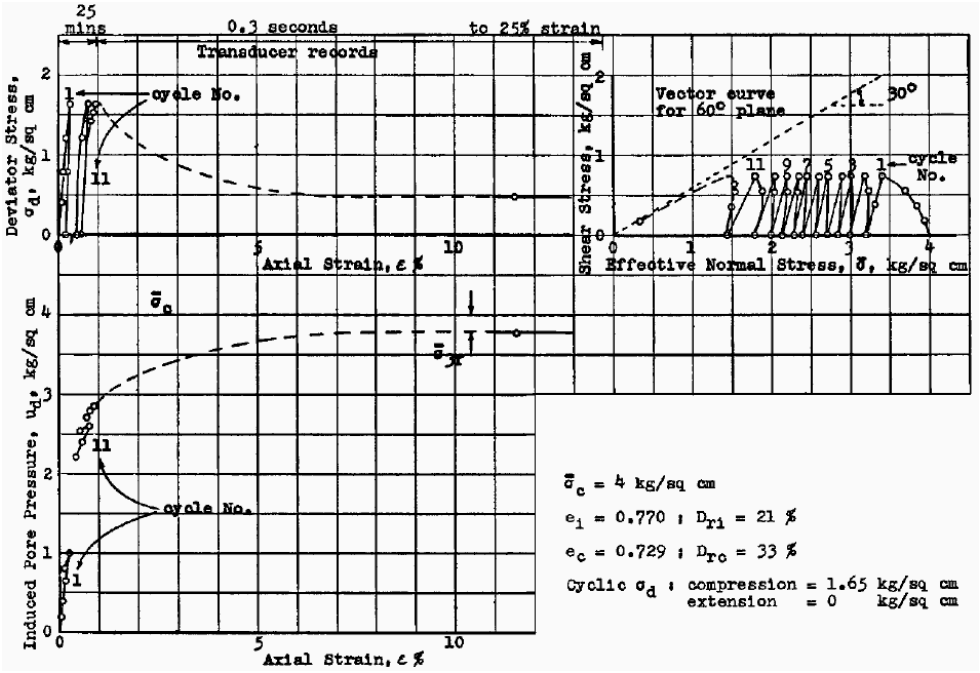

Figure 2.16 Cyclic liquefaction behavior of soil (Castro 1969)

According to Vaid and Chern (1985), Vaid et al. (1989) and Hyodo et al. (1994), the following conditions are necessary for liquefaction to take place during cyclic loading:

- The sand must be contracting during the monotonic loading.
- The maximum value of the cyclic amplitude shear loading ($\tau_{cy} + \tau_s$) must be greater than the residual value (Figure 2.17).
- The number of cycles applied must be sufficient so that the path of the effective stresses migrates towards the failure line and reaches it.

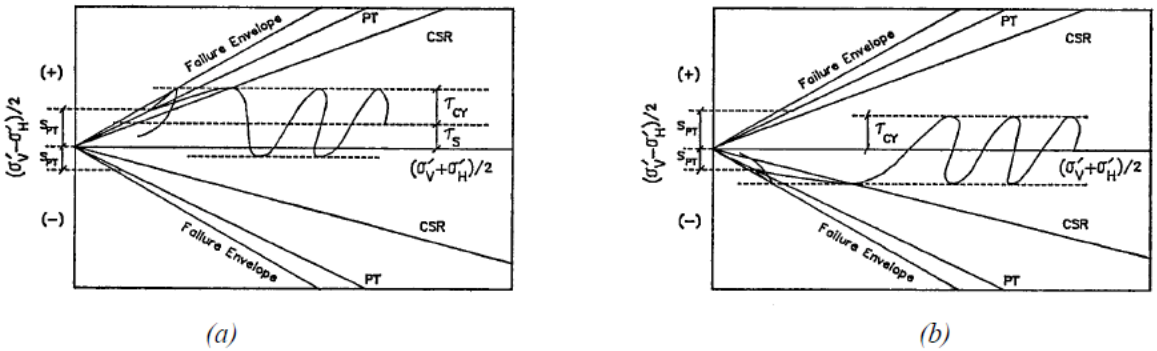

Figure 2.17 Initiation of cyclic liquefaction (Vaid et al. 1989).

a) In compression; b) In extension

Figures 2.18 presents the behavior of Hostun sand carried out by Benahmed 2001. This figure shows clearly the comparison of the responses observed under non-alternating monotonic loading and cyclic loading, in the planes ($q - \varepsilon_a$), ($\Delta u - \varepsilon_a$), and (q - p'). The tests were carried out with identical initial conditions for two different cyclic amplitudes (45 kPa and 100 kPa). There is similarity in the soil behavior at liquefaction state although the liquefaction is triggered by different loading types, the curve in the monotonic experiment seems to be the contour in the cyclic test.

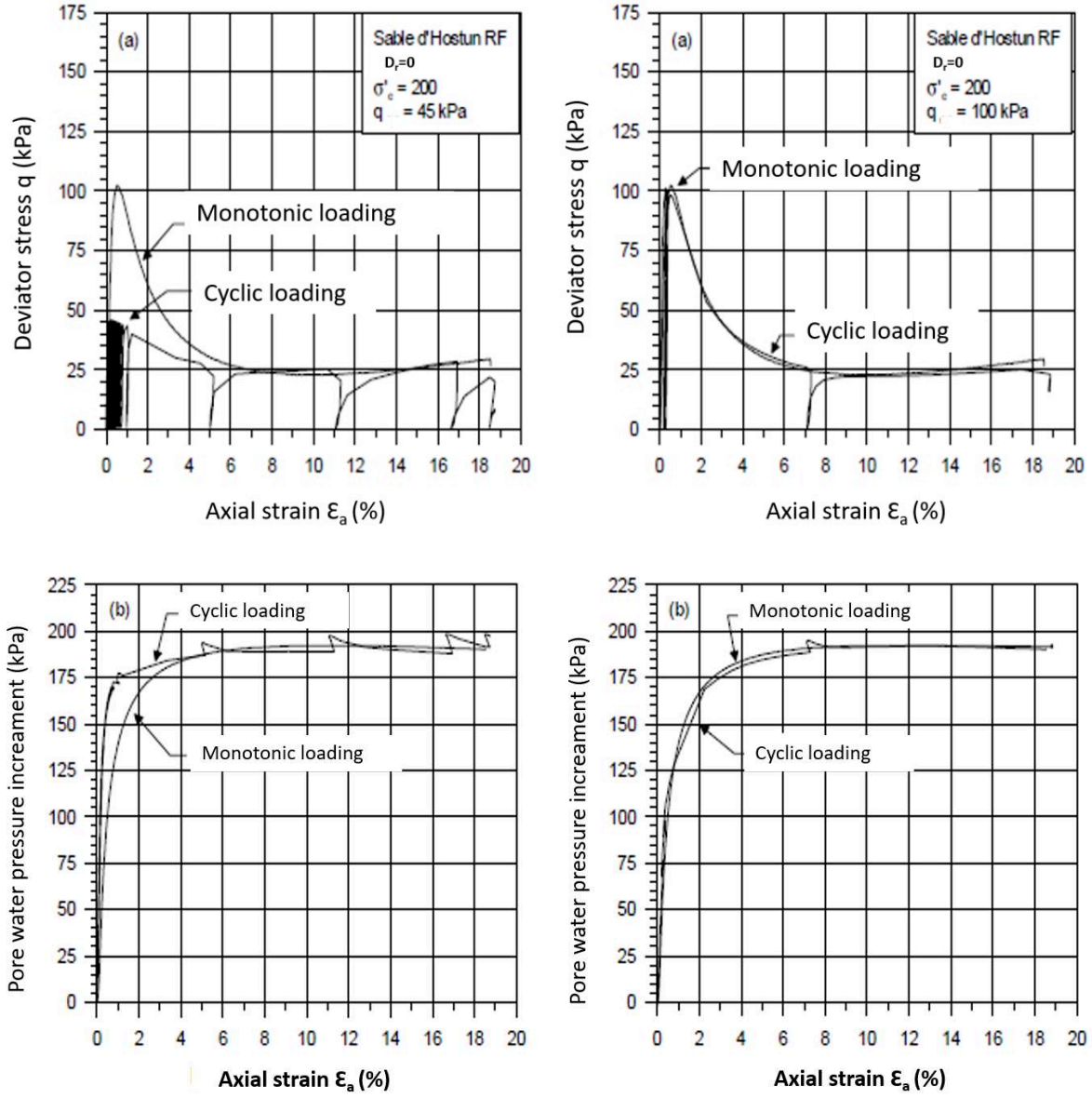

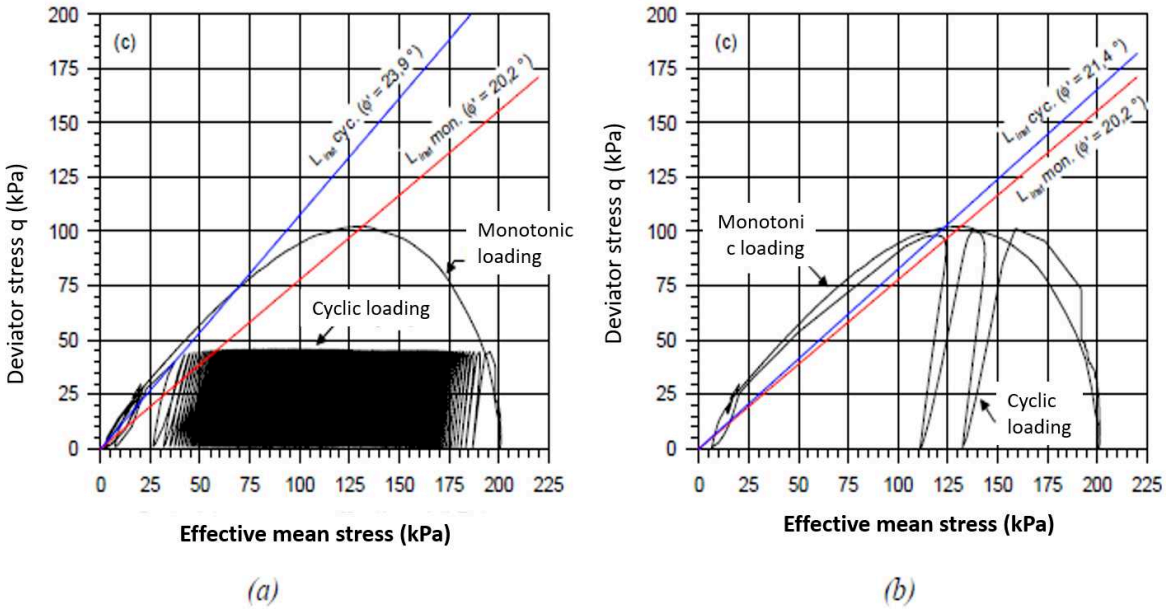

Figure 2.18 Comparison between monotonic and cyclic behavior for the same initial conditions and different cyclic amplitudes for Hostun sand (contracting case); $\sigma_c' = 200$ kPa (a) q_{cyc} = 45 kPa; (b) q_{cyc} = 100 kPa. (Benahmed 2001)

II.1.6. Factors influencing the liquefaction of soil under cyclic loading

II.1.6.1. Influence of relative density

The relative density is considered as the most affecting factor in the cyclic behavior of sands subjected to cyclic loading. It is because of its effect on the nature of the cyclic response (liquefaction or cyclic mobility) and the value of the shear strength. Some authors have shown that the increasing density decreases the liquefaction potential (Lee and Seed 1967, Seed and Idriss 1971, Seed 1979). In other words, the shear stresses to cause failure by one or the other of the two phenomenons increases with the increase of the relative density (Figure 2.19). The same findings have been reported in other works (Ishihara et al. 1975; Castro and Poulos 1977; Vaid et al. 1985).

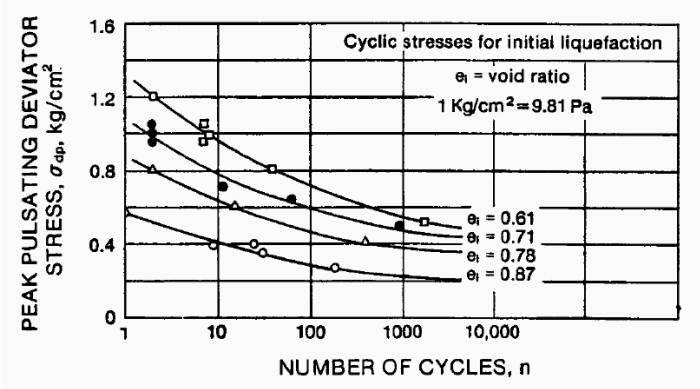

Figure 2.19 Influence of the void index on the cyclic shear strength (Lee and Seed, 1967).

For the sand Hostun, the effect of initial density on the number of cycles is demonstrated in figure 2.20. In the study of Benahmed (Benahmed 2001), the tests were carried out on the loose samples with relative density varying from zero to 0.2 and cyclic stress ratio CSR of 0.05 and 0.062. Effective confining stress was maintained at 200 kPa. From this figure it can be seen that for a given value of cyclic stress ratio, the number of cycles with liquefaction increases very quickly with the increase in relative density, and this increase is more obvious when the cyclic shear ratio is low.

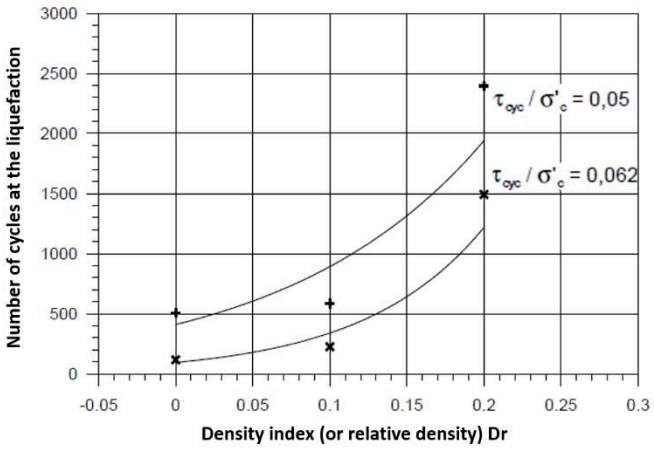

Figure 2.20Influence of the density index on the number of cycles triggering cyclic liquefaction of Hostun RF sand (Benahmed 2001).

II.1.6.2. Influence of initial static shear stress.

Generally, the soil is often subjected to initial static shear stress due to the load caused by the mass of constructions and facilities above the ground or the self-load of the soil layers.

Therefore, its behavior under cyclic stress could be affected by the presence of this initial stress. It is therefore very important to know whether the existence of the initial static shear stress has an advantage or a disadvantage to stability of soils.

Lee and Seed (1967) and Seed (1979) showed that the resistance to liquefaction increases with the value of the initial stress deflector (K_c). However, Yoshimi and Oh-oka (1975) presented opposite results indicating that the presence of an initial deflector has a bad effect on the shear strength. This last observation was also found by Vaid and Finn (1979), Mohkam (1983) and Hyodo et al. (1994).

In a very detailed study on the influence of the presence of the initial static stress, Vaid and Finn (1979) and Vaid and Chern (1985) found that the resistance to cyclic loading could increase, decrease or remain unchanged as a function of the relative density, of the value of K_c and of the failure criterion retained (level of deformations allowed) (Figure 2.21).

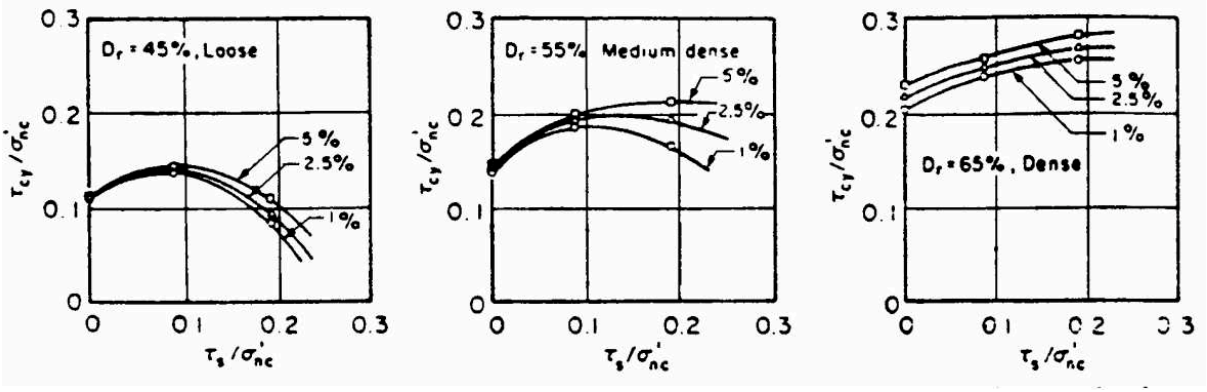

Figure 2.21Effect of initial static stress on the cyclic stress ratio causing several levels of deformation in ten cycles (Vaid and Chern, 1983).

II.1.6.3. Influence of the over consolidation

The over-consolidation increases the cyclic shear resistance of the soil. At the same density, over-consolidated sand has a higher liquefaction resistance than that of normally consolidated sand (Seed and Peacock 1971; Tokimatsu et al. 1986). The effect of over consolidation on the number of cycles causing the peak cyclic pore pressure ratio of 100% and the axial strain of 5% (the two conditions for liquefaction) are presented in figure 2.22

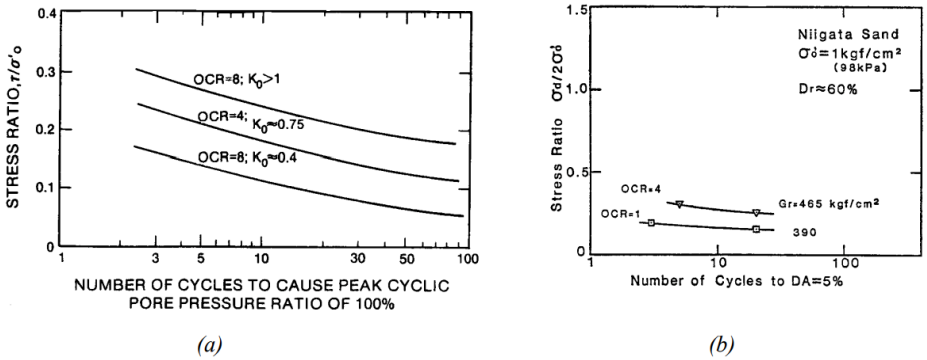

(a) (b)

Figure 2.22 Effect of over consolidation on the characteristics of liquefaction (a) Seed and Peacock 1971), (b) Tokimatsu et al. 1986.

II.1.6.4. Influence of the stress history

Some studies have pointed out that the stress history affects significantly to the liquefaction susceptibility of soil. Finn et al (1970) show that when a sample of sand is subjected to a small shear deformation before applying cyclic loading, its resistance to liquefaction increases. However, if this pre-deformation is significant, its resistance reduces. These results have been confirmed by the work of Ishihara and Okada (1978) and Vaid et al. (1979).

The difference in soil cyclic resistance is shown in figure 2.23. Two samples were subjected to cyclic loading. One had not been undergone preloading and the other had been subjected to small deformations simulating weak seismic vibrations (Seed et al. 1977). Although no significant densification was noted on the preloaded sample, it presents resistance to liquefaction 1.5 times greater than that of sand without preloading (Figure 2.23a).

The effect of stress history on the cyclic resistance of sand was analyzed clearly by Tokimatsu and Hosaka (1986). The tests with pre-deformations of 0.3; 0.5; 1; 2 and 3% were carried out to simulate the history of shear stresses during sampling operations. The results obtained were compared to the sample which had not undergone any stress history (Figure 2.23b). It is noted that the resistance of the preloaded samples decreases with the growth of the axial deformation of preloading. Samples subjected to 2 and 3% axial deformation have only 20 to 30% of the shear strength of the non-pre -sheared sample.

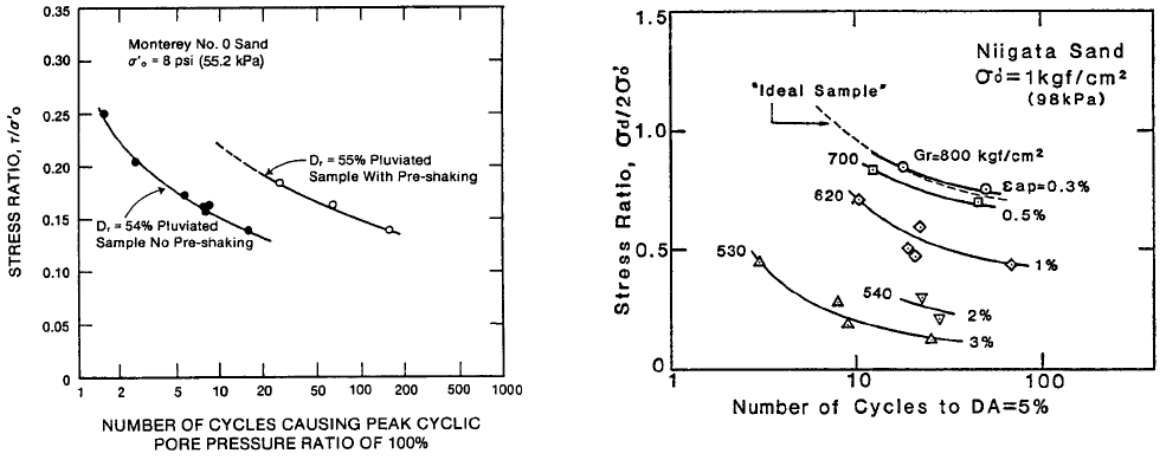

(a) (b)

Figure 2.23 Effect of the history of shear stresses on liquefaction characteristics. (a) Seed et al. (1977), (b) Tokimatsu and Hosaka (1986).

II.1.6.5. Influence of sample reconstitution method

The sample reconstitution method affects the granular structure of the samples. Figure 2.24 show the different granular structure of the samples made from RF Hostun sand and prepared by different methods.

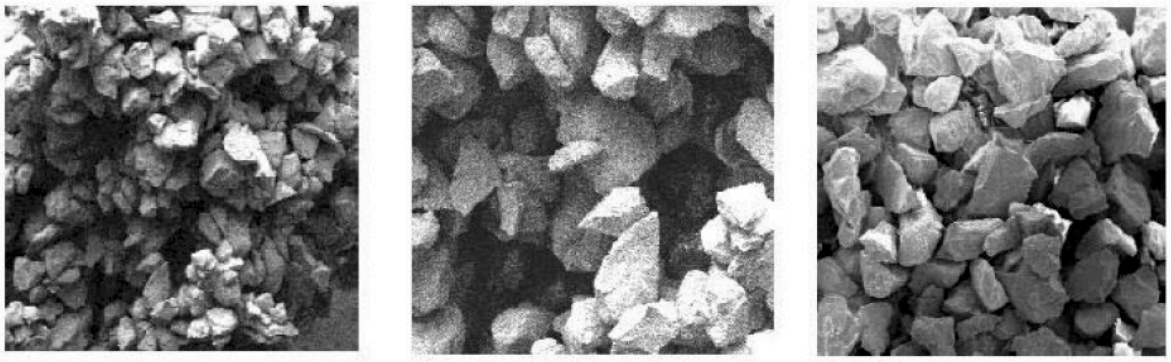

(a) (b) (c)

Figure 2.24 The microscopic image of the sample prepared by different methods to highlight the different granular structures (a) by wet tamping method (b) water sedimentation (c) dry deposition (Benahmed et al. 2007)

Studies by Ladd (1977), Mulilis et al. (1977) and Miura and Toki (1994), Tatsuoka et al. (1986) indicated that the sample reconstitution method has a significant influence on the characteristics of the cyclic loading behavior of sand. A series of cyclic triaxial stress-controlled tests were carried out by Mulilis et al. (1977) on Montery sand samples manufactured at the same density index but with different preparation methods. The results is shown in Figure 2.25 These results show that the cyclic shear strength varies from one deposition mode to another and that the densification (compaction) method also has an effect. However, Mulilis et al. (1977) indicated that this variation was not the same for all types of soil. Yamashita and Toki (1993) confirmed these results on the sand of Toyoura, the sand of Tohbetsu and the sand of Soma by using three different manufacturing methods named: multiple sieving pluviation (MSP), vibration method (VIB), and centrifugal force method (CE).

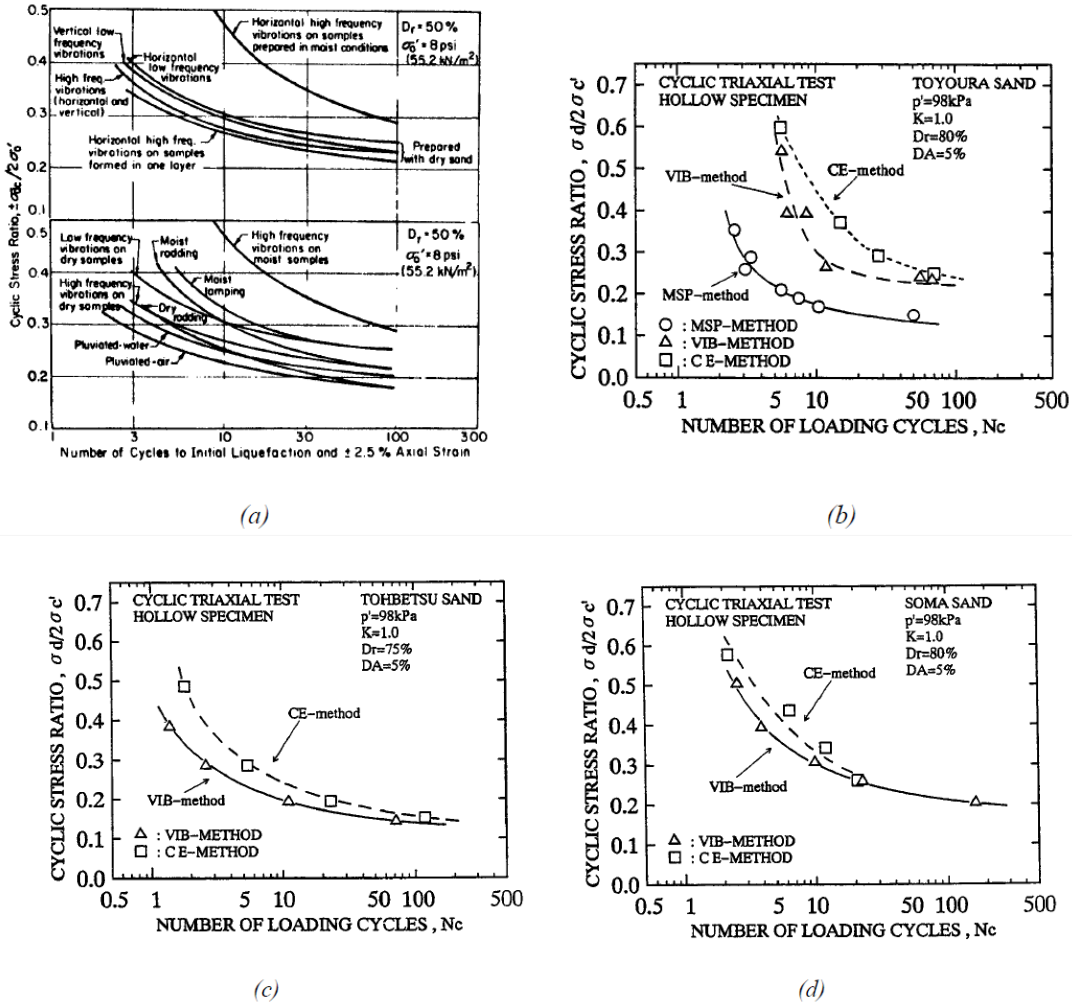

Figure 2.25 Influence of the deposition method using several manufacturing methods. (a) Mulilis et al. 1977; (b), (c) and (d) Yamashita and Toki 1993.

II.1.6.6. Influence of the fines content

The fines content plays an important role in the behavior of sands. However, their effect on resistance to liquefaction remains linked to their plasticity index and raises many differences of opinion (Erten and Maher 1995; Singh 1996).

II.1.6.7. Influence of the failure criterion

Figure 2.26 shows the influence of failure criteria to the liquefaction resistance evaluation of the soil. The criterion for liquefaction is usually taken equal to 5% of axial strain. However, it can be changed in some special cases. This influences less significantly for loose sands where rupture occurs by the flow and the liquefaction is initiated suddenly and large deformations develop suddenly and quickly. Nevertheless, in the case of dense sands, the relationship between the magnitude of the cyclic stress and the number of cycles leading to failure varies according to the failure criterion adopted (Lee and Seed 1967; Vaid and Chern 1985; Ishihara 1985; Toki et al. 1986).

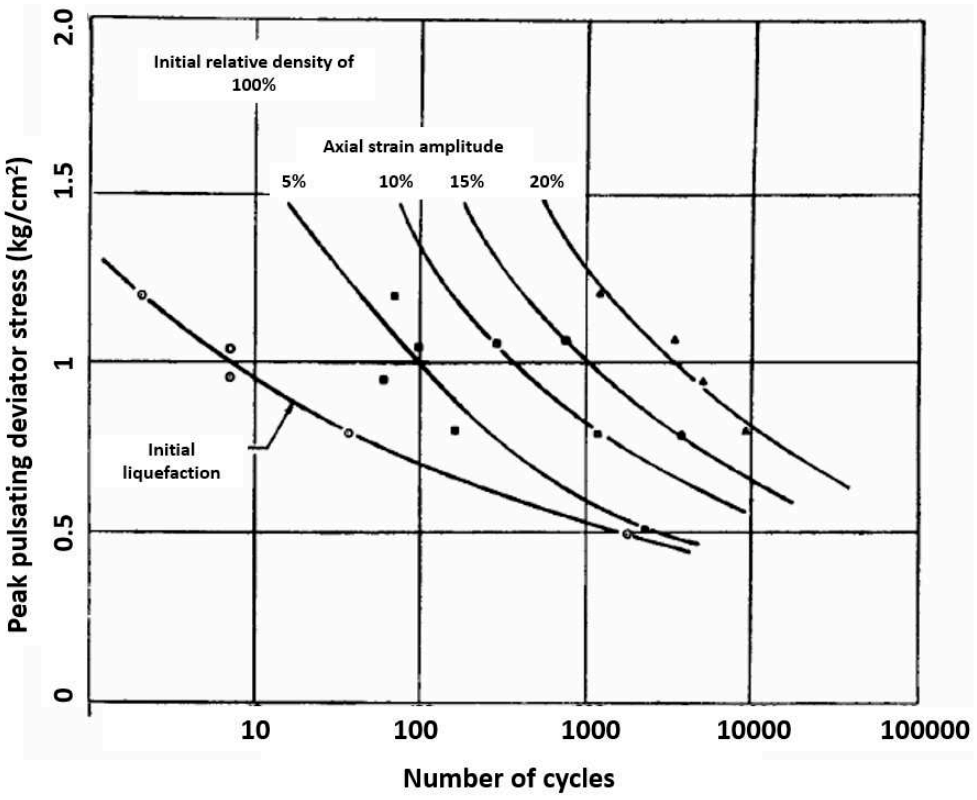

Figure 2.26 Influence of the failure criterion on the stress conditions inducing the failure (Lee and Seed 1967).

II.1.6.8. Influence of the certain experimental parameters

Factors like load frequency, membrane penetration, sample dimensions, the duration of sample consolidation were studied in a program launched by five laboratories in Japan. The results were that the effect of load frequency could be negligible while there was a light effect of the sample dimensions and membrane penetration (Tatsuoka et al. 1986). These influences are shown in figure 2.27 below.

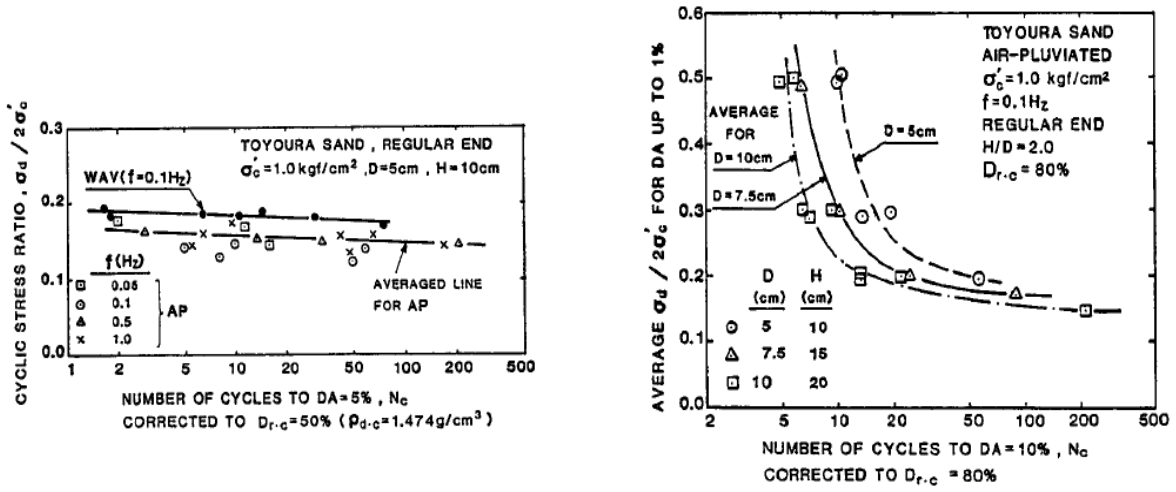

(a) (b)

Figure 2.27 Influence of certain experimental parameters on cyclic resistance (Tatsuoka et al. 1986)

(a) influence of the loading frequency; (b) influence of the diameter (D) and height (H)of the samples.

II.1.6.9. Influence of saturation degree

Resistance to liquefaction is affected significantly by the saturation degree of the soil. Martin et al. (1978) had theoretically shown that a reduction in the degree of saturation from 1 to 0.98 squarely doubles the value of the stress ratio leading to liquefaction for a given number of cycles (Figure 2.28a). These theoretical results have been experimentally confirmed by Xia and Hu (1991) (Figure 2.28b). The effect of saturation degree is mentioned more clearly in part II.2 of this chapter.

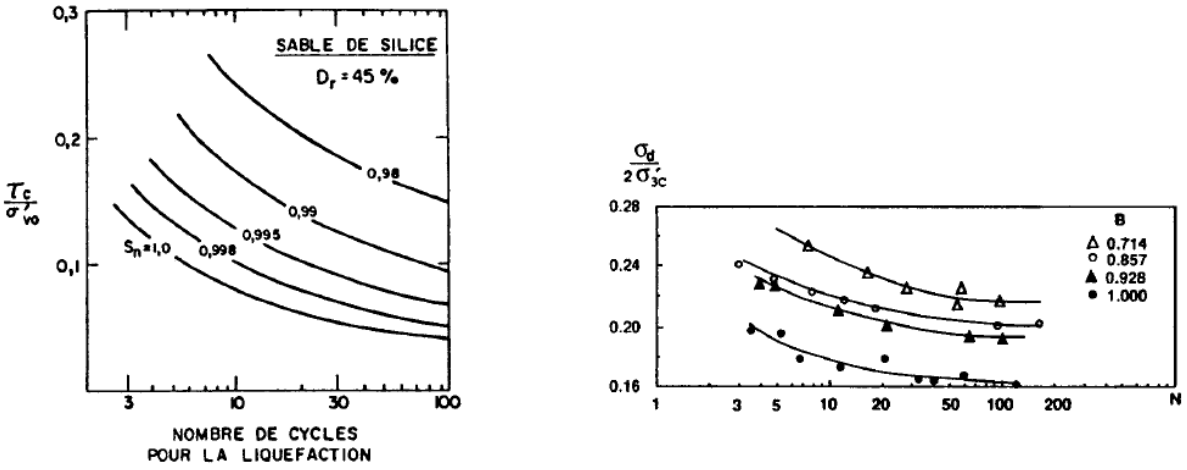

Figure 2.28 Influence of saturation degree on the cyclic shear strength. (a) Martin et al. (1978); (b) Xia and Hu (1991) (B: Skempton's coefficient).

II.1.7. Liquefaction assessment

II.1.7.1. Liquefaction assessment procedures overview

Seed and Idriss (1971) proposed a methodology called "simplified procedure" to assess the earthquake-induced liquefaction resistance of soils. Since then, this methodology has become a standard and a large volume of literatures has been added to this system.

The essential point of liquefaction assessment is the comparison of cyclic strength and mobilized shear stress, which is presented in the equation 2.1:

$$FS_l = \frac{CRR}{CSR} \qquad \text{(Eq. 2.1)}$$

where CRR (cyclic resistance ratio) is defined as the ratio between cyclic resistance and the vertical effective stress. CSR (cyclic stress ratio) is defined as the mobilized shear stress over the vertical effective stress. In general, the soil is out of liquefaction potential if the factor of safety FS_l higher than unit and the soil is susceptible to liquefy if the factor of safety smaller than unit. However, it also suggests that the analysis to determine the liquefaction susceptibility should be done with the safety factor nearly to the unit.

The determination of CSR is initially proposed by Seed and Idriss (1971). It depends on the maximum horizontal accelerate of ground in the earthquake and several other parameters (Equation 2.2).

$$CSR = \frac{\tau_{av}}{\sigma'_{vo}} = 0.65 \frac{a_{max}}{g} \frac{\sigma_{vo}}{\sigma'_{vo}} r_d \quad \text{(Eq. 2.2)}$$

where a_{max} is the peak horizontal acceleration at the ground surface determined in the earthquake. In practice, this parameter is taken in the ground accelerate maps which can be found in related design standards, however, it also depends on the specific geological conditions (Idriss 1991); g is gravitational acceleration; σ_{v0} and σ'_{v0} are total and effective over-burden stress, respectively; r_d is stress reduction coefficient, the meaning of this parameter is that the shear stress underneath is smaller than that on the ground surface because of the deformability of soil column (Ishihara 1993).

There are several experimental methods proposed to determine the CRR, including laboratory tests, CPT, SPT, elastic wave velocity. Youd et al. (2001) gave a brief summary of these different methods.

II.1.7.2. Pore pressure prediction

Another important factor with correlation to the liquefaction phenomenon is the pore pressure increment. Generally, the pore water pressure increases during cyclic loading results in the decrease of effective stress according to the effective stress principle. In the literature, there are two types of models for the prediction of pore pressure generation under cyclic loadings. The first type (Seed et al. 1975) aims to obtain the relationship between pore pressure and the number of cycles as shown in Figure 2.29. The equation is given as:

$$r_u = \frac{u_g}{\sigma'_0} = \frac{2}{\pi} \arcsin\left(\frac{N}{N_L}\right)^{1/2\theta} \quad \text{(Eq. 2.3)}$$

where, r_u is the pore pressure ratio, this parameter is defined as the pore pressure over the initial effective over-burden pressure; N is the number of cycles applied; N_L is the number of cycles causing liquefaction, and θ is an empirical parameter ranging from 0.5 to 0.9. The second pore pressure prediction method correlating the pore pressure generation to shear strain level is shown in Figure 2.30 (Dobry et al. 1982). Note that, there is a shear strain threshold below which pore pressure increment cannot be observed. This could imply shear modulus at small strain is larger than that at large strain. By measuring the in-situ pore pressure, Chang et al. (2007) pointed out that the induced shear strain rather than shear stress is more suitable for the simulation of pore pressure generation.

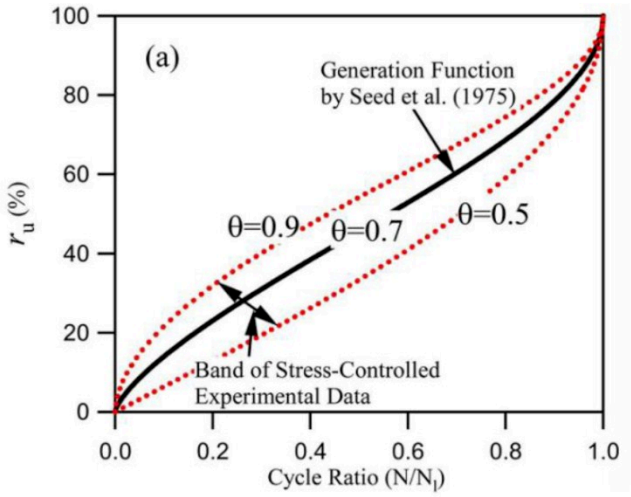

Figure 2.29 Pore pressure generation models for cyclic stress-controlled tests (Seed et al. 1975)

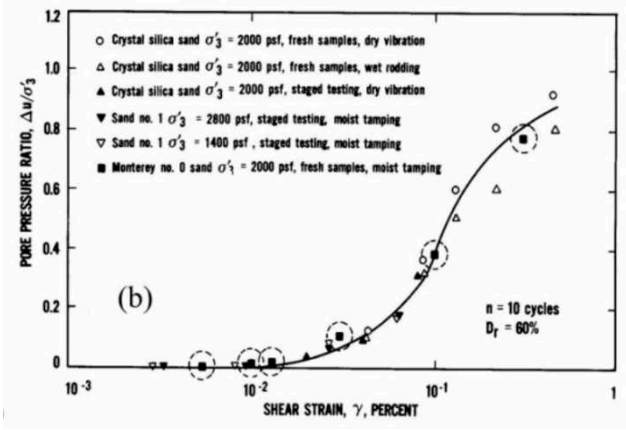

Figure 2.30 Pore pressure generation models strain-controlled cyclic triaxial tests (Dobry et al. 1982 after Chang et al. 2007)

II.1.8. Regulatory context

From the literature review, it can be seen that the soil liquefaction can be induced by various reasons and circumstances. The damages caused by this phenomenon have a wide range of effects, causing damage not only economically but also culturally and humanly. Therefore, the regulations to prevent this phenomenon appear in the standards of many countries.

With France, since 2010, the regulatory context has been changed three times (Brule and Javelaud 2014; Vernay 2018). The first improvement relates to the redefinition of the level of the importance of the constructions, its equipment. The first modification also related to the

redefinition of the five seismicity zones in French territory. The second modification related to the implementation of new European standards, in particular, the Eurocodes EN 1998-5. The third modification is the completion of the seismic zone dividing. On the left of figure 2.31, the old seismic map is presented, and on the right, the new seismic map as defined by decree n° 2010-1255. From this comparison, it can be seen that the possibility of the earthquake induce in the territories of France has been increasingly modified compared to the previous seismic zone map.

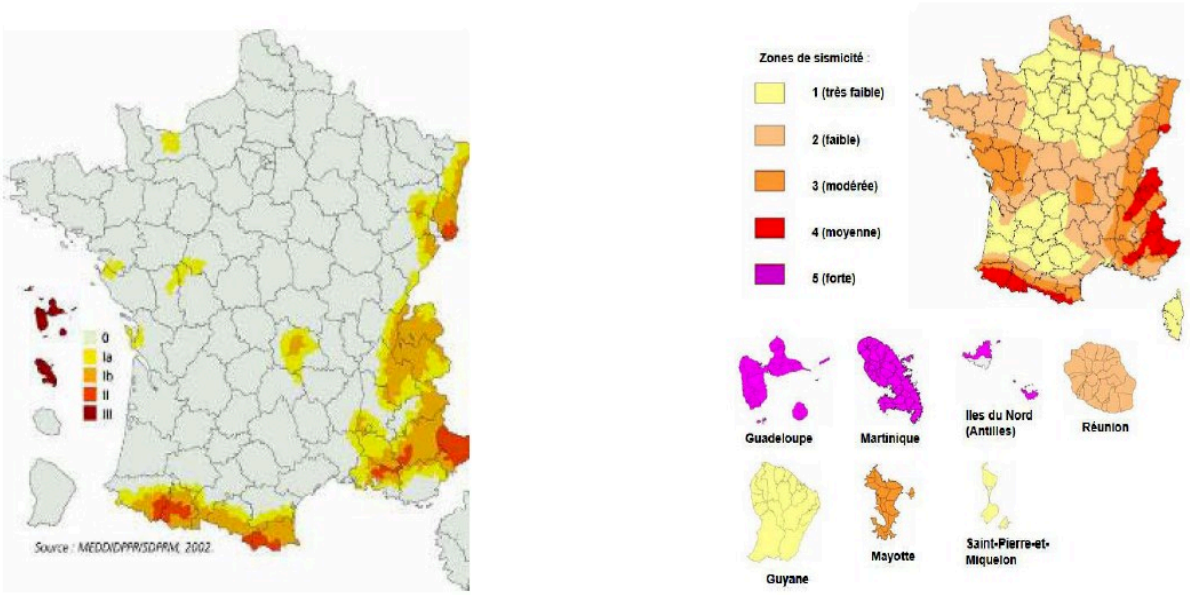

Figure 2.31 Map of earthquake risk in France. Old map on the left and new map on the right.

The definition of liquefaction in Eurocode 8 (EN 1998) is presented as: “A decrease in the shear strength and/or stiffness caused by the increase in pore water pressures in saturated cohesionless materials during earthquake ground motion, such as to give rise to significant permanent deformations or even to a condition of near-zero effective stress in the soil.”

The Eurocode also indicates that the assessment of the sensitivity to liquefaction must be carried out when the foundation soil comprises extensive layers or thick lenses of loose sand, with or without silt/clay fines, beneath the water table level, and when this level is close to the ground surface. This assessment shall be executed for the free-field site conditions (ground surface elevation, water table elevation) existing during the lifetime of the structure. In order

to assess the liquefaction potential, the European standard recommends carrying out in-situ tests including standard penetration (SPT) or static penetration (CPT) tests as well as the determination of grain size distribution curves in the laboratory.

Eurocode 8, part 5, paragraph 4.1.3 gives the users the conditions under which the risk of liquefaction can be neglected. These conditions apply on criteria of:

- Vertical stress, reflecting limit depths beyond which the risk is no longer to be considered.
- Amount of fines, soils with a high proportion of fines are not considered to be liquefiable
- Granulometry, coarse, draining materials are not considered as liquefiable.
- The relative density of soil. The soil in dense state is considered to have high liquefaction resistance strength.

In the case of Vietnam, the regulations on soil liquefaction assessment are also based on EN 1998-5 standards, so there is some similarity between Vietnamese regulation and French regulation. However, it is not exactly the same between Vietnamese standard and Eurocode. In Vietnam, the map of seismic areas includes four zones with the risk of earthquakes ranging from level 1 to 4; the change of color from white to dark yellow shows the increasing of seismic ground acceleration (Figure 2.32). Another seismic magnitude scale used in Vietnam is the Medvedev–Sponheuer–Karnik scale (MSK). This magnitude scale is based on the standard of Russia. But, the same point for almost the current seismic resistance standards of nations is that the calculations are based on the ground acceleration, thus, it is switchable between standards. Similar to EN1998-5, the risk of liquefaction can be ignored when the maximum ground acceleration is smaller than 0.15 and some conditions below are fulfilled:

- Sand has clay content greater than 20% with plasticity index PI> 10;
- Sand has a fines content greater than 35% and at the same time the number of SPT after being standardized with the depth and the energy ratio $N_1(60)> 20$;
- Clean sand, with SPT index after being standardized with soil self-pressure and with energy ratio $N_1(60)> 30$.

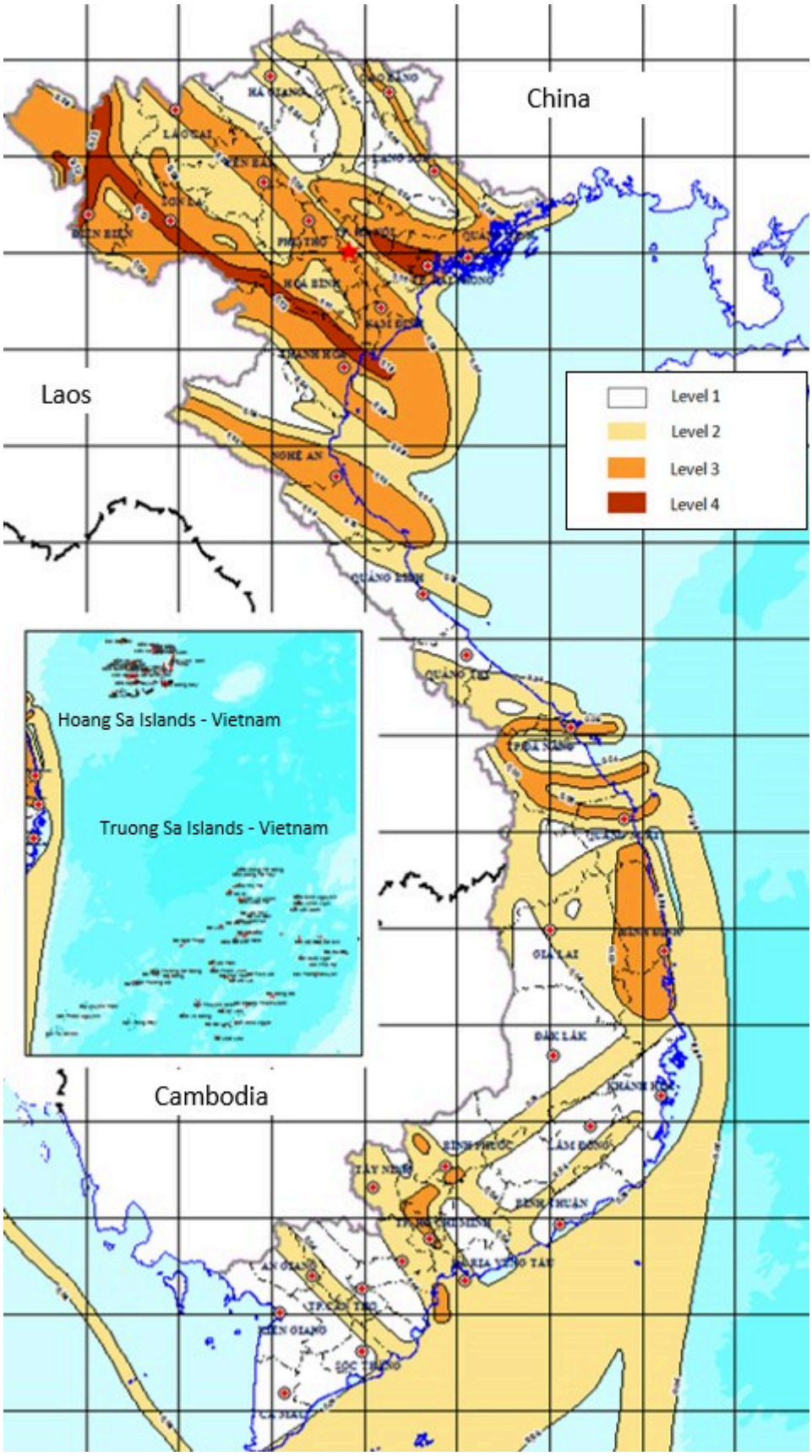

Figure 2.32 Map of earthquake risk following Vietnamese standard

From the review of some standards, it can be seen that the risk of liquefaction has been recognized, and better understood; however, there have been still some unconvinced points. The standard presents that the liquefaction of soil can be evaluated thought the SPT or CPT index. From this perspective, the soil layers close to the ground surface with low CPT or SPT index have a high susceptibility of liquefaction. But the recent studies show that besides the mechanical parameters, the liquefaction resistance of soils is strongly affected by the un-saturation which usually appears in these soil layers. On the other hand, the evaluation of the liquefaction potential of soils is mainly performed through the particle size characterization of the materials, as well as by the evaluation of its mechanical resistance and its density. The standard considers liquefiable potential only on fully saturated soils, "below the level of the water table". There is therefore still no evaluation of the liquefaction potential of soils layers above the level of the water table.

II.1.9. Conclusions

It is clear that the liquefaction is a natural phenomenon that can occur worldwide, causing great damages. Liquefaction is often associated with earthquakes and related to cohesionless saturated soil. However, it can also be caused by other natural or artificial factors such as vibrations of machines, wind, etc.

This phenomenon has long been studied and the mechanical behavior of cohesionless saturated soils is well understood. There are some definitions of liquefaction, but it is generally understood as the failure of the ground due to the increase in pore water pressure when the soil is subjected to static or dynamic loadings.

Liquefaction susceptibility of soil depends strongly on some parameters including saturation degree. The standards of many countries refer to the liquefaction assessment as a mandatory part of the seismic resistance calculation of constructions. However, the effect of saturation degree has been neglected while most of the soil closed to the ground surface is unsaturated.

II.2. Effect of the degree of saturation on liquefaction phenomenon

II.2.1. Context

Yoshimi et al. (1989) described that the liquefaction of soil incompletely saturated had been firstly studied with two objectives: i) to assess the experimental errors due to the compressibility of pore fluids that would cause an overestimation of liquefaction resistance, and ii) to study the behavior of natural soil deposits that were not completely saturated for some reasons. The studies of the first type (Chaney 1978) have resulted in the limitation of Skempton's parameter B (= 0.96) for soil to be considered as full saturation. It is understood that when B is higher than 0.96 for sandy soil, the compressibility of pore fluids equals to the compressibility of water. As an example of the second objective, Sherif et al. (1978) presented some results carried out in the laboratory on samples with the saturation degrees higher than 80%. Following these results, the liquefaction resistance of clean, fine sand increases significantly when the degree of saturation decreases.

Recently, another attempt has been made to increase the liquefaction of resistance of soil by reducing the degree of saturation by lowering the water table or by generating the air bubbles into the pores of the soil (He 2013; Yegian et al. 2007). Besides, Tsukamoto et al. (2014) revealed that the air bubbles can be found at 5 m below the groundwater table. It means that most of the building structures could be based on unsaturated soil layers. This shows the need to study the effect of unsaturation on the liquefaction behavior of soil. On the other hand, the experiences of the recent earthquakes and its damages propose an issue that it is necessary to study the liquefaction behavior of unsaturated soil in a relationship to factors like cyclic or monotonic loading before and after the main reason causing liquefaction (ICOLD 2012; Tran et al. 2018).

II.2.2. Some observations on the liquefaction potential of partially saturated soils

The risk of liquefaction for unsaturated soil has been not only demonstrated by laboratory results but also the observations in situ. In situ investigations were carried out after the 2003 Sanriku-Minami earthquake that attacked the city of Tsukidate in Japan and significant damages due to liquefaction were reported. Very large brutal landslides were observed, as well as a large amount of water present on the surface, a signal of pore water pressure increment in soil. At the same time, it was reported from the meteorological agency that it had not rained in this area during the week before the earthquake. Based on the knowledge of the

local geography, and the properties of the material in place, the traces in situ, it was concluded that the ground was liquefied although it is unsaturated (Unno et al. 2006).

The liquefaction of unsaturated soil has been also observed on coastal structures. Mory et al. (2007) presented the results of field experiments performed around a bunker from the Second World War situated on the beach. This construction was surrounded by water when the tide increases and subject to intense wave forcing. By positioning pressure sensors at different levels inside the soil, a series of pore pressure measurements at the same time was obtained. The results revealed that the temporary liquefaction was observed as the appearance of an upward pressure gradient, which could be higher than the effective stress caused by the sediment layer weight. They also used the Fourier analysis to demonstrate that the soil is unsaturated. This in situ observation confirmed that the liquefaction phenomenon can be observed under conditions of partial saturation. Michallet et al. (Michallet et al. 2012) carry out a physical model of these coastal structures and confirm that under heavy loads induced by high tide, pore pressures develop in loose and partially saturated sand and a liquefaction threshold is reached.

Liquefaction is a phenomenon that is mainly observed on surface soils. However, as reported by Fredlund and Rahardjo (Fredlund and Rahardjo 1993), the majority of soils on the surface are partially saturated. Moreover, the saturation conditions below the level of the water table are also still questionable. Authors such as Tsukamoto et al. (Tsukamoto et al. 2014) reported the results of wave velocity measurements through different soil layers to significant depths below the water level. These results show that the air bubbles can be found 5 meters below the water table. Breul et al. (2008) had also demonstrated through geoendoscopy that despite the appearance of a thin layer of saturated sediment the ground surface, there was still a significant amount of air in lower layers. More recently, authors such as (Cubrinovski et al. 2019) have studied some soil profiles subjected to liquefaction damage in the Christchurch earthquake in New Zealand. They reported that although some areas have the same water table level and soil profiles, the damage of liquefaction is different. It, therefore, appears from their observations that the level of the water table is ultimately not a unique critical threshold for the assessment of liquefiable layers

II.2.3. Studies of liquefaction on unsaturated soils

Sherif et al. (1977) studied the effect of initial saturation on the cyclic behavior of sand. They used a hollow cylinder device to carry out liquefaction tests on Ottawa sand, the clean sand with parameters: D_{50} = 0.4, D_{10} = 0.2, coefficient of uniformity = 2.1. The different levels of saturation were obtained by varying the volume of water circulating through the sample during the sample saturation process. After that, the relationship between the Skempton's coefficient and the degree of saturation was used to evaluate the saturation degree of the sample. This relationship between B and the saturation degree was obtained using Boyle's law and Henry's law.

In their study, the development of pore water pressure in the sample with different saturation degrees was compared. Figure 2.33 shows the typical liquefaction test data for three values of B. The sample with B = 0.9 was considered to be fully saturated and the two lower B samples were considered not fully saturated. They commented that even the very low B samples do liquefy; the trend of residual pore-pressure rise in samples with low B value is quite small, especially in early cyclic loading. They also explained this phenomenon by the fact that as the degree of soil saturation decreases, the Coulomb-type frictional stresses within the soil increase, which in turn will decrease the magnitudes of the stresses transferred to the fluid of the soil.

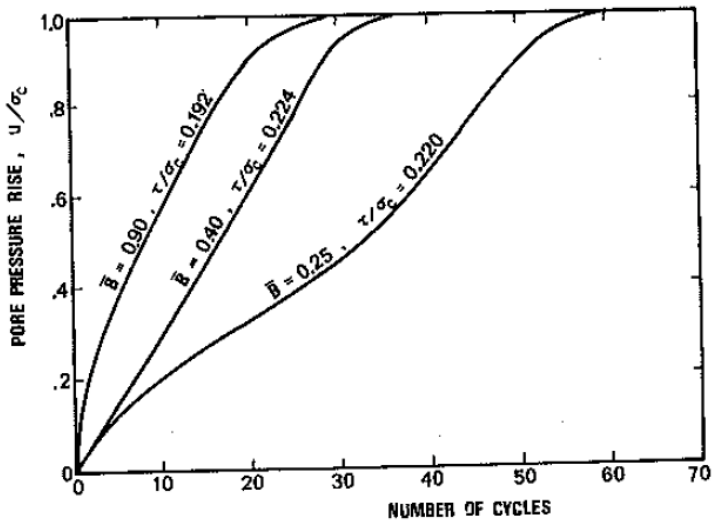

Figure 2.33 Typical pore water pressure increment versus the number of cycles for low B and high B samples (Sherif et al. 1977)

This study also showed that the liquefaction resistance of soil depends on the saturation degree. The lower saturation degree corresponds to the higher *CSR* needed to liquefy the

samples. Additional to that, when plotting the relationship between cyclic stress ratio (*CSR*) and the number of cycles causing liquefaction in an axis with a logarithmic scale, it seems to have linear form (Figure 2.34).

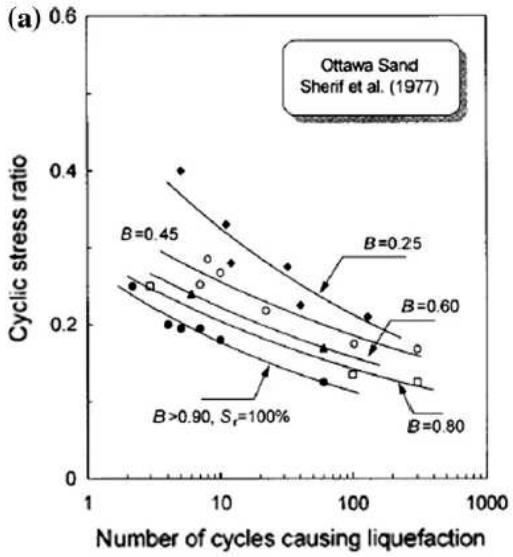

Figure 2.34 Degree of saturation effect on laboratory tests results of liquefaction resistance of Ottawa sand (Sherif et al. 1977)

Chaney et al. 1978 investigated the effect of the degree of saturation on the cyclic response of compacted Monterey sand by using tri-axial test. The samples were prepared at two relative densities. The cyclic loading was applied until reaching 5% of axial strain. The results showed that at a constant cyclic stress ratio, the number of cycles to reach a specified strain increases with decreasing B values. The relationship between B value and the logarithm of the number of cycles causing liquefaction is linear for both loose and dense samples, and the effect of B on cyclic strength is more obvious when the cyclic stress is low (Figure 2.35).

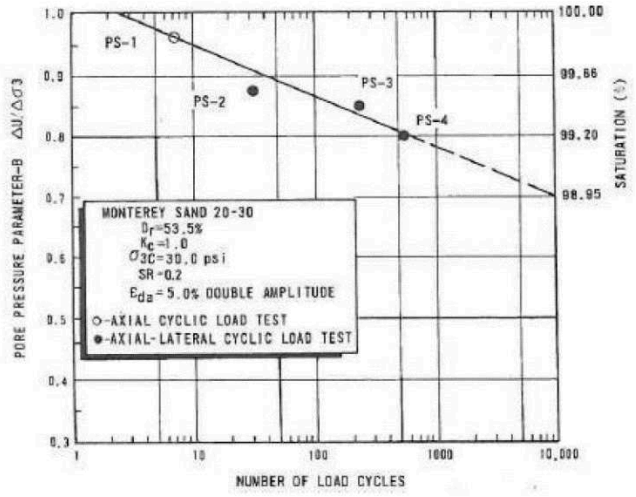

Figure 2.35 The number of cycles to reach 5% of axial deformation as a function of the Skempton's coefficient (Chaney 1978)

In 1989, Yoshimi (Yoshimi 1989) carried out experiments to determine the effect of saturation on liquefaction resistance of Toyoura sand. The sand has physical properties: specific gravity of soil particles = 2.64, D_{50} = 0.175, D_{10} = 0.129, uniformity coefficient = 1.52, fines content = 0 percent, maximum dry density = 1.645 g/cm^3, minimum dry density = 1.335g/cm^3. The samples were prepared by the air-pluviated method at a relative density of 60%. The saturation degree was calculated thought the B-Sr relationship and the measurements at the end of tests based on the water content and the dry weight of the samples. The results of this study showed that: 1) the liquefaction resistance increased significantly with a decrease in saturation degree, the liquefaction resistance for the sample with 70 percent of saturation degree was about three times that of the full saturation sample (Figure 2.36); 2) the liquefaction resistance also was inverse proportion with B value (Figure 2.37); 3) the cyclic shear behavior of the unsaturated sand was like to that of denser saturated sand, exhibiting high strength as well as stable deformation characteristics.

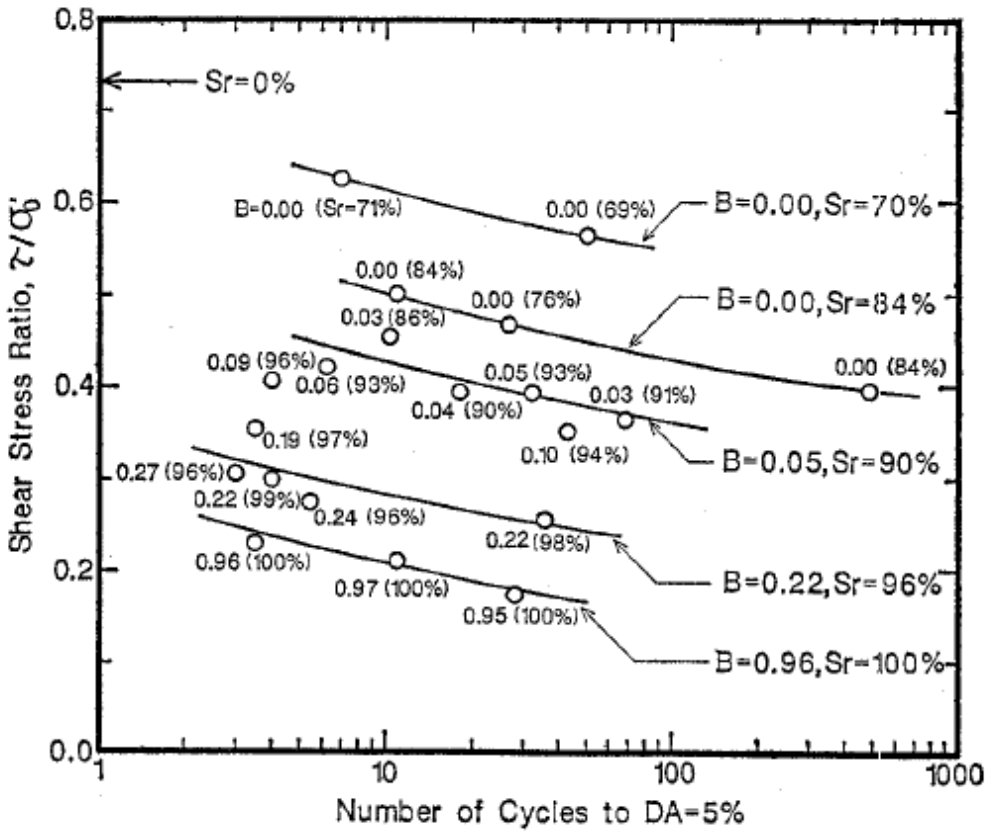

Figure 2.36 Effects of degree of saturation on liquefaction characteristics of sand (Yoshimi 1989)

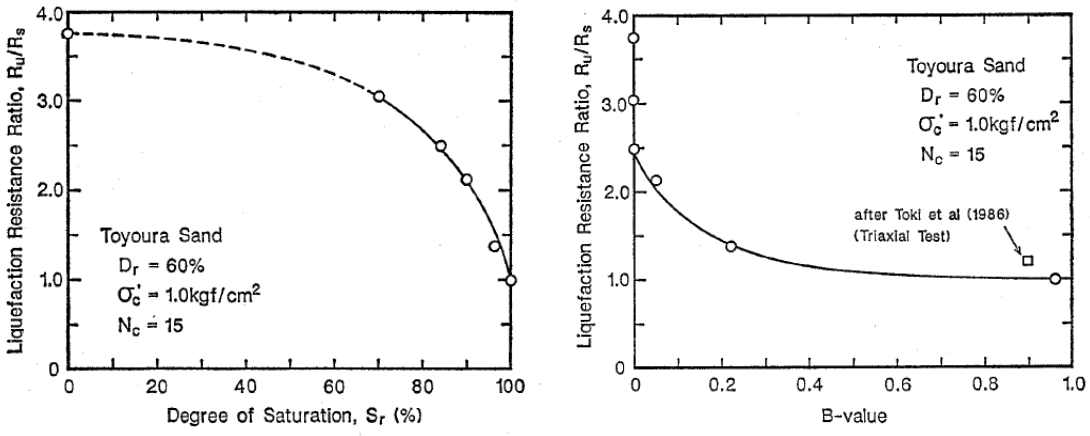

Figure 2.37 Effect of the un-saturation to liquefaction resistance ratio of Toyoura sand (Yoshimi 1989)

a) relationship between degree of saturation to the liquefaction resistance ratio b) relationship between Skempton's parameter B to the liquefaction resistance ratio.

Yoshimi and his colleagues, therefore, highlighted that for a "low" degree of saturation, the response of sand under cyclic loading is more like the cyclic mobility phenomenon than the cyclic liquefaction (Figure 2.32).

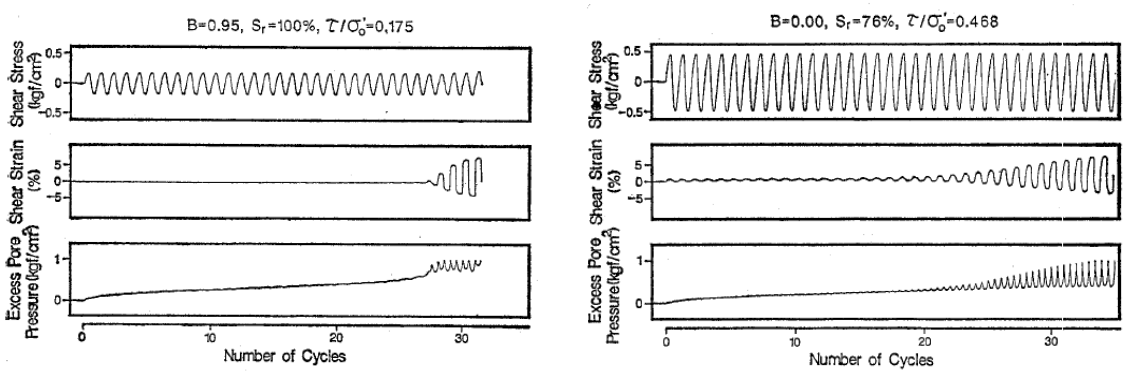

Figure 2.38 The behavior of soil under cyclic loading (Yoshimi 1989).

a) full saturated sample b) unsaturated sample

Xia and Hu (1991) investigated the influence of saturation degree and back pressure on the liquefaction resistance of a fine sand taken from the drill holes at the site of Tong Jaizhi Power Station by conducting cyclic triaxial tests ((Figure 2.33). The sand has a coefficient of uniformity C_u = 3.7, median size of particle D_{50} = 0.0995 x 103 m, and specific gravity G_s = 2.74. Their results show that a very remarkable increase of the liquefaction resistance of the tested sand had been caused by a slight decrease of degree of saturation from 100% to 99.5%, only 0.5% lower in the degree of saturation, the ratio of cyclic stress ratio increases sharply; and the decrease of the saturation degree of the samples does not result in such a sensitive increase of liquefaction resistance of the sand when the saturation degree of the sand is below a certain value. When the saturation degree is lower than 99.5, It can be considered that the ratio of cyclic stress ratio increases linearly with the decrease of the degree of saturation.

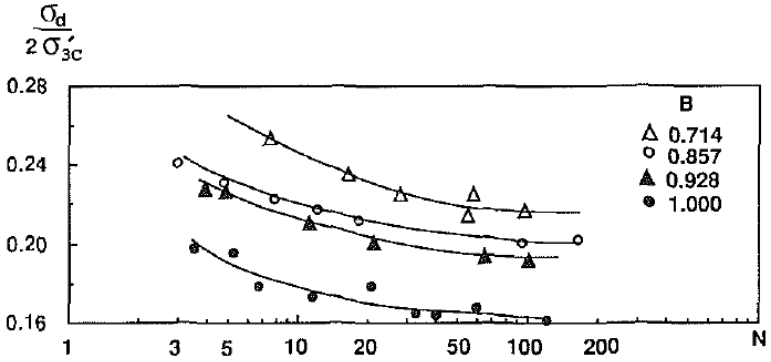

Figure 2.39 Effect of saturation degree on the liquefaction resistance of sand (Xia and Hu 1991)

The effect of back pressure on the cyclic resistance of unsaturated soil was also investigated in their study (Figure 2.40). All the samples had the same initial degree of saturation of about 99.8%, corresponding to a Skempton's pore pressure coefficient B = 0.97. The applied effective confining stress was 98.1 kPa while the back pressure varied from 0 kPa to 382 kPa. The liquefaction resistance of the sand increased significantly with the higher values of back pressures. It even became much higher than the liquefaction resistance for the samples without back pressures.

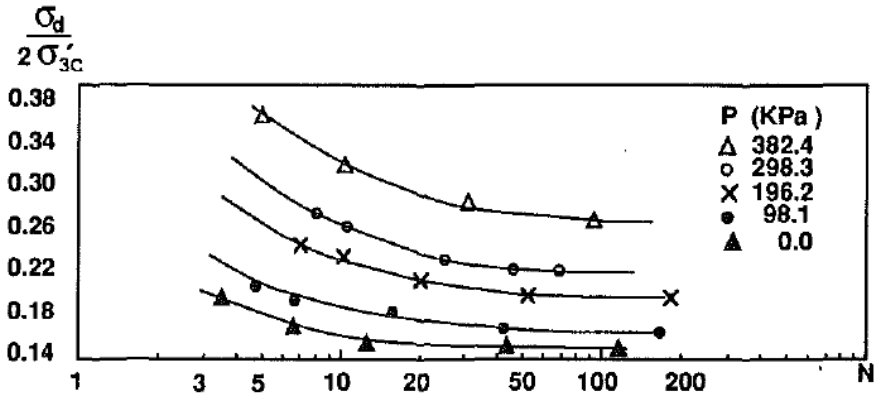

Figure 2.40 Effect of back pressure on the liquefaction resistance of unsaturated sand (Xia and Hu 1991)

For their part, Fourie et al. (2001) conducted monotonic test on the disturbed and undisturbed unsaturated tailings sand. By study the undisturbed sample, the evidence that the degree of saturation below the phreatic surface of the Syncrude tailings sand is less than unity was given (Figure 2.41). They concluded that the existence of air bubbles, even if existing only in very small volumetric percentages, affects apparently on the response of the pore water pressure within the samples under undrained monotonic loading condition. Therefore, the liquefaction potential of unsaturated tailings sand under undrained loading may be decreased compared to that when the soil is fully saturated.

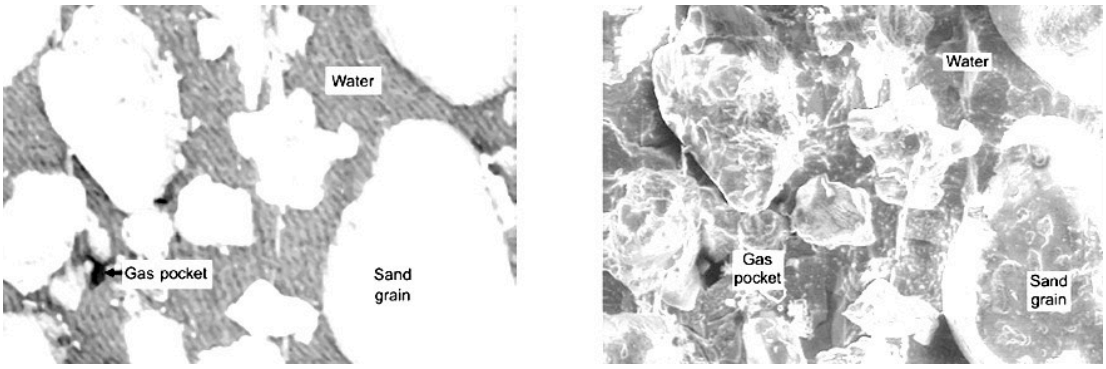

Figure 2.41Appearance of gas pocket inside the tailing sand (Fourie et al. 2001)

Okamura and Soga (Okamura and Soga 2006) studied the effects of the compressibility of the pore fluid on the liquefaction susceptibility of unsaturated sands. In this study, Okamura and Soga stated the effects of suction and compressibility of air on the behavior of unsaturated soils. However, the role of suction is small compared to that of air compressibility since, according to them, taking this parameter into account is not relevant with regard to the type of material studied (sand), the suction was about 4 kPa when the saturation degree was 70%. They pointed out that the presence of matrix suction within a material has an effect on increasing the value of the effective stress compared to the completely saturated soil when the saturation degree is small. They, therefore, focused only on the second mechanism involved in increasing the resistance to liquefaction of unsaturated soils, the compressibility of the pore fluid. More specifically, the role of air present in the pores of unsaturated soil is to absorb excess pore water pressure by reducing its volume and this volumetric reduction resulted in a unique relationship between the normalized liquefaction and the potential volumetric strain as shown in figure 2.42.

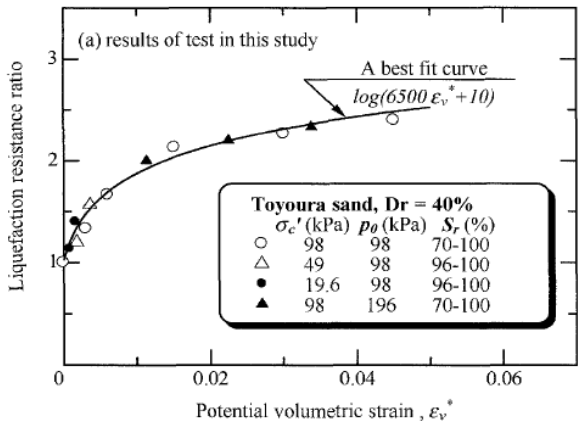

Figure 2.42 Relationship between hypothetical volumetric strain and liquefaction resistance of partially saturated sand normalized with that of fully saturated sand (Okamura and Soga 2006)

They also showed that for unsaturated sands, the degree of saturation significantly affects the liquefaction resistance of sand. The liquefaction resistance also depends on the initial backpressure and the initial effective stress (Figure 2.43).

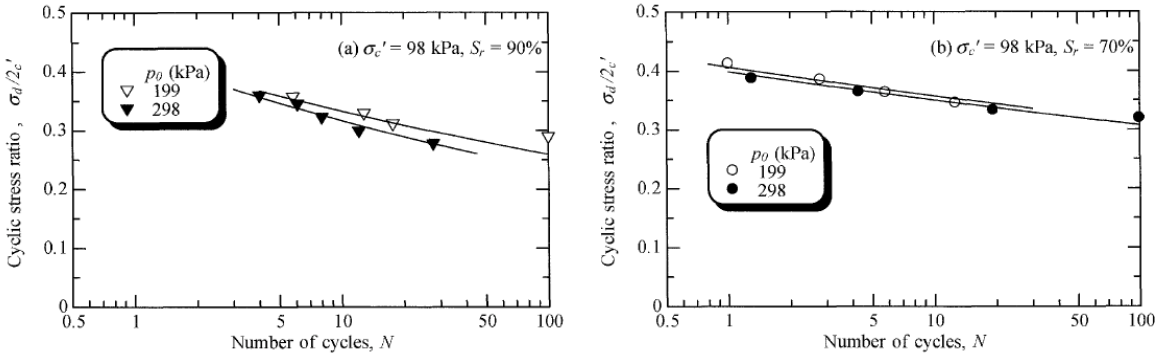

Figure 2.43 Effect of initial pore pressure on the relationship between cyclic stress ratio and number of cycles (Okamura and Soga 2006)

In the studies presented above, the effect of saturation degree is represented through Skempton's parameter B; however, this parameter is not easy to measure in situ. Some authors have tried to make a relation between saturation degree and suction by measuring the pore water pressure and pore air pressure in the voids of soil. Unno et al. (2008) carried out a series of tests to get a better understanding of the general liquefaction of unsaturated soils. The samples had the relative densities at 26% and 60%, the degree of saturation varied from 39.5% to 100% for the samples with the relative density of 60 % and from 0% to 100% for the sample with the relative density of 26%. After that, the stepping axial deviator stress was applied under undrained condition (Figure 2.44). In these tests, the pore air pressure and the pore water pressure were measured continuously.

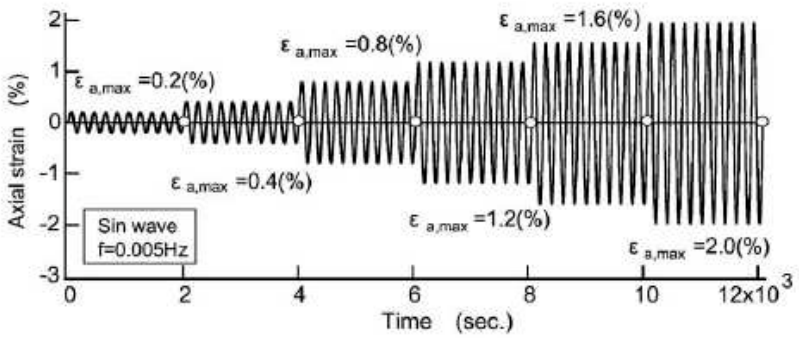

Figure 2.44 Time history of axial strain during cyclic loading process (Unno et al. 2008)

The behavior of soil under controlled axial strain loading is shown in figure 2.45. After cyclic loading, the samples were liquefied. During the cyclic loading, both pore-water pressure and pore air pressure increased. The pore air pressure was always higher than pore water pressure; however, their peaks were the same and equaled to the initial effective stress when the samples liquefied.

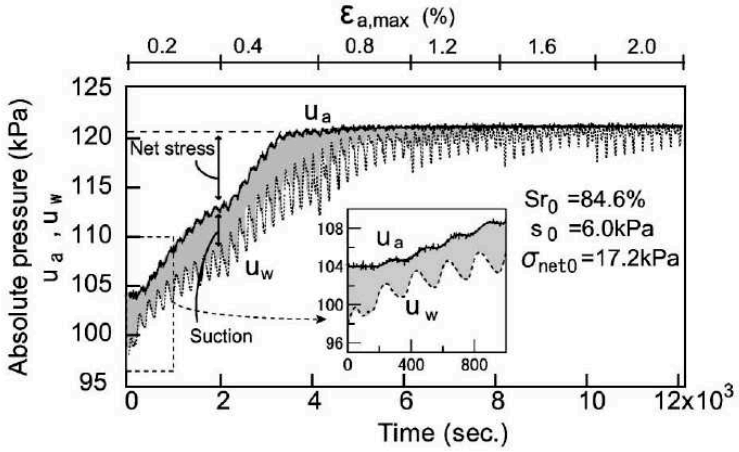

Figure 2.45 Time history of pore air pressure and pore-water pressure (Unno et al. 2008)

Figure 2.46 presents the results obtained for undrained triaxial tests carried out on Toyoura sand for different values of initial degrees of saturation (100%; 83.8%; 75.4%; 43.3%) and a low initial relative density (D_r = 26%). This graph shows the evolution of the effective stress reduction ratio as a function of time (bottom axis) and strain-controlled loading (top axis), in which, effective stress reduction ratio was defined as equation 2.4

$$\text{The effective stress reduction ratio} = 1 - \frac{\sigma'_m}{\sigma'_{m0}} \qquad \text{(Eq. 2.4)}$$

where σ'_{m0} is the initial mean principal effective stress, σ'_m is the mean effective stress. This index indicates the degree of effective stress loss ranging from zero to unity. The effective stress reduction ratio equals to 1 corresponding to the completed liquefaction state.

The initial net stress is the same (approximately) for the three unsaturated samples, around 20 kPa. Some points can be observed from this figure:

- The fully saturated sample (Sr = 100%) liquefies very quickly at a low axial strain value;

- The reduction in the effective stress is slower for the samples having lower degrees of saturation.

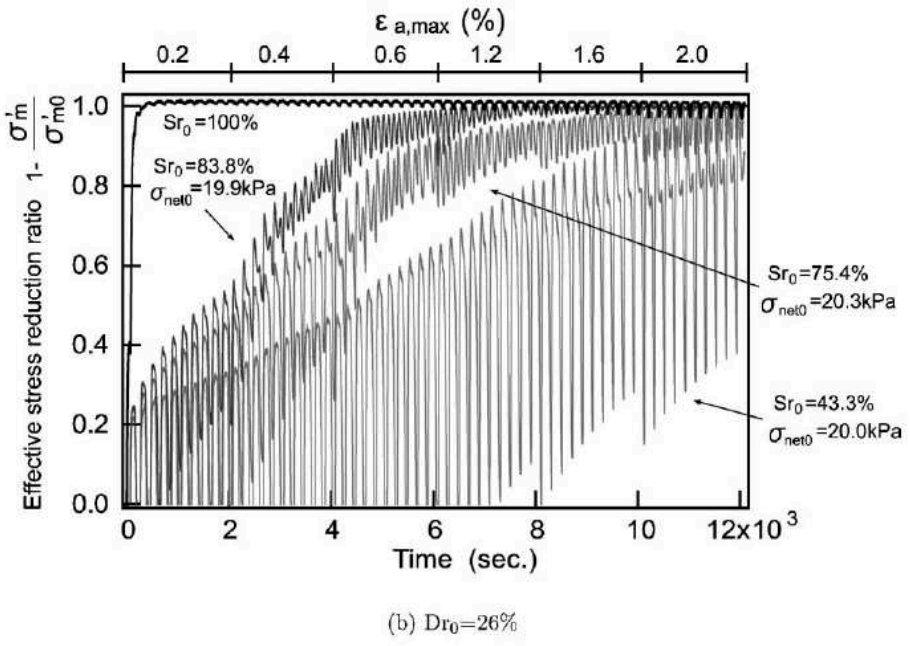

(b) Dr_0=26%

Figure 2.46 Time history of effective stress reduction ratio for Toyoura sand samples having relative density of 26% (Unno et al. 2008)

Figure 2.47 shows the evolution of effective stress reduction ratio as a function of time (bottom axis) and axial deformation (top axis), for four initial degrees of saturation (100%; 84.6%; 64.8%; 82%) and an initial density Dr = 60%. The two samples initially saturated at 84.6% and 64% have net stress of 20 kPa (approximately), the sample initially saturated at 82% has initial net stress of 60 kPa. We can, therefore, observe here the influence of the confining stress on the cyclic response of unsaturated samples. The effect of initial relative density also observed when comparing the evolution of effective stress reduction ratio of the samples with the same saturation degrees (Sr = 100 % and Sr = 84%) but different initial relative densities (26 % in figure 2.46 and 60% in figure 2.47). The samples with higher relative density are more difficult to liquefy than the samples with lower relative density.

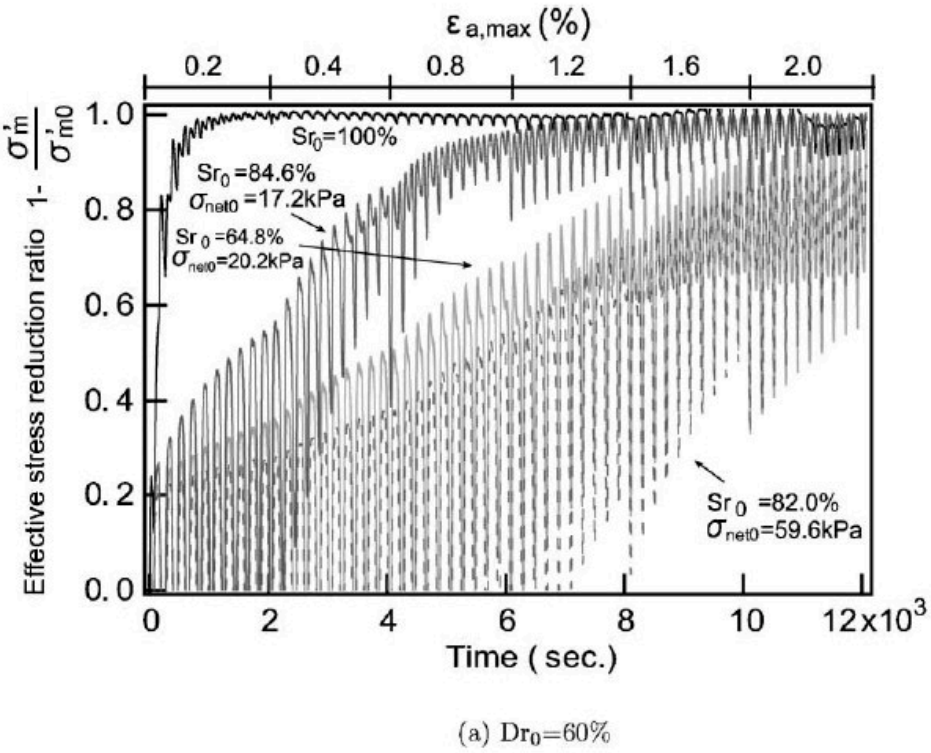

(a) Dr_0=60%

Figure2.47 Time history of effective stress reduction ratio for Toyoura sand samples having relative density of 60% (Unno et al. 2008)

From this study, the results revealed that the soil with low saturation degree can liquefied under cyclic axial strain controlled loading. The pore pressure increased due to the decrease of soil skeleton. The amount of volume change at zero effective stress state depends on three parameters: the volume compressibility of soil skeleton, the degree of saturation, and the initial confining stress. The liquefaction potential of unsaturated soil can be evaluated by comparing the volume compressibility of the soil particle skeleton with the volume change required to reach liquefaction (figure 2.48).

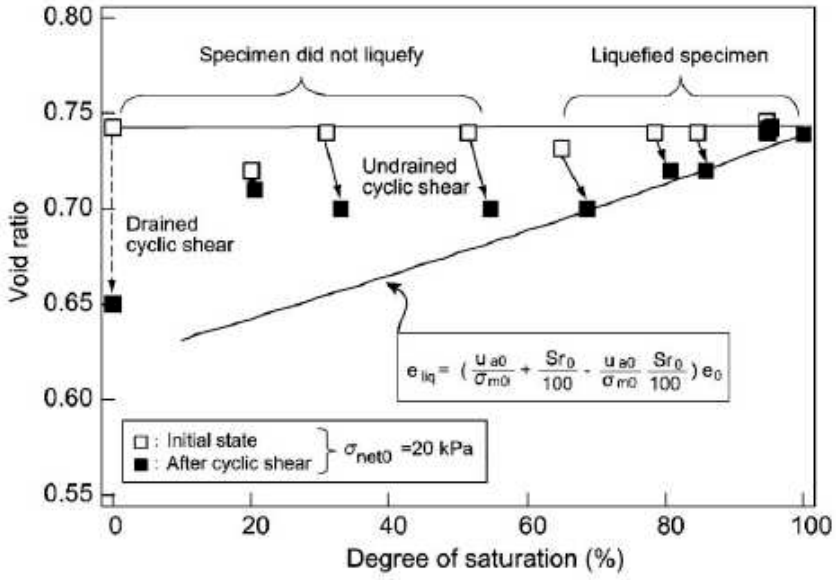

Figure 2.48 Liquefaction prediction of the test result using Toyoura sand at Dr = 60% (Unno et al. 2008)

In 2007, Kamata and his team (Kamata et al. 2007) presented a campaign of monotonic undrained triaxial tests performed on two kinds of sand, using the axis translation technique to impose initial matrix suction value on the material. Using this method, they could independently apply and measure pore-air and pore-water pressures. The limitation of this method, as they admitted, was that the conditions reproduced in laboratories were not completely equivalent to those found in situ. The results of their tests are presented in Figure 2.43 and show the evolution of the deviatoric stress as a function of the axial deformation for different values of degrees of saturation. The presence of initial suction leads to a slight increase in shear stress (figure 2.49).

Using the ordinary triaxial apparatus and the special triaxial apparatus which allowed measure the pore water pressure and pore air pressure independently, Tsukamoto et al. (2014) investigated the liquefaction of two silty sands at three zones of saturation: unsaturation, partially saturation, and full saturation. The samples were loaded under the stress-controlled and undrained condition. During the cyclic loading process, the volume change was also measured. The results showed that for the samples with a low saturation degree, the pore water pressure and pore air pressure increase until reaching a limitation, and then the samples failed due to the excessive accumulated axial strain (Figure 2.50).

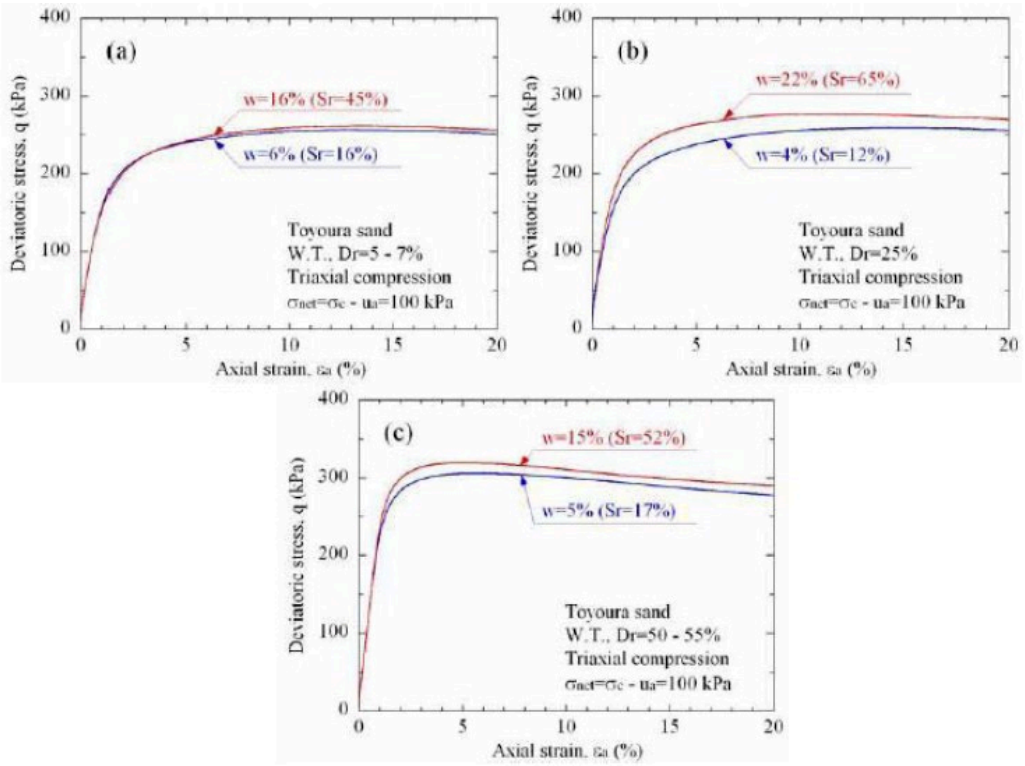

Figure 2.49 Results of monotonic tri-axial test carried out on Toyoura sand at deferent initial saturation degrees (Kamata et al. 2007)

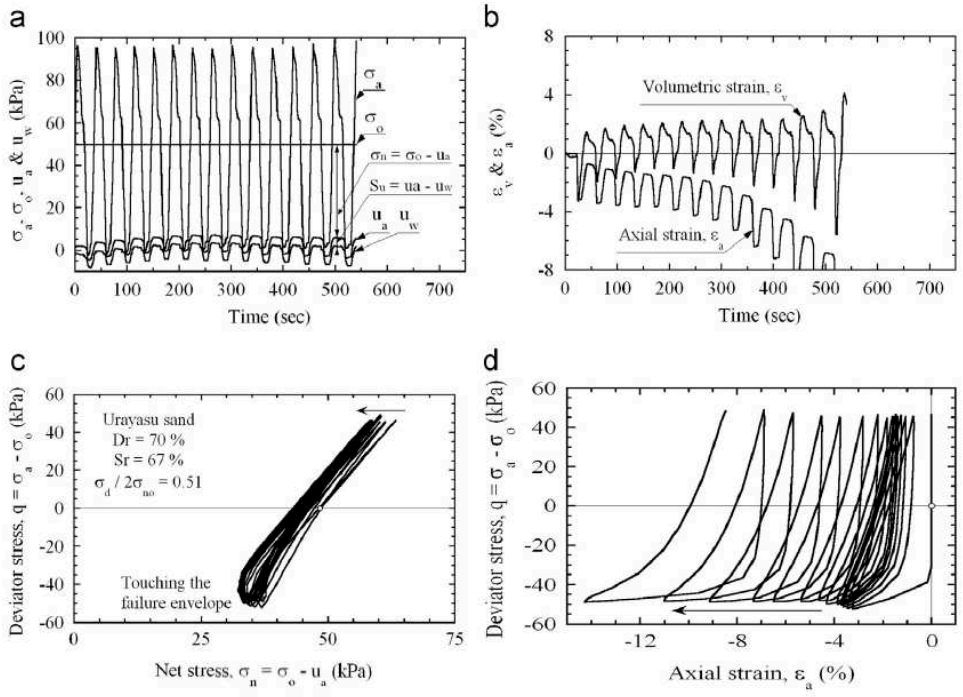

Figure 2.50 Behavior of unsaturated silty sand subjected to cyclic loading (Tsukamoto et al. 2014)

The volumetric strain of samples was investigated in this study to evaluate the liquefaction potential of sand subjected to cyclic deviator stress. Figure 2.51 shows the maximum volumetric strain of the samples at 5% of axial strain against the initial saturation degree. The maximum value, minimum value, and medium values are respectively the upper amplitude, lower amplitude, and the middle value of volumetric strain in the cycle corresponding to the axial strain of 5%. The threshold $\varepsilon_{v,l}$ is the minimum value of volumetric strain causing the zero effective stress state. Tsukamoto et al calculated this parameter based on an observation of Unno et al 2007 that the pore air pressure and pore water pressure equal to confining stress at the onset of liquefaction. The volumetric threshold triggering liquefaction is presented in the equation 2.5 below:

$$\varepsilon_{v,l} = \left(1 - \frac{u_{a0_{abs}}}{\sigma_{0_{abs}}}\right).\frac{e(1-Sr)}{1+e} = \left(1 - \frac{u_{a0_{abs}}}{\sigma_{0_{abs}}}\right).\varepsilon_{va} \qquad \text{(Eq. 2.5)}$$

where $u_{a0_{abs}}$, $\sigma_{0_{abs}}$, and ε_{va} are the absolute pore air pressure, absolute confining stress, and pore air volumetric strain. In their study, u_{a0} = 0 kPa, σ_0 = 50 kPa in gauge pressures. However, both Unno et al. (2007) and Tsukamoto et al (2014) did not show the calculation for u_{a0-abs} and σ_{0-abs} , thus, it is not clear that if the pore air pressure part caused by the surface tension of air bubbles had been taken in to the account. From figure 2.51 they suggested that the soil is liquefied when the saturated is higher than 70%.

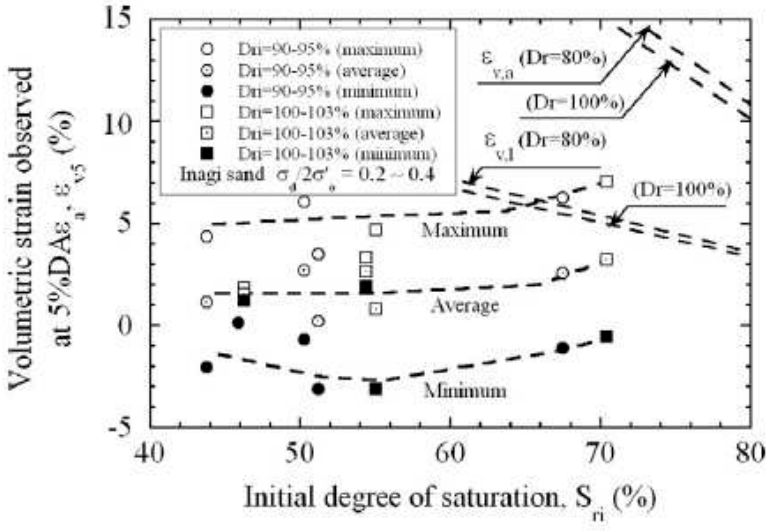

Figure 2.51 Plots of volumetric strain observed at 5% of double axial strain against intial degree of saturation S_{ri} for Inagi sand (Tsukamoto et al. 2014)

Otherwise, using undrained monotonic and cyclic triaxial tests, Arab et al. (2016) studied the liquefaction of unsaturated RF Hostun sand, according to the value of Skempton's coefficient B. The samples were prepared at relative density of about 50% by wet tamping method. They showed that the saturation degree affects soil behavior characteristics including initial stiffness, shear strength, cyclic shear strength, and the sample deformation during cyclic loading. The effect of B on the cyclic shear strength appears from the first cycle (Figure 2.52). Skempton's coefficient also affect significantly on the sample deformation.

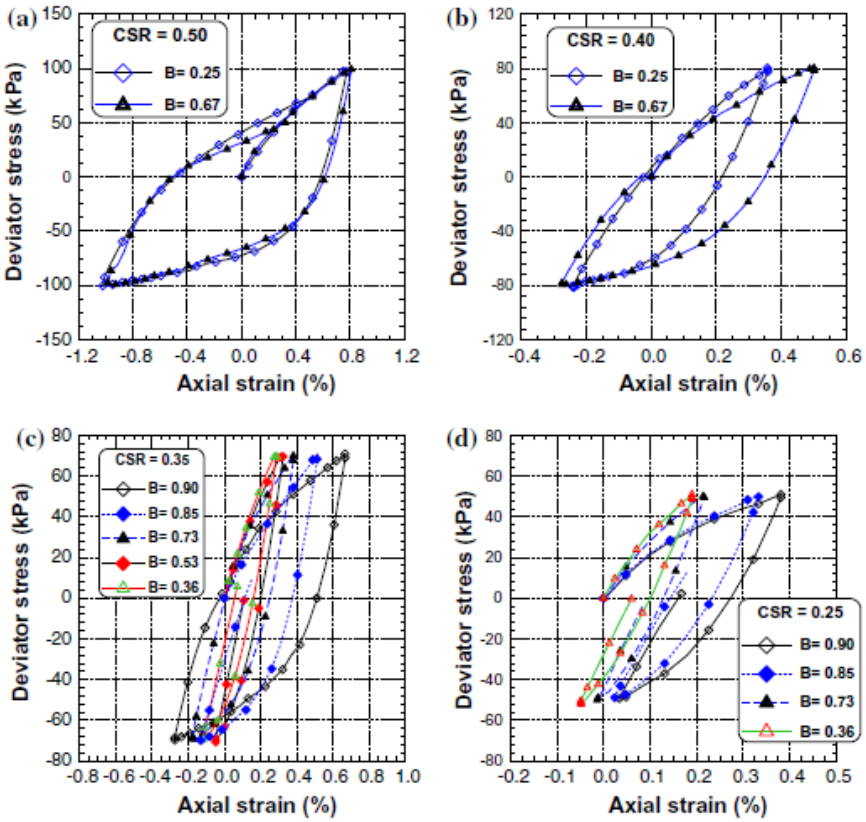

Figure 2.52 Effect of Skempton' parameter B on the first cycles of soil behavior under cyclic loading (Arab et al. 2016)

The cyclic test results show that the cyclic shear strength of soil is inversely proportional to Skempton's coefficient (B) (Figure 2.53). A limitation of this study is that the saturation degree was not measured directly; it was calculated based on the modeling results of the B-Sr relationship.

Mase et al. (2019) studied the cyclic shear strength behavior of sand using the cyclic triaxial test on undisturbed specimens. The specimens were taken from Osaka Bay onshore area by the freezing sample method. In this study, the excess pore water pressure ratio, hysteresis

loop, and effective stress path were investigated (Figure 2.54). The results showed that the sample taken from situ was not full saturated; however, it was liquefiable under different deviator stresses. The experimental results of cyclic behavior were also compared to the modeling results.

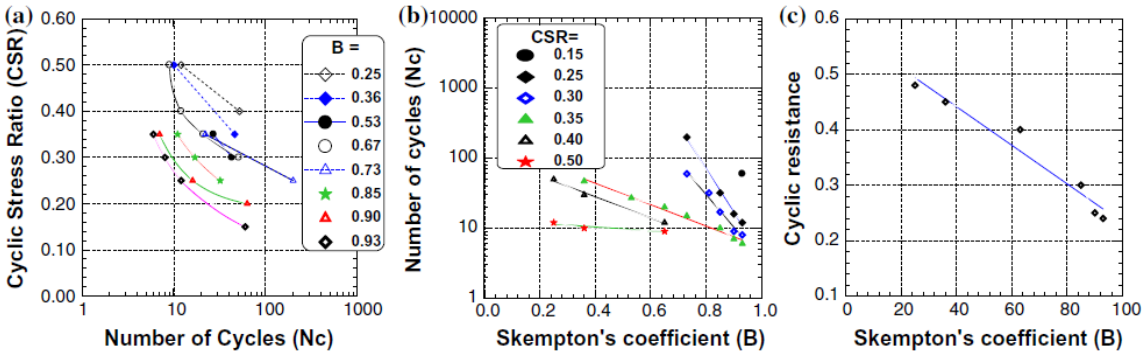

Figure 2.53 Influence of saturation degree on the cyclic undrained response of the Hostun Rf sand (Arab et al. 2016)

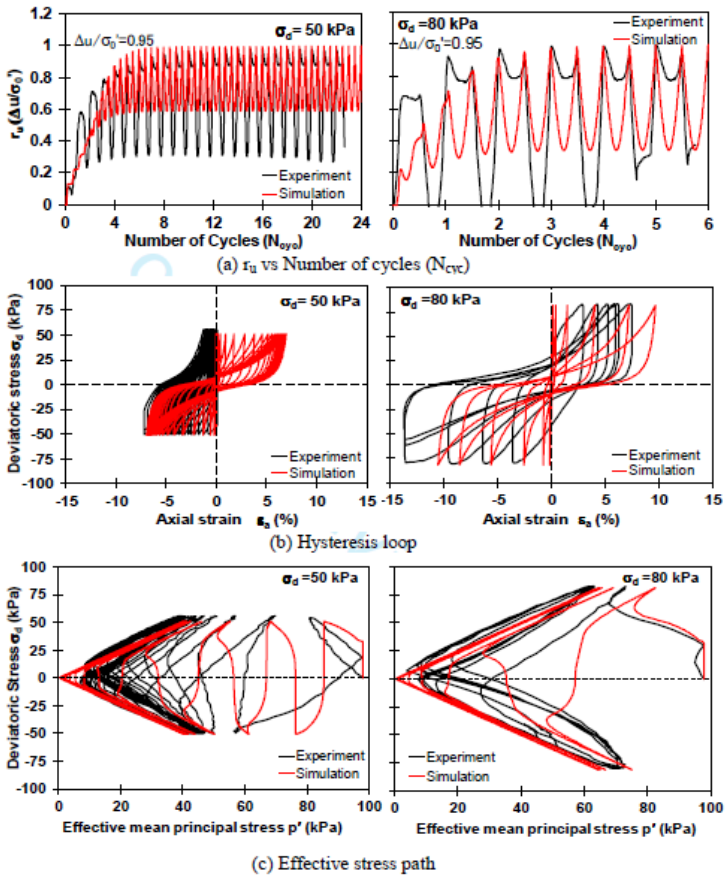

Figure 2.54 Cyclic triaxial test and model simulation results for the samples having a saturation degree of 63% (Mase et al. 2019)

Recent studies in the liquefaction of unsaturated soil have been carried out in France by Vernay and her colleagues. Vernay et al. (2015) carried out the triaxial test on the sample in the loose state (D_r = -0.1 – 0.18) with B value between 0.22 and 0.97. They concluded that the liquefaction can take place in unsaturated soil. This conclusion is also confirmed again by Vernay et al. (2016; 2017).

Vernay (2018) and Vernay et al. (2019) investigated the effect of suction, pore fluid compressibility, and saturation degree on the unstable behavior of Fontainebleau sand samples using cyclic triaxial tests. They divided the saturation degree into three zones to study.

- The unsaturated zone is characterized by a continuous gas phase and positive suction values. In this study, it ranges between 70% and 95% degree of saturation

- The quasi-saturated zone is characterized by a discontinuous gas phase, present in the form of dissolved air, or occluded bubbles. It ranges between 95% and 100% (excluded) degree of saturation;

- The last zone is the totally saturated zone, characterized by a single pore fluid, water. It corresponds to the particular case Sr = 100%.

Their results showed that the samples with an initial state in the quasi-saturation domain exhibited mechanical behavior similar to that of fully saturated samples. They all liquefied under the cyclic loading with CSR of 0.6. Besides, it can be seen that the lower the initial degree of saturation, the more the initiation of instability is delayed in terms of the number of loading cycles. Figure 2.55 shows the effect of the initial saturation degree on the liquefaction potential of the samples. In which the critical cycle is defined as the cycle having rapid and sudden decrease in shear strength, strong and rapid development of axial deformation, associated with strong development of pore overpressures.

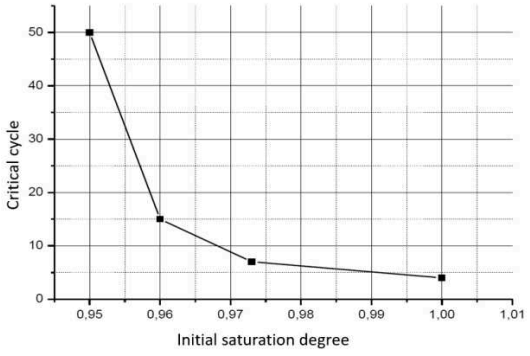

Figure 2.55 The critical cycle versus the initial degree of saturation (Vernay 2018)

Their study also showed clearly the effect of saturation degree on the development of pore water pressure in the samples having the same void ratio, subjected to the same cyclic loading but different initial saturation degree. Figure 2.56 shows the development of pore water pressure in function of number of cycles.

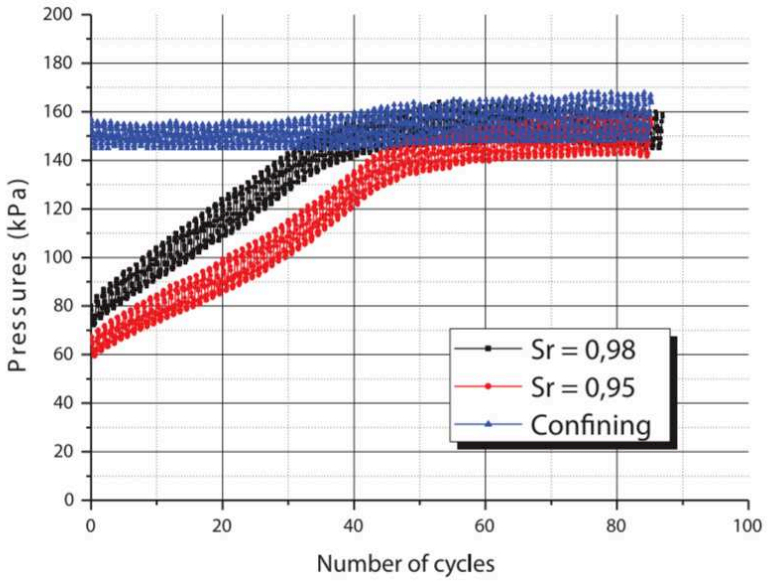

Figure 2.56 Development of the pressure ratio as a function of the number of cycles (Vernay et al. 2019)

When carrying out the test on the samples in the unsaturated zone, they found that there is a strong difference between saturated and quasi-saturated behavior and unsaturated behavior. Under the same condition including the CSR and initial relative density, the samples in the quasi-saturation zone were liquefied while there was no liquefaction observed on the samples in the unsaturated area.

When studying the volumetric behavior of the samples, they found that at the end of the cyclic loading, the samples with initial saturation degree lower than 100% reached a level of saturation very close to the state of total saturation. The development of the saturation degree and the void ratio in function of the number of cycles is shown in figure 2.57. It can be seen clearly that the saturation degree at end of the process is 100%.

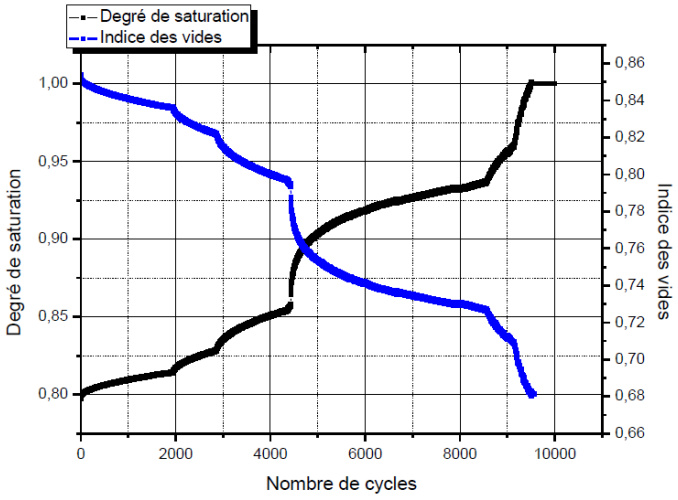

Figure 2.57 Development of the pressure ratio as a function of the number of cycles (Vernay 2018)

II.3. Conclusions

From the literature review of the liquefaction of unsaturated soil, it can be seen that this phenomenon has been considered by researchers since 1970s of the last century. These studies allow making a clear state of art and identify the issues needed to be solved to make better understanding of this phenomenon.

The first studies based on triaxial compression equipment confirmed the liquefaction ability of unsaturated soil. These studies also established the relationship between saturation and soil liquefaction intensity through parameter B. However, since the difficulty in the determination of this parameter in situ, the authors tried to make a relation between B with and saturation degree through experimental and modeling results. Subsequent studies have been carried out on undisturbed samples taken from the field which have shown the presence of air bubbles in the soil and the liquefaction potential of the undisturbed samples.

More recent studies have clarified the liquefaction mechanism of unsaturated sand. The studies have focused on the effect of the compressibility of voids in unsaturated sand on its liquefaction potential. This effect can be seen through the effect of some parameters on the liquefaction potential of sand like the backpressure and the sample volumetric strain during cyclic loading. Some authors have suggested using the possible volumetric strain as criteria for evaluating the liquefaction possibility of unsaturated soil.

Several studies have shown that the sand with a saturation degree less than 70% has no possibility of liquefaction. Meanwhile, it is clear that with saturation greater than 70%, the matrix suction in the sand is very small. Thus, the effect of the soil suction on the liquefaction potential is questionable and needs to be clarified.

Despite some achievements, much remain unclear about the behavior of unsaturated soil, there are still issues needing to be clarified such as: (i) the behavior before and after the main shock and their effect on the liquefaction potential; (ii) effect of the saturation degree on the cyclic stress ratio.

CHAPTER 3: MATERIALS AND METHODS

III.1 Introduction

From the literature review, it can be seen that the liquefaction of unsaturated soil has been poorly understood. This issue is partly due to the technical difficulty in working with samples in the unsaturated state; thus, not many laboratories could perform these experiments. The first challenge comes from the apparatus for dynamic triaxial testing; this device is always very expensive and complicated to master. The techniques to reconstitute the sample have also made some controversy. Most of the studies have used three techniques to reproduce the samples including wet tamping, dry deposition, and water sedimentation; however, they seem not able to make the samples exactly similar to the soil in the site. The wet tamping method is the most usually used method in triaxial testing, but the homogeneity in the sample produced by this method and its effect on the liquefaction of dense soil is not clear. Unlike the loose samples, the dense samples at the unsaturated state could be liquefied after a large number of cycles, and the heterogeneity of the soil in each sample can cause a big difference in the number of cycles causing liquefaction between tests although they have the same initial global void ratio. Another difficulty is the method to make the sample with a high saturation degree. Arab et al. (2016) used CO_2 and de-aired water to circulate the sample until reaching the required saturation degree. We tried to use this method but it seemed to take a lot of time to increase the saturation degree. Xia and Hu (1991) mixed the dry sand with the water in vacuum condition after that they reconstitute the sample. The advantage of this method is that the saturation degree can be controlled well but its possibility of applying on the sample with a high relative density is questionable. Besides, there are also many difficulties in accurately measuring parameters such as initial void ratio, volume deformation during loading, etc. which have been ignored in many previous studies. This study tries to provide some answers to these questions.

III.2 Material, apparatus

III.2.1. Material – RF Hostun sand

The material is fine quartz sand (Hostun RF) from Sika Co, a reference material in France to study liquefaction phenomenon (Colliat 1986; Fargeix 1986; Doanh et al. 1997; Benahmed 2001; Canou et al. 2002; Arab et al. 2016). This sand is mined from the Hostun quarry located in the Drôme region. It is a gray-white to beige-pink sand, siliceous (SiO_2> 99%), with sub-

angular to angular grains. A real image of sand is shown in figure 3.1 and a microscope photo of the sand particles at different enlargements is shown in figure 3.2 and they are angular to very angular grains. The grain size distribution is inside the zone of liquefiable soils defined by Iwasaki (1986) (Figure 3.3).

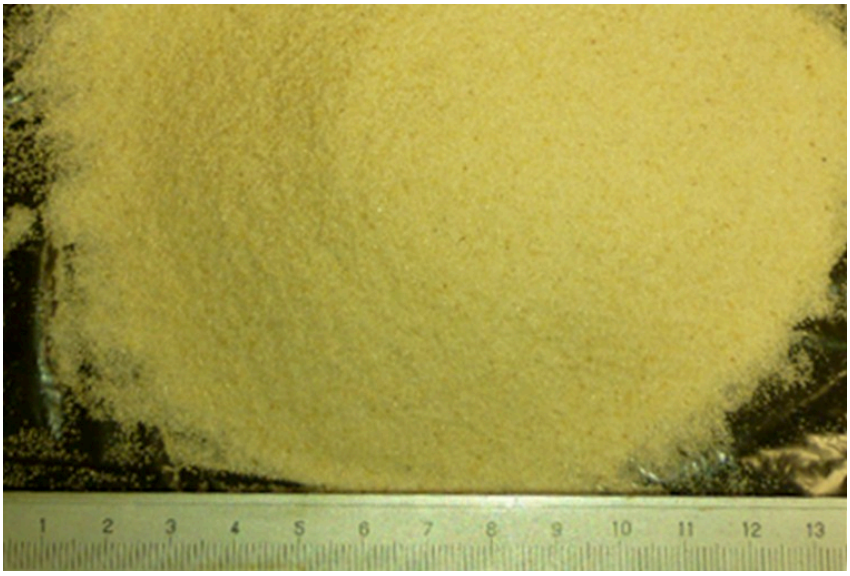

Figure 3.1 RF Hostun sand

This material has the following parameters: specific gravity 2.65 g/cm^3, maximum grain size 0.6 mm, minimum grain size 0.12 mm. Other parameters are shown in table 1. D_{10}, D_{50}, D_{60} are the diameters corresponding to 10, 50 and 60% of particles passing through the sieve, respectively, e_{max} and e_{min} are the standardized maximum and minimum values of void ratio.

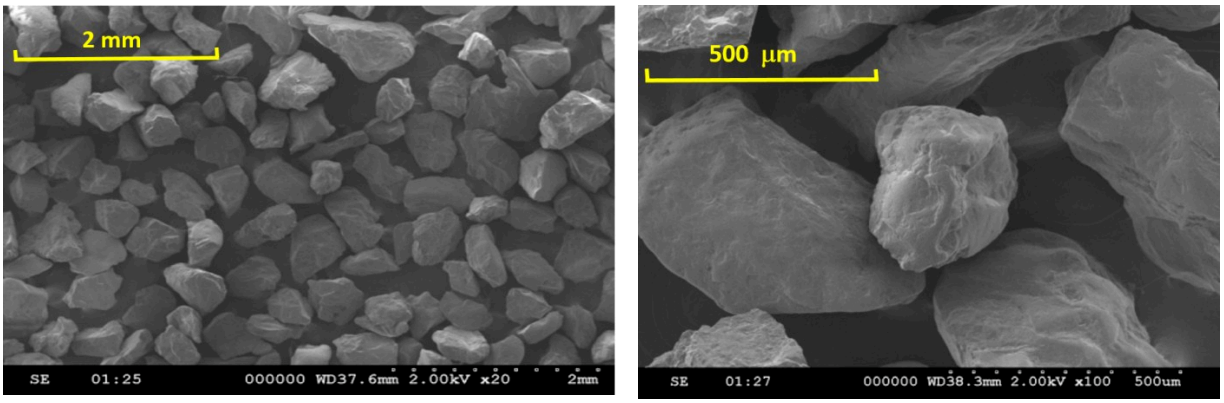

Figure 3.2 RF Hostun sand at different scales

Relative density or density index is defined as the ratio of the difference between the void ratios of the soil in its loosest state (e_{min}) and current state (e) to the difference between its void ratios in the loosest (e_{min}) and densest states (e_{max}). The relative density is calculated by equation 3.1:

$$D_r = \frac{e_{max} - e}{e_{max} - e_{min}} \qquad \text{Eq. 3.1}$$

Thus, the densest state corresponds to the relative density of 100% and the loosest state corresponds to the relative density of 0%.

The uniformity coefficient C_u of the grain size distribution is calculated as equation 3.2:

$$C_u = \frac{D_{60}}{D_{10}} \qquad \text{Eq. 3.2}$$

Table 3.1. The parameters of RF Hostun sand. (Fargeix 1986)

D_{50} (µm)	D_{10} (µm)	D_{60} (µm)	e_{max}	e_{min}	C_u
300	200	400	1.041	0.648	1.57

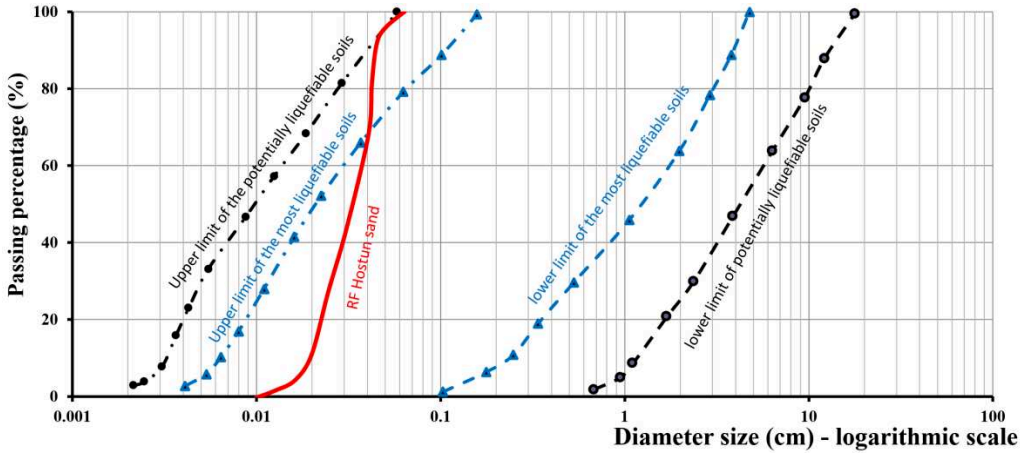

Figure 3.3 Comparison of the grain size distribution of Hostun RF sands to other liquefiable sands (Iwasaki 1986)

III.2.2. Dynamic triaxial system

III.2.2.1. Apparatus overview

The real picture of the apparatus used for dynamic tri-axial tests used in this study is shown in Figure 3.4 and its schema is presented in figure 3.5. The Dynamic (Cyclic) Triaxial Testing System 5Hz/5kN provided by VJ tech includes a dynamic controller to generate and control

dynamic parameters, i.e. force, displacement and pore water pressure. It is capable of providing fully automatic high frequency and load dynamic triaxial testing.

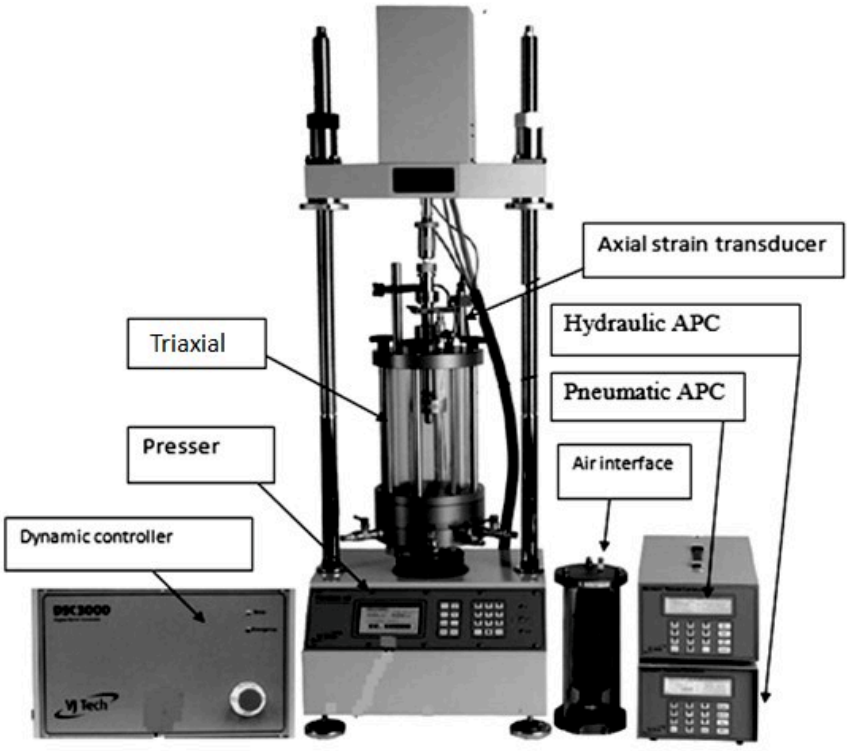

Figure 3.4 Triaxial dynamic testing apparatus

The cell pressure and back pressure are controlled by a Pneumatic Automatic Pressure Control (APC) device and a Hydraulic APC device, respectively. The pressure imposed by the Pneumatic APC is transmitted to the cell through an Air-Water Interface, in order to make the pressure more responsive.

The specimens used are 70 mm in diameter and 140 mm in high. Back pressure is applied on both top and bottom of the sample, while the pore water pressure is measured only at the bottom of the sample. The displacement can be measured by the dynamic controller or by the axial displacement transducer.

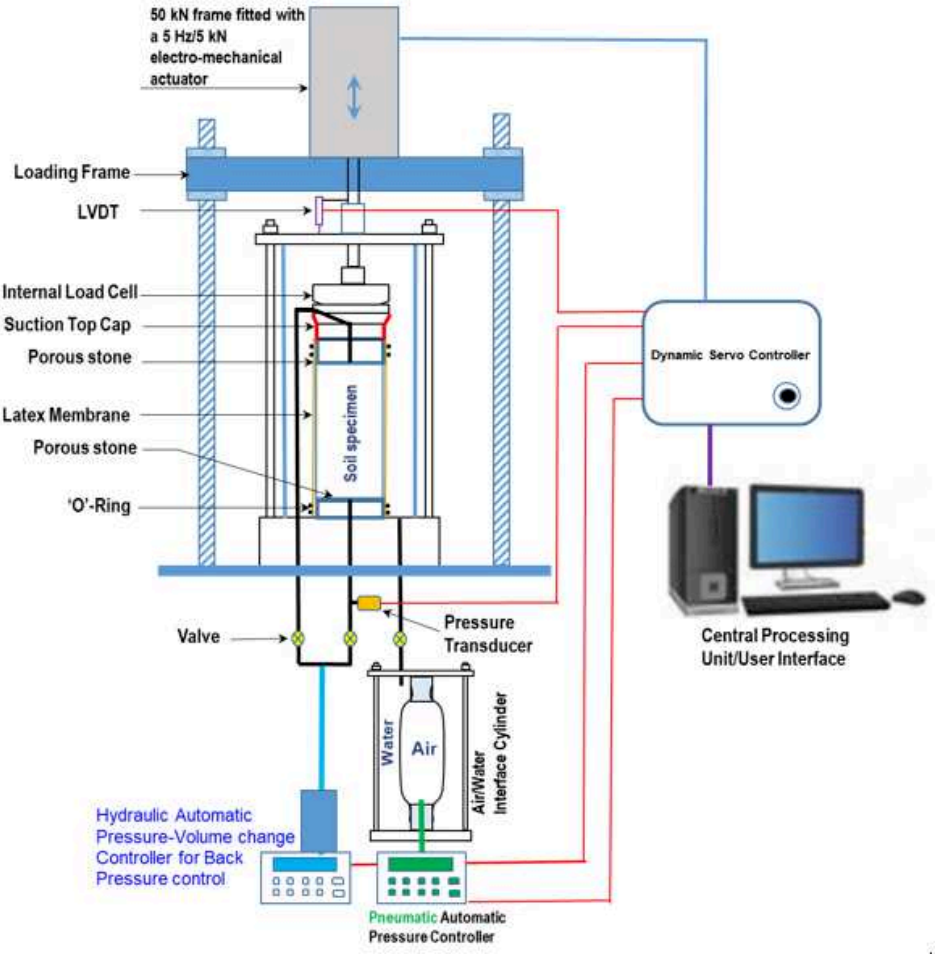

Figure 3.5 Schema of the triaxial dynamic testing apparatus

III.2.2.2. Axial loading and frequency calculation

The axial load with the maximum value of 5 kN is applied on top of the sample. The load is generated by an electro-mechanical actuator placed on the horizontal loading frame (Figure 3.4 and 3.5). There are two transducers used to measure the load. One is integrated with the electro-mechanical actuator and the other is placed on the top of the sample (Figure 3.5). This transducer allows measuring the load more exactly than the first one because the effect of connections and the inertia of the piston have been eliminated. This device also enables axial deformation control at a maximum speed of 90mm/min. The piston can fluctuate with a stroke $\Delta l = 95$mm, from the highest position to the lowest position.

As mentioned, one criterion for liquefaction is the double amplitude of axial strain in one loading cycle reaches 5%, from this condition, it can be calculated that with the sample

having the height of 140mm in this study, the position of the piston must be able to change at least 7mm in one cycle. The maximum value of the piston movement is 90mm/minute (or 1.5mm/second) so the maximum frequency is 0.1 Hz as calculated by equation 3.3 and the figure 3.6:

$$v_{max} = \frac{2.\varepsilon_a}{T_{min}/2} \leftrightarrow f_{max} = \frac{1}{T_{min}} = \frac{V_{max}}{4.\Delta_a} \qquad \text{(Eq. 3.3)}$$

where v_{max} is the maximum speed of the piston. This parameter depends on the apparatus. T_{min} and f_{max} are the minimum period and maximum frequency of the cyclic loading respectively. $2.\Delta_a$ is the double amplitude of axial deformation corresponding to the 5% of axial strain.

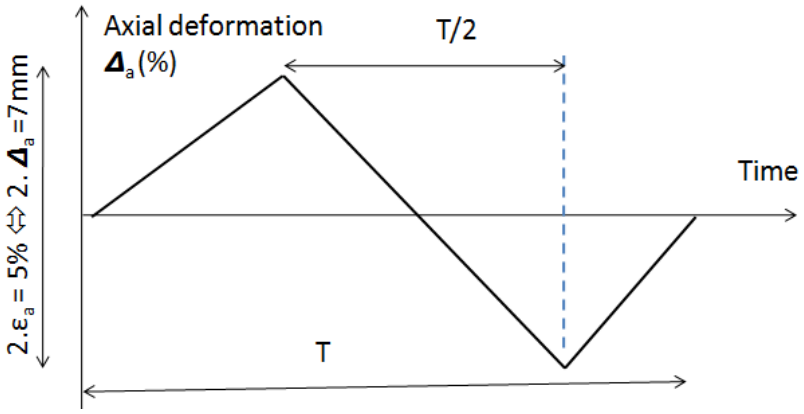

Figure 3.6 Diagram for loading frequency calculation.

III.2.2.3. Back pressure control system and pore water pressure transducer

The hydraulic automatic pressure control system allows applying back pressure in a range between 0 and 1000 kPa. It is also used to measure the sample volume change in drained saturated tests. This system can reserve maximally 200 cm^3 of water in its tank, thus, in the tests with soils in a very dense state when the sample volume changes significantly, it is necessary to set the initial amount of water appropriately. This device also allows programming to increase or decrease automatically the pressure at a given rate. This process is called RAMP and used to saturate completely the samples. To have the high accuracy in the sample volume change measurements, it is necessary to avoid loading tap water to this device because the tap water exists in the pipes under high pressure with a lot of dissolved air. When the tap water goes inside the device, under low pressure, the dissolved air is released and air

bubbles can appear inside the tank of the device. When the pressure increases, these air bubbles dissolve in the water again. In our laboratory, a solution, which is used to avoid this error, is using de-aired water instead of tap water.

The pore water pressure is measured at the bottom of the sample by a transducer. The range of this transducer is between 0 and 1000 kPa.

III.2.2.4. Cell pressure control system

The cell pressure is controlled by a Pneumatic Automatic Pressure Control (APC) device. The pressure imposed by the Pneumatic APC is transmitted to the cell through an Air-Water Interface. This device's duty is to make the pressure smoother and more responsive. It includes a rubber ball embed in a cell. The pressure generator controls the air pressure inside the rubber ball instead of cell pressure directly. Due to the construction characteristics of this device, the surface tension of the rubber membrane can affect the cell pressure measurement. In the process of carrying out the tests, it is necessary to avoid this error by filling the cell with enough water to have good shape of the membrane (Figure 3.7). With this device, the cell pressure can be controlled between 0 kPa and 900 kPa.

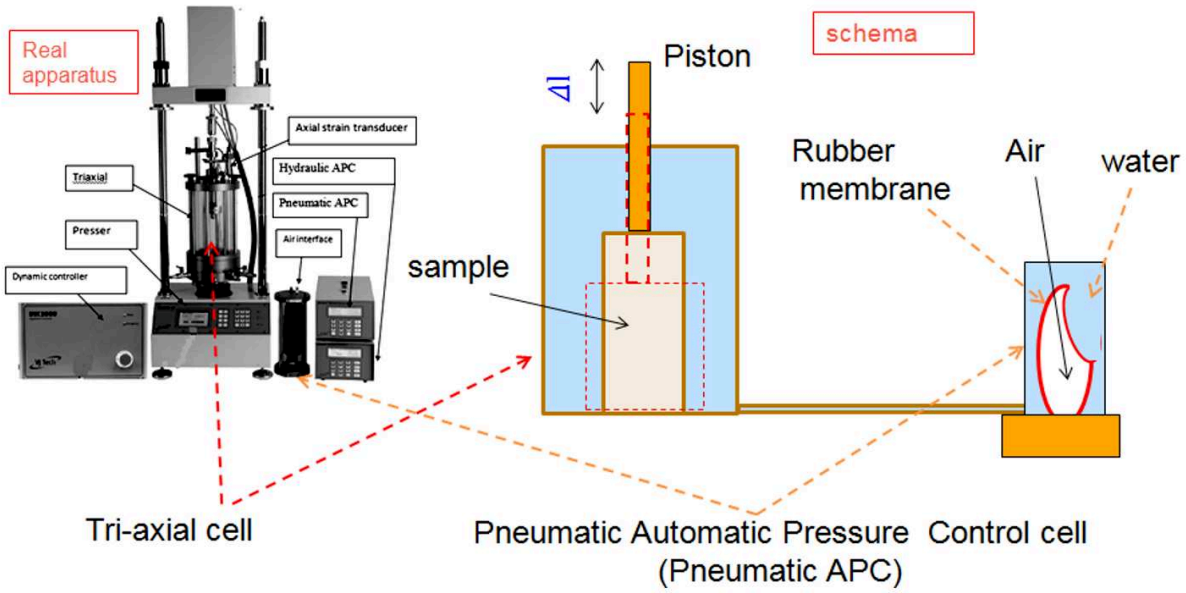

Figure 3.7 Cell pressure controller Pneumatic APC

III.2.2.5. De-air water supply system

De-air water is usually used to circulate the samples. The remaining air bubbles after the first stage of sample saturation dissipate into the de-aired water easier than tap water. Thus, de-aired water is important in making the sample with a high saturation degree. Figure 3.8 shows the de-aired water system in our laboratory. This system was also used to apply the vacuum to the sample in order to make the sample at a desired saturation level.

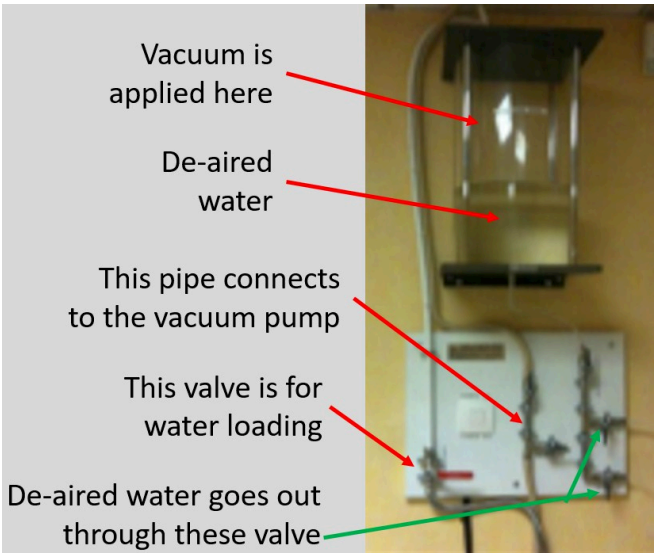

Figure 3.8 De-aired water system

III.2.2.6. Porous stone and permeable paper

In this study, the pore air was not measured. Thus, the porous stones installed at the two ends of the sample are to help draining the sample more easily (Figure 3.9). When the saturation degree is high, the air exists in the sample as bubbles (Zienkiewicz et al. 1999; Fredlund and Rahardjo 1993). These air bubbles cannot pass the permeable paper and the porous stone in draining processes like sample consolidations before and after cyclic loading mentioned later. Therefore, the volume of air in the sample is assumed to be unchanged throughout the experiment if the pore water pressure is stable. Besides, the permeable papers and porous stones are also useful in preventing the soil particles from entering the HAPC device.

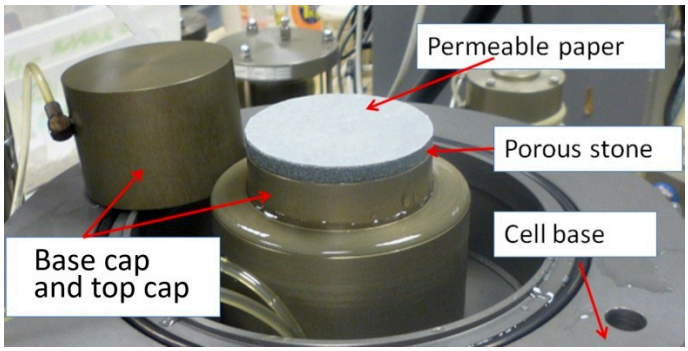

Figure 3.9 Porous stone with two layers of permeable paper.

III.2.2.7. Axial strain measurement

The axial strain varies during the test and it is measured by two transducers. One is integrated with the electro-mechanical actuator. The axial strain measured by this transducer has low accuracy due to the errors caused by the connections between parts of the device. The other transducer is fixed to the piston. This transducer allows measuring the relative movement between the piston and the cell ceiling (Figure 3.10). It is more exact than the first transducer because the errors caused by the connections have been eliminated. Its range is quite small, about 50 mm. This measuring method has some disadvantages as summarized by Vernay (2018):

- It is an external measurement system. The measurement obtained corresponds to the measurement of the displacement of the piston, which is assimilated to the vertical deformation of the sample, without taking account of the displacements which can be induced by other factors;

- This system is not precise enough on the measurement of small deformations and not suitable for detecting the start of deformation.

- The bad contact between the piston and the cell ceiling can cause a measurement error.

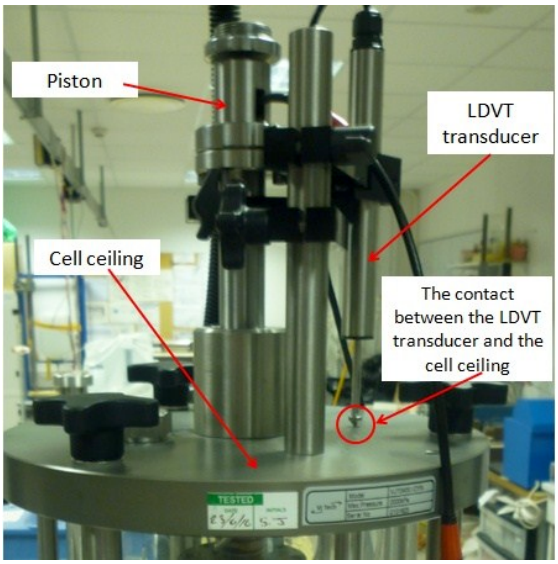

Figure 3.10 LVDT transducer

There is a notation when installing the LVDT transducer. As mention, the range of this transducer is quite small. Therefore, in the monotonic test when the required axial strain is high (20%), it is necessary to estimate primarily the position of this transducer. With the tests in this study, all the samples are in dense state, the initial appropriate position is corresponding to the initial strain input between 20 and 25mm

III.3 Test procedure

III.3.1. Sample preparation by the wet tamping method

From the literature review (Dang 2019), there are three methods often used to reconstitute samples: wet tamping, dry deposition, and water sedimentation. Amini et al. (2000) have shown that the resistance to liquefaction of soil prepared by the wet tamping and sedimentation methods are not significantly different. When the samples are prepared by the wet tamping method (Ladd 1978; Mullilis et al. 1978; Canou 1989), it is possible to prepare samples with a wide range of relative densities, even with negative relative densities, according to NF P94-059 French standards. It also avoids segregation between sand particles and gives effective control of the general relative density of the samples. When the samples are prepared by the dry deposition method (Ishihara 1993; Yamamuro and Lade 1997), the maximum void ratio that can be reached is considerably decreased and is comprised between the minimum and maximum void ratios given by NF P94-059 French standard. On the other hand, a number of studies have shown that specimens prepared by the wet tamping method

were generally more susceptible to liquefaction than water- or air-pluviated specimens (DeGregorio 1990; Hird and Hassona 1990; Vaid et al. 1999; Vaid and Sivathayalan 2000; Chu et al. 2003; Eliadorani and Vaid 2003). Wet tamping was also used in some of the most important tests to build up concepts depicting soil liquefaction, such as the steady-state or critical state (Poulos 1981), the state parameter defined as the combination of void ratio influence, stress level with reference to a steady state to describe sand behavior (Been and Jefferies 1985), etc. Since this study focuses mainly on the liquefaction phenomenon, the wet tamping method was chosen to prepare all the specimens as shown in figure 3.11 and figure 3.12. To prepare the samples, first, the sand was dried and then, a fixed quantity of water was added to have a mixture with the initial water content of 8%. Finally, the samples were made by compacting layer by layer until reaching the relative density of 83%. The sample size is 70 mm in diameter and 140 mm high. The specific steps are listed below to prepare the sample with an initial void ratio of 0.71

Step 1: Mix 824.9 (g) of dry sand with 204.57(ml) of water. Divide the mixture into 5 equal parts. Each part weighs 205.9 (g) (Figure 3.11)

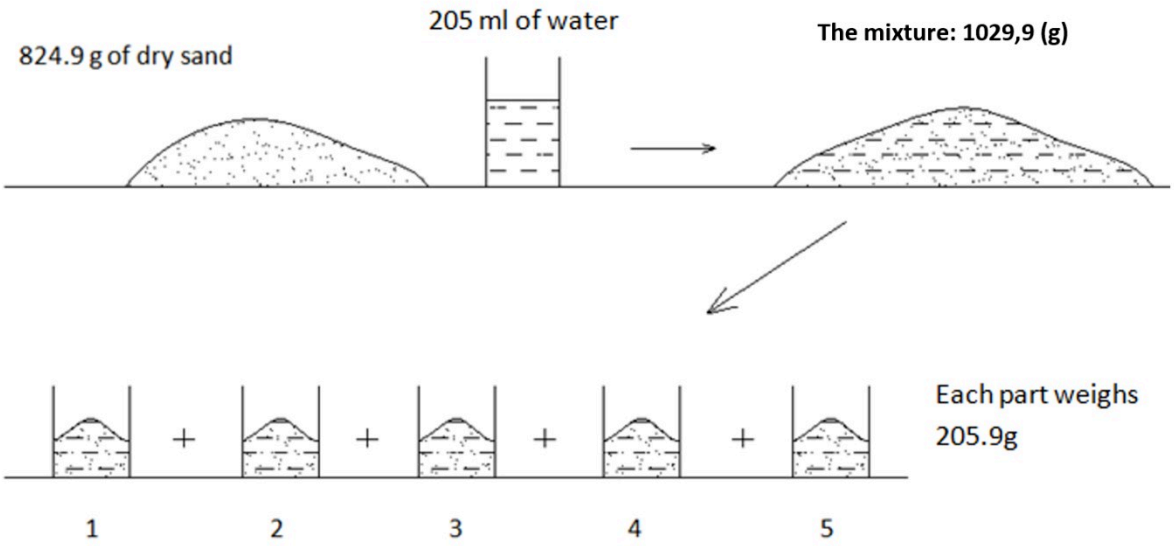

Figure 3.11 Mixing the dry sand with the water to have the mixture having 8% of water content.

Step 2: Installing the porous stone, the membrane, and the mold to the triaxial apparatus (figures 3.12 and 3.13b).

Step 3: The samples are formed by compacting layer by layer, each layer thickness is 28 mm. Put one by one part of the mixture into the mold, compact it until reaching the required height level. (Figure 3.12 and 3.13c)

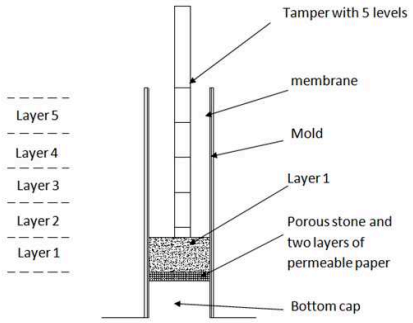

Figure 3.12Sample compaction in wet tamping method

Step 4: Installing the sample Top Cap, silicone funnel, and measuring the sample's dimensions (figure 3.13e and 3.13f)

Step 5: Installing the cell and transducers (Figure 3.13g)

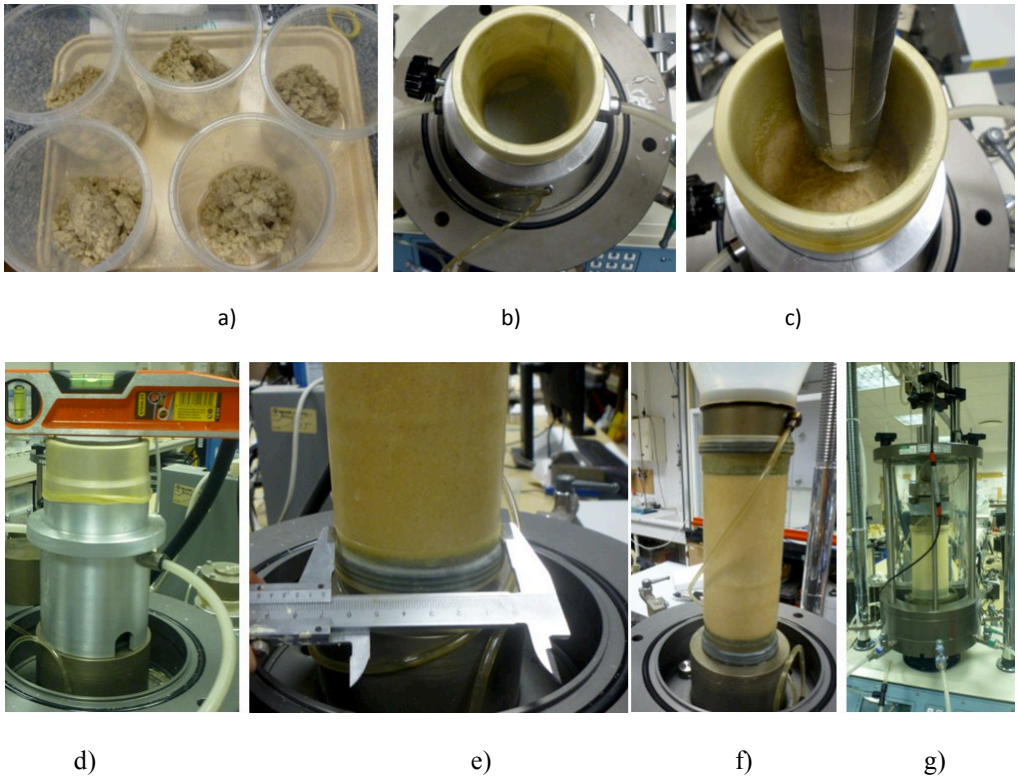

Figure 3.13 Sample preparation by wet tamping method

a) five parts of the sample, b) Porous stone, membrane, and mold installation, c) Sample compaction, d) Upper stone installation and sample balance check, e) Sample measurement, f) Sample top cap and silicone funnel installation, g) Installing the cell and axial strain transducer

III.3.2. Sample saturation and Skempton's parameter B measurement

There are a number of techniques to saturate samples prepared by wet tamping method. The first technique which is the most basic one is flowing de-aired water through the sample from the bottom to the top. However, this method does not result in full saturation because there are still air bubbles existing in the sample even if they do not appear in the outlet pipe. From our experience, the maximum saturation degree achieved in sand by this method is approximately 70%.

The second technique usually used to saturate the sample is saturation under vacuum. This method is more complicated, nevertheless more effective; samples are saturated by flushing water under vacuum condition. Similar to the first technique, the technique of using vacuum does not result in full saturation. According to our experience, the maximum saturation degree achieved by this method for sand is nearly 98%. To saturate completely the sample, after carrying out one of the two above-mentioned techniques, the third technique consists in increasing the cell and back pressures to 620 and 600 kPa, respectively. As mentioned in chapter I, the solubility air into water is proportional to the air pressure, thus, the higher the applied back pressure is, the easier the air dissolve into water. However, the maximum back pressure also depends on the capacity of the back pressure generator (HAPC). In our case, preliminary tests showed that the chosen values are a good compromise to fulfill these conditions. After reaching the target value, the pressures were left to equilibrate for 4 days to be sure that the air dissipates completely into water. A technique was used to predict the full saturation state of samples. Under high pressure, the remaining air bubble was contracted and dissolved into the de-aired water. To maintain the backpressure, the water from Hydraulic APC came into the sample to replace the dissipated air volume. This trend finished when air bubbles inside the sample have been dissolved completely and de-aired water stopped coming into the sample. It also means the stabilization of water volume in Hydraulic APC was used as an indication for a full saturation state.(see figure 3.14). In this study, we used the second and third techniques for saturated tests, and the second technique for unsaturated tests.

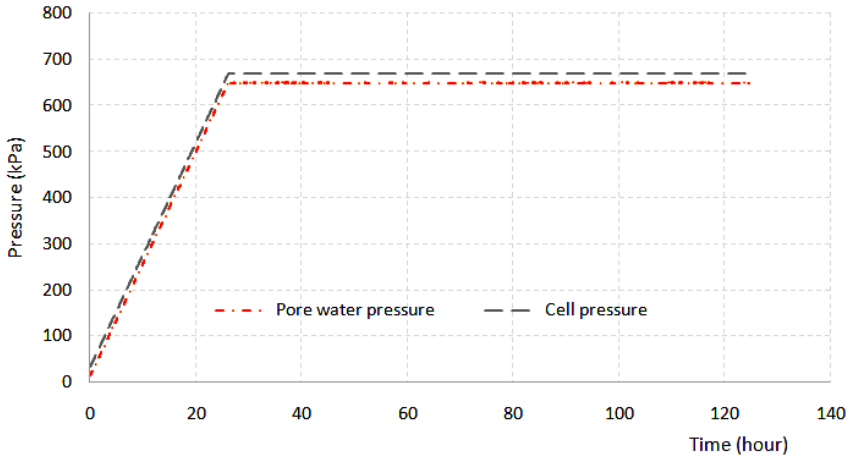

Figure 3.14 The variation of controlled pore-water pressure and cell pressure during sample full saturation process

After sample saturation, Skempton's coefficient B was used to check the saturation of the samples. To do this experiment, first, all the back pressure valves are locked. Then, the cell pressure is increased. This growth of pressure results in an increase in the pore water pressure. The ratio between the measured pore pressure increase and the imposed cell pressure increase is defined as Skempton's coefficient B:

$$B = \frac{\Delta u_w}{\Delta \sigma_3} \qquad \text{(Eq. 3.4)}$$

where $\Delta\sigma_3$ and Δu_w are the imposed increment of confining stress and the resulting measured increment of pore water pressure, respectively.

III.3.3. Sample consolidation

To consolidate the sample, firstly, all back pressure valves were closed and then the cell pressure was increased to have the difference of 100 kPa between the cell pressure and the back pressure. Then the back pressure valves were opened. The water went out of the sample through both ends due to the imbalance between the back pressure and the increased pore water pressure. The effective stress increased gradually and reached 100 kPa at the end of the process. The variations of cell pressure and back pressure during B measurement (B check) and sample consolidation process of the saturated tests and the unsaturated tests are respectively shown in figure 3.15 and figure 3.16.

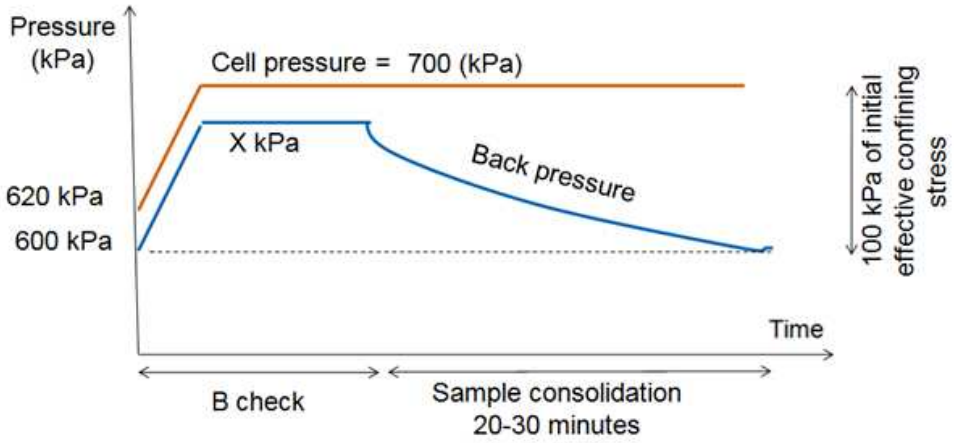

Figure 3.15 Cell pressure and back pressure variations during Skempton's parameter B measurement and sample consolidation process of saturated tests.

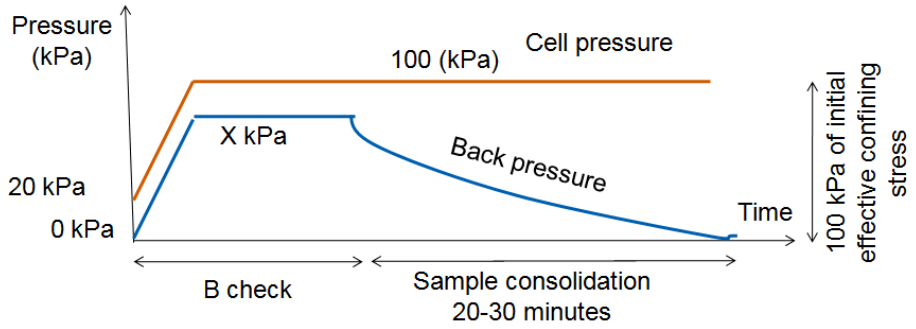

Figure 3.16 Cell pressure and back pressure variations during Skempton's parameter B measurement and sample consolidation process of unsaturated tests.

III.3.4. Deviator cyclic loading

III.3.4.1. Load parameters

In most studies of the liquefaction phenomenon, the load was chosen with the aim to reproduce similarly the load appearing during the earthquakes. During an earthquake, the waves do not propagate in a single direction but in several directions. In one direction, the earthquake wave includes two elements: the horizontal wave and the vertical wave. Seed and Idriss (1982) recognized that the waves propagating as vertical direction are predominant. Under these earthquake waves, the soil grains tend to move closer together, the void between grains decreases and water in the void tend to drain. However, the earthquake waves usually impact a very large area; thus, the water cannot drain in a short period of time during the earthquake. This happens even with sandy soils, which have good permeability. One method

to simulate these conditions is applying the cyclic load to the sample in the triaxial cell in the undrained condition. What needed to consider here are the parameters during the experiment including the form of cyclic loading wave, the load frequency, and the value of the cyclic stress ratio (CSR). It can be seen that the effects of these parameters have been understood clearly in saturated liquefaction tests but not obviously in the tests on unsaturated soils. The frequency of the cyclic loading in laboratory tests usually chosen based on two factors: the first one is the ability of the apparatus and the second one is to simulate similarly the real frequency in earthquakes. As calculated in part III.2.2.2 this chapter (equation 3.3), the maximum frequency which can be performed by this apparatus is 0.1 Hz. For the second factor, load frequency, from the literature review performed by Vernay (2018), there is not much information regarding the proper frequency using for cyclic testing on unsaturated soils. On the other hand, there has been more work done on the influence of the shear rate on the shear strength measurements of unsaturated samples. Fredlund and Rahardjo (1993); Ho and Fredlund (1982) have worked extensively on the influence of shear rate on the measurement of shear strength in soils. They showed that the shear speed must be chosen according to the physical properties of the material tested (compressibility and coefficient of permeability), as well as according to the drainage conditions. They gave some guidance but this guidance is for monotonous loading tests. Authors such as Unno et al. (2008) and Tsukamoto et al. (2014), who work extensively on the cyclic behavior of unsaturated sands, used the frequency of 0.01 Hz for their cyclic triaxial tests. The specific frequency for each group of tests in this study is chosen so that the experiment time was not too long and the frequency is also not too high in order to avoid the errors caused by the limited capacity of the apparatus.

Similar to the load frequency, there is an ambiguity in the effect of the waveform of the cyclic loading on the liquefaction behavior of unsaturated soil although many studies have pointed out that this parameter does not affect significantly to the liquefaction behavior of the saturated soils.

Another important parameter in cyclic liquefaction testing is the cyclic shear stress (CSR). It is defined by the equation 3.5:

$$CSR = \frac{q^c_{\max}}{2\sigma^{'}_{3c}} \qquad \text{Eq. 3.5}$$

Where $q^c_{\max}/2$ is the maximum cyclic shear stress, $q^c_{\max}$ is the amplitude of deviator dynamic stress. $\sigma^{'}_{3c}$ is the effective consolidation stress.

In this study, the tests were classified into two groups. The choice of the specific frequency, the waveform, and the CSR for each group of tests are presented in detail in the next parts.

III.3.4.2. First group: Cyclic loading with constant CSR

In the first group of tests, all samples at different level of saturation degree were subjected to the cyclic loading until liquefaction. The cyclic stress ratio (CSR) varies between tests; however, is constant in each test. The frequency of cyclic loading was 0.05Hz. Figure 3.17 shows the wave form and other parameters for the load case having CSR of 0.15.

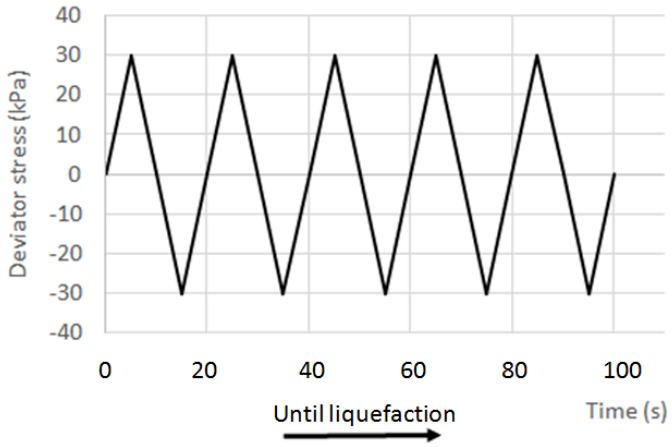

Figure 3.17 Constant CSR cyclic deviator stress

III.3.4.3. Second group: Cyclic loading with stepping CSR

One hundred cycles of loading-unloading with a saw-tooth form and a frequency of 0.1 Hz were applied to the top of the sample.

The amplitude of the deviator stress was chosen initially to be 30 kPa corresponding to the cyclic stress ratio of 0.15. After 100 cycles of the first cyclic load case, if the sample was still not liquefied, the amplitude of the CSR was increased to 0.20 (i.e. by steps of 0.05) and 100 cycles were applied, until liquefaction. In case the sample showed a clear tendency to liquefaction, the test was continued with unchanged CSR and, in that case, the number of cycles of the final load case would be larger than 100, such as in Test 2. Otherwise, the CSR was increased of 0.05 to 0.25, and so on (Figure 3.18).

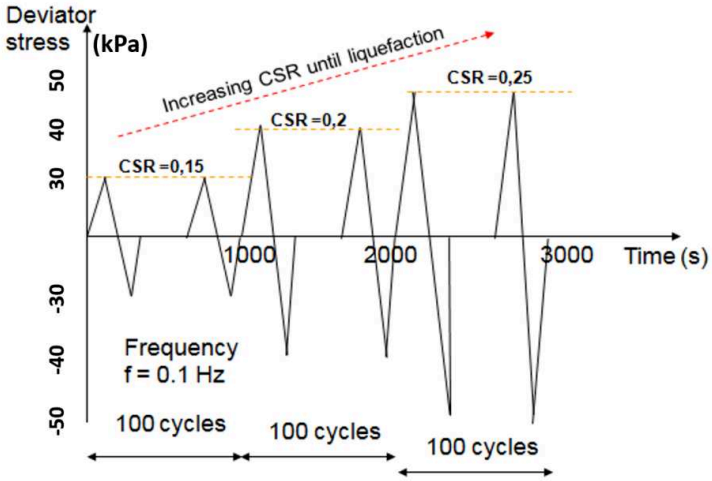

Figure 3.18 Stepping CSR cyclic loading

III.3.5. Monotonic loading after liquefaction

Two series of tests were carried out to evaluate the residual strength of soil after liquefaction. The first series of tests were carried out on the sample liquefied under constant CSR cyclic loading. The second series were carried out on the sample liquefied under stepping CSR cyclic loading. The loading process for each series is presented more detailing bellow.

III.3.5.1. Compressed monotonic loading

After liquefaction, the samples were subjected to monotonic strain controlled loading. The tests were carried out in drained condition. The samples were compressed until the relative axial strain reaches 20% to study their residual strength. The axial strain variation is illustrated in figure 3.19

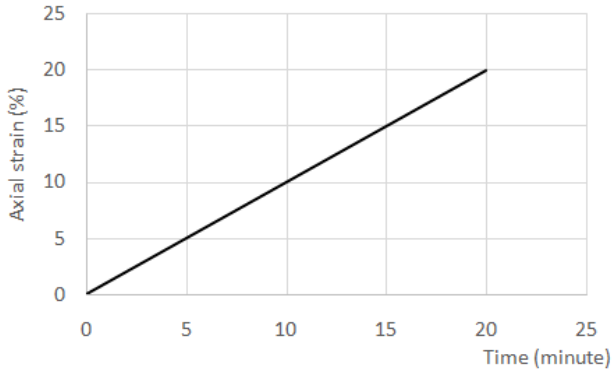

Figure 3.19 Axial strain variation for the sample monotonic loading after being liquefied by constant CSR cyclic loading

III.3.5.2. Closed loop monotonic loading

After liquefaction during earthquake or other dynamic loadings, the pore water pressure dissipates and the soil is reconsolidated. To better understand the unsaturated sand behavior after liquefaction, the sample in drained condition was compressed to reach axial strain of 5 %, which was chosen so as not to damage the sample. After that, the samples were stretched to -15% to study the residual strength in extension. The axial strain variation is illustrated in figure 3.20 and the tests were in drained condition.

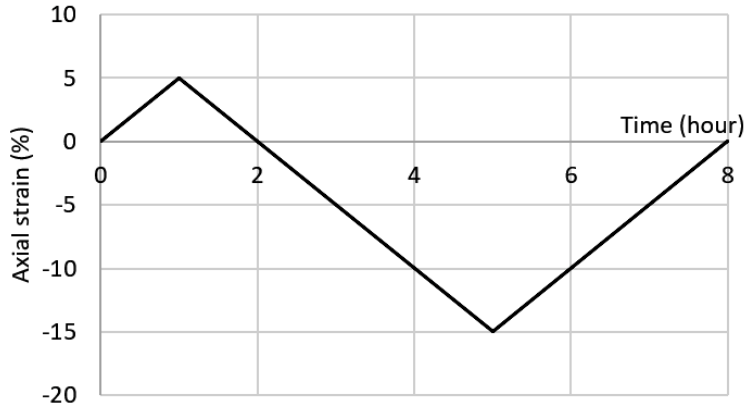

Figure 3.20 Axial strain variation for the sample monotonic loading after being liquefied by stepping CSR cyclic loading

III.3.6. Sample removal after the tests

The sample removal is to measure the water volume and the dry sand weigh inside the saturated sample. From this value of water volume, it is possible to calculate the sample volume and the void ratio before and after liquefaction. This test is necessary because from the sample preparation phase to the shearing phase, the sample undergoes significant volume variations which essentially take place during the mould removal, the saturation phase and the consolidation phase. These changes significantly modify the void ratio. If they are ignored, these variations in volumes can constitute a significant source of error in the exact estimation of the voids ratio before shearing which consequently generates an error in the determination of the ultimate resistance of the soil when assessing the liquefaction potential.

The volume variations during the consolidation phase can easily be determined by making direct measurements of the volume of water going out of the sample. However, the volume variations caused by saturation are quite difficult to measure. Indeed, the circulation of water

through the sample during this phase decreases the capillary force created by the humidification of the sand during the sample preparation by the wet tamping method. As a result, collapse-like deformations result, this leads to the densification of the sample. Although this problem has attracted particular attention from researchers, the number of solutions proposed remains quite limited.

Castro (1969) was the first to note the densification of the sample during the saturation phase. Based on the isotropic deformation hypothesis, he corrected the final void ratio by taking the volume deformation equal to three times the axial deformation he measured. Sladen and Handford (1987), noting that the densification of samples during saturation is very important and increases with the percentage of fine elements, propose a direct method of evaluation of the void ratio based on the freezing method and the calculation of their water content at the end of the tests.

Verdugo and Ishihara (1996) made a comparison between the commonly used method based on direct measurements of the height and diameter of the sample and that based on the measurement of the amount of water present in the sample at the end of the test. They show that the latter gives more precise results of the value of the void ratio.

The above studies were carried out on the saturated sample. However, it is more difficult with the unsaturated sample because the sample volume includes three elements: the water volume, the air volume, and the soil particle volume. To overcome the difficulty in calculation caused by the appearance of air bubbles, our solution is saturating completely the sample before carrying out the measurements. There is an assumption used in this method. In the vicinity of saturation, the pore air is considered as the bubbles embedded in pore water (Okamura and Soga 2006; Bian 2007; Fredlund and Rahardjo 1993). Consequently, the pore pressure is due to a homogenized and compressible pore fluid, composed of a mixture of water and occluded air. In this area, Terzaghi's effective stress concept remains valid (Biarez et al. 1991; Fleureau et al. 1992; Fleureau et al. 1993a, b). Therefore, it is reasonable to assume that the increase of saturation degree from this state to the full saturation state does not result in the sample volume change and the air volume does not change if the pore water pressure is kept stable.

The steps to measure the parameters after the tests are presented below:

Step 1: Saturate completely the sample after the test.

With the assumption that the sample volume does not change during this step, the air volume is taken as the water volume going into the sample. This volume is called V_a (Figure 3.21).

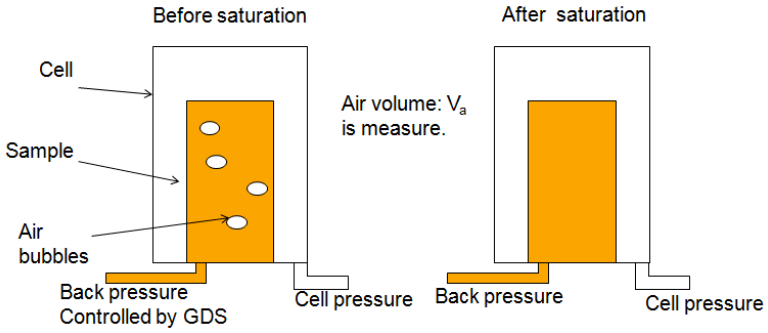

Figure 3.21Sample saturation to measure the saturation degree

Step 2: Remove the sample and measure the water volume, the soil particle weight (figure 3.22). The total volume of the sample is calculated as equation 3.6:

$$V_{T-end} = \frac{M_{water}}{\gamma_{water}=1} + \frac{M_{sand}}{\gamma_{sand}=2.65} \qquad \text{Eq. 3.6}$$

where M_{sand} is the weight of the dried sample after removing; M_{water} is the weight of the water existing in the fully saturated sample at the end of the test. It is calculated by subtracting M_{sand} from the total weight of the sample after removing.

a) b) c) d)

Figure 3.22 Sample removal

a) Sample after removing the triaxial cell, b) drying the membrane, c) removing the sample, d) measure the total weigh of the sample

III.3.7. The measurement of the sample volume changes during the tests

The measurement of total volume change in the unsaturated tests is much more complicated than in saturated tests. Because in saturated soil, there is no air bubble, if the compressibility of the water is negligible, the total volume change is equal to the water volume change, and it can be easily measured by the volume change controller. In the drained tests on unsaturated

soil in a quasi-saturated domain, it is also possible to measure the sample volume change by this method if considering that the air bubbles are embedded in pore water and its volume does not change during the draining process. However, in the unsaturated undrained tests, the volume change is caused by the compressibility of air bubbles inside the samples.

From literature review, there are three methods to measure the sample volume change in tests for unsaturated soil: 1) cell fluid measurement, 2) direct air and water volume change measurement and 3) direct measurement on the specimen. In this study, the first method was used to measure the sample volume change.

If not mention the volume changes when removing the mold and during saturation process, the sample volume changes include the elements as presented in the figure 3.23.

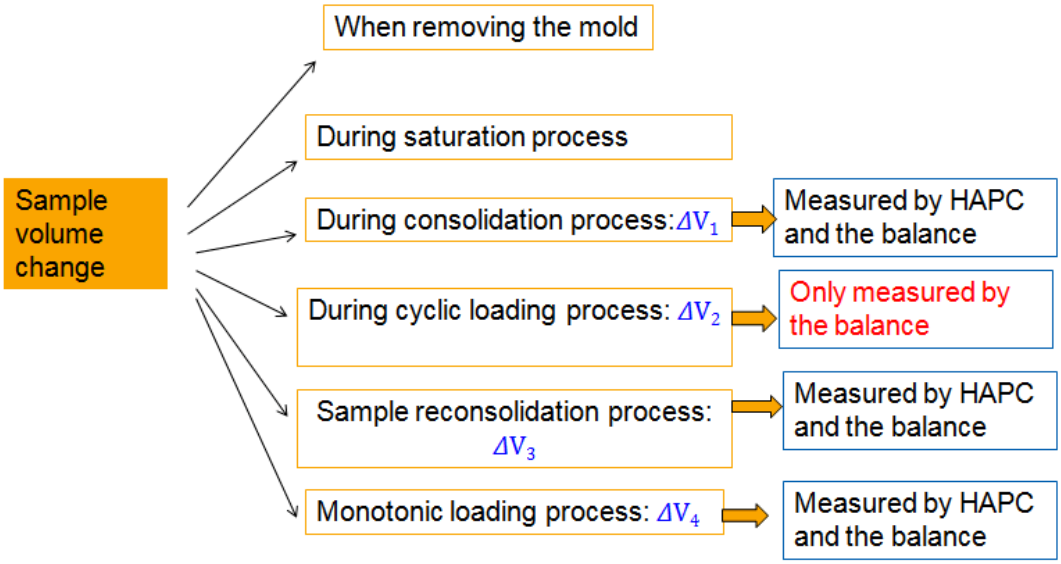

HAPC: *Hydraulic Automatic Pressure-volume Control*

Figure 3.23 Sample volume changes from the consolidation to the end of the tests.

In this study, two methodologies were used to measure the sample volume change in each step of the tests. The first method is using the function of HAPC (Figure 3.4 and 3.5). This device works as a volume change controller and the sample volume changes were measured through the water volume leaving the sample in drained processes (ΔV_1, ΔV_3, and ΔV_4). However, this method cannot be used to measure the sample volume change during cyclic loading because this process is in undrained condition. To overcome this challenge, we developed a method allowing measuring the sample volume change during cyclic loading through the water volume going out or in the triaxial cell (Figure 3.24)

In the second method, the highly sensitive balance was used to measure the water volume change of triaxial cell. The room temperature was controlled at 27^0C. This method can recognize the volume change of 0.1 cm^3 corresponding to the change of 0.1g recorded by the balance. The sample volume change is calculated by the water volume change measured by the balance subtracting the volume change caused by the movement of the piston (Equation 3.7)

$$\Delta_{v2} = \Delta_{v-b} - \Delta_{v-p} \quad \text{(Eq. 3.7)}$$

where Δ_{v2}; Δ_{v-b}; Δ_{v-p} are the sample volume change (figure 3.23), the volume change measured by the balance and the volume change caused by the movement of the piston, respectively.

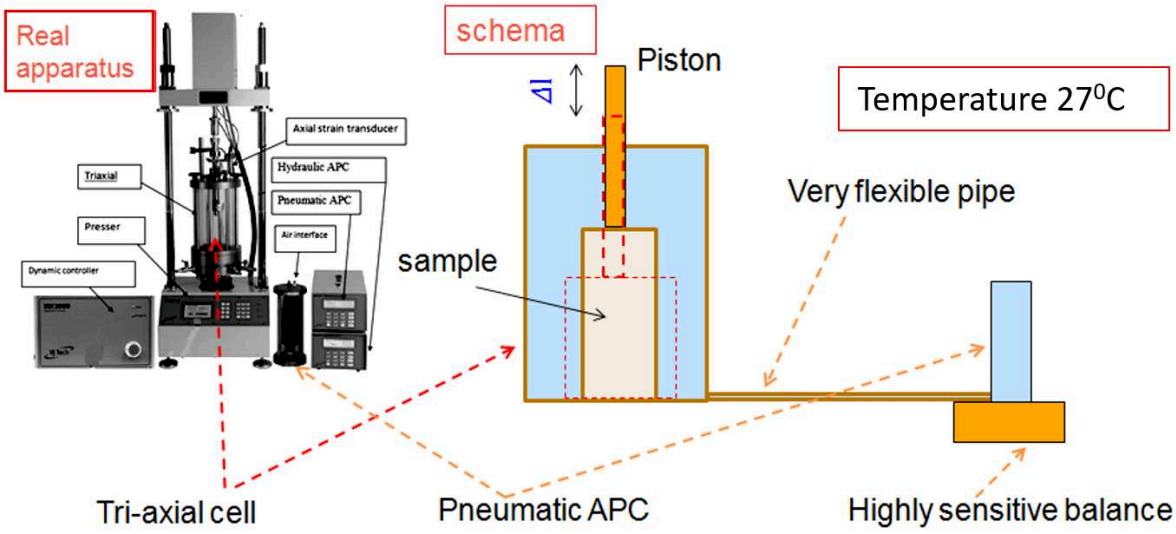

Figure 3.24 Using balance to measure the sample volume change during cyclic loading.

The advantage of the method of using the balance as presented is simple and easy to use in any laboratory; however, it just allows recognizing the initial and the last value of the sample volume change during cyclic loading. It is impossible to follow the sample volume change continuously during the process.

III.3.8. Block diagrams for the test procedure

III.3.8.1. Tests with constant CSR cyclic loading

Figures 3.25 and 3.26 summarize the protocol for the tests on saturated and unsaturated samples subjected to constant CSR cyclic load.

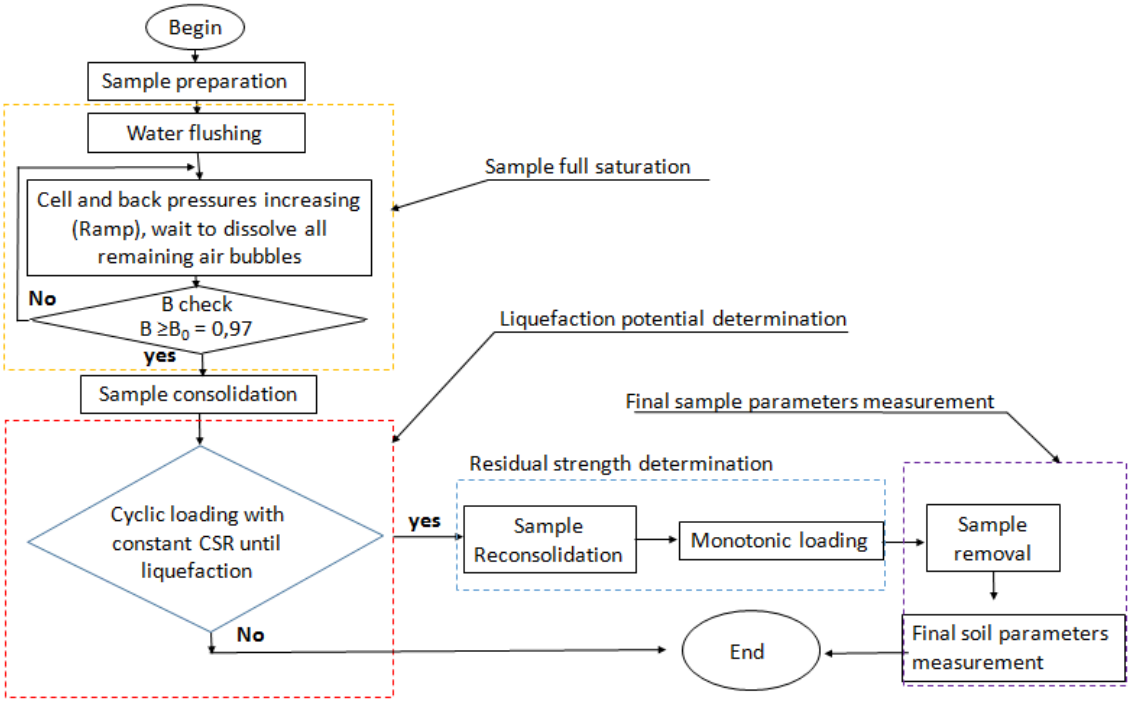

Figure 3.25 Procedure for the saturated tests subjected to constant CSR cyclic loading

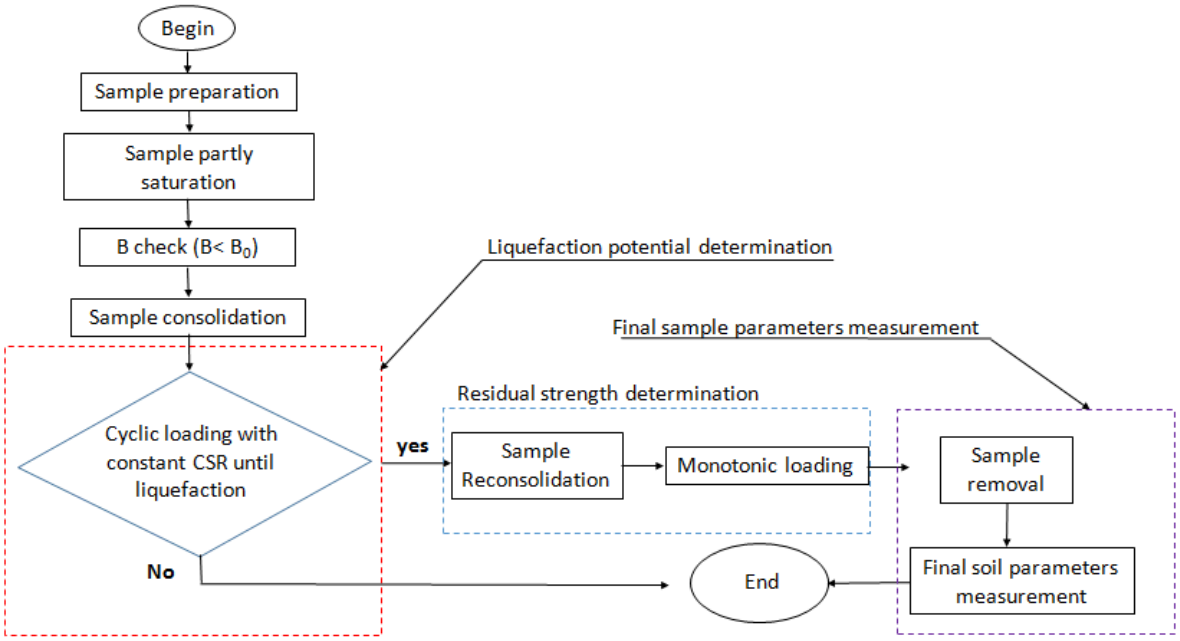

Figure 3.26 Procedure for the unsaturated tests subjected to the constant CSR cyclic loading

III.3.8.2. Tests with stepping CSR cyclic loading

Two following diagrams (figures 3.27 and 3.28) summarize the protocol for the tests on saturated and unsaturated samples subjected to stepping CSR cyclic load.

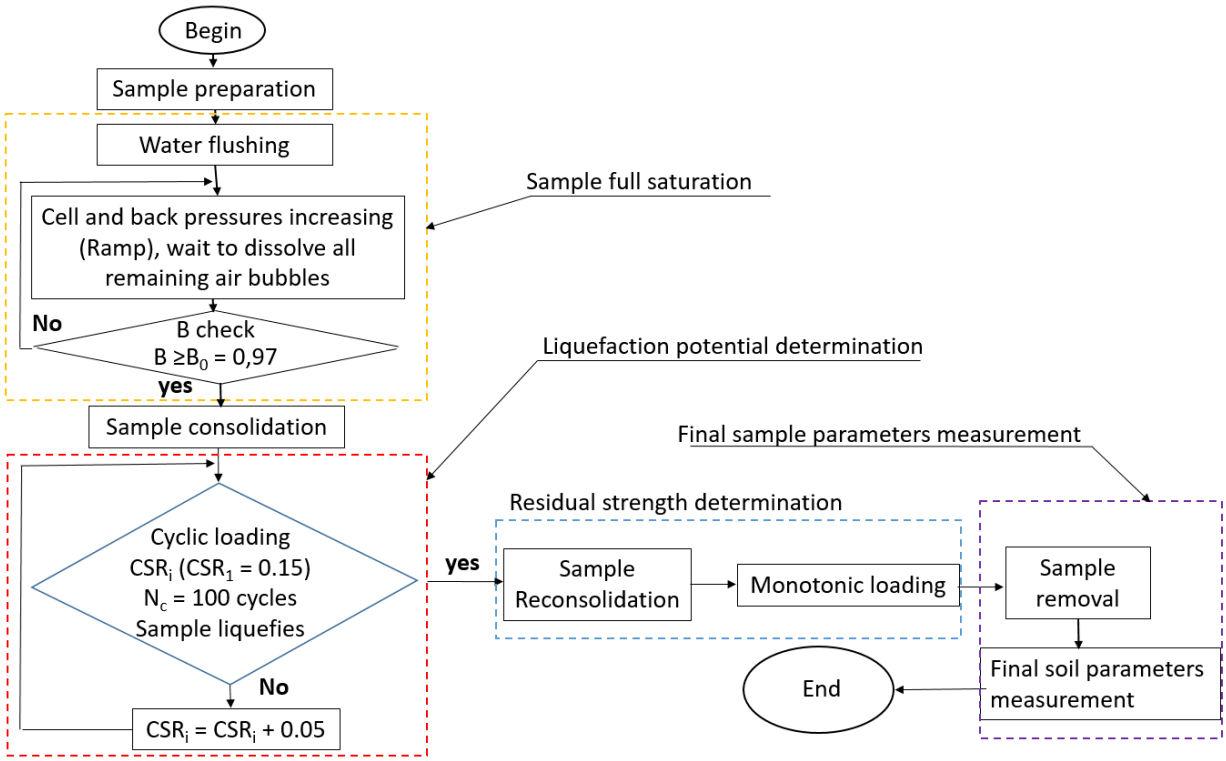

Figure 3.27 Procedure for the saturated tests subjected to stepping CSR cyclic loading

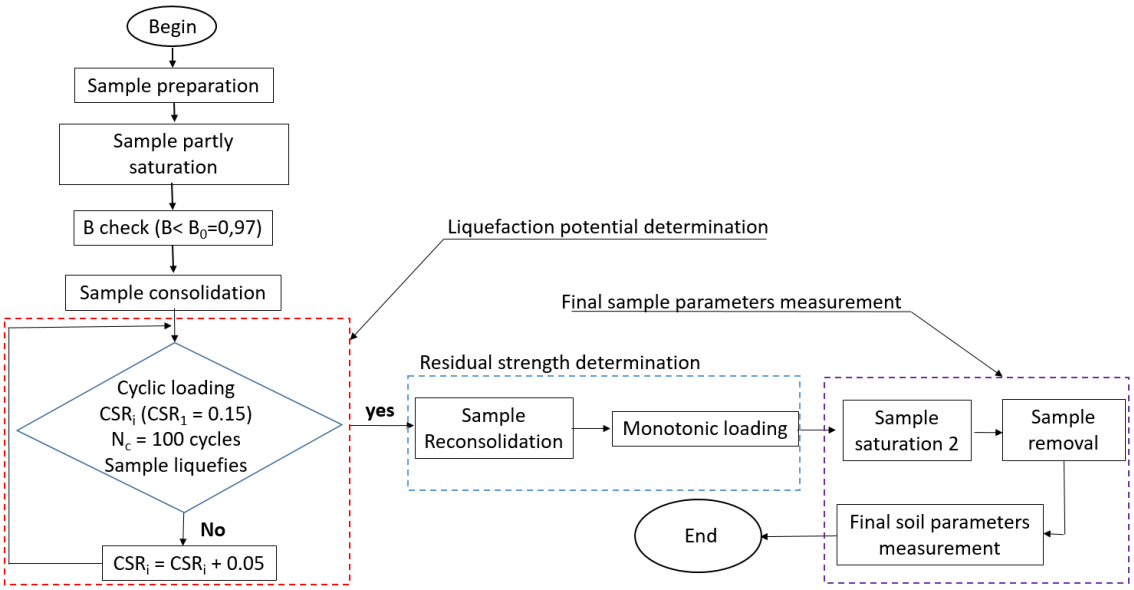

Figure 3.28 Procedure for the unsaturated tests subjected to stepping CSR cyclic loading

III.4 Conclusions

An experimental protocol is established in which the main challenge for the unsaturated soil liquefaction tests has been handled quite well. The protocol allows reconstituting the samples having a saturation degree from unsaturated to fully saturated states. The main parameters of tests including void ratio, saturation degree, and sample volume change can be measured or calculated for each stage of the tests. These parameters are very important to understand the liquefaction behaviour of soil; however, not mentioned in many previous studies. In this protocol:

- The wet tamping method is chosen to make sand samples.
- The samples were saturated by two methods: (i) using vacuum and (ii) using vacuum and increasing pore water pressure and cell pressure to dissolve the remaining air bubbles inside the samples.
- There are two methods of imposing CSR used to liquefy the samples: (i) constant value of CSR until liquefaction and (ii) stepping value of CSR after 100 cycles until liquefaction.
- A method was proposed to measure the volume change of unsaturated tests.
- Two different monotonic loading ways were used to study the residual strength of sand after liquefaction: (i) monotonic loading with the axial strain varying from zero to 20% and (ii) the closed loop axial strain.

- A method was proposed and developed for the unsaturated liquefaction test to measure the void ratio of the sample at the final state.

CHAPTER 4: EFFECT OF UNSATURATION ON LIQUEFACTION POTENTIAL
-Cyclic Loading with Constant CSR-

IV.1. Introduction

Recent studies have achieved some results and it is clear that liquefaction can be observed not only in saturated soil but also in unsaturated sandy soils. The theoretical study of Martin et al. (1978) showed the effect of partial saturation on the cyclic shear strength of sands. They concluded that there is a significant increase in stress ratio causing initial liquefaction with only a small reduction from full saturation. The effect of the saturation degree on soil liquefaction has been also confirmed by the laboratory results (Chaney et al. 1978; Yoshimi et al. 1989; Vernay et al. 2019; Tran et al. 2018a,b; Tran et al. 2019a,b), and tests on undisturbed samples (O-hara et al. 1974;Fourie et al. 2001; Mase et al. 2019).

In this chapter, to study the effect of saturation on the strength of Hostun sand during and after liquefaction, three series of tests were carried out. In the first series, all the samples have the saturation degree at 100%. In the second series, the saturation of the samples is approximately 95%. The saturation in the last series was decreased to approximately 86%. The cyclic loading applied to liquefy the sample has the constant CSR. In other words, the load amplitude was kept stable from the beginning to the end of tests. In each series, the CSR is decreased after each test until no liquefaction observed. One monotonic loading test was applied after the sample liquefaction to study the residual strength of the soil. The summary of these three test series is shown in table 4.1:

Table 4.1. Summary of the test series

N° of the test series	**Initial saturation degree (%)**
Series 1	100
Series 2	95
Series 3	86

IV.2. Liquefaction potential and residual strength of saturated sand

IV.2.1. Liquefaction potential of saturated sand

IV.2.1.1. Test program

The first series of tests were carried out on the samples with saturation degree of 100% to study the liquefaction behavior of saturated soil. The initial void ratio is almost 0.83. This value was calculated based on the measurement at the end of tests. The samples were

subjected to a constant CSR cyclic loading until liquefaction. The value of CSR was decreased after each test. To study the residual strength of the soil in the full saturation state, the monotonic loading was applied after the liquefaction (Test CS1). The information of tests in the first series is presented in table 4.2.

Table 4.2. Series 1: tests on the full saturated samples.

Tests	e_0	B	Sr_0 (%)	q_{max}	σ_3	u_0	CSR	N_{Liq}	Liquefaction criterion	Monotonic test after liquefaction
CS1	0.827	0.97	100	60	700	600	0.3	3	DA& EPP	Yes. Test : MT1
CS2	0.834	0.97	100	50	700	600	0.25	9	DA& EPP	No
CS3	0.828	0.97	100	40	700	600	0.2	89	DA& EPP	No
CS4	0.83	0.97	100	28	700	600	0.14	163	DA& EPP	No

DA: *Double amplitude (of axial strain) reaches 5%*
CS1: *Cyclic saturated test 1*
EPP: *Excess pore water pressure equals to cell pressure*
MT1: *Monotonic Test 1 after liquefaction.*

IV.2.1.2. Results

Figure 4.1 shows the variation of the deviator stress versus the number of cycles in four tests, from CS1 to CS4, having the similar initial saturation degree but subjected to different CSR cyclic loading. The initial deviator stress of tests varies from 28 kPa to 60 kPa corresponding to the CSR increase from 0.14 to 0.3, respectively.

The first test CS1, with CSR of 0.3 is presented in figure 4.1a. It can be seen that the test was stopped after 3.5 cycles. In the first two cycles, the deviator stress path is linear. It consists of connected lines but it becomes nonlinear from the 3rd cycle where the horizontal lines appear in the graph each time the deviator stress passes zero. This phenomenon shows good agreement with the analysis of cyclic mobility phenomenon which has been studied in chapter 2.

In test CS2, when the initial deviator stress was decreased to 0.25, the test was finished after 10 cycles due to the liquefaction (figure 4.1b). The deviator stress in the first 7 cycles was kept stable; however, its decreases after the 8^{th} cycle. Similar to test 1 (figure 4.1a), after cycle 8^{th}, there is an appearance of a period in which the deviator stress path goes horizontally.

In test CS3 (figure 4.1c), the initial deviator stress is 40 kPa corresponding to a CSR of 0.2. The sample stopped after 89 cycles; however, the signal of liquefaction appears after cycle 80, when the deviator stress shows the decreasing tendency in its amplitude.

In the figure 4.1d, the deviator stress variation of test CS4 with initial value of 28 kPa is shown. The test stopped after 163 cycles. In the first 140 cycles, the deviator stress amplitude is stable at 28 kPa. From the cycle 141st, the sample shows the signal of liquefaction. During the testing process, the apparatus recognized the softening of the sample and it tried to offset the loss in deviator stress by increasing automatically the amplitude of deviator stress. That is why there is a slight increase in deviator stress amplitude before the sudden decrease.

In general, the first four tests on saturated sample show the behavior of sand at the relative density of almost 55%. The decrease of CSR results in the increase of the number of cycles causing liquefaction (N_{liq}); however, this increase is not linear with the decrease of CSR. The decrease of CSR from 0.3 to 0.25 results an increase of the N_{liq} from 3.5 to 10, while the decrease of CSR from 0.25 to 0.2 results in a 79-cycle increase of N_{liq}. The effect of CSR decrease on (N_{liq}) is more obvious when the CSR is small.

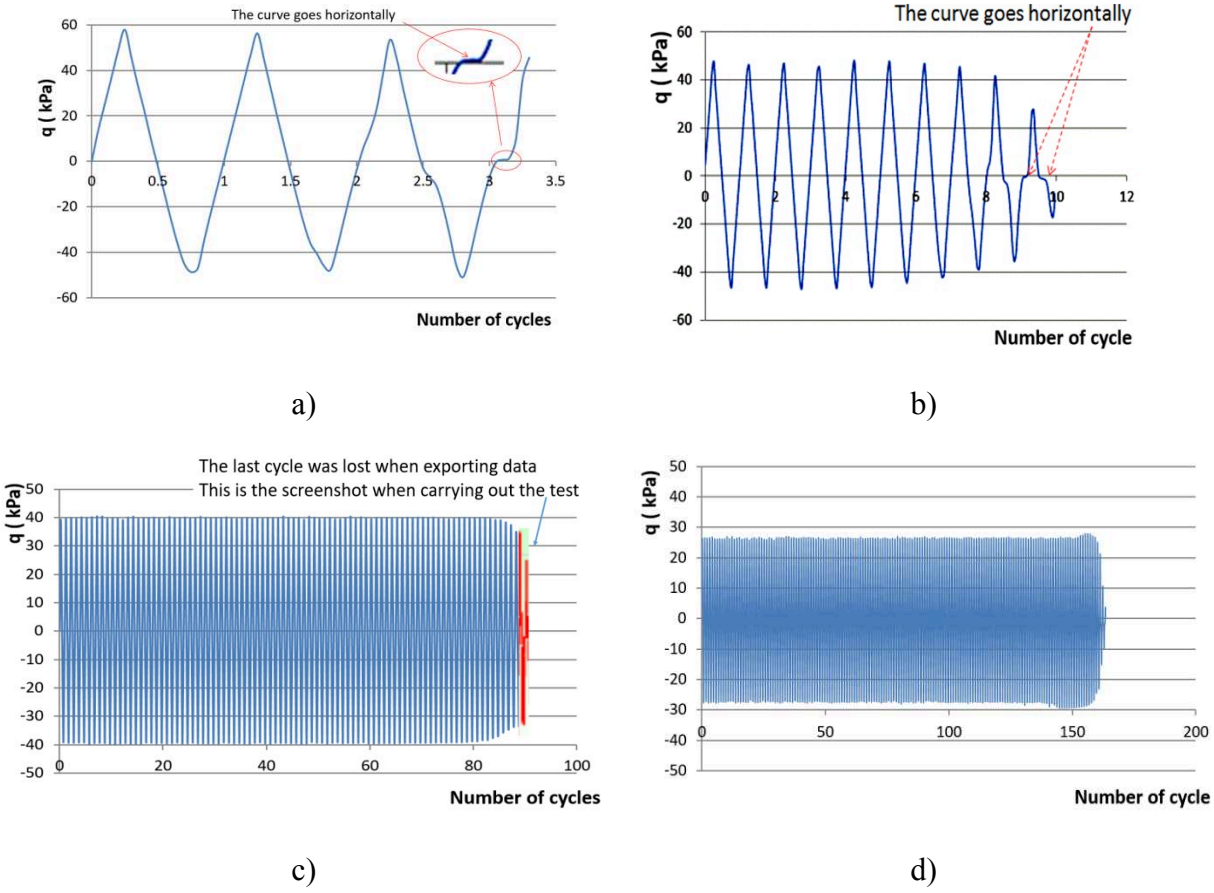

Figure 4.1 Deviator stress versus number of cycles for saturated tests.
a) test CS1 with the CSR of 0.3, b) test CS2 with the CSR of 0.25, c) test CS3 with the CSR of 0.2, d) test CS4 with the CSR of 0.14.

The pore water pressure increment of tests is presented in figure 4.2. All tests have the initial effective confining stress of 100 kPa. In test CS1 with the initial CSR of 0.3, the two-peak mechanism appears from the 3rd cycles. This is a characteristic of cyclic mobility as mentioned by some other authors (Benahmed 2001, Vernay et al. 2019, etc.). It can be seen that this mechanism occurs at the same time with the appearance of the horizontal lines in the curve of deviator stress versus the number of cycles as mentioned above. In figure 4.2a, this mechanism appears in one cycle before the liquefaction. The presence of two-peak mechanism is more obvious in test 2 where the number of cycles is large enough. The increase of pore water pressure in undrained tests shows the contraction of the sample volume in drained condition and vice versa. Therefore, in cycles where the two peaks mechanism appears, the number of times the sample changes its state from contraction to dilation or from dilation to contraction is two times as it is in the normal cycles. The two peak mechanism is also observed in test CS3 and CS4 (figure 4.2c and 4.2d); however, due to the high density of cycles displayed in these figures, it is not shown clearly. With test CS3, there is a note that the data of the last cycle has been lost when exporting the data so the pore water pressure displayed in the figure is a little lower than the initial effective cell pressure.

In the figure 4.2c and figure 4.2d, when the number of cycles is big enough, it can be seen cleanly that the development of the pore water pressure includes three phases.

- In the first phase, the peak points of pore water pressure form a nonlinear curve. In test CS3 with initial CSR of 0.2 (figure 4.2c), the first phase starts from cycle 1 and ends at cycle 18. The test CS4 with initial CSR of 0.14, the first phase is from the first cycle to the 25th cycle.
- In the second phase, the peak points of the pore water pressure curve form an increasing linear line. In figure 4.2c, the second phase is from the 19th cycle to the 80th cycle while it is from the 26th cycle to the 150th cycle in figure 4.2d.
- The last phase shows the sudden increase of pore water pressure. The pore water pressure reaches the initial effective confining stress.

Figure 4.2 also shows that the amplitude of pore water pressure fluctuation depends on the value of the CSRs. The increase of CSR results in the increase of pore water pressure amplitude.

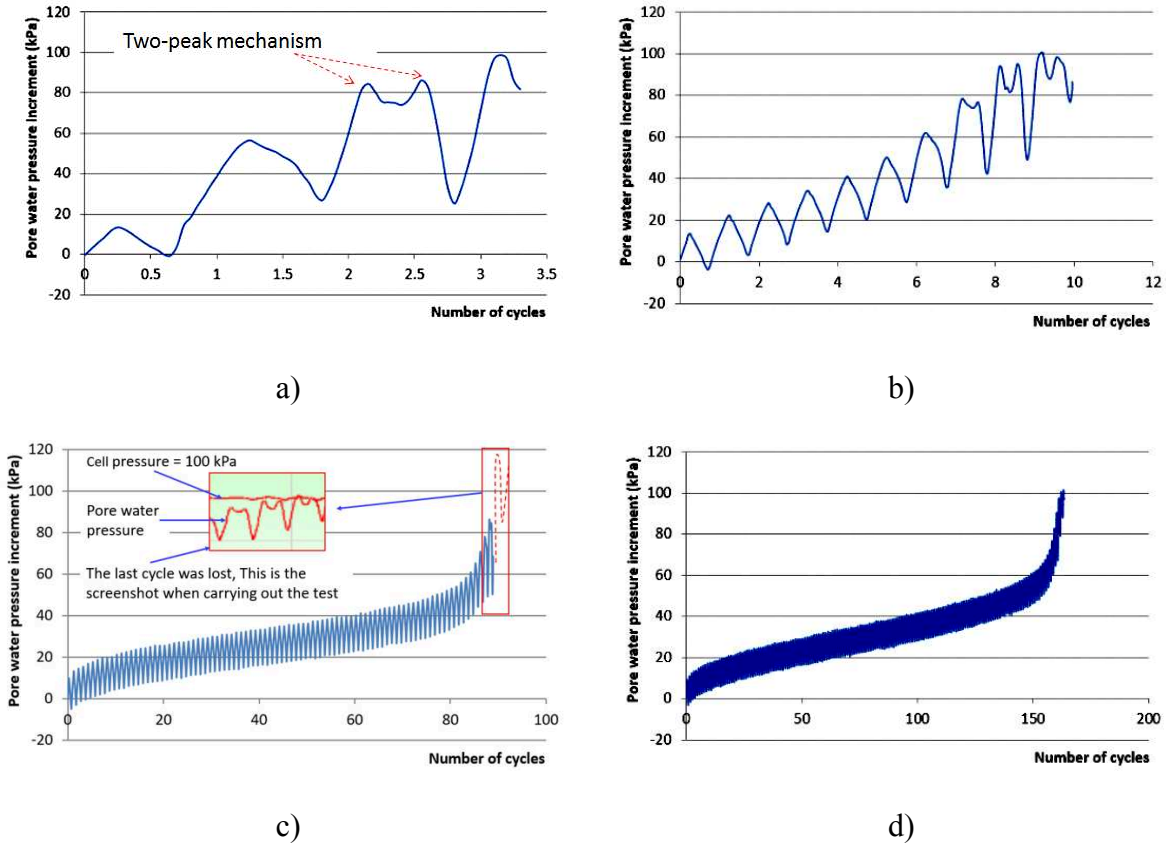

Figure 4.2 Pore water pressure versus number of cycles for saturated tests.
a) test CS1 with the CSR of 0.3, b) test CS2 with the CSR of 0.25, c) test CS3 with the CSR of 0.2, d) test CS4 with the CSR of 0.14.

The developments of the axial strain of tests are shown in figure 4.3. As presented in chapter 2, one criterion for liquefaction assessment is the axial strain in one cycle reaches 5%. It can be seen that with the saturated samples, at the time of liquefaction, all tests have the axial strain near 5% (note that the data of the last cycle of test CS3 was lost when exporting data from Clipstudio, the software controls the apparatus). The axial strain develops mainly to the negative direction reveals that the samples were stretched during cyclic loading. The reason for this mechanism will be discussed more clearly when studying the stress path of tests.

The development of axial strain is low in some first cycles; however, it increases rapidly at several last cycles, especially, in the cycles where there is the appearance of the two-peak mechanism presented at the beginning of this part. The difference between the two phases of axial strain increment is shown more visibly when the CSR is low (figure 4.3c and figure 4.3d). In figure 4.3d the accumulated axial strain is almost 1% after 160 cycles; however, it increases to 5% after the last three cycles.

It is noted that in most cycles from the beginning of the tests, the upper peaks of the axial strain develop towards the negative direction, it means that the samples were stretched; however, in some last cycles, it can be seen that these peaks go upward (figure 4.3c). This tendency appears at the same time with the appearance of the two-peak mechanism presented in the plane of deviator stress versus number of cycles.(note that the data of the last cycle of test CS3 was lost when exporting data from Clipstudio, the software controls the apparatus. The last cycle presented in figure 4.3c is taken from the screenshot when carrying out the test)

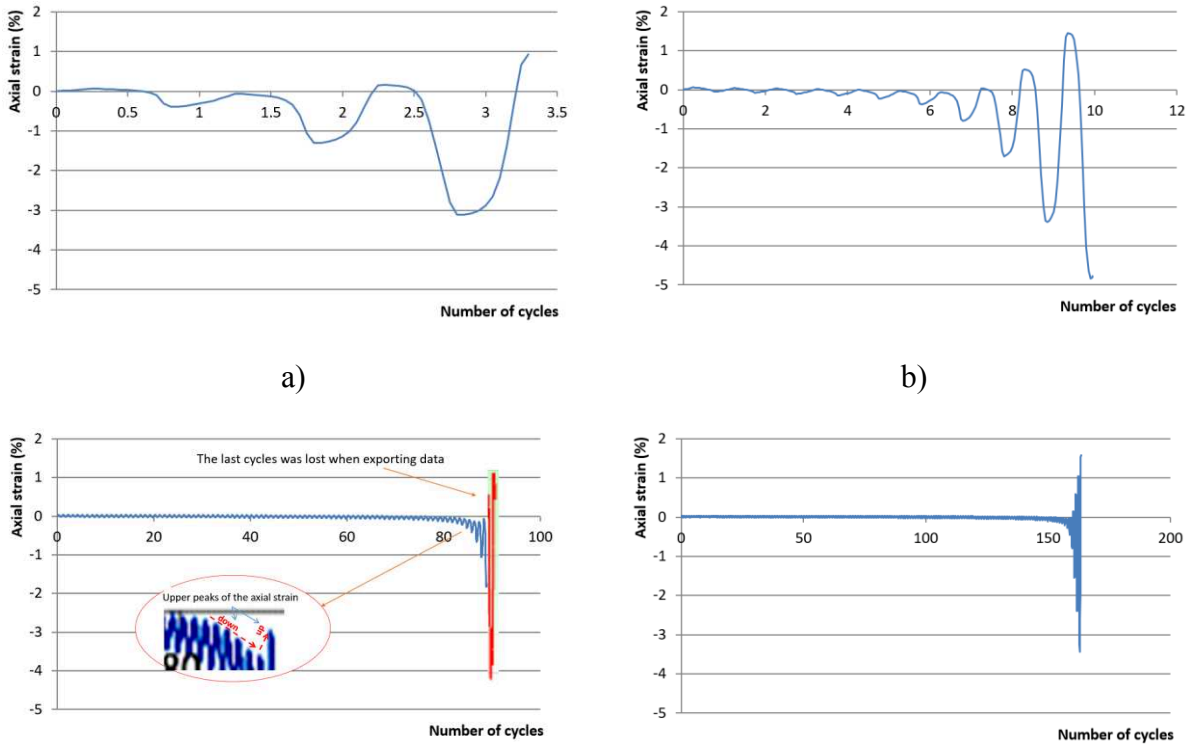

Figure 4.3 Axial strain versus number of cycles for saturated tests.
a) test CS1 with the CSR of 0.3, b) test CS2 with the CSR of 0.25, c) test CS3 with the CSR of 0.2, d) test CS4 with the CSR of 0.14.

Along with the increase of the pore water pressure is the decrease of the effective confining stress. Figure 4.4 shows the reduction of the effective confining stress after each cycle. With the cyclic mobility phenomenon, the effective confining stress is not stable at zero. It is only zero at some points (note that the data of the last cycle of test CS3 was lost when exporting data from Clipstudio, the software controls the apparatus).

Similar to the increment of pore water pressure and the axial strain, the change of the effective confining stress manifests most clearly in the last cycles where the appearance of the two-peak mechanism can be also observed.

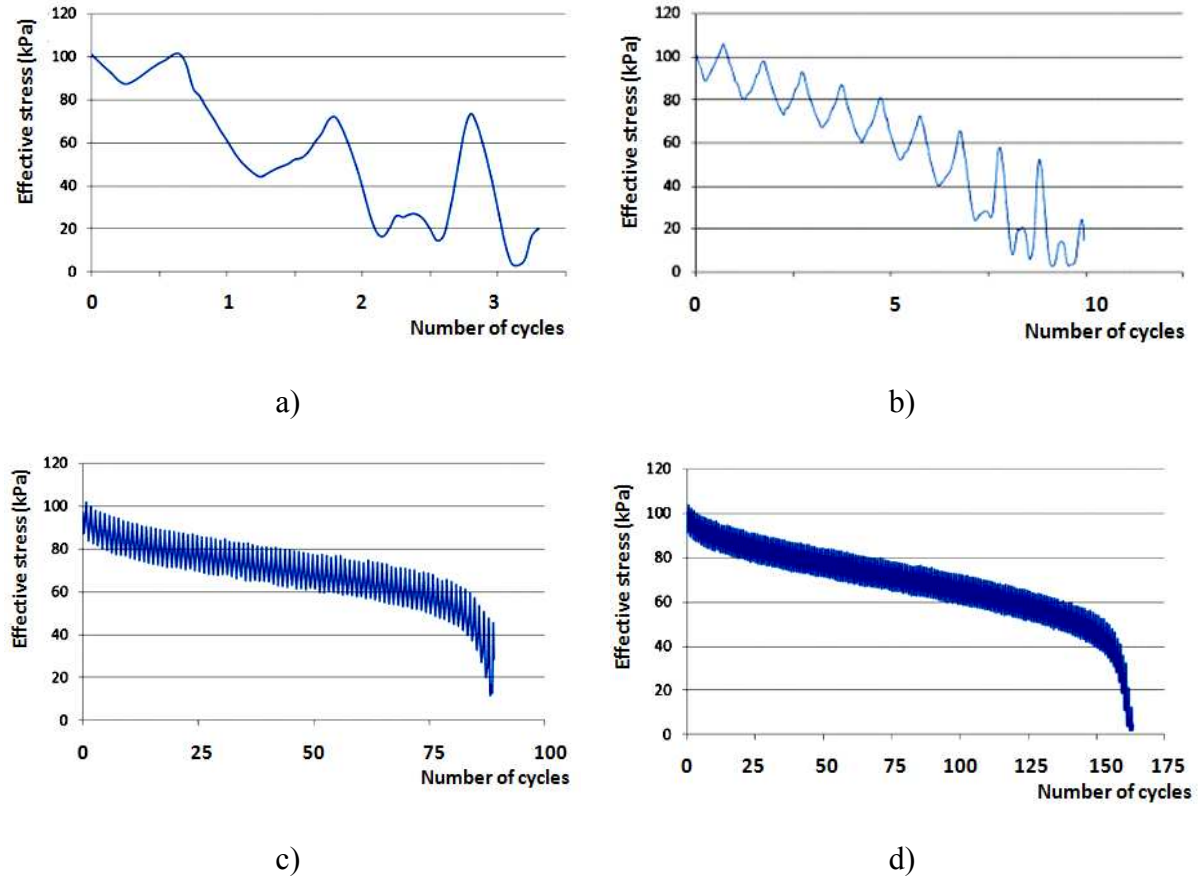

Figure 4.4 Pore water pressure versus number of cycles for saturated tests.
a) test CS1 with the CSR of 0.3, b) test CS2 with the CSR of 0.25, c) test CS3 with the CSR of 0.2, d) test CS4 with the CSR of 0.14.

Another way to demonstrate the liquefaction without the appearance of the initial effective confining stress and pore water pressure increment is using the excess pore water pressure ratio concept. This ratio is calculated by normalizing the excess pore water pressure generated during undrained cyclic loading for the effective consolidation stress. It is shown in the following equation:

$$r_u = \frac{\Delta_u}{\sigma'_{3c}} \qquad \text{(Eq.4.1)}$$

where Δu is the excess pore water pressure and σ'_{3c} is the initial effective stress.

The maximum possible value for r_u is 1.0 (or 100 %), which occurs when the pore water pressure equals cell pressure or the effective confining stress equals zero. At the maximum

value of r_u, the sample is considered to be liquefied. Figure 4.5 shows the development of this parameter for four mentioned saturated tests

The overall evolution of this pressure ratio depends on the applied CSR. In figure 4.5a, r_u develops strongly from the beginning of the test and reaches the unit after three cycles. In figure 4.5b, r_u increases relatively slowly at some first cycles then accelerates to the unit. In figure 4.5c and figure 4.5d, where the CSRs are low, the development of r_u shows obviously three different phases (note that the data of the last cycle of test CS3 was lost when exporting data from Clipstudio, the software controls the apparatus). It can be also commented that the curves in these two figures have the form different from those in figure 4.5a and figure 4.5b. In the first phase, r_u increases quickly in some first cycles. The second phase shows the linear increase of r_u. The last phase lasts in some several last cycles, where r_u increases sharply to reach the maximum value equal 1.

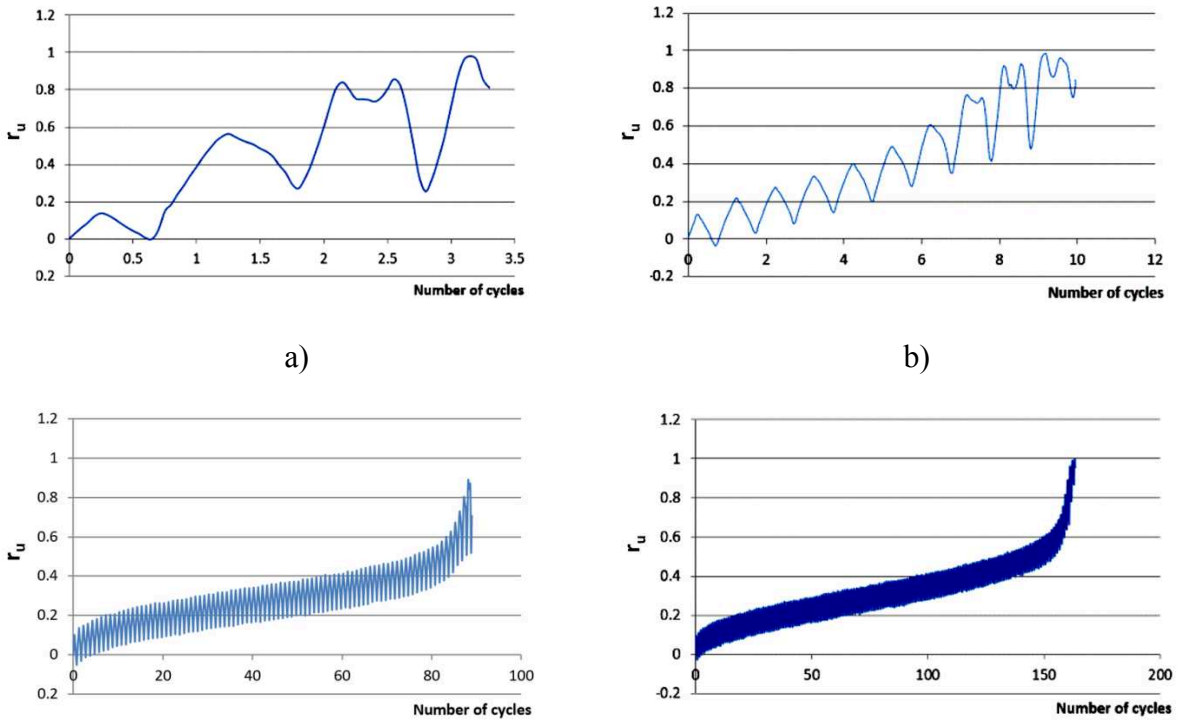

Figure 4.5Normalized Excess pore water pressure ratio r_u versus number of cycles for saturated tests.

a) test CS1 with the CSR of 0.3, b) test CS2 with the CSR of 0.25, c) test CS3 with the CSR of 0.2, d) test CS4 with the CSR of 0.14.

The relationship between the mean effective stress and the deviator stress of the tests are presented in figure 4.6. The figures are butterfly shape, a characteristic of the cyclic mobility phenomenon. The q-p' curve approaches the failure criteria lines and fluctuates (q is the deviator stress and p' is the effective mean stress). The relationship between the slope of the failure criterion lines and the friction angle is shown in equations (4.2) and (4.3). From these curves, it can be seen that the failure criteria with slopes of M=1.37 in compression and M=-0.94 in extension, corresponding to the friction angle of 34°, suit best for both saturated and unsaturated samples.

$$M = \frac{6.sin\emptyset}{3-sin\emptyset}$$ (in compressed domain) (Eq. 4.2)

$$M = -\frac{6.sin\emptyset}{3+sin\emptyset}$$ (in extended domain) (Eq. 4.3)

The representation of the tests in the plane of the stresses (q, p') shows that the path of the effective stresses firstly migrates gradually towards the origin of the axes with a reduction of the effective mean stress p' after each cycle of loading. From the first crossing of the characteristic state threshold, the form of the curves changes and is the butterfly form. From there, the samples show strongly contracting and dilating tendency during each cycle of the cyclic loading, both in compression and in extension expressed through the strong increase and fluctuation of pore pressures. This causes the mean effective stresses migrating rapidly towards the origin. One important characteristic shown in this graph is that after the first time the effective stress path touches the failure line in the extension domain, an increase of the deviator stress from the minimum value to the maximum value in a half of the loading cycle corresponds to the two different trends of the mean effective stress, first is decreasing and then increasing. This shows that the change in pore water pressure affects the value of the mean effective stress. And as being known, the change of pore water pressure in the undrained experiment relates to the volumetric behavior of materials. The reverse of mean effective stress, in this case, is caused by the transformation of the sample from the contraction phase to the dilation phase. The locus of points marking the phase transformation of the sample is called the phase transformation lines or the characteristic state lines of the material. In figure 4.6a, the phase transformation lines are expressed by the two yellow lines in two domains of the plane, one is in compression domain and the other is in the extension domain. The samples collapse initially due to instability in the tension domain, the stress path touches the failure line in this domain corresponding to the negative deviator stress. When the

cyclic loading continues, the stress path migrates to the origin, and then touches the failure lines in the compression domain. From this cycle, the axial strain develops strongly to the both directions: compression, and extension.

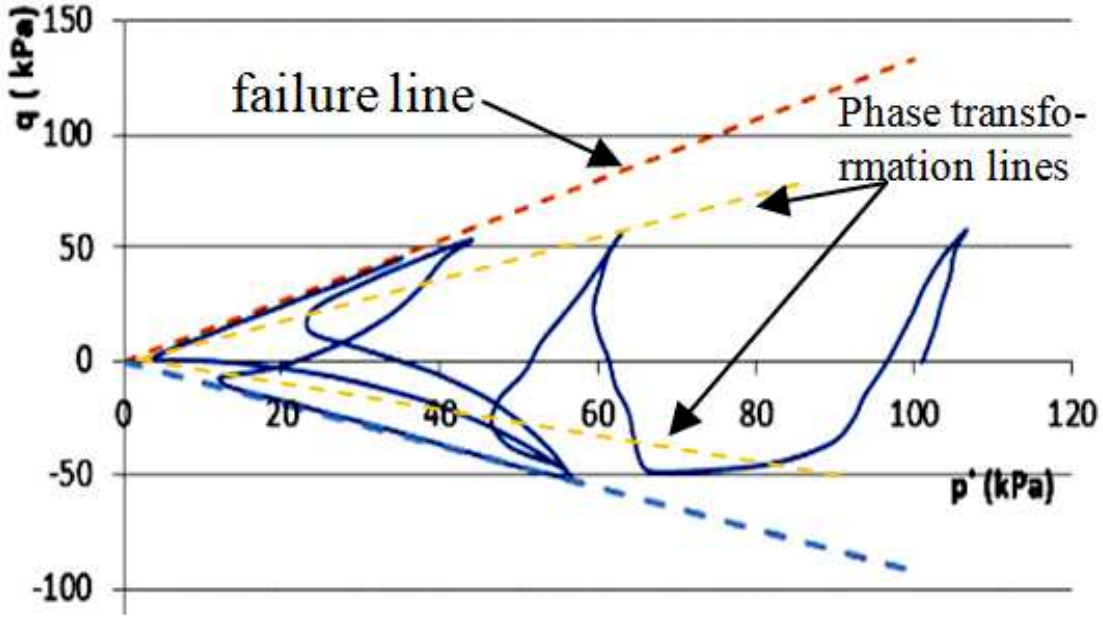

(a)

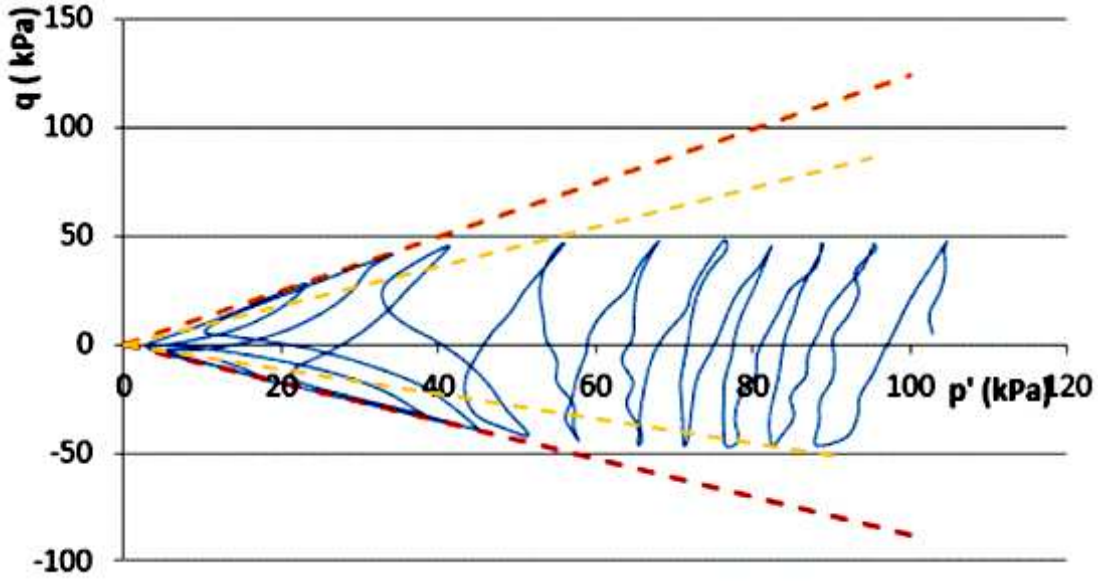

(b)

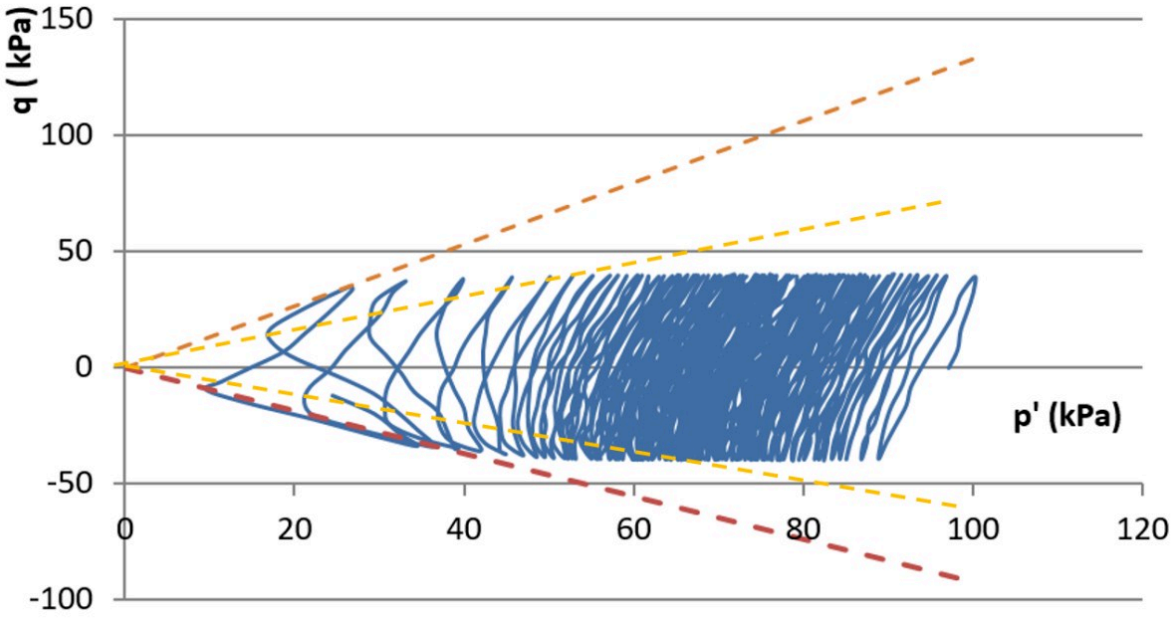

(c)

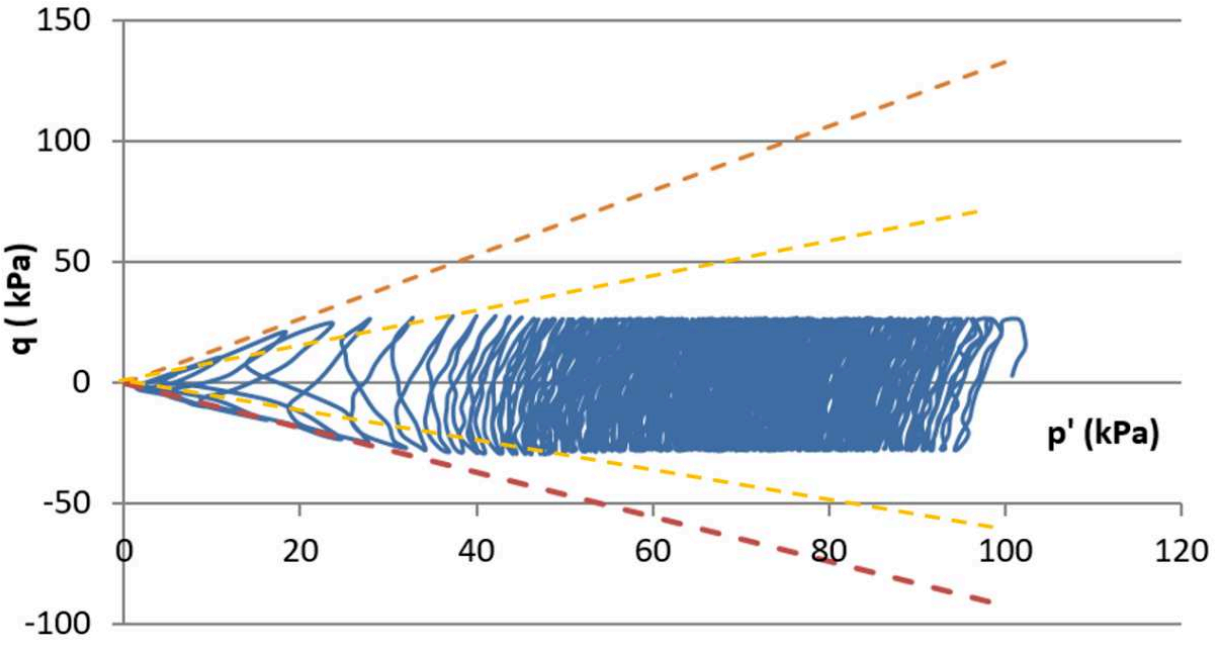

(d)

Figure 4.6 Mean effective stress versus deviator stress for saturated tests.
a) test CS1 with the CSR of 0.3, b) test CS2 with the CSR of 0.25, c) test CS3 with the CSR of 0.2, d) test CS4 with the CSR of 0.14.

Comparison was done with the friction angle derived from the literature on the same sand with one deduced from the cyclic test in this study. Many authors have carried out monotonous triaxial tests on the Hostun RF sand at different relative densities and different drainage conditions. Table 4.3 presents a synthesis of these results. It can be seen that the angle of friction varies from 34.5° to 37° depending on the authors and the test conditions. These values seem to be very consistent and in a good agreement with the one deduced from the cyclic tests in this study.

Table 4.3. The friction angle of Hostun sand in literature.

References	Type of the tests	Friction angle (degree)	Relative density D_r (%)
Dang 2019	Drained monotonic triaxial test	35.21 (in critical state)	D_r = 0 (void ratio e=1.04)
		36.59 (in critical state)	D_r = 40
Arab et al. 2016	Undrained monotonic triaxial test	35 (mobilized friction angle, not related to the relative density)	D_r= 8;64;78
Benahmed 2001	Drained monotonic triaxial test	34.5 (in critical state)	D_r = 50
		35 (in critical state)	D_r = 70

Figure 4.7 shows the relationship between the axial strain versus the deviator stress. At some initial cycles of the cyclic loading, the axial strain shows small development; however, it increases rapidly at some last cycles. All tests stop when the double amplitude of axial strain in one cycle reaches 5%, corresponding to the second condition for liquefaction assessment (except test CS3, because some information of the last cycles was lost during the exporting data from the software Clip-studio, the software controls the apparatus). The important information observed from this figure is that the axial strain increases quickly not at the moment when the deviator stress reaches maximum or minimum values but when this stress

passes zero. In each cycle, there are two times the axial strain develops sharply, and each time is in a different direction.

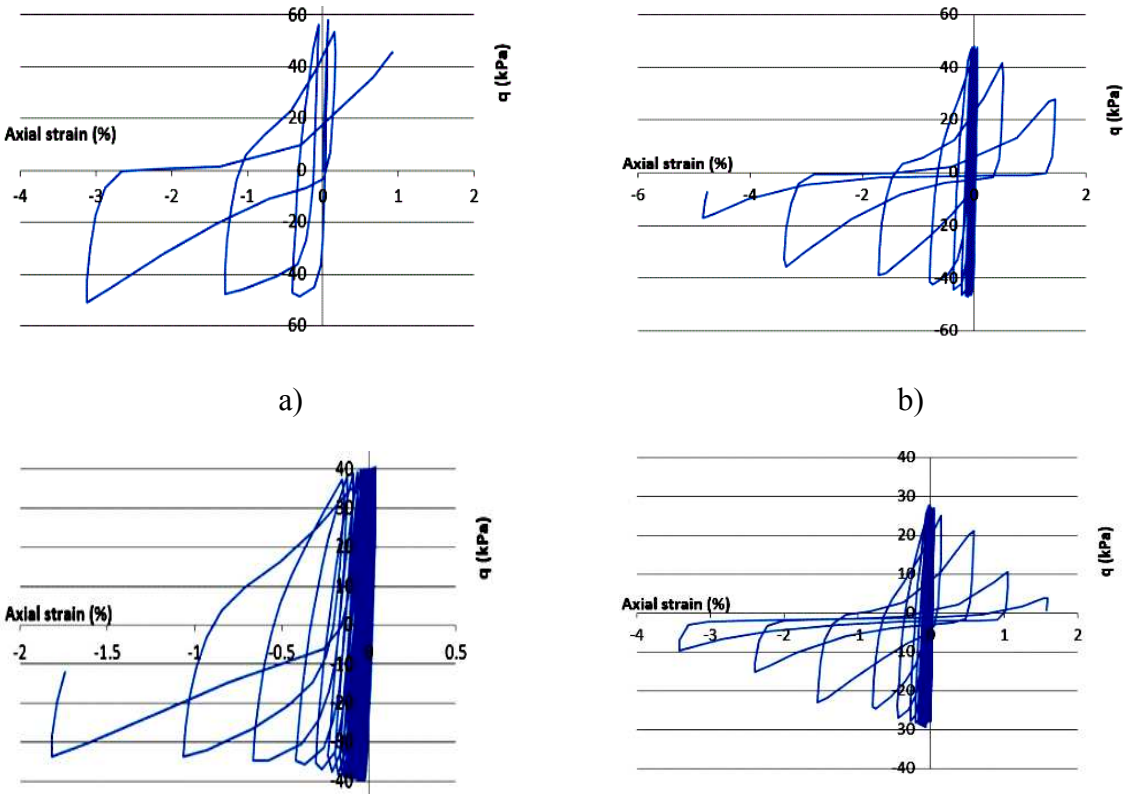

Figure 4.7 Axial strain versus deviator stress for saturated tests.
a) test CS1 with the CSR of 0.3, b) test CS2 with the CSR of 0.25, c) test CS3 with the CSR of 0.2, d) test CS4 with the CSR of 0.14.

The presentation of the results in the pore water pressure – axial strain plane shows the development of each parameter (figure 4.8). At the beginning of each curve, the pore water pressure and the axial strain accumulates slowly after each cycle. However, these parameters increase strongly at some last cycles. Focusing on these cycles, it can be seen that at the edges of each loop, the axial strain develops slowly due to the low pore water pressure corresponding to a high effective confining stress. The axial strain develops rapidly when the pore water pressure reaches its highest values.

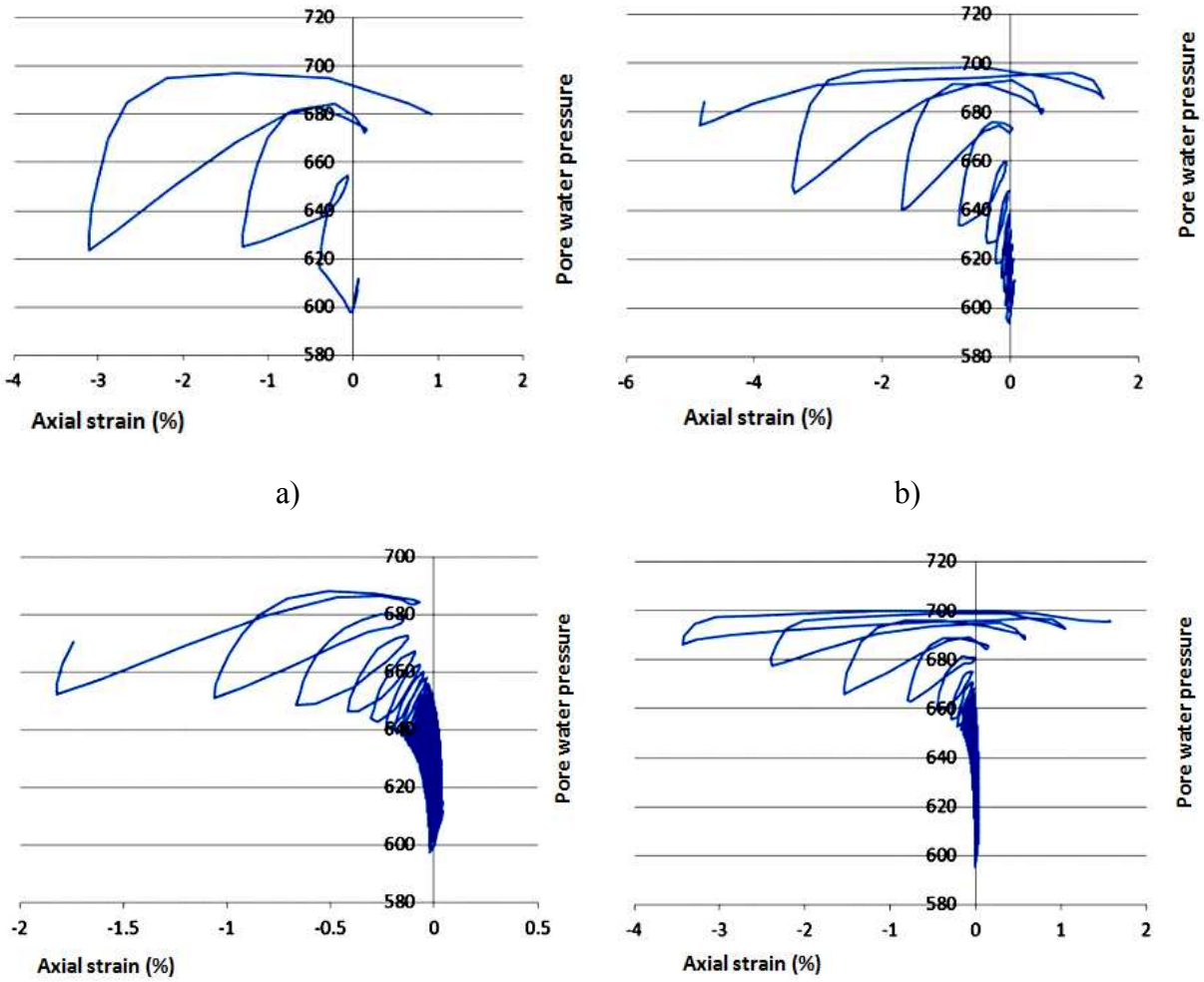

Figure 4.8 Axial strain versus pore water pressure for saturated tests.

a) test CS1 with the CSR of 0.3, b) test CS2 with the CSR of 0.25, c) test CS3 with the CSR of 0.2, d) test CS4 with the CSR of 0.14.

IV.2.2. Residual strength after liquefaction of saturated sand

IV.2.2.1. Test program

After cyclic loading, the samples were subjected to monotonic loading to study the residual strength of the sand after liquefaction. In reality, after liquefaction, there are two possible behaviors:

- If the pore pressure dissipates after liquefaction, the residual strength can be studied in drained condition. This means that the permeability of the soil is sufficiently great to dissipate the pore water pressure in short time.

- If the permeability of the soil is low enough the pore water pressure cannot dissipate in short time the residual strength must be studied in undrained condition.

In this study, only the first case is studied. The tests and their parameters are presented in table 4.4.

Table 4.4. Residual strength tests on the fully saturated samples.

No	**Name**	**Preceded cyclic test**	**Void ratio before monotonic loading: e_{m0}**	**Sr**	**σ_3 kPa**	**U kPa**	**Axial strain variation (ε_a) %**
1	MT1	CS1	0.808	100	100	0	0.5 → 20.5

MT1: *Monotonic Test 1 after liquefaction* CS1: *Cyclic Saturated test 1*

IV.2.2.2. Results

Figures from 4.9 to 4.12 present the results of the residual strength test on the sample with saturation degree of 100%. In figure 4.9, the deviator stress is plotted in function of axial strain. The axial strain of the state after liquefaction is 0.5% and it is increased to 20.5% during monotonic compression. This axial strain increment results in an increase of the deviator stress from 50 kPa to 320 kPa.

Figure 4.10 shows the deviator stress versus the mean effective stress. It can be seen that the stress path is linear. The stress path increases until contacting the failure line in compression domain. Noting that these failure lines are the same with the failure lines presented in the cyclic loading results.

Figure 4.11 exhibits the sample volumetric strain in relationship with the axial strain. From this figure, it can be concluded that the sample is in dense state. The sample volume decreases in short term at the beginning of the test, after that the sample dilates. This result shows a good agreement with the cyclic mobility observed when loading the sample cyclically. The sample volumetric change results in the change of the sample void ratio which is shown in figure 4.12. The void ratio increases from 0.81 to 0.88 during the monotonic loading test.

From these figures (4.9, 4.10, 4.11, 4.12), it can be seen that after liquefaction, the pore water pressure dissipates and the sand residual strength recuperates and its behavior is similar to the behavior of sand in dense state, and the void ratio of the sample is perhaps more homogenous; however, it is necessary to make more tests to verify this assumption.

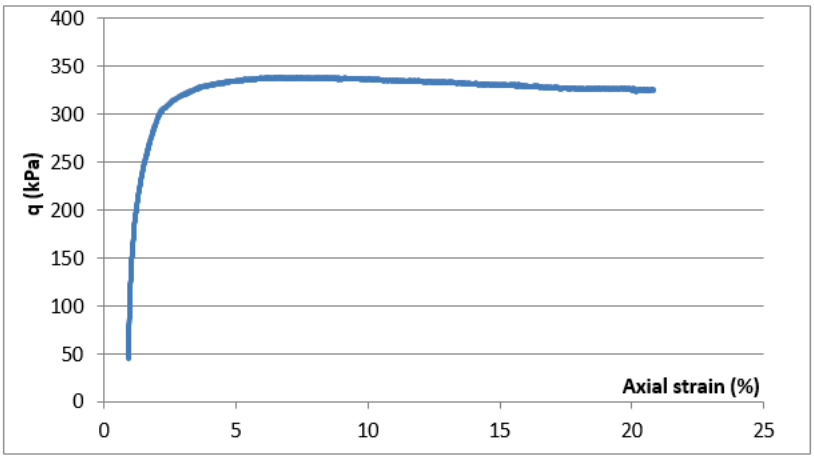

Figure 4.9. Deviator stress versus axial strain for monotonic saturated test MT1

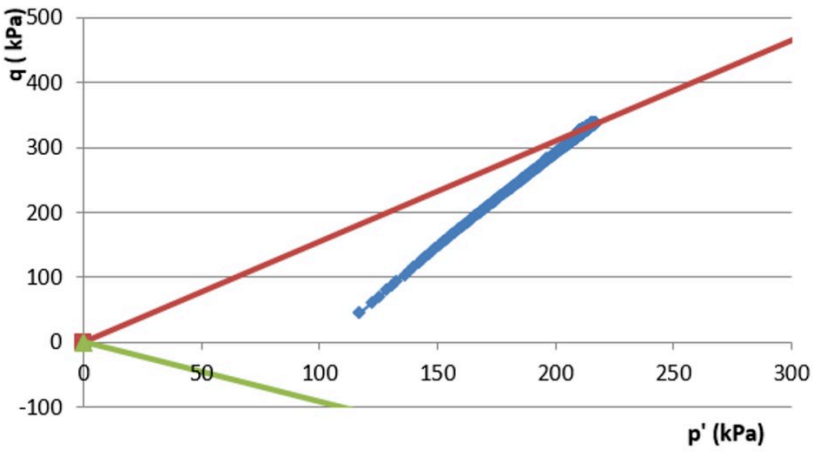

Figure 4.10 Deviator stress versus mean effective stress (p') for monotonic saturated test MT1

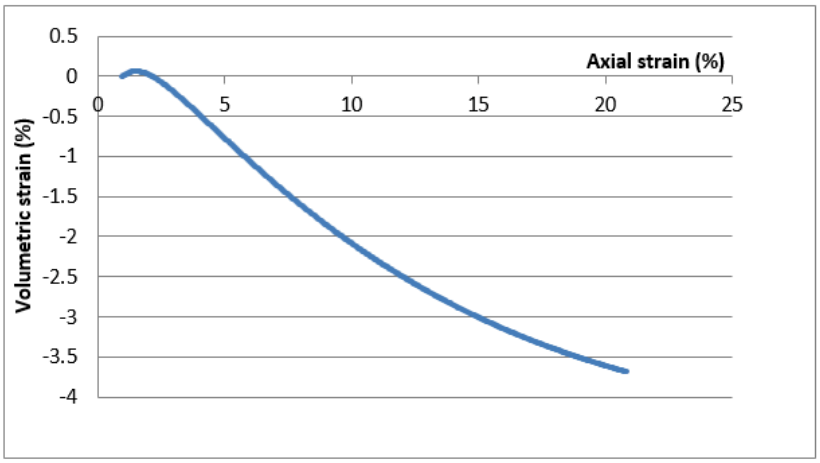

Figure 4.11 Volumetric strain versus axial strain for monotonic saturated test MT1

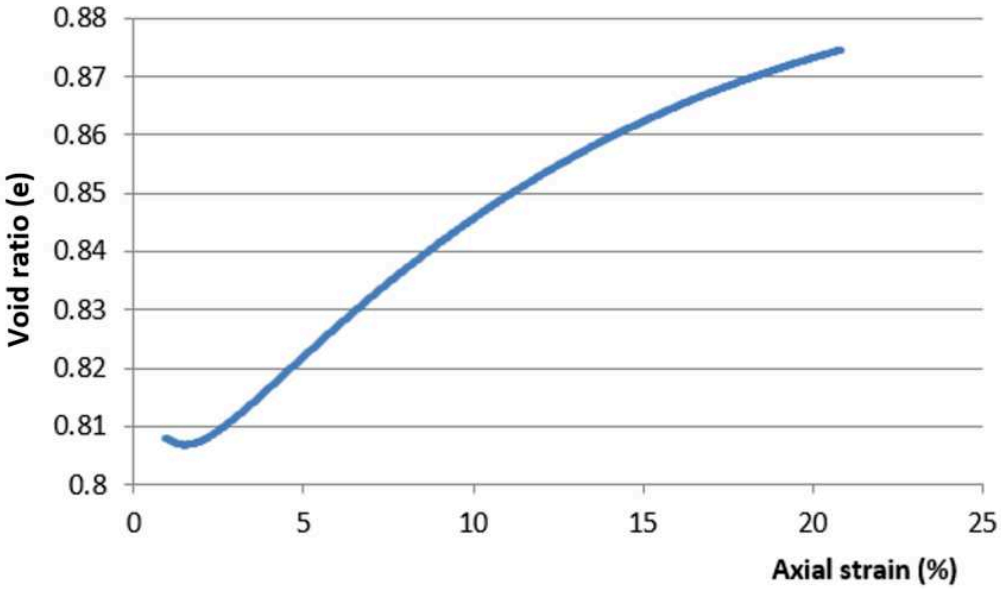

Figure 4.12 Void ratio versus axial strain for monotonic saturated test MT1

IV.2.3. Test parameter variation during the saturated test

With our experimental protocol, the parameters of test were measured or calculated for all stages of tests. The table 4.5 presents the parameter for saturated test CS1 + MT1. The parameters of other tests will be presented in the appendix. Figure 4.13 summaries the variation of saturation degree and the void ratio during the test. Because the test was carried out on the saturated sample, the saturation degree was stable at 100%. While the void ratio changes in each stage of the test. It decreases in sample consolidation processes and increases in monotonic loading process. In cyclic loading stage, the test was in un-drained condition so the void ratio was maintained.

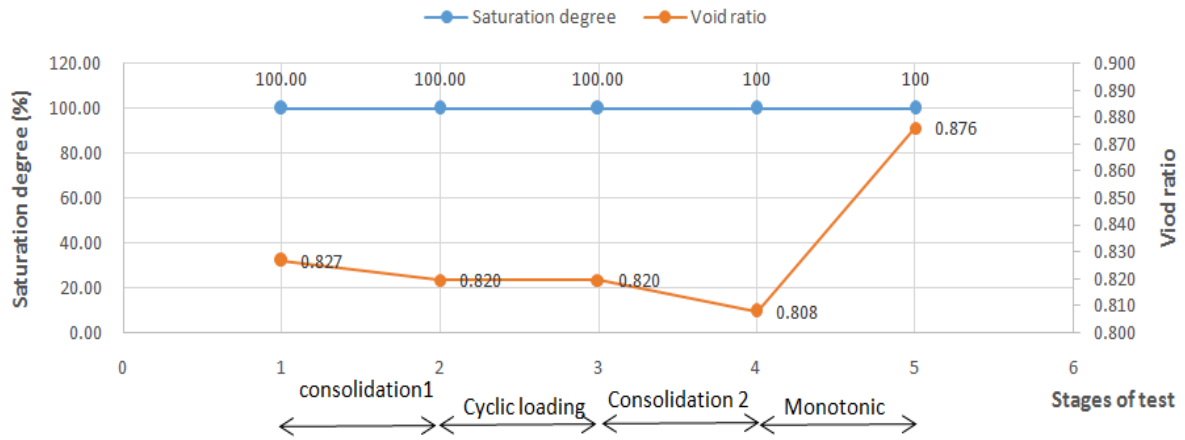

Figure 4.13 Summary of saturation degree and void ratio changes for each stage of saturated test CS1 + MT1.

Table 4.5. Variation of parameters during saturated test CS1 + MT1.

Parameters	**Before consolidation (Initial state)**	**After consolidation 1**	**After cyclic loading**	**After consolidation 2**	**Final state- after monotonic loading**
B	0.97	-	-	-	-
S_r %	100.00	100.00	100.00	100.00	100
void volume (cm^3)	240.3	238.2	238.2	234.8	254.6
Water volume (cm^3)	240.3	238.2	238.2	234.8	254.6
Dry weigh of sample (g)	770.1	770.1	770.1	770.1	770.1
Sand particle volume (cm^3)	290.61	290.61	290.61	290.61	290.61
Total sample volume (cm^3)	530.9	528.8	528.8	525.4	545.2
Void ratio: e	0.827	0.820	0.820	0.808	0.876
n	0.453	0.450	0.450	0.447	0.467
Sample volume change cm^3	0	2.1	2.1	3.4	-14.3
Volumetric strain (%)	0	0.39	0.39	0.64	-2.70

IV.3. Liquefaction potential and residual strength of unsaturated sand.

IV.3.1. Liquefaction potential of unsaturated sand

IV.3.1.1. Test program

To study the liquefaction of unsaturated sand, two series of tests with different saturation degree were carried out. The first series includes 4 tests. The saturation degree of tests in this series is around 95%. The deviator stress is decreased after each test, from 70 kPa to 40 kPa corresponding to the CSR decrease from 0.35 to 0.2. The monotonic loading test was applied after cyclic test named CUI2 to study the residual strength of soil after liquefaction. In the

second series, tests were carried out on the samples with saturation near 86%. There were five tests carried out. The CSR varies from 0.45 to 0.3 corresponding to a decrease of deviator stress from 90 kPa to 60 kPa. At the CSR of 0.3, there was no liquefaction observed. Similar to the second series, the monotonic test was applied after the cyclic test CUII-4 to study the residual strength of the soil. The program for the second series and the third series of tests are presented in the table 4.6 and table 4.7 below:

Table 4.6. Series of tests on the samples with saturation near 95 %.

No	Tests	e_0	B	Sr_0 (%)	q_{max}	σ_3	u_0	CSR	N_{Liq}	Liquefaction criterion	Monotonic test coming after liquefaction
1	CUI-1	0.842	0.21	95.98	70	100	0	0.35	10	DA& EPP	No
2	CUI-2	0.826	0.22	95.85	60	100	0	0.3	14	DA& EPP	Yes. Test : MT2
3	CUI-3	-	0.21	94.82	50	100	0	0.25	468	DA& EPP	No
4	CUI-4	0.826	0.21	94.3	40	100	0	0.2	-	NL	No

CUI: *Cyclic Unsaturated test (Group I)*
MT: *Monotonic Test after liquefaction*
DA: *Double Amplitude (of axial strain) reaches 5% in one cycle*
EPP: *Excess Pore-water Pressure equals to the initial effective confining stress*
NL: *No liquefaction*

Table 4.7. Series of tests on the samples with saturation near 86 %.

No	Tests	e_0	B	Sr_0 (%)	q_{max}	σ_3	u_0	r_u	N_{Liq}	Liquefaction criterion	Monotonic test coming after liquefaction
1	CUII-1	-	0.057	86.5	90	100	0	0.45	5	DA	No
2	CUII-2	0.823	0.056	86.26	80	100	0	0.4	12	DA	No
3	CUII-3	0.836	0.07	87.39	70	100	0	0.35	28	DA	Yes. Test : MT3
4	CUII-3b	0.83	0.067	87.1	70	100	0	0.35	22	DA	No
5	CUII-4	0.823	0.056	86.26	60	100	0	0.3	-	NL	No

CUII-4: *Cyclic Unsaturated test4 (group II with a saturation degree around 86%)*
MT3: *Monotonic Test 3 after liquefaction*
DA: *Double Amplitude (of axial strain) reaches 5% in one cycle*
NL: *No Liquefaction*

IV.3.1.2. Results

IV.3.1.2.1. Samples with saturation near 95 %:Liquefaction of soil due to the increase of pore water pressure and the excess development of axial strain

Figure 4.14 shows the deviator stress versus the number of cycles for four tests with the nearly similar initial saturation degrees but subjected to different CSR cyclic loading. The initial saturation degree of all tests is almost 95% corresponding to B = 0.2-0.21 as presented in the table 4.6. The initial deviator stress of test CUI-1 was chosen at 70 kPa corresponding to the CSR of 0.35. The CSR were decreased after each test with step of 0.05 until there was no liquefaction observed. The minimum value of CSR was 0.2 corresponding to the deviator stress applied equal to 40 kPa. With this CSR, the sample did not show any signals of liquefaction after 500 loading cycles.

Figure 4.14a presents the deviator stress in a function of the number of cycles for the first unsaturated test CUII-1. It can be seen that the test was stopped after 10 cycles. At the beginning of the test, the maximum value of the deviator stress is 70 kPa while the minimum value is approximately -60 kPa, a little higher than the expected value (-70 kPa). This is because the deviator stress is approximately the extension strength of the material and the sample became very soft. Thus, the apparatus could not increase the deviator stress to the desired value. In the next cycles, the apparatus adjusted the rate of load increase to reach the desired amplitude but the sample liquefied after a small number of cycles. However, in general, the amplitude of the deviator stress was kept stable during the test. In the first 7 cycles, the graph is linear form. It consists of straight lines but it becomes nonlinear from the 8^{th} cycle. From this cycle, the two-peak phenomenon is also observed in the pore water pressure versus number of cycles which will be presented later.

In test CUII-2, the CSR was decreased to 0.3 corresponding to the deviator stress of 60 kPa; the test was finished after 14 cycles (figure 4.14b). The deviator stress in the first 10 cycles was kept stable; however, it decreases from the 11^{th} cycle. Similar to figure 4.14a, from the cycle 11, there is the appearance of nonlinear periods in the curve.

In test CUI-3, the deviator stress fluctuated between -50 kPa and 50 kPa (CSR=0.25). Figure 4.14c shows that the deviator stress was well controlled during the test. The test stopped after 468 cycles; however, the signal of liquefaction appears from the 460^{th} cycle when the amplitude of the deviator stress shows the decreasing tendency.

The three presented un-saturated tests show the behavior of sand in unsaturated state. The increase of CSR results in the increase of the number of cycles causing liquefaction (N_{liq}) and similarly to the saturated tests, the effect of CSR decrease on N_{liq} is more obvious when the CSR is small.

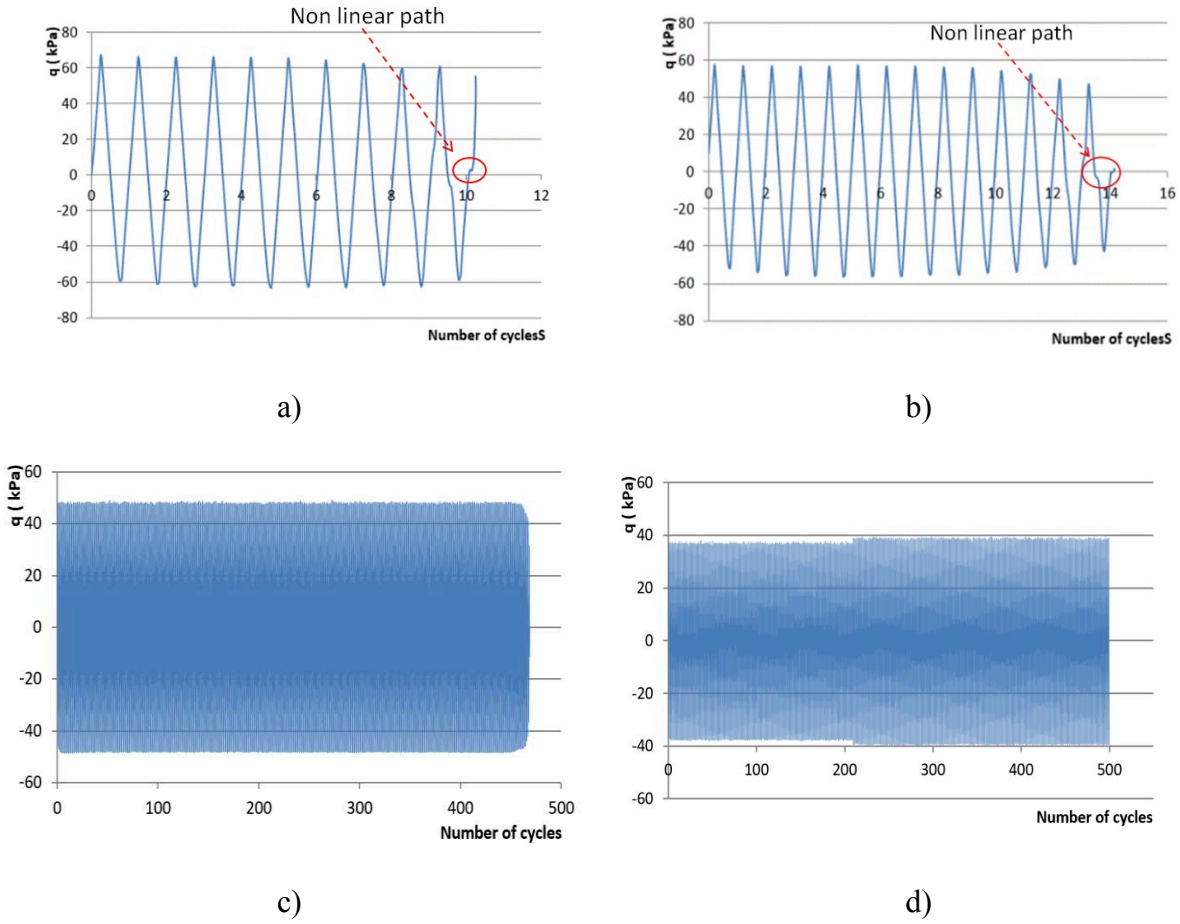

Figure 4.14 Deviator stress versus number of cycles for the samples with saturation degree of approximately 95%.

a) test 1 CUI-1with the CSR of 0.35, b) test CUI-2 with the CSR of 0.3, c) test CUI-3 with the CSR of 0.25, d) test CUI-4 with the CSR of 0.2.

The blue curves in figure 4.15 shows the pore water pressure in a function of the number of cycles for all four unsaturated tests while the orange curves show the value of the cell pressure. As presented in chapter 3, all unsaturated tests have the initial pore water pressure at

0 kPa after sample consolidation, the initial cell pressure of 100 kPa and it was kept stable during cyclic loading.

Based on the first criterion for liquefaction that the pore water pressure reaches the cell pressure, the sample in test CUI-1with CSR of 0.35 (figure 4.15a) liquefies after 10 cycles. The sample in test CUI-2 with CSR of 0.3 (figure 4.15b) liquefies after 14 cycles, and the sample in test CUI-3 with CSR of 0.25 liquefies after 463 cycles while there is no liquefaction observed in test 4 after 500 loading cycles.

The two-peak mechanism also appears in these unsaturated tests similar to the saturated tests presented above. In literature, the appearance of the two-peak mechanism on unsaturated tri-axial tests has been also seen in other studies (Vernay 2018, Xia and Hu 1991, Yoshimi et al. 1989).

The development of the curves depends on the value of CSR. In figure 4.15c, the curve includes three phases. The first phase observes a sharp increase in pore water pressure. This phase includes several first cycles. After that, the second phase appears with the linear increase of the peaks of the pore water pressure. The third phase witnesses the non-linear increase of the peaks of the pore water pressure. In some last cycles of this phase, the pore water pressure reaches the cell pressure and the sample is liquefied as cyclic mobility phenomenon. While, in figure 4.15a and figure 4.15b, we do not see clearly the division of these curves into three phases as figure 4.15c.

The accumulated axial strain after each cycle of loading is presented in figure 4.16 for 4 tests. Similar to the saturated tests, the development of axial strain is low in some first cycles and increase sharply in several last cycles, especially, in the cycles where there is the appearance of two-peak mechanism in the deviator stress – number of cycles plane. And in these cycles, the upper peaks of the axial strain curve develop upward (figure 4.16a), while they decrease in the previous cycles.

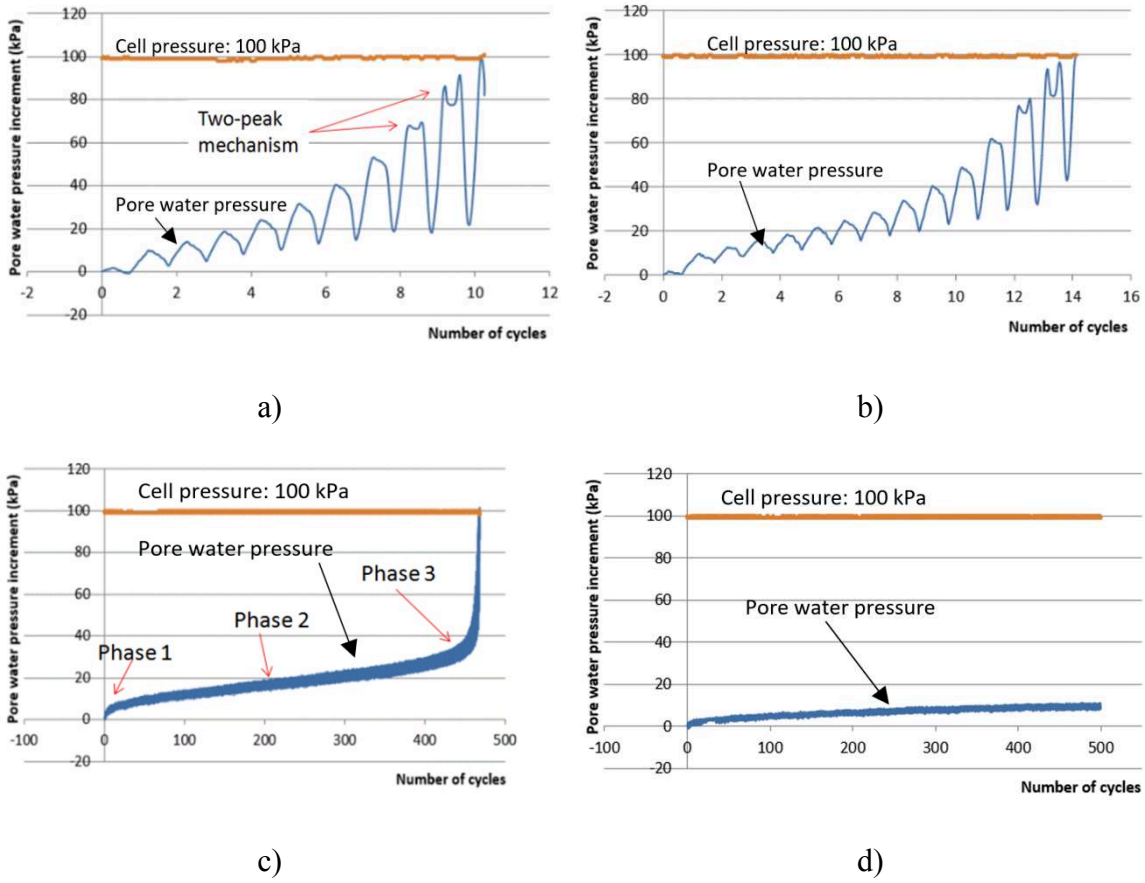

Figure 4.15 Pore water pressure versus number of cycles for the samples with saturation degree of approximately 95%.

a) test CUI-1 with the CSR of 0.35, b) test CUI-2 with the CSR of 0.3, c) test CUI-3 with the CSR of 0.25, d) test CUI-4 with the CSR of 0.2.

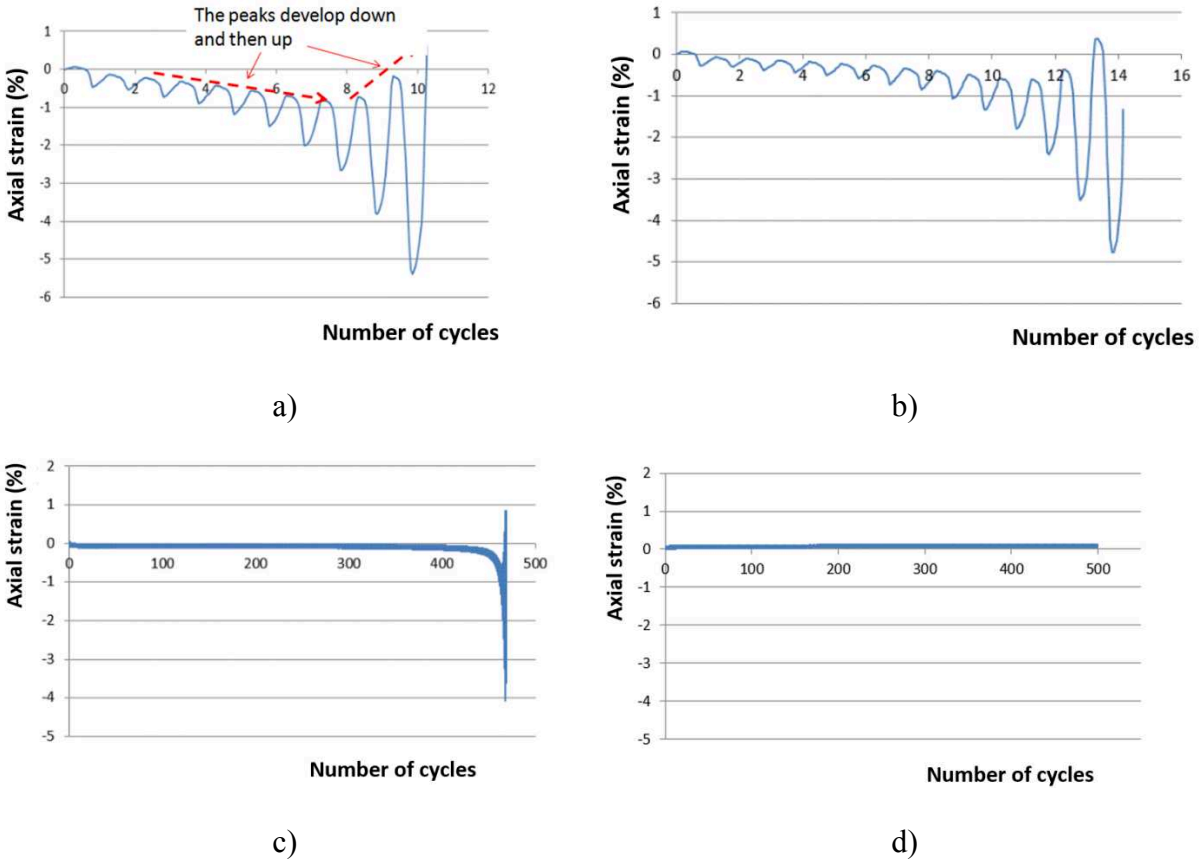

Figure 4.16 Axial strain versus number of cycles for the samples with saturation degree of approximately 95%.

a) test CUI-1with the CSR of 0.35, b) test CUI-2 with the CSR of 0.3, c) test CUI-3 with the CSR of 0.25, d) test CUI-4 with the CSR of 0.2.

Figure 4.17 presents the relationship between the effective confining stress versus the number of cycles. In the vicinity of saturation, the pore air is considered as the bubbles embedded in pore water (Okamura and Soga 2006; Bian 2007; Fredlund and Rahardjo 1993). In this area, Terzaghi's effective stress concept remains valid (equation 4.4) (Biarez et al. 1991; Fleureau et al. 1992; Fleureau et al. 1993a, b).

$$\sigma' = \sigma - u_w \qquad \text{(Eq. 4.4)}$$

Along with the increase of the pore water pressure is the reduction of effective confining stress. The change of the effective confining stress in some last cycles allows relating to the two-peak mechanism in the plane of the pore water pressure versus the number of cycles.

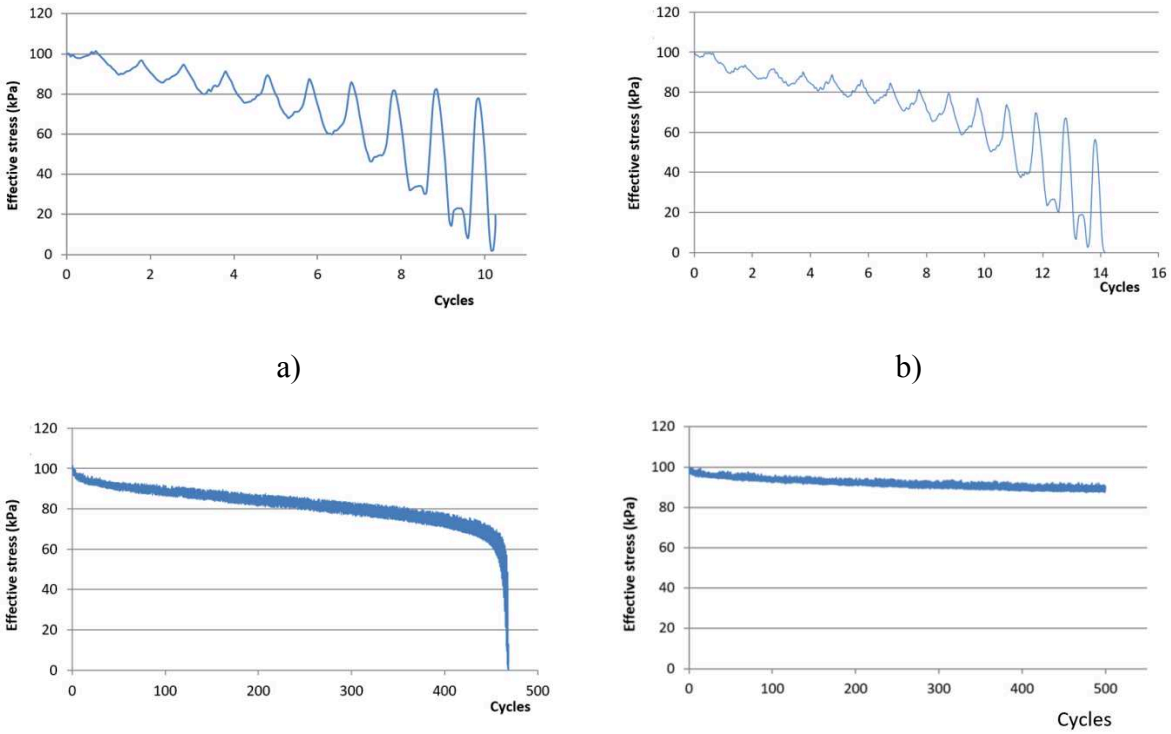

Figure 4.17 Effective confining stress versus number of cycles for the samples with saturation degree of approximately 95%.

a) test CUI-1 with the CSR of 0.35, b) test CUI-2with the CSR of 0.3, c) test CUI-3with the CSR of 0.25, d) test CUI-4with the CSR of 0.2.

The development of normalized pore water pressure is presented in figure 4.18. It can be seen that the two-peak mechanism is also observed in this figure. Figure 4.18c shows three phases of the development of this parameter. The first phase and last phase witness the non-linear rapid increase of r_u, while, in the second phase, this parameter increase linearly. The classification into three phases in this figure is the same with the phases presented in figure 4.15. Similar to the saturated tests, this three-phase form is not clear in the figure 4.18a and figure 4.18b when the CSRs are 0.35 and 0.3, respectively.

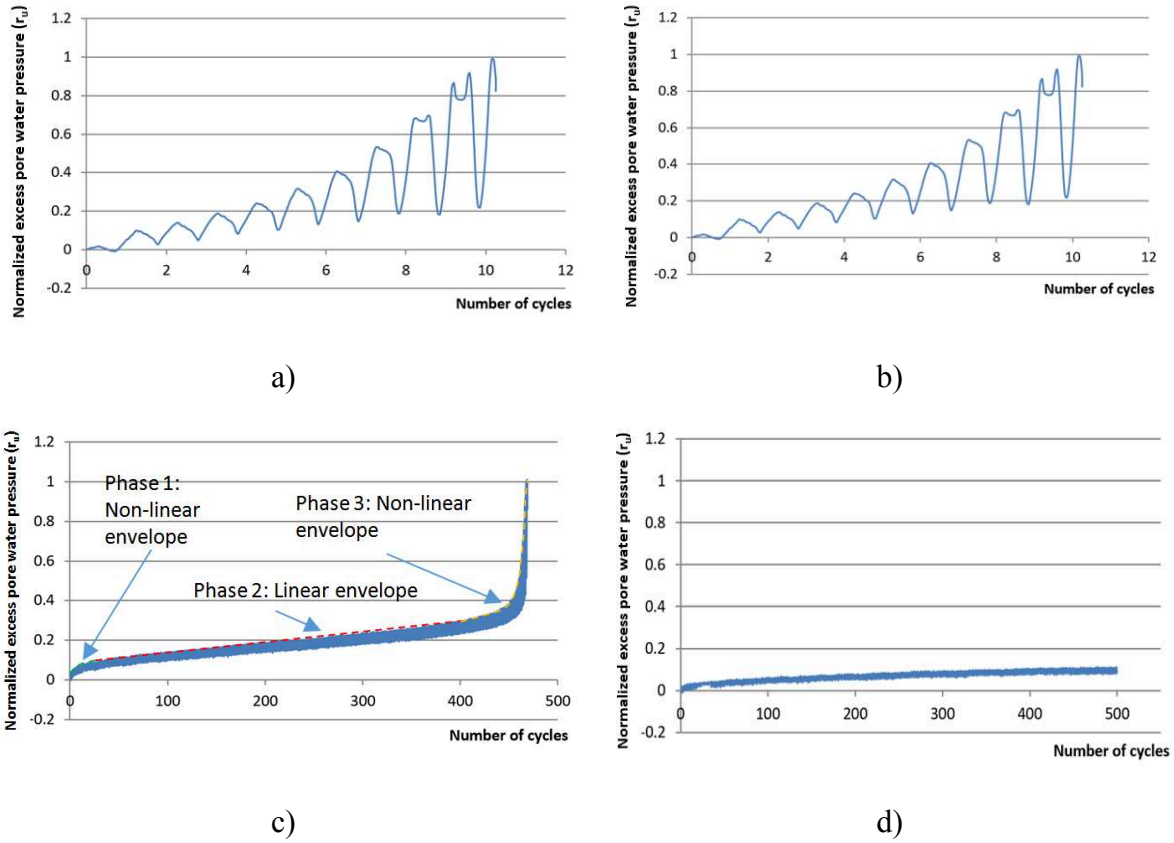

Figure 4.18 Normalized excess pore water pressure versus number of cycles for the samples with saturation degree of approximately 95%.

a) test CUI-1 with the CSR of 0.35, b) test CUI-2with the CSR of 0.3, c) test CUI-3with the CSR of 0.25, d) test CUI-4with the CSR of 0.2.

The relationship between the deviator stress and the mean effective stress is presented in figure 4.19 in which, the mean effective stress of unsaturated soil in the vicinity of the full saturation state is calculated as equation 4.5:

$$p' = \frac{\sigma_1' + \sigma_2' + \sigma_3'}{3} = \sigma' + q/3 \qquad \text{(Eq. 4.5)}$$

here, σ' is the effective confining stress calculated as equation 4.4.

The relationship between the slope of the failure lines and the friction angle is also calculated following equation 4.2 and 4.3. The experimental results show that the slope of the failure lines is the same despite of the decrease of the initial saturation degree from 100% to almost 95%. In both cases, the friction angle is 34^0.

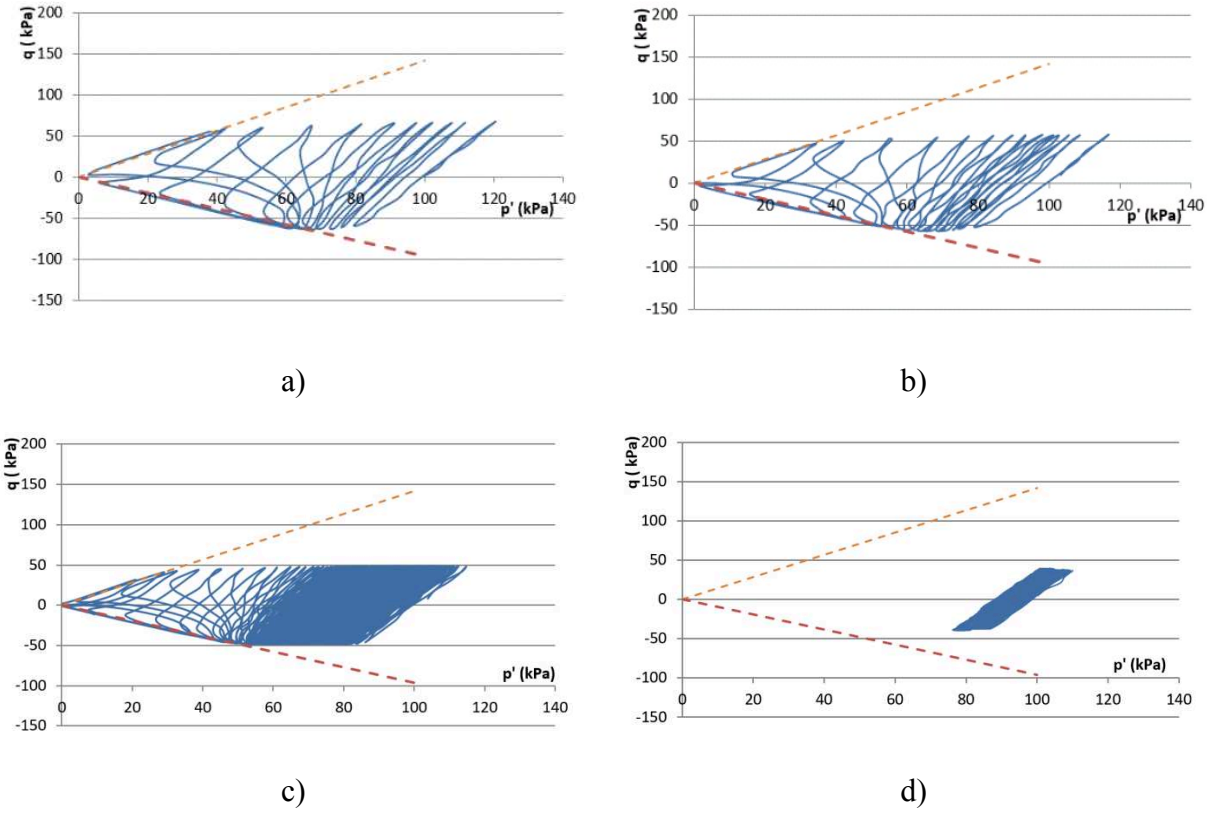

Figure 4.19 Deviator stress versus mean effective stress for the samples with saturation degree of approximately 95%.

a) test CUI-1with the CSR of 0.35, b) test CUI-2with the CSR of 0.3, c) test CUI-3with the CSR of 0.25, d) test CUI-4with the CSR of 0.2.

The accumulated axial strain after each cycle of deviator stress is demonstrated in figure 4.20. The axial strain of all tests reaches 5% when the samples liquefy. In some last cycles, the axial strain develops sharply each time the deviator stress passes zero. After that is a period, in which the axial strain develops more slowly and the deviator stress is restored.

The presentation of tests in the plane of pore water pressure versus axial strain shows that the axial strain develops at a highest rate when the pore water pressure reaches its peaks (figure 4.21).

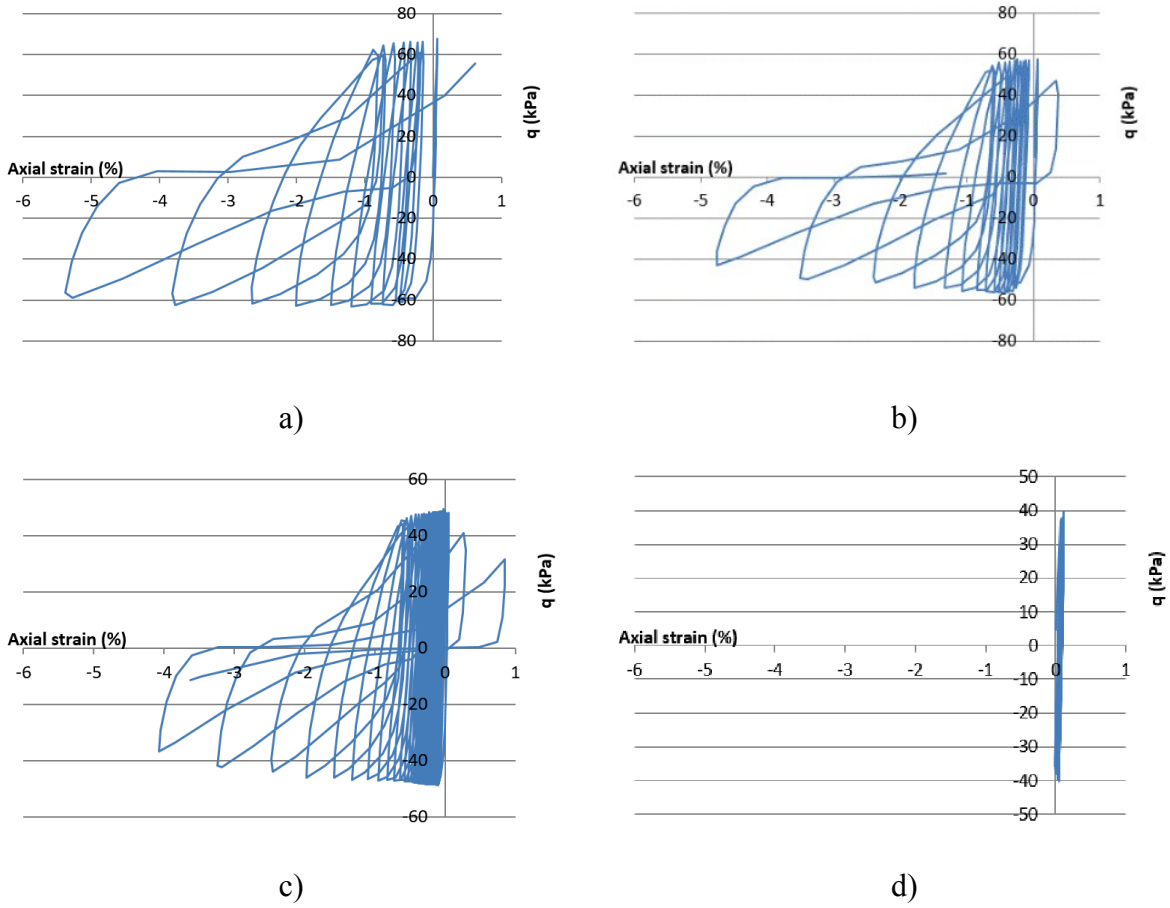

Figure 4.20 Deviator stress versus axial strain for the samples with saturation degree of approximately 95%.

a) test CUI-1with the CSR of 0.35, b) test CUI-2with the CSR of 0.3, c) test CUI-3with the CSR of 0.25, d) test CUI-4with the CSR of 0.2.

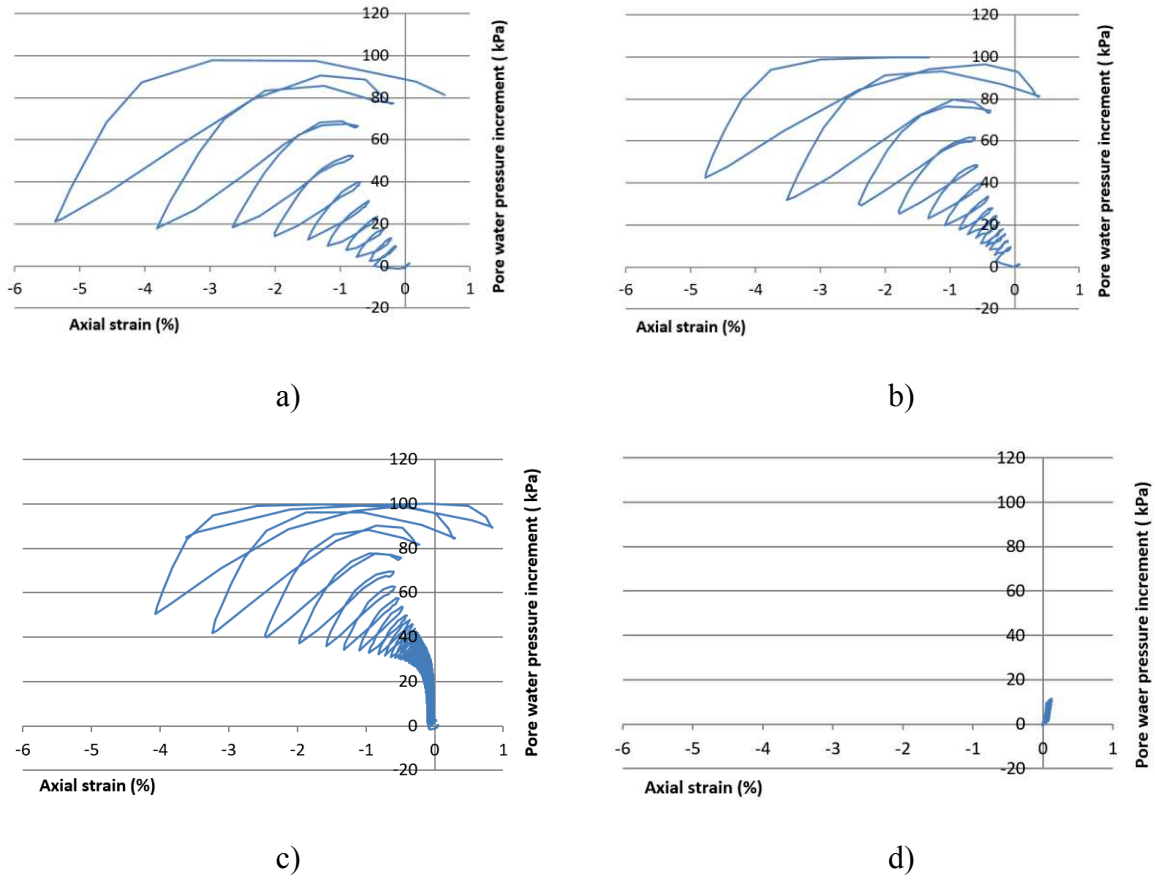

Figure 4.21 Pore water pressure versus axial strain for the samples with saturation degree of approximately 95%.

a) test CUI-1with the CSR of 0.35, b) test CUI-2with the CSR of 0.3, c) test CUI-3with the CSR of 0.25, d) test CUI-4with the CSR of 0.2.

IV.3.1.2.2. Samples with saturation near 86 %: Liquefaction of soil due to the excess development of axial strain

The initial saturation of tests is almost 86% as presented in table 4.7. The desired CSR for tests decreases from 0.45 to 0.3 with the step of 0.05 after each test. Figure 4.22 shows the real applied deviator stress in a function of the number of cycles. In test CUII-1 (figure 4.22a), the deviator stress fluctuates between 85 kPa and approximately -70 kPa. The test stops after 5 cycles of loading. Noting that when the deviator stress reaches -70 kPa, the stress path in these figures seems to contact with the lower failure line. Thus, the sample becomes very soft and the apparatus could not generate the desired amplitude in the negative direction. That is

why the minimum value of the deviator stress is only approximately -70 kPa. In test CUII-2 (figure 4.22b), the positive amplitude of the deviator stress is 80 kPa corresponding to CSR of 0.4. Similar to test CUII-1, the negative amplitude of the deviator stress is approximately -70 kPa. In test CUII-3 (figure 4.22c), the positive amplitude is 70 kPa corresponding to the CSR of 0.35 and the negative amplitude reaches -70 kPa. In test CUII-4 (figure 4.22d), the CSR is approximately 0.3 and the test finishes after 500 cycles of loading without any liquefaction signals observed.

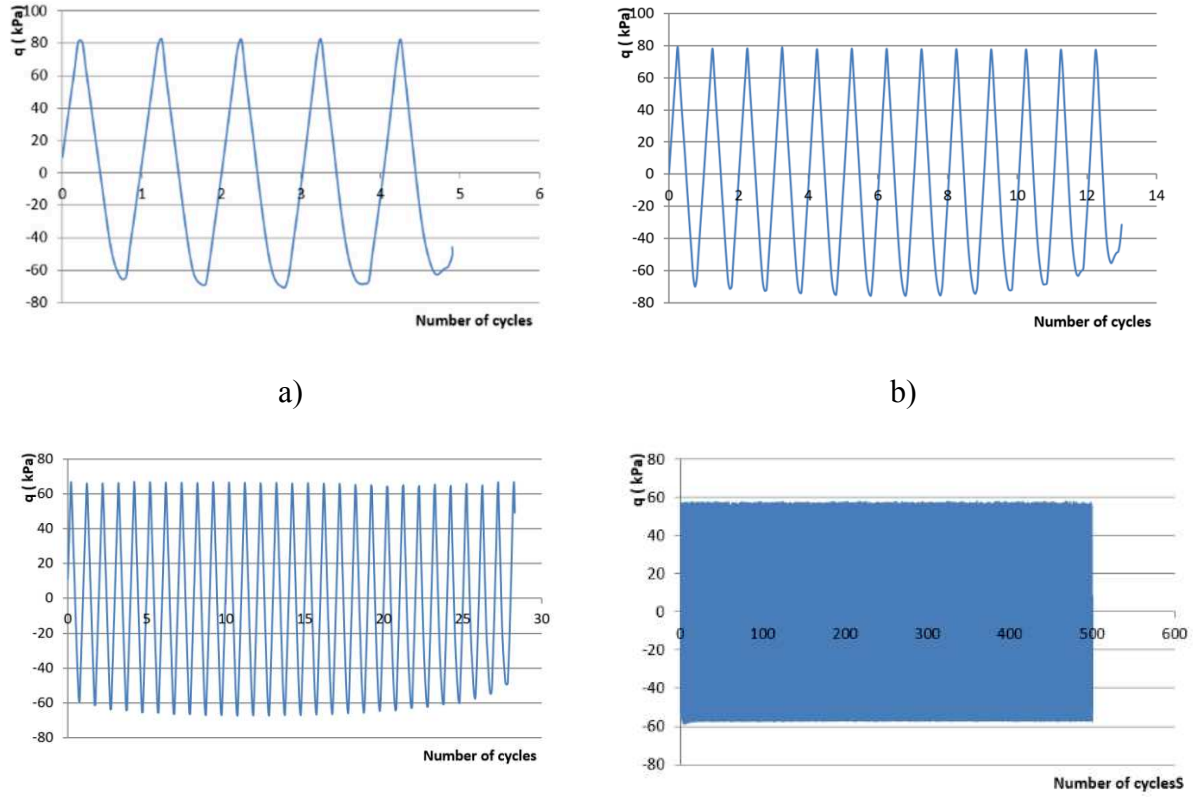

Figure 4.22 Deviator stress versus number of cycles for the samples with saturation degree of approximately 86 %.

a) test CUII-1with the CSR of 0.45, b) test CUII-2with the CSR of 0.4, c) test CUII-3with the CSR of 0.35, d) test CUII-4with the CSR of 0.3.

Figure 4.23 shows the development of accumulated pore water pressure after each loading cycle. For easy understanding, it is necessary to note that the initial pore water pressure after the sample consolidation were 0 kPa. The cell pressure was kept stably at 100 kPa during the tests. In these figures the deviator stress of all tests does not reach the initial confining stress.

In tests CUII-1 and CUII-2, the pore water pressure increases to 20 kPa before the stop of tests. In test CUII-3, the pore water pressure increment is 50 kPa, a little higher than two previous tests; however, much lower than the initial confining stress. It can be concluded that in these tests, the first criterion for liquefaction, the pore water pressure equals to cell pressure, is not observed.

Considering the change of pore water pressure in each cycle, it can be seen that there are not the two-peak mechanism appearing in tests like the two previous series of tests presented above (the first series is on the saturated samples and the second one is on the samples with the initial saturation of almost 95%). In tests CUII-2 and CUII-3, there is a period where the upper amplitude of pore water pressure is kept constant at a value.

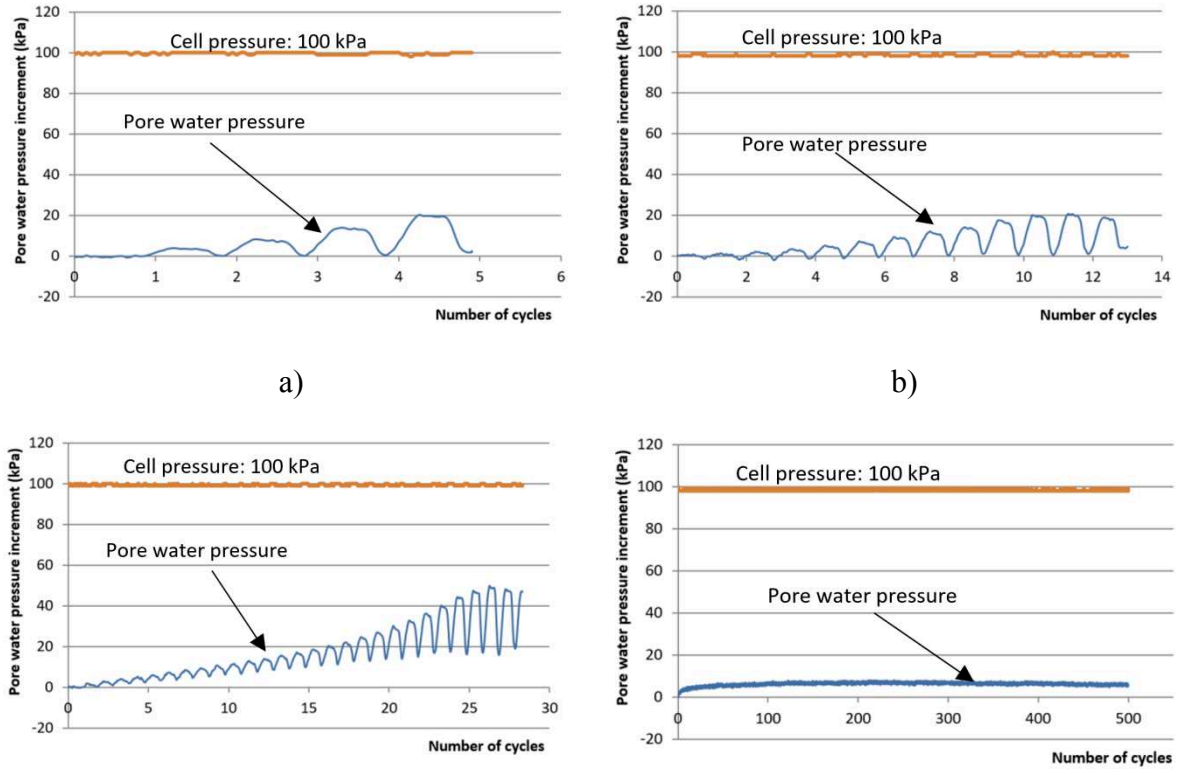

Figure 4.23 Pore water pressure increment versus number of cycles for the samples with saturation degree of approximately 86%.
a) test CUII-1 with the CSR of 0.45, b) test CUII-2 with the CSR of 0.4, c) test CUII-3 with the CSR of 0.35, d) test CUII-4 with the CSR of 0.3.

Figure 4.24 shows the accumulated axial strain in a function of the number of cycles. The axial strain increases after each cycle. In tests CUII-1, CUII-2, and CUII-3, the double

amplitude of axial strain in the final cycles reaches 5% and these samples are considered to be liquefied (following the second criterion). While, the axial strain of test CUII-4 is much lower than 5% after 500 load cycles, thus, the test has been stopped and the sample is considered to be non-liquefied. It can be seen that the upper and lower peaks of axial strain develop only toward the negative direction without the stage in which these peaks develop to both negative and positive sides like the two previous series of experiments. The axial strain development of test CUII-4 is very small (figure 4.24d)

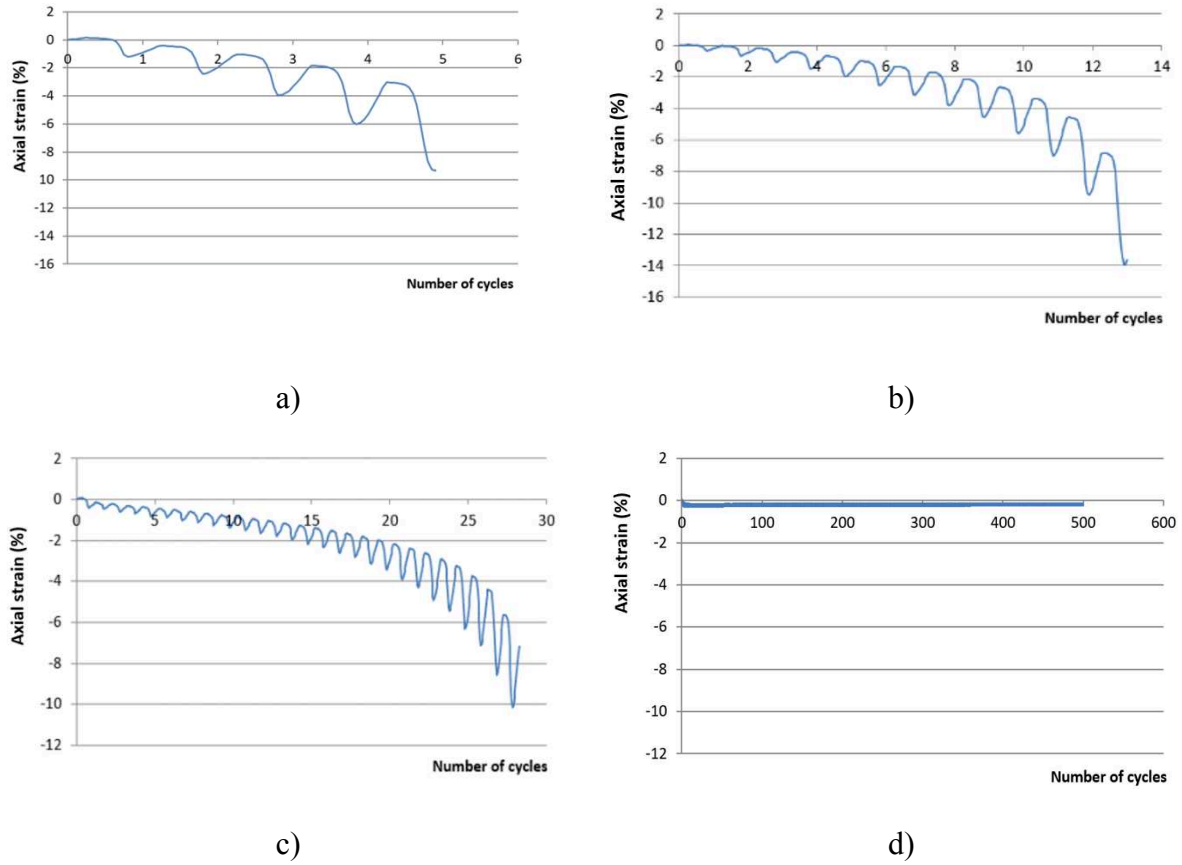

Figure 4.24 Axial strain versus number of cycles for the samples with saturation degree of approximately 86%.

a) test CUII-1 with the CSR of 0.45, b) test CUII-2 with the CSR of 0.4, c) test CUII-3 with the CSR of 0.35, d) test CUII-4 with the CSR of 0.3

Figure 4.25 displays the effective stress versus the number of cycles of the tests. In this series of tests, the effective confining stress is still similar to the second series of tests on the samples with the initial saturation degree of approximately 95%. At the time the samples liquefy, the effective stress is not equal zero. In figures a) and b), the effective confining stress at the end of tests is 80 kPa at some points. In figure c, the effective confining stress decrease

from 100 kPa to 50 kPa after 28 cycles. In figure d, the effective confining stress is almost 90 kPa after 500 cycles.

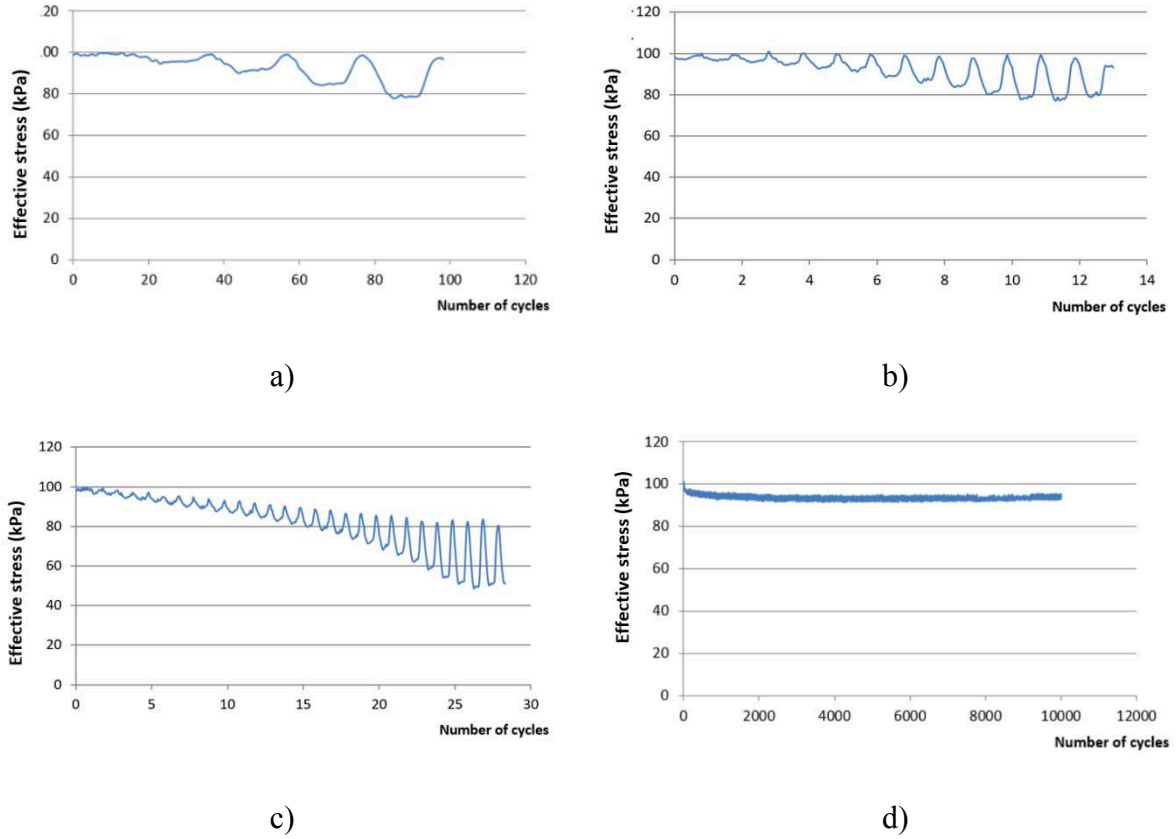

Figure 4.25 Effective confining stress versus number of cycles for the samples with saturation degree of approximately 86%.
a) test CUII-1 with the CSR of 0.45, b) test CUII-2 with the CSR of 0.4, c) test CUII-3 with the CSR of 0.35, d) test CUII-4 with the CSR of 0.3

Figure 4.26 exhibits the increment of normalized excess pore water pressure ratio r_u for all the tests. In figure 4.26a and 4.26b this ratio reaches a peak of 0.2 when the samples liquefy. In figure 4.26c, this ratio reaches a peak of 0.5 when the sample liquefies. And this ratio is almost zero with test CUII-4 (figure 4.26d) after 500 loading cycles. These results show agreement with the development of pore water pressure presented in figure 4.23. Because the pore water pressure does not reach the initial confining stress, r_u is much lower than the unit for all tests.

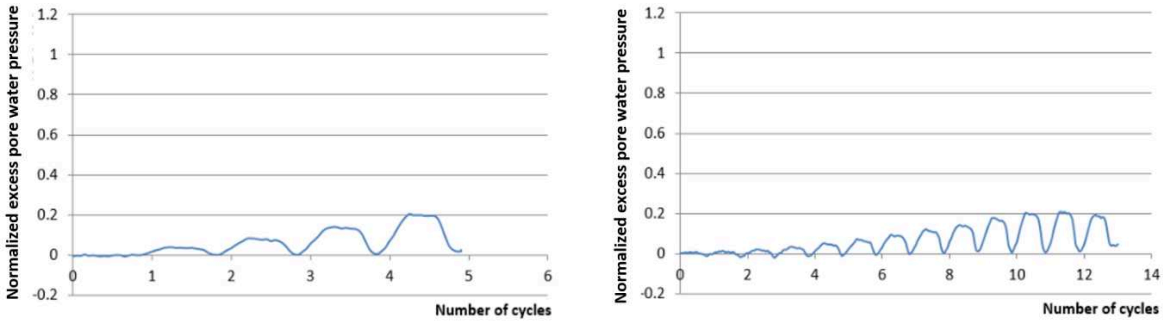

a)

b)

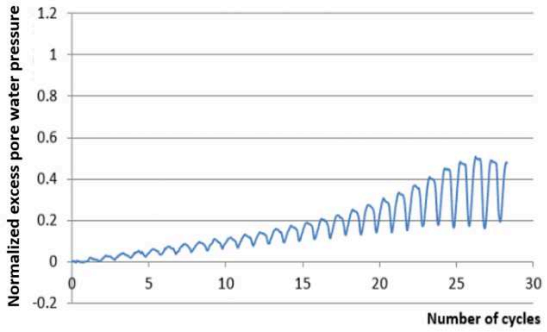

c)

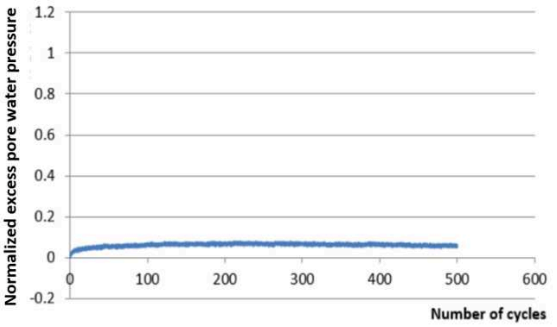

d)

Figure 4.26 Normalized excess pore water pressure versus number of cycles for the samples with saturation degree of approximately 86%.
a) test CUII-1 with the CSR of 0.45, b) test CUII-2 with the CSR of 0.4, c) test CUII-3 with the CSR of 0.35, d) test CUII-4 with the CSR of 0.3

The stress paths of tests are presented in the plane of deviator stress versus mean effective stress. It can be seen that in figure 4.27a and figure 4.27b the stress paths reach the failure line (in extension domain) from the first cycle. Due to this, the samples becomes very soft and that is why the deviator stress, in this case, stops at -70 kPa although the apparatus had been programmed to generate higher values.

In figure 4.27c, when the applied CSR is 0.35 corresponding to the deviator stress fluctuating between -70 kPa and 70 kPa, the stress path approaches the failure line in the extension domain. In the cycles before touching the failure line, the mean effective stress decreases slowly after each cycle of loading. However, after reaching the failure line for the first time, the stress path goes rapidly toward the origin.

Figure 4.27d presents the results of test CUII-4 when the deviator stress is 60 kPa corresponding to the CSR of 0.3. The mean effective stress decreases a little after 500 cycles. The figure shows a very dense loops and the stress path is far from the failure line.

From figures 4.27 a, b and c, it can be seen that these samples liquefied because the stress paths contact with the lower failure line. This explains that why the peaks of the axial strain develop only to the negative side. It is deferent from the two series of studied tests on the sample having initial saturation of 100% and 95% when there are the developments of the peaks of the axial strain toward both negative and positive directions.

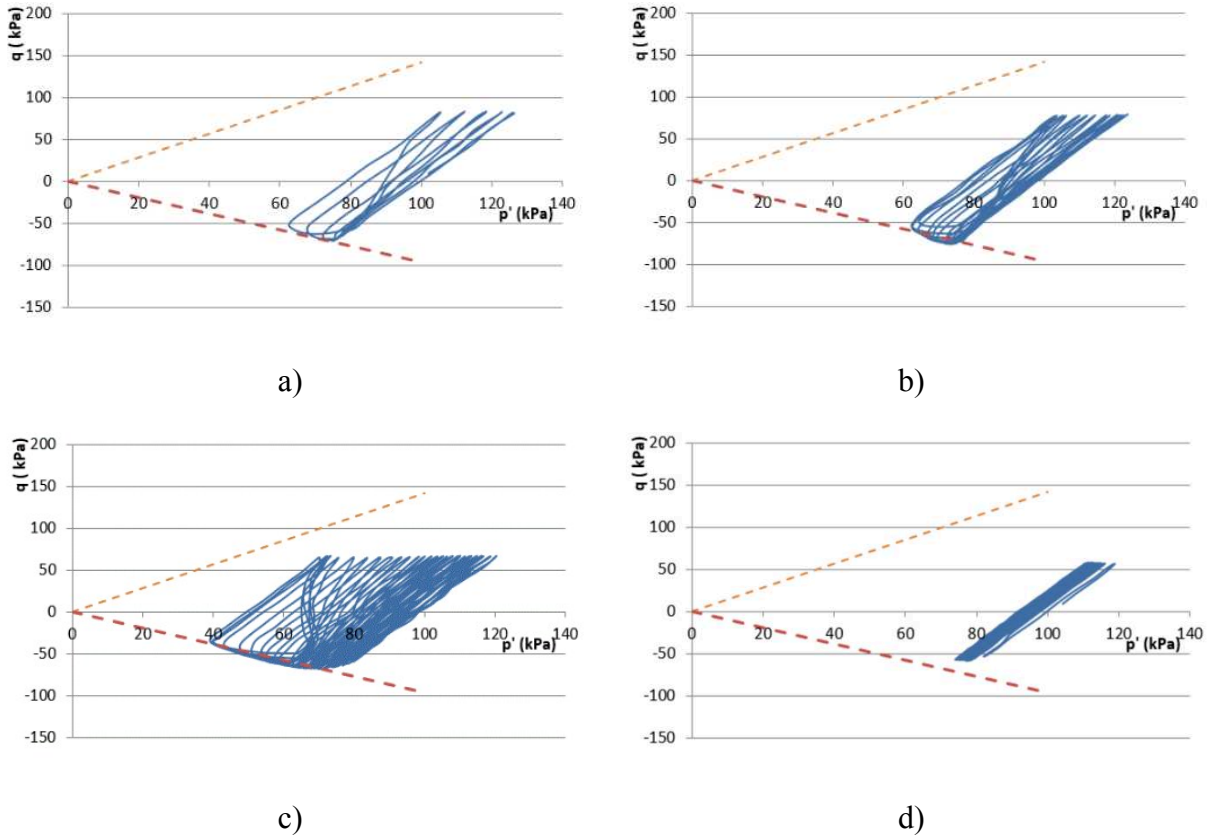

Figure 4.27 Deviator stress versus mean effective stress for the samples with saturation degree of approximately 86%.

a) test CUII-1 with the CSR of 0.45, b) test CUII-2 with the CSR of 0.4, c) test CUII-3 with the CSR of 0.35, d) test CUII-4 with the CSR of 0.3

The stress-strain path of tests is demonstrated in the plane of the deviator stress versus axial strain (figure 4.28). The double amplitude of the axial strain of the first three tests reaches 5% when the samples liquefy. The stress-strain path in these figures shows the difference from that in the two previous series of tests. In these tests, the axial strain develops suddenly when

the deviator stress reaches it minimum value, not at the time when the deviator stress passes zero like the samples in the two previous series. The peaks of the stress-strain curves develop only toward the negative direction.

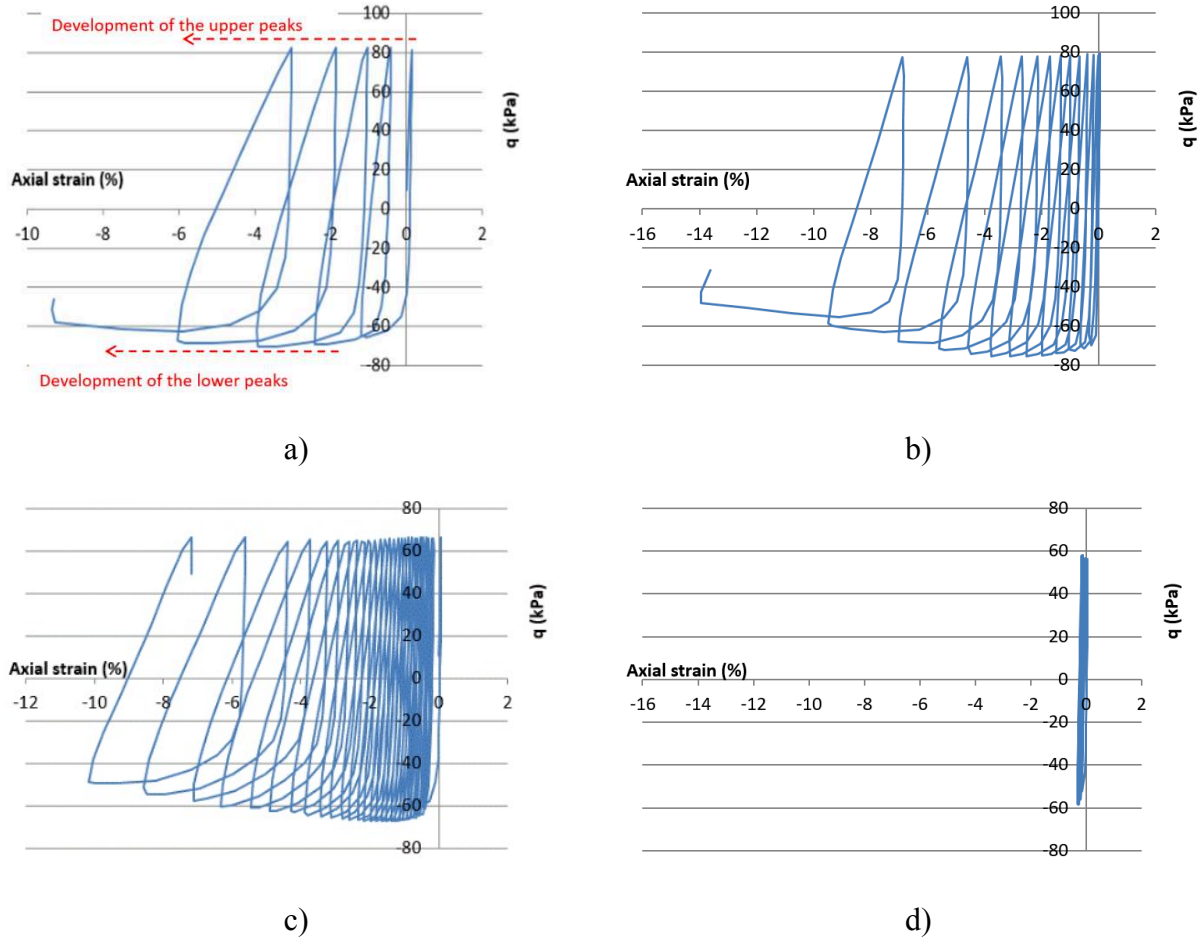

Figure 4.28 Stress – strain path for the samples with saturation degree of approximately 86%. a) test CUII-1 with the CSR of 0.45, b) test CUII-2 with the CSR of 0.4, c) test CUII-3 with the CSR of 0.35, d) test CUII-4 with the CSR of 0.3

The presentation of the results in the pore water pressure – axial strain plane shows the development of each parameter (figure 4.29). At the beginning of each curve, the pore water pressure and the axial strain are small, and they accumulate slowly after each cycle. However, these parameters increase strongly at some last cycles. It can be seen that the axial strain develops most rapidly not at the time the pore water pressure reaching its highest values.

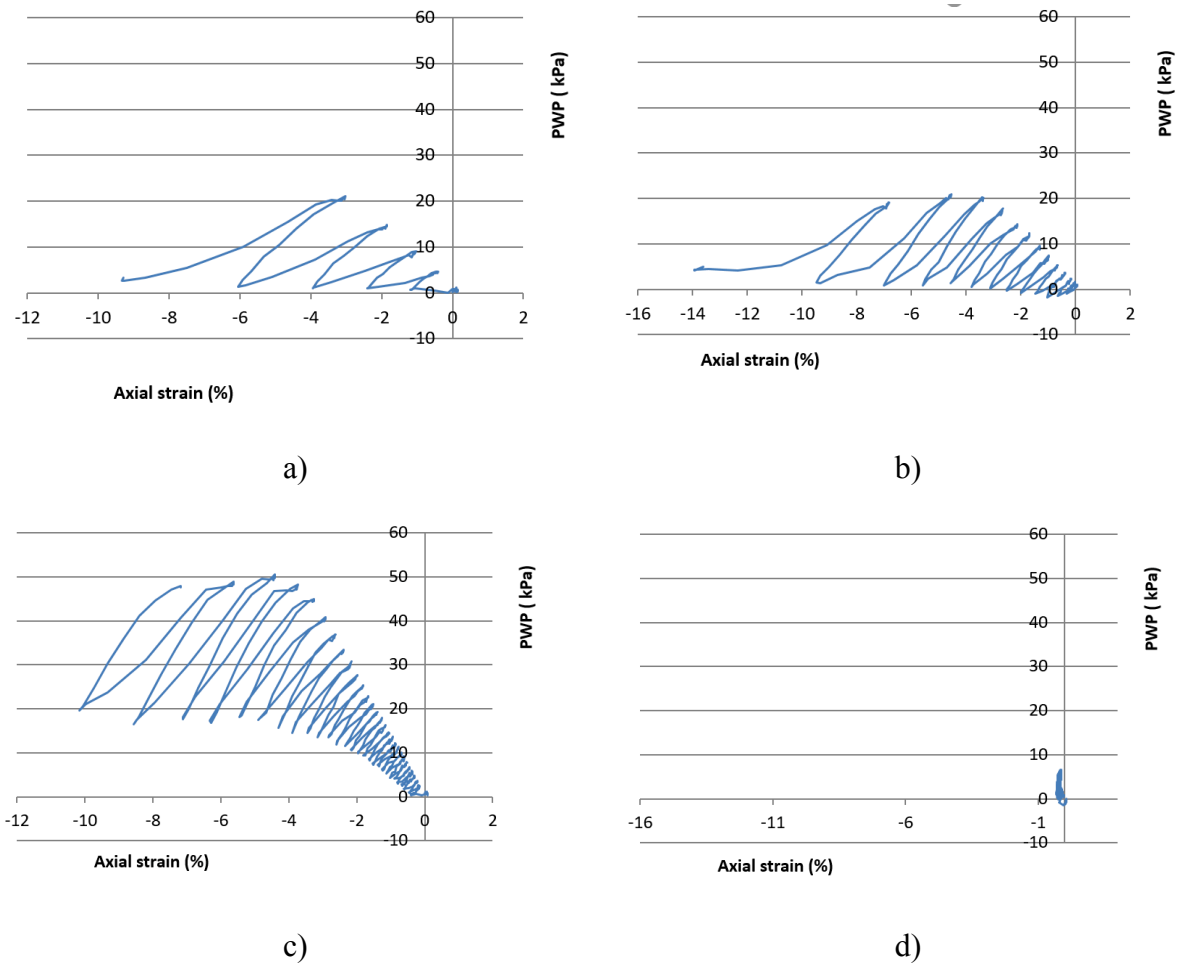

Figure 4.29 Deviator stress versus pore water pressure for the samples with saturation degree of approximately 86%.

a) test CUII-1 with the CSR of 0.45, b) test CUII-2 with the CSR of 0.4, c) test CUII-3 with the CSR of 0.35, d) test CUII-4 with the CSR of 0.3

IV.3.2. Residual strength after liquefaction

IV.3.2.1. Test program

Two monotonic tests on unsaturated samples were carried out to study the residual strength of the sand after liquefaction (Table 4.8). The axial strains before the monotonic compressed tests are not the same because these values depend on the ending moment of the preceded cyclic loading tests. The axial strain of test MT2 varies from -2% to 16% while the axial strain of test MT3 varies from -9% to 10%. The total axial strain of both tests is approximately 20%.

Table 4.8. Monotonic tests on unsaturated samples.

No	Name	Preceded cyclic test	Void ratio before monotonic loading: e_{m0}	S_r before monotonic loading	σ_3 kPa	U kPa	Axial strain variation (ε_a) %
1	MT2	CUI-2	0.802	95.6	100	0	[-2 ; 16]
2	MT3	CUII-3	0.79	87.4	100	0	[-9 ; 10]

MT: *Monotonic test after liquefaction*
CUI: *Cyclic unsaturated test (group I with saturation degree around 95%)*
CUII: *Cyclic unsaturated test (group II with saturation degree around 86%)*

IV.3.2.2. Results

Figure 4.30 shows relationship between the deviator stress and the mean effective stress of the monotonic test MT2. For easy understanding, the stress path of the preceded cyclic test and the second consolidation after liquefaction were added. The cyclic loading starts at point A, after 14 cycles of cyclic loading, the sample liquefies and the test stops at point B. In the second consolidation process, the pore water pressure was dissipated, and during this process, the axial strain was maintained, so the deviator stress decreased slightly and the mean effective stress increased. In the last stage, the monotonic loading was applied and the result is presented by the line CD. It can be seen that the stress path in this stage is linear, and it ends at the intersection with the failure line in the compression domain. This figure also demonstrates that the cyclic loading test and the monotonic loading test have the same failure line.

In figure 4.31, the void ratio change is plotted in a function of axial strain. Through this figure, it is clear that the sample behaves as it is in dense state. The void ratio decreases a little at the beginning of test. After that, it shows a strong increase. The variation of the volumetric strain and the deviator stress are also demonstrated in figure 4.32 and figure 4.33.

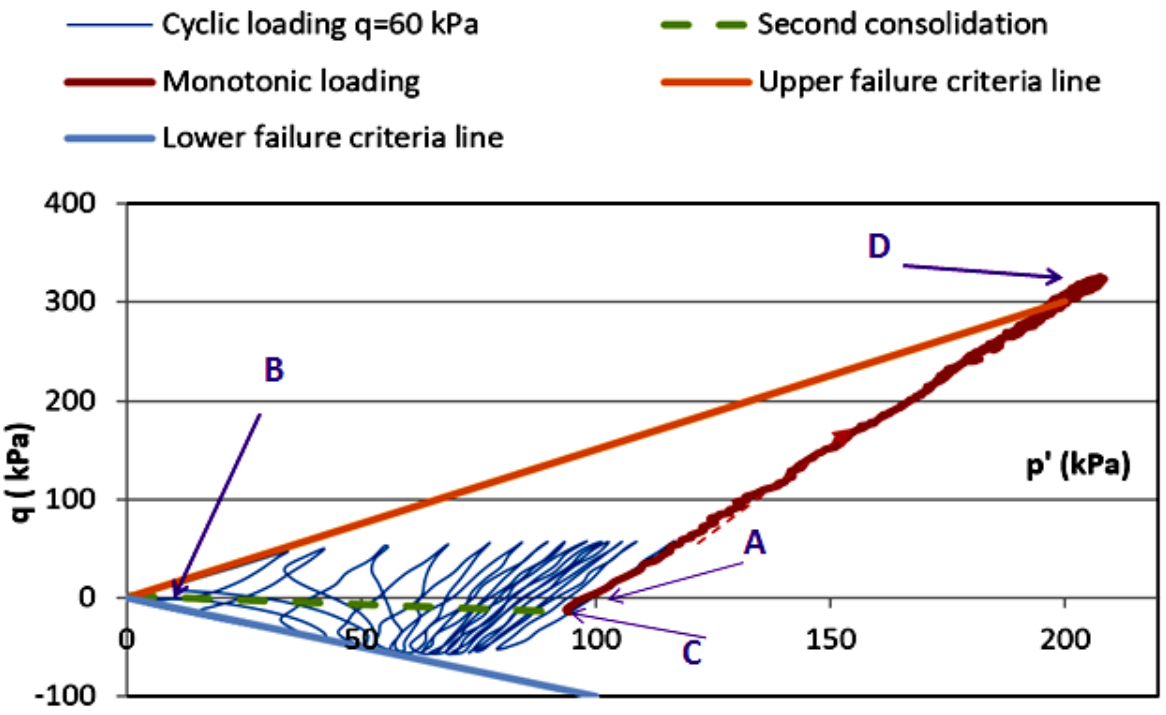

Figure 4.30. Deviator stress versus mean effective stress for unsaturated test CUI2 + MT2

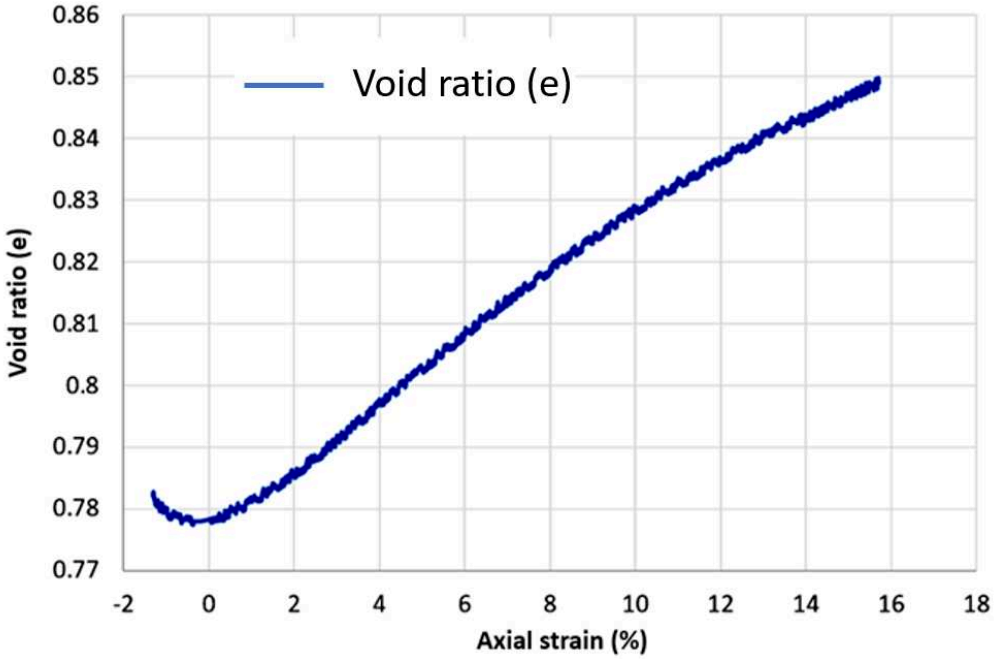

Figure 4.31 Void ratio versus axial strain for monotonic unsaturated test MT2.

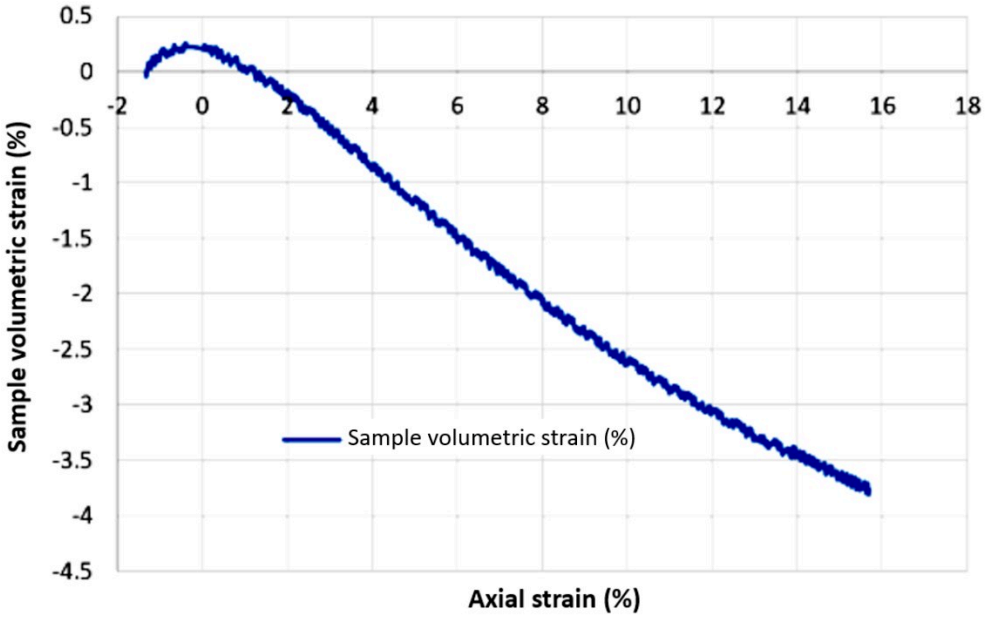

Figure 4.32. Sample volumetric strain versus axial strain for monotonic unsaturated test MT2.

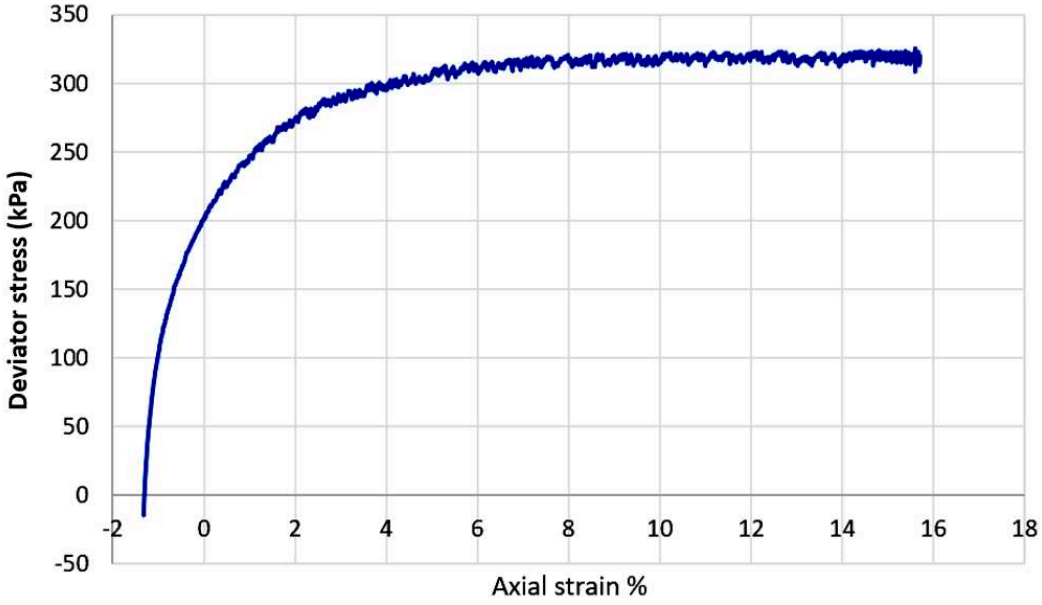

Figure 4.33Deviator stress versus axial strain for monotonic unsaturated test MT2.

IV.3.3. Test parameters variation during the unsaturated test

The protocol developed in this study allows following or calculating the test parameters not only on the saturated test but also on the unsaturated tests. The parameters of the unsaturated test CUI2+MT2 are presented in table 4.9.

Table 4.9. Variation of parameters during the unsaturated test CUI2+MT2.

Parameters	**Before consolidation (initial state)**	**After consolidation 1**	**After cyclic loading**	**After reconsolidation**	**After monotonic loading**	**After final saturation**
B	0.22	-	-	-	-	-
S_r %	95.85	95.81	97.72	95.6	95.97	100
Void volume (cm^3)	240.9	238.7	234.0	228.2	248.4	248.4
Water volume (cm^3)	231.0	228.7	228.7	218.2	238.4	248.4
Dry weigh of sample (g)	773.4	773.4	773.4	773.4	773.4	773.4
Sand particle volume (cm^3)	291.84	291.84	291.84	291.84	291.84	291.84
Total sample volume(cm^3)	532.8	530.5	525.9	520.1	540.3	540.3
Void ratio(e)	0.826	0.818	0.802	0.782	0.851	0.851

The variation of saturation degree and the void ratio during the saturated test CUI2+MT2 is exhibited in figure 4.34. The test was carried out on the unsaturated sample, the initial saturation degree is 95.85%, and it decreases slightly after the sample consolidation process. During the cyclic loading process, the sample volume decreased, and the air bubbles were compressed so it can be seen in figure 4.34 that the saturation degree increases strongly. The void ratio changes in each stage of the test including the cyclic loading, even though this process was carried out in an undrained condition.

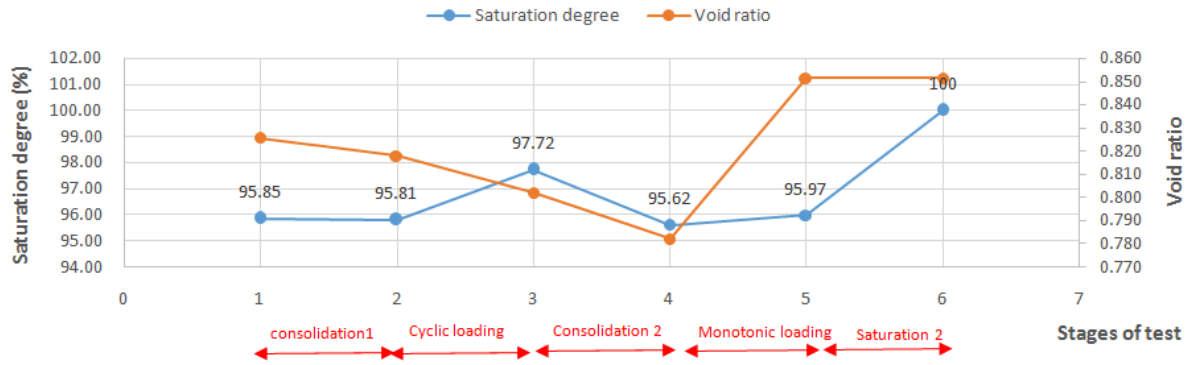

Figure 4.34 Saturation degree and void ratio changes during the unsaturated test CUI2+MT2

IV.4. Effect of saturation degree on the liquefaction potential of sand

In order to study the effect of saturation degree to the liquefaction behavior of sand, the summary results of tests are presented in figures from 4.35 and 4.37.

Figure 4.35 shows the effect of the saturation degree on the liquefaction resistance of the sand. It can be seen that the increase of liquefaction resistance is not linear with the decrease of saturation degree. The 5% decrease of saturation degree, from 100% to 95%, results in an increase of liquefaction resistance which is higher than that caused by the decrease of saturation degree from 95% to almost 86%. The liquefaction resistance is more sensitive to the change of saturation degree in the domain near 100%.

The results in figure 4.35 can be compared to the results of Arab et al 2015 (figure 4.36). In their study, the tests were carried out on the samples having the initial relative density of 50% a litter lower than that in this study (≈54%). There is a small difference between two studies when comparing the two curves corresponding to the highest B values in two figures. However, it is not clear that the relative density in their study is calculated before or after the sample consolidation, and also the methodology to measure this parameter was not presented.

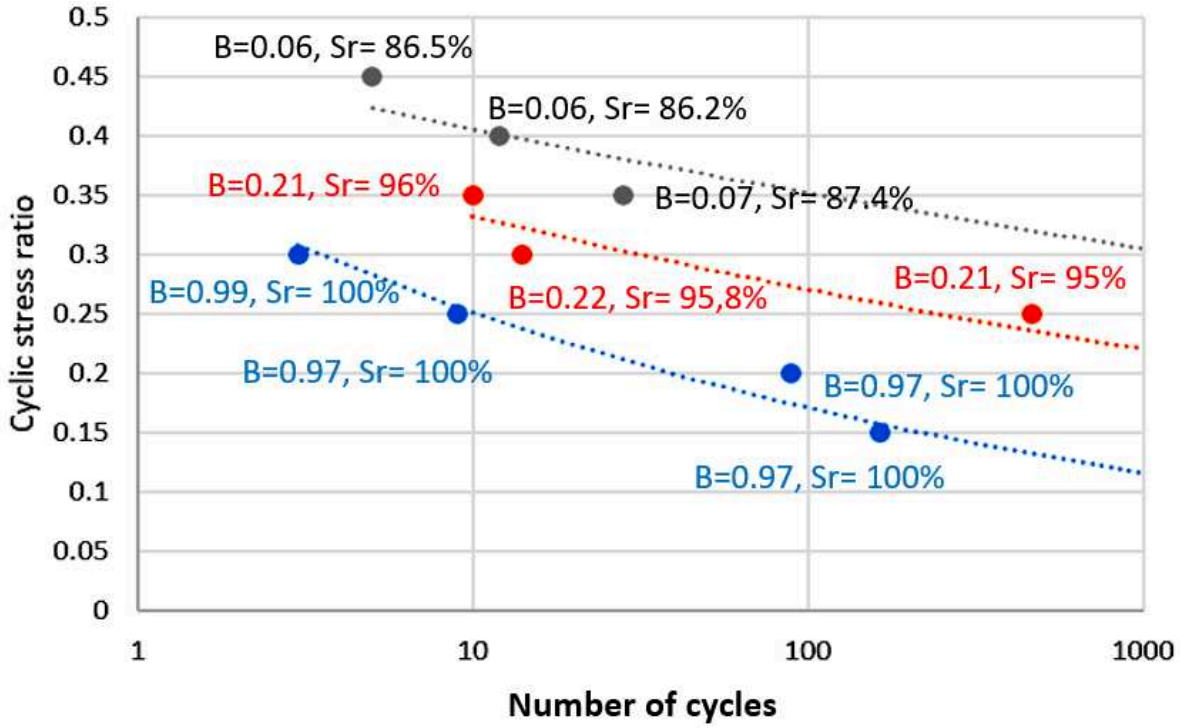

Figure 4.35 Influence of saturation degree on the liquefaction potential of Hostun Rf sand

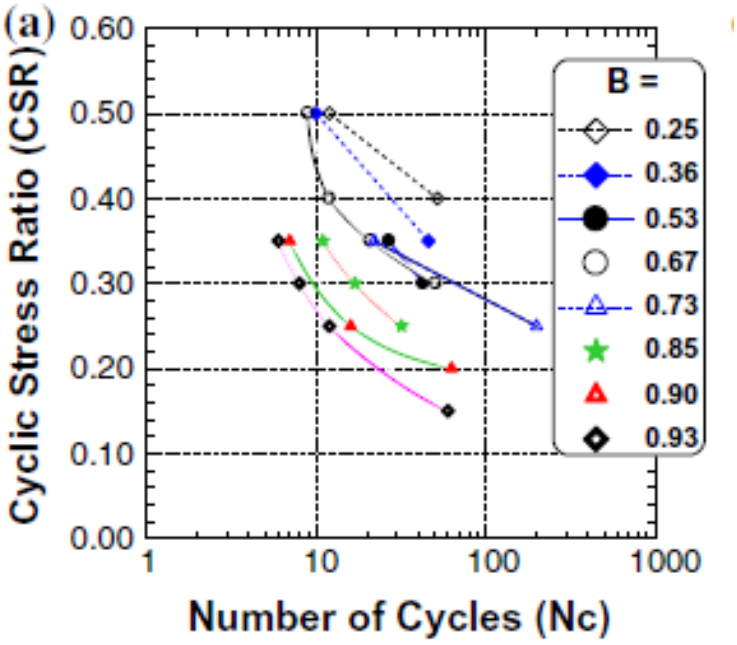

a)

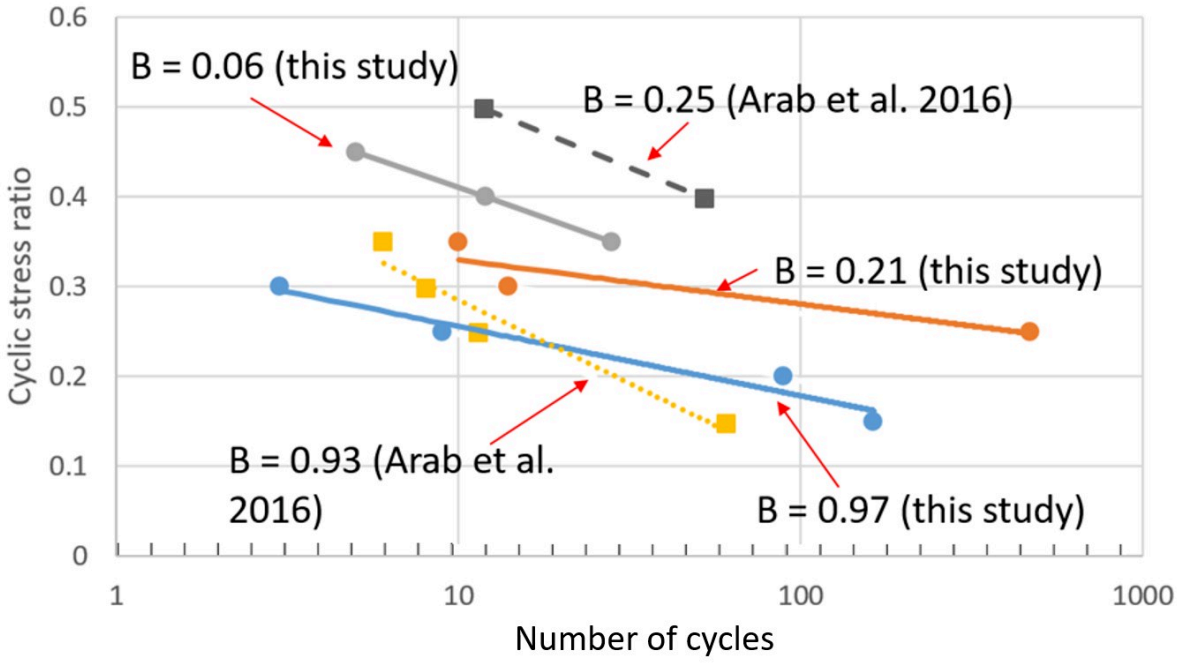

b)

Figure 4.36 Influence of Skempton's coefficient (saturation degree) on the cyclic un-drained response of the Hostun Rf sand.

a) the results of Arab et al. (2016); b) The results of this study in comparison with Arab et al. (2016)

IV.5. Volumetric strain at the liquefaction state

Figure 4.37 presents the sample volume change at the liquefaction state versus the saturation degree. Because the cyclic loading was applied under the un-drained condition, the full saturated samples have a volumetric strain of 0%. When the saturation degree decreases to almost 95%, there are air bubbles appearing inside the pore fluid and make the pore fluid possible to be compressed. Under cyclic loading, the samples contract, and this results in the increase of pore water pressure. Figure 4.38 shows the void ratio variation versus the saturation degree. From the modeling in the study of Unno et al. (2008), the void ratio change at the state of null effective stress is linear with the saturation degree (figure 4.39). Because the relationship between the void ratio change and the sample volume change is linear (equation 4.6), it can be inferred that the sample volumetric strain at the null effective stress state (liquefaction state due to the excess pore water pressure) is linear with the saturation degree. In relation to this study, the curve in figure 4.37 can be divided into two parts. In the area of the line AB, the relationship between volumetric strain at liquefaction state and the

saturation degree is linear. In this domain, the two conditions of liquefaction (the excess pore water pressure and double amplitude of 5%) are observed. While, in the domain of the line BC, at liquefaction state, maybe only the 5% of double amplitude criterion is observed. However, it is noted that the volumetric strain in this domain increase with the decrease of CSR. At point C, when the CSR applied is 0.35, the volumetric strain is 2% while at point D, the volumetric strain is only 1.1% when the CSR applied is 0.4. And it can be predicted that the excess pore water pressure criterion for liquefaction will appear on the sample with a saturation degree of 86% if the volumetric strain reaches 2.7% (point E) and certainly under the CSR lower than 0.35. The curves BD, BF, BC, BE can represent for the sample volume change at liquefaction states caused by the different CSRs.

$$e_t = e_0 + \varepsilon_v.(1 + e_0) \leftrightarrow \Delta_e = \varepsilon_v.(1 + e_0) \quad \text{(Eq. 4.6)}$$

where, e_0 and e_t is the initial void ratio and the last value of void ratio, respectively. ε_v is the volumetric strain of the sample.

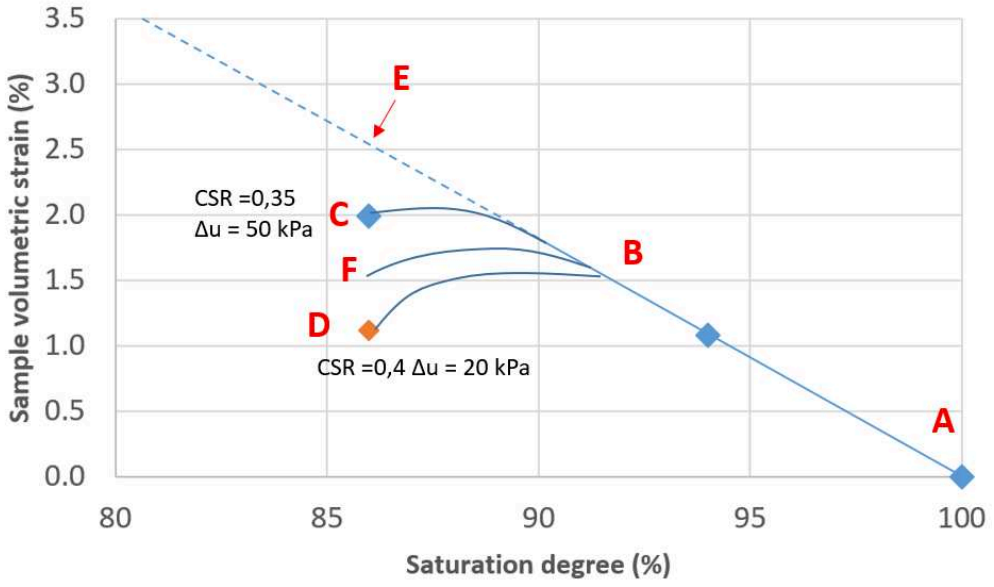

Figure 4.37 Volumetric strain at liquefaction state versus the degree of saturation

Figure 4.38 presents the void ratio change in a function of saturation degree with different applied CSR. This figure helps to refer to the study of Unno et al. (2008) more clearly. The initial void ratio of all samples is approximate 0.826 (red dashed line in the figure). With unsaturated samples, the appearance of air bubbles inside the voids makes the pore fluid compressible. When the samples contract, the pore air is compressed and the pore water pressure increases. The increase of the sample volume change results in the increase of the

pore water pressure. Following the modeling of Unno et al. (2008), the sample volume change needed to increase the pore water pressure to cell pressure is linear with the saturation degree (line AB). From the figure 4.38, it can be seen that when the saturation degree is on the left of point B (B is an assumed pointed near 90%), only one double amplitude criterion (DA) is observed at liquefaction state. This is because the sample does not contract enough to increase the pore water pressure to the cell pressure. The void ratio of the tests having initial saturation degree of 86% decreases from 0.826 (point O) to 0.79 (point C), this value is higher than the value needed to increase the pore water pressure to cell pressure (point E with void ratio of 0.78). When the saturation degree is on the right of point B, two signals of liquefaction are observed at liquefaction state.

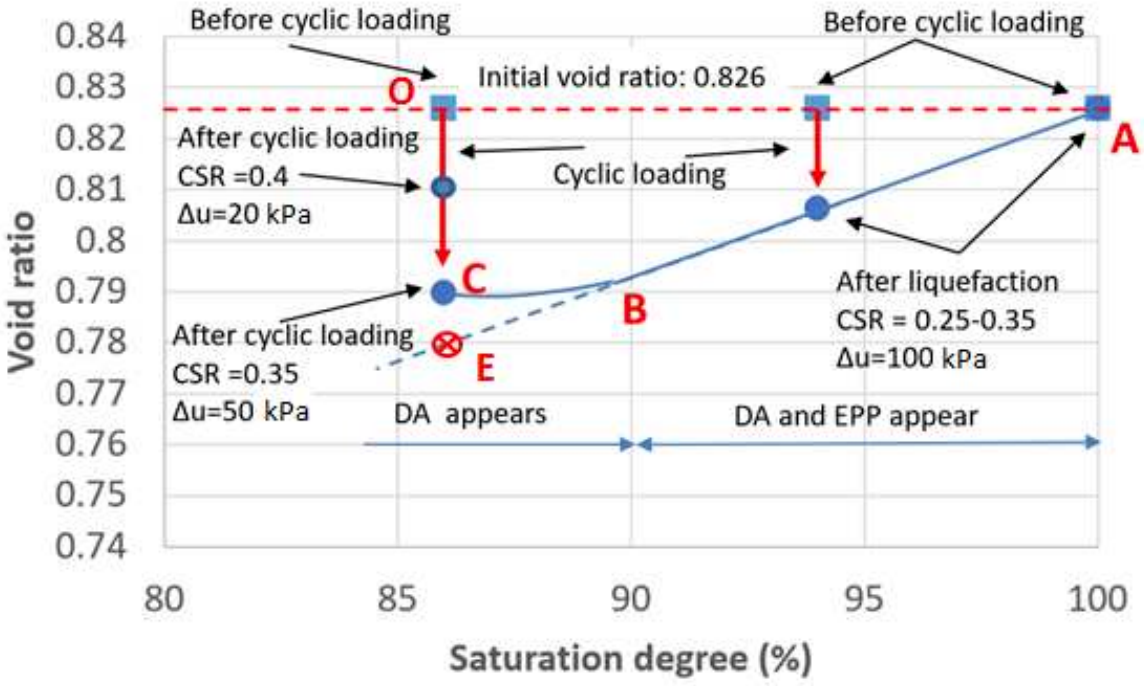

Figure 4.38 Void ratio change in relationship with the initial saturation degree.

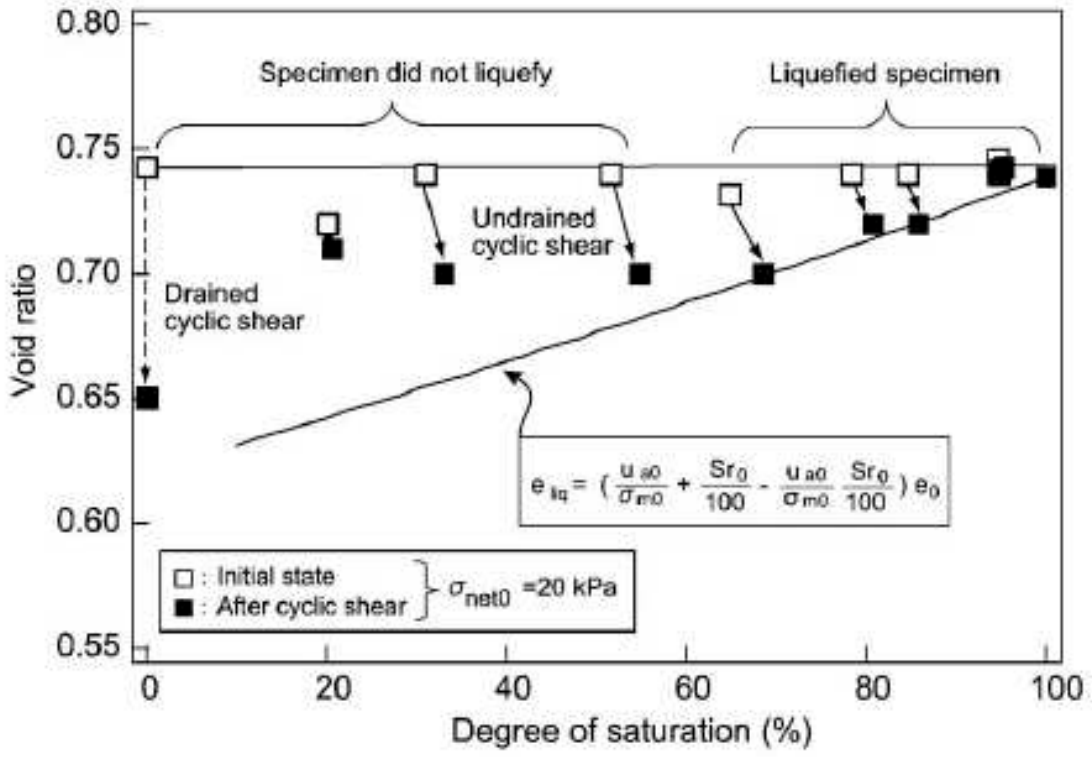

Figure 4.39 Sample volumetric strain prediction in relationship with saturation degree (Unno et al. 2008)

IV.6. Conclusions

The decrease in the initial degree of saturation tends to improve the liquefaction resistance of the sand. The greater the amount of initial air within the granular material, the more the initiation of instability is delayed, and consequently liquefaction as well.

It is clear that the relationship between the increase of liquefaction resistance and the decrease of saturation degree is not linear. The decrease of saturation degree from 100% to 95%, results in an increase of liquefaction resistance higher than that caused by the decrease of saturation from 95% to 86%. The liquefaction resistance is more sensitive to the change of saturation degree in the domain near 100%.

At a high saturation degree, the liquefaction state can result in both the null effective stress and the double amplitude of 5% conditions. However, there is an existence of a threshold for which the saturation degree is smaller than**,** maybe only one criterion of liquefaction (double amplitude) is observed. This result is somewhat similar to that of Vernay (2018) and Vernay et al. (2019). In that study, they showed that there is a difference between the cyclic behavior of soil in the zone of saturation higher than 95% and the zone of saturation lower than 95%.

With the saturation degree smaller than the criteria value mentioned above, the sample volume change is inverse proportional with the value of CSR applied.

The monotonic loading after liquefaction demonstrates that after the liquefaction, the pore water pressure dissipates and the soil residual strength recuperates.

The results of tests with a saturation degree of 86% and 95% suggest an interesting issue. The axial strain at liquefaction in tests having high saturation degree (95%) is mostly due to the increase of pore water pressure (the axial strain develops at the state when the deviator stress passes zero) while the axial strain at liquefaction state in tests having a lower saturation degree (86%) is mostly because the deviator stress reaches the extension strength of the material (Axial strain develops at the state when the deviator stress reaches its lowest value and contacts the lower failure line). This suggests that there is a value of saturation degree, at which, the axial strain caused by two reasons (the deviator stress passes zero and the deviator stress reaches the extension strength) is equal.

CHAPTER 5: EFFECT OF UNSATURATION ON LIQUEFACTION POTENTIAL

-Cyclic Loading with Stepping CSR-

V.1. Introduction

The earthquakes motion, in reality, may include foreshocks, main shocks, and aftershocks. During the earthquake of 2011 in Japan, soil liquefaction occurred and resulted in damages to many houses and buildings. Tamari et al. (2011) showed that, in some areas, sand boiling, a characteristic of liquefaction, first occurred during the main shock and expanded during the aftershocks; however, in some areas, there was no liquefaction during the main shock but only during the aftershocks. Besides, this earthquake was followed by a tsunami, which severely damaged the Japanese Fukushima Daiichi power plant in March 2011. This proposes an issue that it is necessary to study liquefaction behavior of soil before and after the main reason causing liquefaction (ICOLD 2012). Especially, statistics show that foreshock activity has been observed in about 40% of all medium to large earthquakes (National Research Council U.S. 2003), and about 70% of events with M > 7.0 (Kayal 2008). This observation shows the need to have more studies focusing on the behavior before and after the main shock and the effect of foreshocks on the liquefaction potential.

In this chapter, four series of tests were carried out to study the effect of saturation degree on the behavior of sand before and after liquefaction. The first series of tests is performed on the samples subjected to monotonic loading to study the undrained behavior of sand in dense state. The second series of test was carried out on the saturated samples while the third series of test was carried out on the unsaturated samples with different saturation degree. These saturated and unsaturated tests are followed by monotonic loading tests to study the residual strength after liquefaction (series 4). The cyclic loading on the samples has the stepping CSR. As presented in chapter 3, the CSR increases after each one hundred cycles of loading until the appearance of liquefaction. In case the samples show the clear signs of liquefaction after 100 cycles, the CSR will not be increased. Due to this protocol, the number of cycles of each load case is normally 100; however, the last load case of tests may have lower or higher than 100 cycles. This cyclic loading method allows relating to the foreshocks in earthquakes. The summary of the series of tests is presented in table 5.1 below.

Table 5.1. Series of stepping CSR tests.

Series	Saturation state	Test description
Series 1	Fully saturated state B = 0.97	Monotonic compression test in undrained condition
Series 2	Fully saturated state B = 0.97	Cyclic stepping CSR in undrained condition
Series 3	Quasi – saturated state B = 0.6 – 0.87	Cyclic stepping CSR in undrained condition
Series 4	Depend on the preceded liquefaction tests (Series 2 and 3): B=0.6-0.97	Monotonic compression test after liquefaction in drained condition

V.2. Undrained behavior of RF Hostun sand

V.2.1. Test program

To study the un-drained behavior of RF Hostun sand under monotonic loading, the following test (table 5.2) was carried out. The sample was produced with an initial relative density of 83% corresponding to the void ratio of 0.71 by using the wet tamping method. The initial parameters and the sample preparation protocol are the same as those of the cyclic tests which will be presented in the next contents of this thesis. Under the un-drained compression, the axial load increased sharply and the test stopped at the axial strain of 5%.

Table 5.2. Test program for undrained behavior of Hostun sand.

N0	Test name	Test type	Sample preparation method	σ_3 (kPa)	u_0 (kPa)	e_0	D_r
1	CUT1	CU	Wet tamping method	1050	950	0.71	83%

CU: *Consolidated Undrained condition.*
CUT1: *Consolidated Undrained Test 1*

V.2.2. Results

Figure 5.1 shows the behavior of the sample subjected to monotonic compression loading. In figure 5.1a, the deviator stress increases rapidly to 2000 kPa when the axial strain reaches 5.5%. The characteristics of dense sand are shown through the development of pore water pressure and the stress path during the monotonic loading process (figure 5.1b and c). The pore water pressure firstly increases from the initial value of 950 kPa to 980 kPa when the axial strain increases from zero to 1%. After that, it decreases and reaches 400 kPa at the axial

strain of 5.5%. Due to the decrease of the pore water pressure, the effective confining stress increases from 100 kPa to 750 kPa. The test stops at the axial strain of 5.5% and the pore water pressure of 400 kPa. This value of pore water pressure is much lower than the initial pore water pressure and this can lead to the appearance of air bubbles in the pore water. The stress path in figure 5.1d shows the relationship between the deviator stress and the mean effective stress. As presented in chapter 2, this form of stress path corresponds to the characteristic of sand in a dense state. The path goes up to the right and approaches to the failure line. The angle of this failure line can be calculated as equations 4.2 and 4.3 presented in chapter 4 and the result shows that the friction angle in this case is 37°. If we compare this friction angle with the results carried by other authors on the same material (table 4.3), it can be seen that there is a good agreement between the studies.

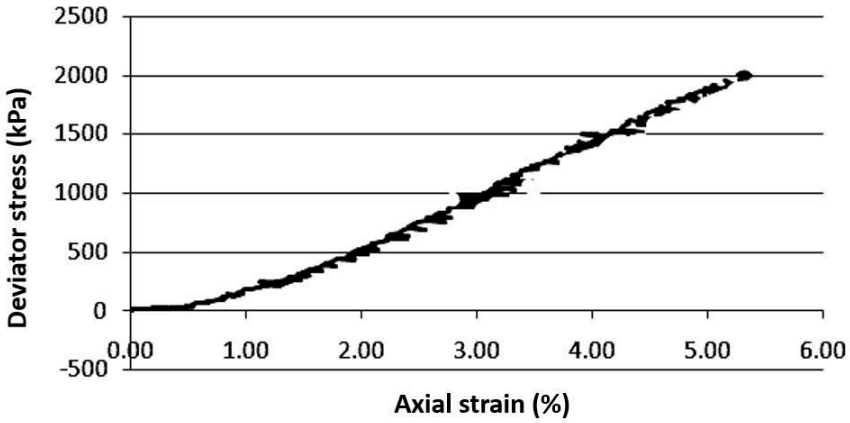

a) Deviator stress versus axial strain

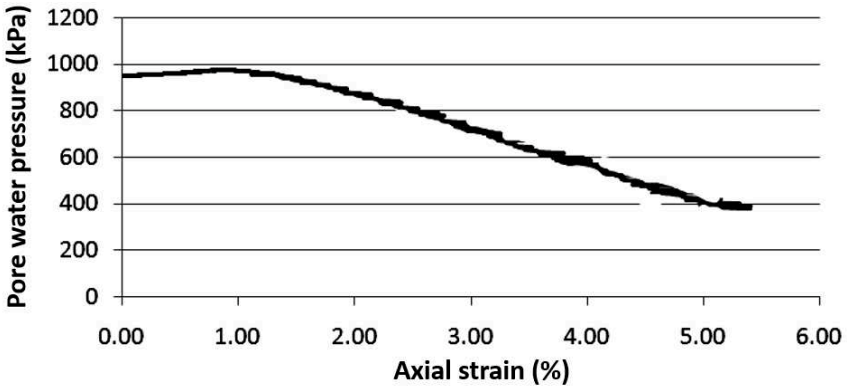

b) Pore water pressure versus axial strain

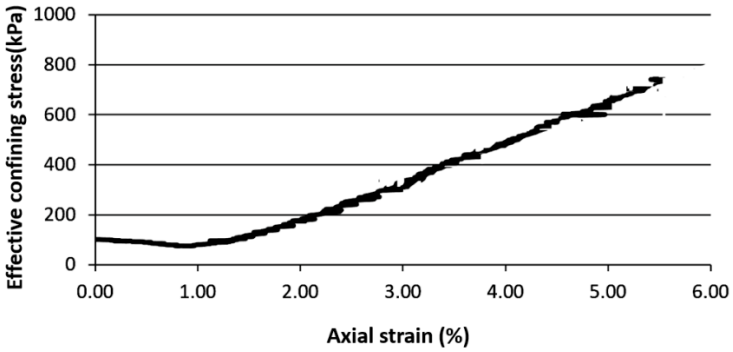

c) Effective confining stress versus axial strain

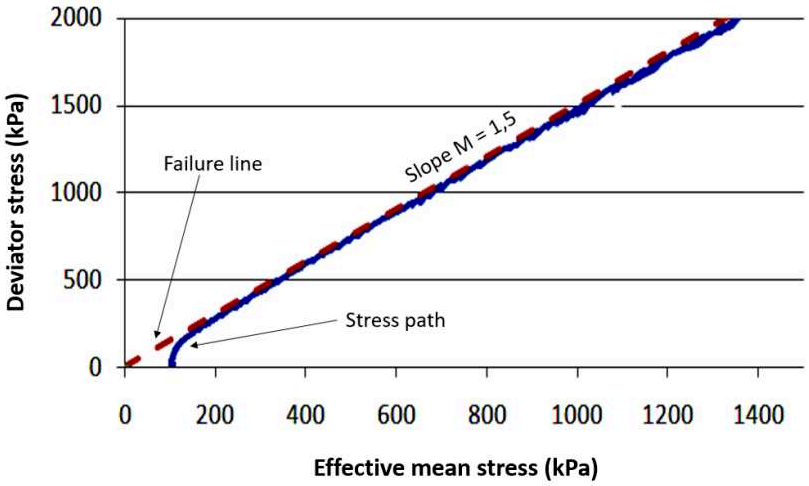

d) Deviator stress versus effective mean stress

Figure 5.1 Undrained behavior of RF Hostun sand at a relative density of 83% under the compressed monotonic loading

V.3. Saturated sand: Liquefaction potential and residual strength

V.3.1. Liquefaction potential

V.3.1.1. Test program

Three saturated cyclic tests with the same initial conditions were carried out (Tests CSST1 to CSST3) to study the behavior of saturated sand under stepping CSR cyclic loading. These tests also allow studying the effect of the sample preparation method to the liquefaction susceptibility of sand in dense state. After 100 cycles of the first and second load case with deviator stress of 30 kPa and 40 kPa, all samples were not liquefied or showed the signals of

liquefaction. The CSR was increased to 0.25 corresponding to deviator stress of 50 kPa. With this CSR all the samples were liquefied. The information of tests is shown in the table 5.3

Table 5.3. The test series on saturated samples subjected to the stepping CSR cyclic loading

Tests No	e_0	B	Sr_0 (%)	q_{max} (kPa)	σ_3	u_0	CSR	N_{Liq}	Liquefaction criterion	Monotonic test coming after liquefaction
CSST1	0.715	0.97	100	50	800	700	0.25	222	EPP	Yes. Test : CSST-M1
CSST2	-	0.97	100	50	800	700	0.25	272	EPP	-
CSST3	-	0.97	100	50	800	700	0.25	310	EPP	-

EPP*: Excess Pore water Pressure equals to the initial effective confining stress*
CSST-M1*: Monotonic saturated test 1 after liquefaction.*
CSST*: Cyclic Saturated Stepping (CSR) Test*
N_{liq}*: Number of cycles at liquefaction*

V.3.1.2. Results

The following figures show the results for test 1. The variation of each parameter under each step of loading are studied. The results of other tests are shown in the appendix.

Figure 5.2 shows the applied deviator stress. The deviator stress is firstly 28 kPa corresponding to the CSR of ≈0.15. After 100 cycles, the deviator stress is increased to 38 kPa corresponding to the CSR of 0.19. At the last load case, the deviator stress fluctuates between -40 kPa and +48 kPa. It can be seen that in the last load case, the horizontal axis is no longer the symmetrical axis of the deviator stress. This issue can be explained by the asymmetry between the lower failure line and the upper line. From the cycles 203^{th}, the deviator stress incrementally decreases and the test stops after 222 cycles.

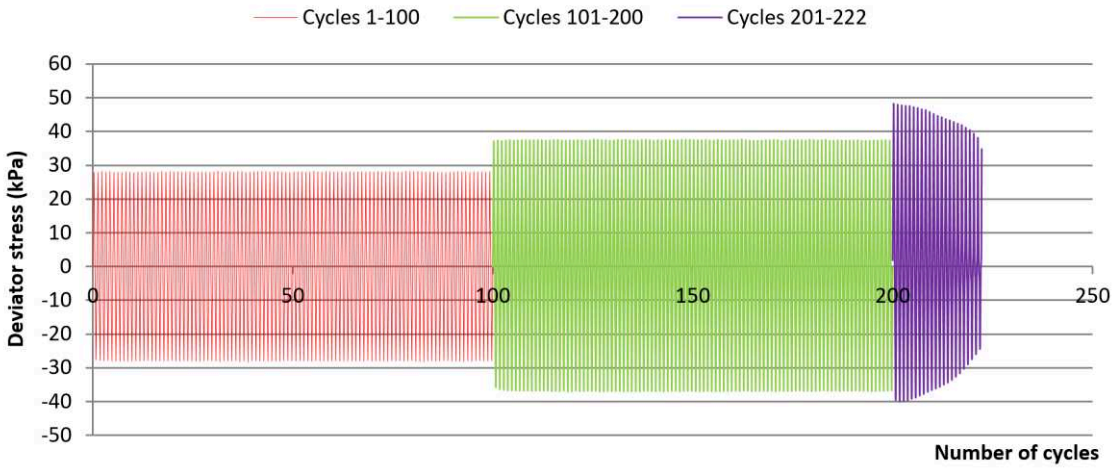

Figure 5.2 Deviator stress in a function of number of cycles for the saturated stepping CSR test.

The development of axial strain in a function of deviator stress is presented in figure 5.3. The results for the first one hundred cycles and the second one hundred cycles are shown in red and green color, respectively. In these load cases, the axial strain fluctuates in small amplitude. The relationship between the deviator stress and the axial strain appears to be linear. The result of the last 22 cycles is shown in purple color. When studying deeply these cycles, it can be seen that in the first 5 cycles (cycle 200 to 204), the axial strain develops mainly when the deviator stress reaches its minimum value. In the plane of deviator stress versus mean effective stress (figure 5.8), this issue is demonstrated by the close distance between the stress path and the lower failure line. However, from cycles 205 to the end of the test, the axial strain develops mainly when the deviator stress passes zero. It is a characteristic of the liquefaction phenomenon; the axial strain develops due to the excess pore water pressure development at the zero effective stress state.

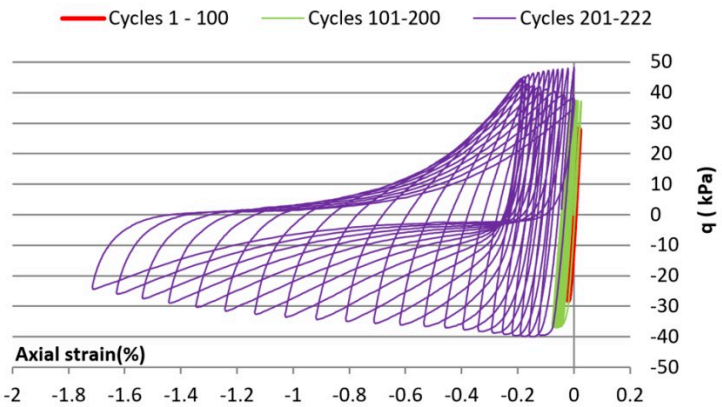

Figure 5.3 Axial strain versus deviator stress for the saturated stepping CSR test.

The development of the pore water pressure after each cyclic loading cycle is shown in figure 5.4a. It can be seen that the pore water pressure increases slowly during load case 1 and load case 2. However, it increases sharply in load case 3. In the first one hundred cycles with CSR = 0.15, the pore water pressure increases from 0 kPa to 20 kPa (the maximum value). While with the CSR of 0.19, the pore water pressure increases from 15 kPa to 45 kPa after 100 cycles. In the last load case, the pore water pressure increases from 45 kPa to 100 kPa in only 22 cycles. Along with the increase of the pore water pressure is the reduction in the effective confining stress (figure 5.4b). These figures also demonstrate that the increase of pore water pressure or the decrease of the effective confining stress in the later load cases is affected by the preceded load cases. In this figure, similar to the liquefaction tests presented in chapter 4, the two-peak mechanism is also observed from the cycle 212th.

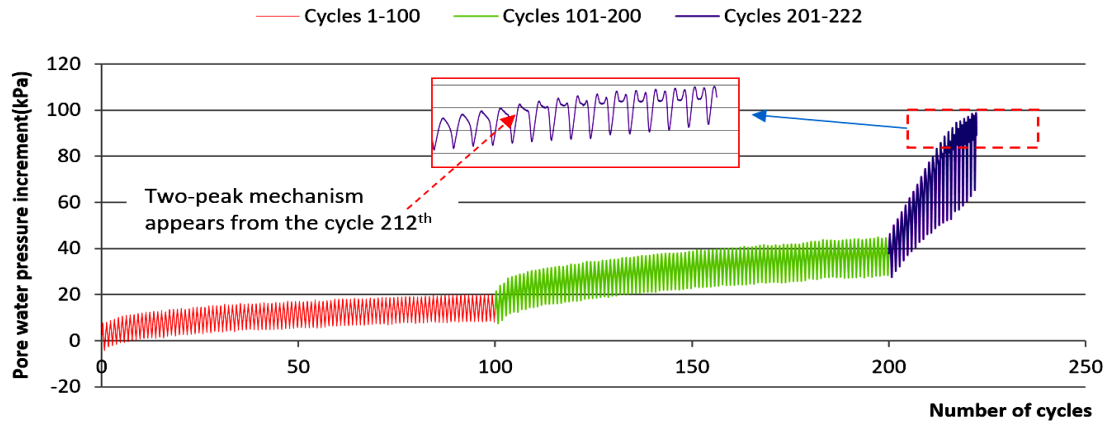

(a)

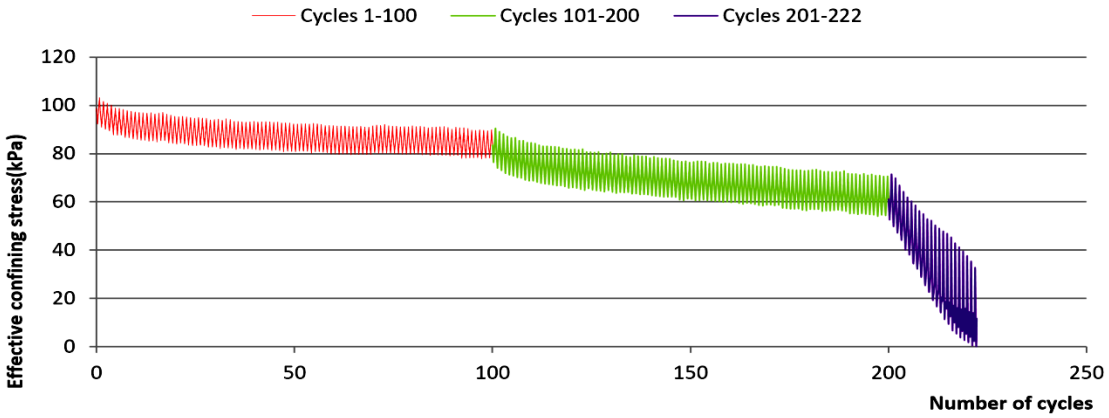

(b)

Figure 5.4 (a) Pore water pressure in function of number of cycles and (b) effective confining stress in function of number of cycles for the saturated stepping CSR test.

The normalized excess pore water pressure increment (r_u)is presented in figure 5.5. Here, this ratio is calculated by normalizing the excess pore water pressure generated during undrained cyclic loading for the initial effective confining stress (equation 5.1). It is noted that the initial effective confining stress used in this equation is the effective confining stress before applying load case 1. This value is used to calculate the normalized excess pore water pressure ratio for all three load cases. This ratio fluctuates due to the change of deviator stress and finally equals to 1 after 22 cycles when the deviator stress is almost 35 kPa.

$$r_u = \frac{\Delta u}{\sigma'_{3c}} \qquad \text{Eq. 5.1}$$

Where Δu is the excess pore water pressure and σ'_{3c} is the effective consolidation stress.

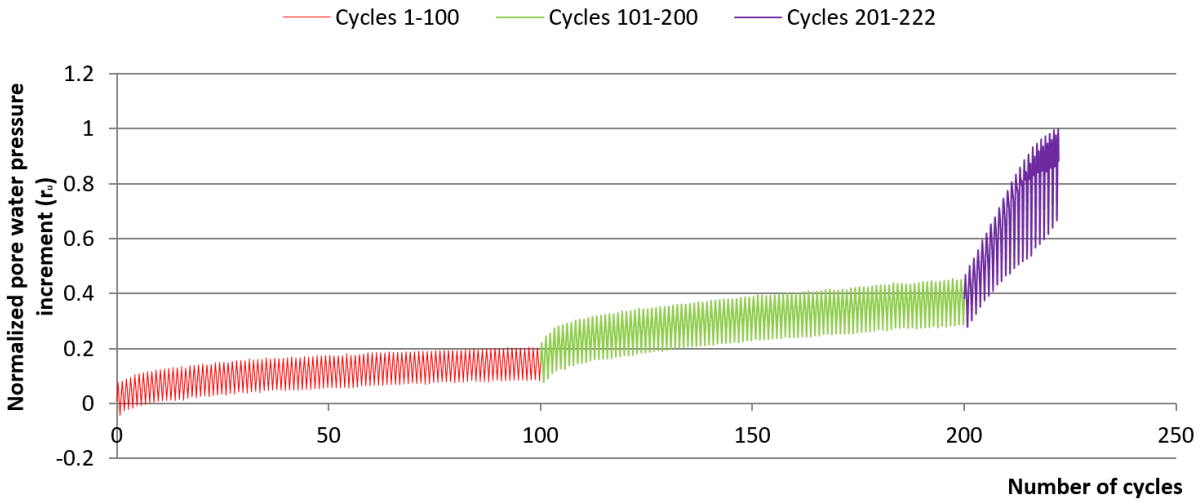

Figure 5.5 Normalized pore water pressure increment r_u for the saturated stepping CSR test.

Figure 5.6 shows the accumulation of the axial strain after each cycle of loading. In the first two hundred cycles, the axial strain is small; however, it increases sharply from the cycle 201 when the CSR is increase to a higher level. Similar to the liquefaction of soil under constant CSR presented in chapter 4, it can be seen that in most cycles from the beginning of the tests, the upper peaks of the axial strain develop towards the negative direction, it means that the samples were stretched; however, from the cycle 212th, the peaks go upward. This tendency appears at the same time with the appearance of the two-peak mechanism presented in the plane of pore water pressure versus number of cycles (figure 5.4a).

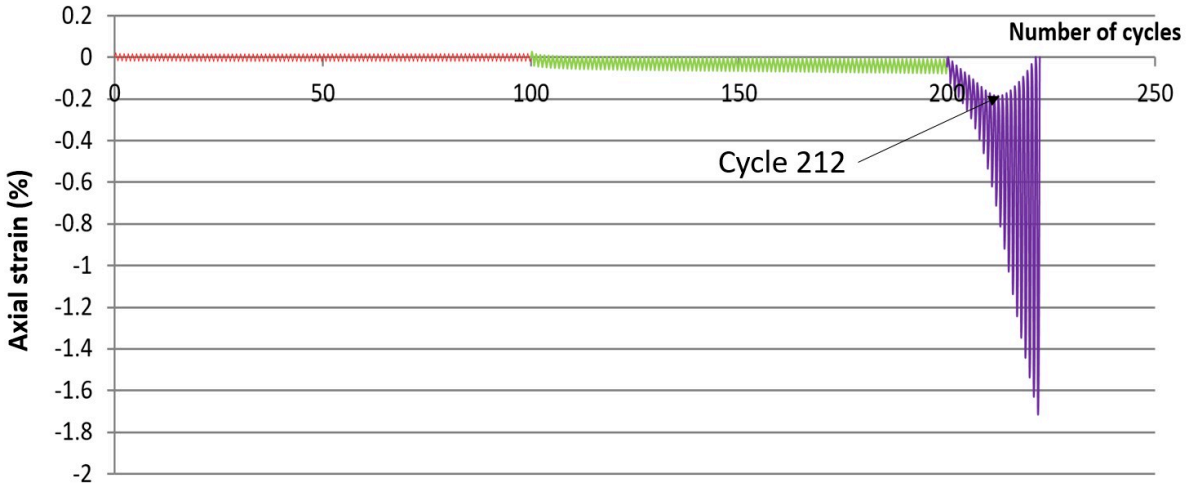

Figure 5.6 Axial strain versus number of cycle for the saturated stepping CSR test.

The relationship between axial strain versus pore water pressure increment is put in the view of figure 5.7. From the cycle 200th, the axial strain develops strongly. However, in cycles from 200th to 205th, the axial strain increases when the pore water pressure is at the lowest points. This is not the characteristic of the liquefaction phenomenon described as: the axial strain develops due to the increase of the pore water pressure results in the decrease of the effective confining stress. From cycle 206th, it is clear that the axial strain increases most strongly when the pore water pressure reaches the highest value. Especially, the axial strain varies suddenly when the pore water pressure increment is equal to the initial confining stress (100 kPa). This is the clearly characteristic of the liquefaction phenomenon.

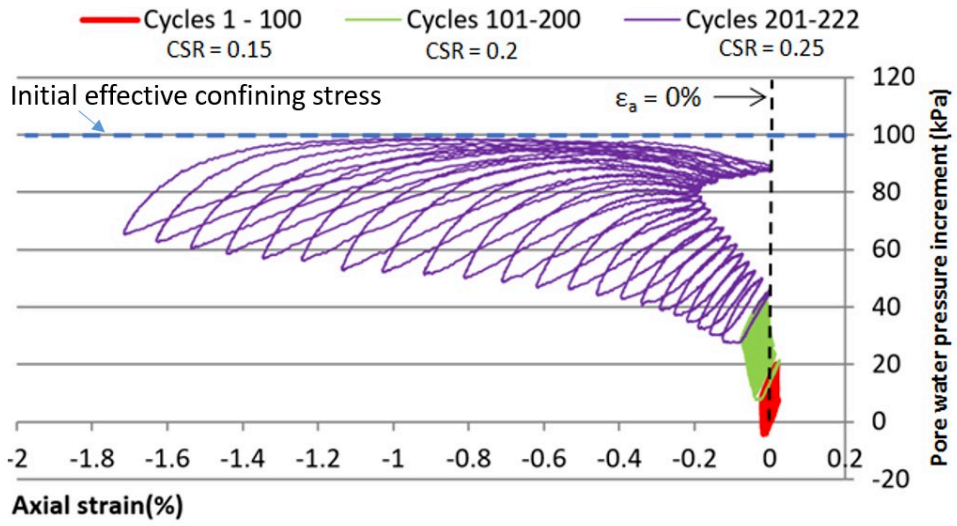

Figure 5.7 Axial strain versus pore water pressure for the saturated stepping CSR test.

The representation of the test in the plane of the stresses q and p' (figure 5.8) shows that the stress path firstly migrates gradually towards the origin with the reduction of the effective mean stress p' for all the load cases. However, in the first and second load cases, the stress path moves rapidly at the beginning and seems to be stable at the end of each loading process. In the last load case, the stress path goes and reaches the origin. From cycles 212th, the form of the curves changes and is butterfly. The path shows the decrease of the mean effective stress. It can be related to the increase of the pore water pressure as being presented in the previous figure. It is clear that in some last cycles, in one half of each loading cycle, the effective mean stress shows two different tendencies: first is decrease and then increase. This can be explained by the change in pore water pressure. That is why we can see the two-peak mechanism in figure 5.4a.

The stress path in this figure also allows determining two lines called failure line. The slope M of these lines relates to the friction angle of the sand and this issue has already presented in chapter 4. In this chapter, the slope of the upper and lower failure lines in figure 5.8 is 1.5 and -1.04, respectively. These values of M correspond to the friction angle of 37°. It demonstrates that there is a good agreement between the friction angle values derived from the cyclic loading, the monotonic loading in section II.2, and the literature.

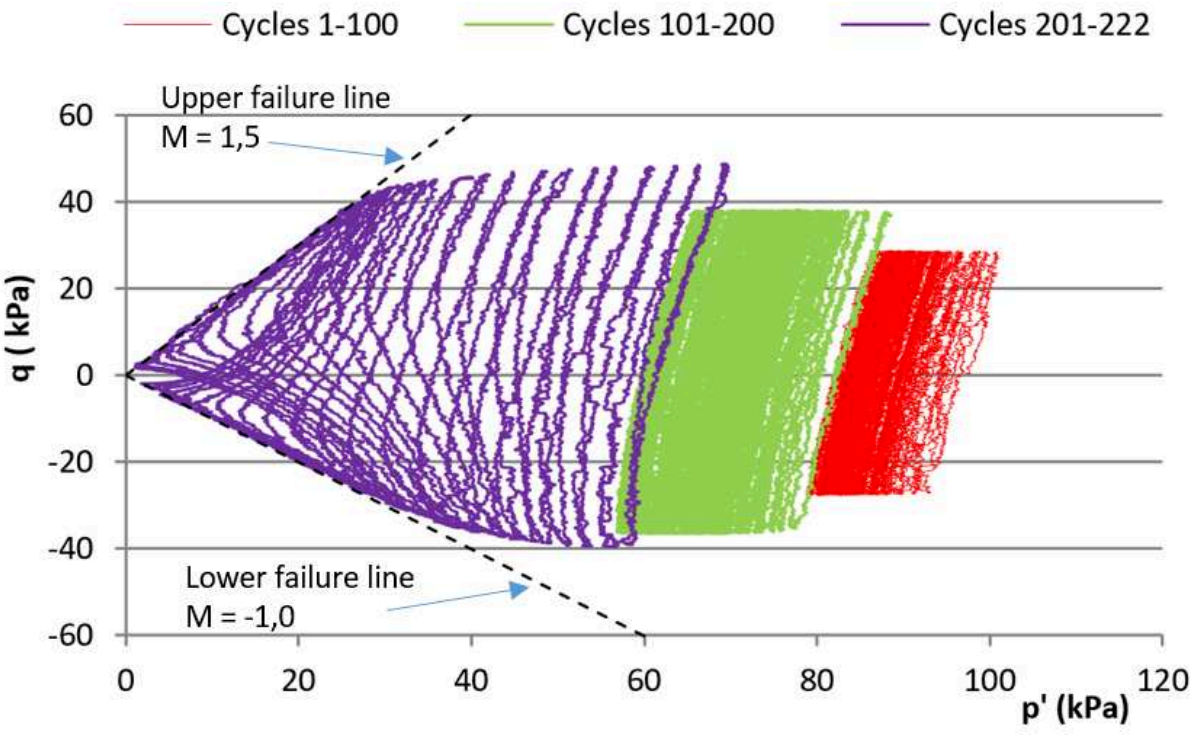

Figure 5.8 Deviator stress versus mean effective stress for the saturated stepping CSR test.

V.3.2. Residual strength after liquefaction

V.3.2.1. Test program

Table 5.4 presents the monotonic saturated test CSST-M1 carried on after cyclic saturated liquefaction test CSST1 to study the residual strength of the sample after liquefaction. At liquefaction state after cyclic liquefaction test CSST1, the pore water pressure is almost 800 kPa and the effective confining stress is approximately zero. To conduct the residual strength test CSST-M1, the increased pore water pressure was dissipated. After that, monotonic loading was applied to the sample. The void ratio of the sample after dissipating the increased pore water pressure due to liquefaction is 0.7. The initial effective confining stress is 100 kPa and the initial pore water pressure is 700 kPa. The sample was first compressed to the axial strain of 5%, then stretched to axial strain of -15%, and finally compressed to the axial strain of 0%.

Table 5.4. Test program for residual strength after liquefaction of saturated sand

Test No	**Preceded cyclic test**	**Void ratio before monotonic loading: e_{m0}**	**Sr**	**σ_3 kPa**	**U kPa**	**Axial strain variation**
CSST-M1	CSST1	0.7	100	800	700	0 →5%→-15%→0%

CSST-M1: *Monotonic saturated test 1 after liquefaction.*
CSST*: Cyclic saturated stepping (CSR) test.*

V.3.2.2. Results

After the liquefaction, the pore water pressure increment was dissipated and the sample was sheared by applying the monotonic loading to study the residual strength after liquefaction. The test was carried out in drained and strain controlled conditions. Figure 5.9 shows the axial strain variation of the test. The axial strain is firstly increased to 5%. This value is enough to study the sample residual strength in compression and not damage the sample. After that, the sample was stretch to -15% of axial strain to study the residual strength in the extension domain. The test lasted in 9 hours to be sure that the pore water pressure inside the sample was well controlled by the HAPC device (figure 5.9).

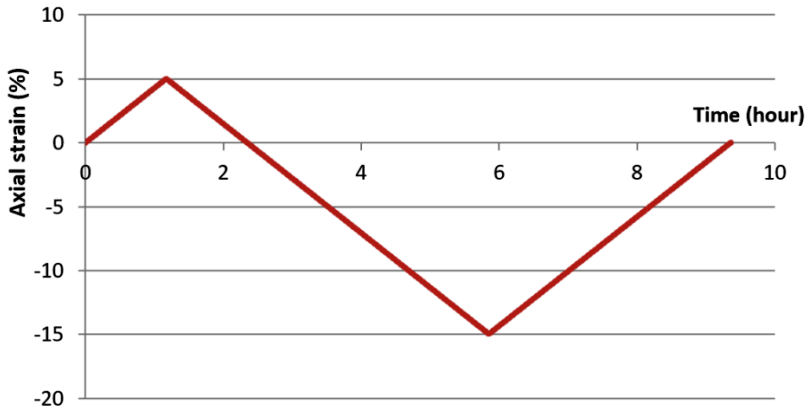

Figure 5.9 The axial strain variation of the monotonic loading after liquefaction

Figure 5.10 shows deviator stress in a function of axial strain. The deviator stress after dissipating the pore water pressure increment due to liquefaction is 60 kPa. The deviator stress increases sharply when the axial strain increases from almost zero to 5%. At the end of this stage (1 →2), the deviator stress seems to be stable at 395 kPa, however, it can be seen that the sample is not failure. In the second stage (2 →3), the deviator stress falls from 395 kPa to -80 kPa and then increases a little to -50 kPa when the axial strain decreases from 5% to -15%. In the last stage (3 →4), the deviator stress increases from -50 kPa to 325 kPa and then level off. Although the sample was compressed in stage 1 and 3, the last value of deviator stress in each stage is not the same.

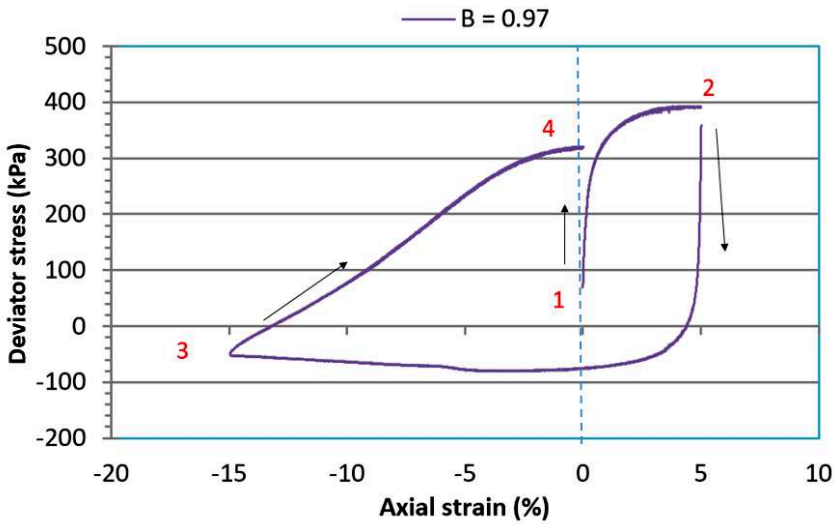

Figure 5.10 Deviator stress in a function of axial strain of the saturated monotonic loading test after liquefaction

The void ratio change of the sample is presented in figure 5.11. In the first stage (1→2) the sample shows a strong dilative behavior. The void ratio increases from 0.7 to 0.75 when the axial strain increases 5%. When the axial strain decreases from 5% to -15%, the void ratio decreases to the minimum value of 0.712 and then increases to 0.754 at the end of the loading process. This stage witnesses the phase transformation of the sample from the contractive behavior to the dilative behavior. It can be seen that the void ratio in the first stage increases when subjected to the compressed monotonic loading. In the second stage of monotonic loading, the void ratio decreases; however, the sample has not reached its initial state. In the last stage (3→4), the void ratio change shows a tendency contrary to the previous stage when the sample is compressed. The void ratio decreases to 0.71 and then increases to 0.75. Note that the maximum and minimum values in stage 3 are almost the same with those in the stage 2.

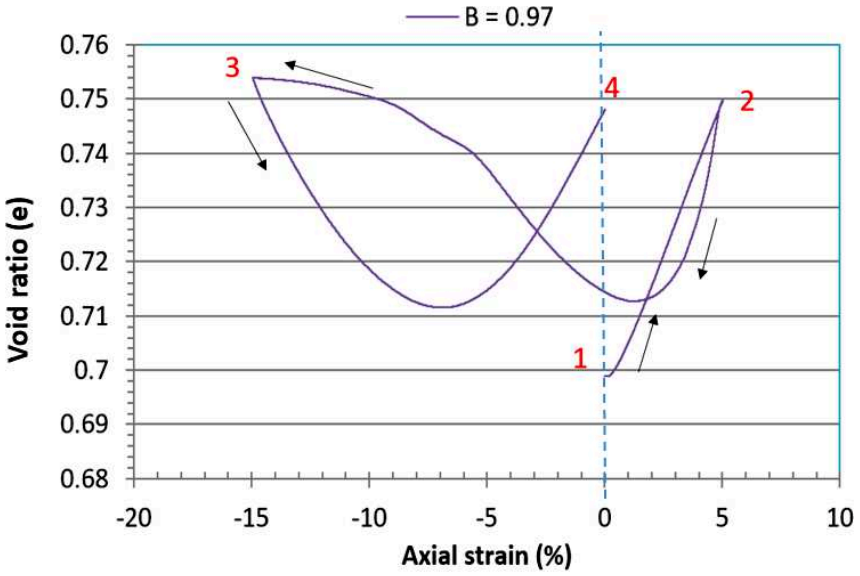

Figure 5.11 Void ratio in a function of axial strain of the saturated monotonic loading test after liquefaction

Figure 5.12 exhibits the void ratio change in a function of effective mean stress. Because the test was carried out in drained condition, the pore water pressure was kept at 0 kPa during the test, and the change in the effective mean stress is only due to the change of the deviator stress. At the beginning of the first stage, the effective mean stress increases sharply corresponding to the sudden increase of the deviator stress as being seen in figure 5.10. After that, it seems to remain while there is a strong increase of the void ratio corresponding to the strong dilative behavior of the sample volume. Stage 2nd also observes a same tendency when

the mean effective stress decreases rapidly at the beginning of the stage. At the end of the process, the mean effective stress changes with a lower rate. It is necessary to note that from the test observation in reality, at the beginning of the stage 1st and 2nd the sample was not failure; however, at the beginning of the stage 3rd, the sample had been damaged due to the large deformation at the end of stage 2nd.

Biarez and Hicher (1994) have suggested correlations for granular media to position the critical state line (CSL) in the [log p'; e] plan. These correlations depend on the uniformity coefficient $C_u=d_{60}/d_{10}$ of the grain size distribution of the granular soil and the shape of the grains. The correlated critical state line is shown in Figure 5.12is for the sand having the shape coefficient R= 0.3 and C_u= 2. It can be seen that point 4 is located in the vicinity of this line.

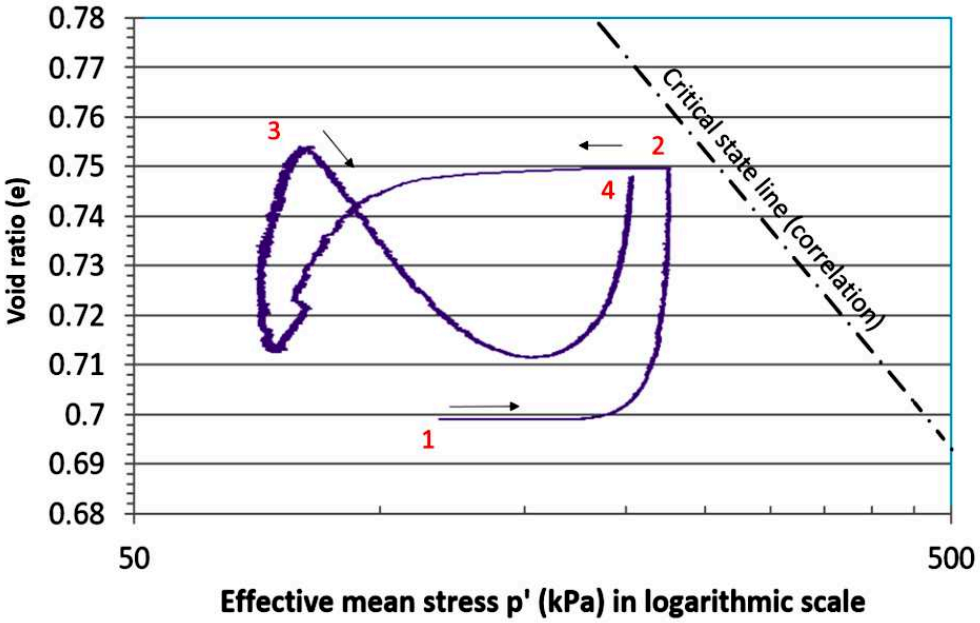

Figure 5.12 Void ratio in a function of effective mean stress of the saturated monotonic loading test after liquefaction

The stress path of the test is exhibited in the plane of deviator stress versus mean effective stress. In the first stage of the test (1→2), the path goes up to the right side and passes the upper failure line. This behavior is valid for the sample in dense state because the sample usually reaches the critical state after a large deformation (see an example for Coarse Hostun sand in figure 5.14). In the second stage (2→3), the stress path goes down to the left and stops

at a point on the lower failure line. After that in stage 3rd (3→4), the stress path goes up and stops at a point on the upper failure line.

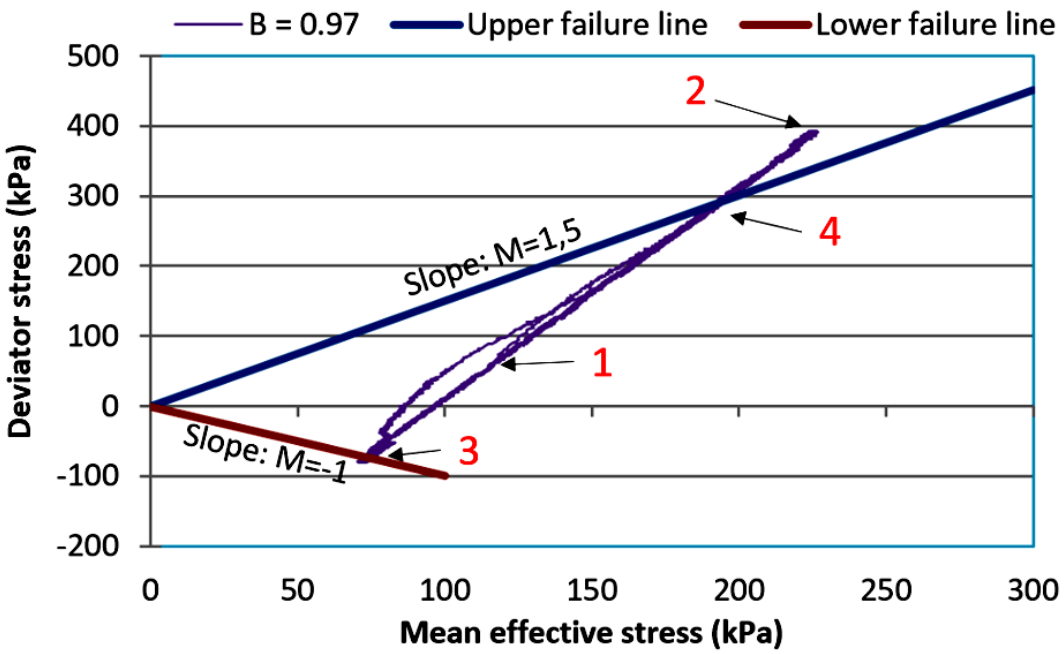

Figure 5.13 Deviator stress versus effective mean stress of the saturated monotonic loading test after liquefaction

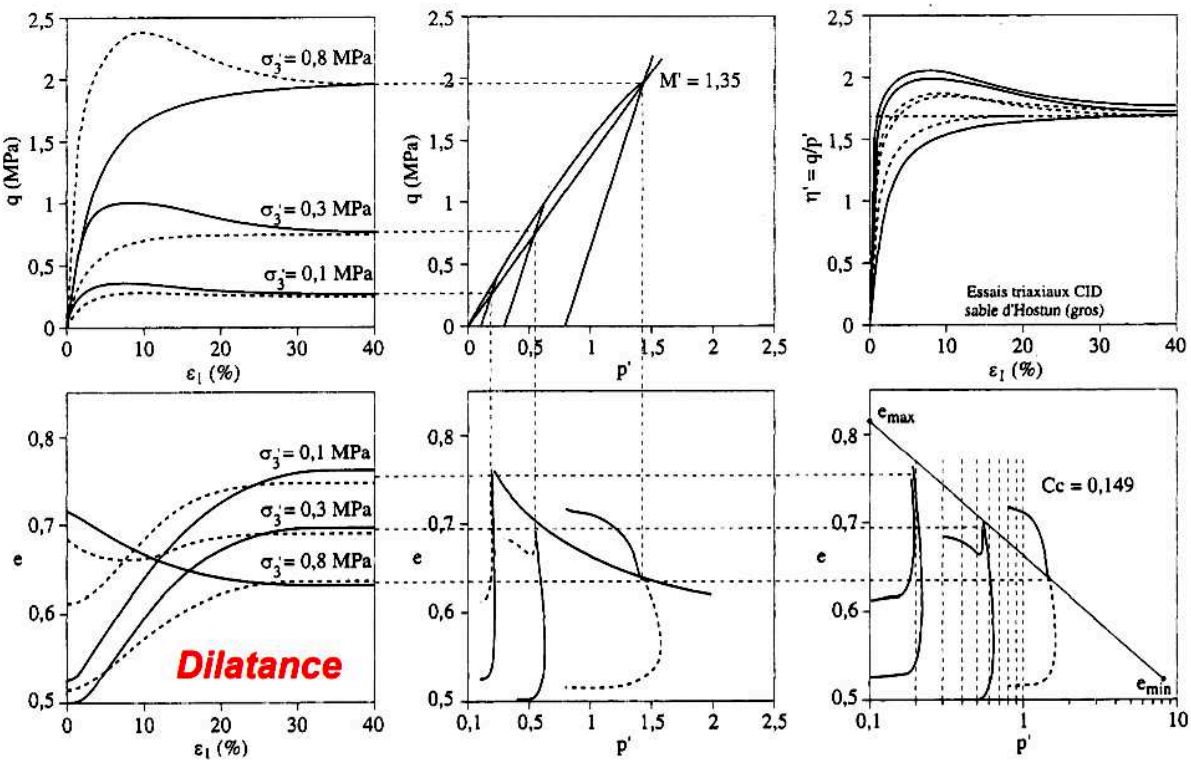

Figure 5.14 Different drained behaviors of (Coarse) Hostun sand (Biarez & Hicher, 1994)

V.4. Unsaturated sand: Liquefaction potential and residual strength

V.4.1. Liquefaction potential

V.4.1.1. Test program

To study the effect of saturation degree on the liquefaction susceptibility of soil, a series of tests was carried out (table 5.5). All the samples were prepared by the same method and have the same initial parameters including the dimensions and the relative density. The tests with different saturation degree were subjected to stepping CSR cyclic loading until liquefaction. The deviator stress was increased to a higher level if, after each one hundred cycles, the sample did not show any signals of liquefaction. With CUST2, after three hundred cycles, the sample shows the signs of liquefaction, so the test was continued and the number of cycles of the last load case is 145 cycles, higher than 100 cycles. Each load case is defined as the cycles at the same CSR, so for each test, the load case 1st includes the first one hundred cycles and so on. The total number of cycles in table 5.5 is the number of cycles causing liquefaction. It equals to the total number of cycles of all load cases.

Table 5.5. Series of tests subjected to stepping CSR cyclic loading.

Test	B	D_r (%)	Numbers of cycles applied					Total number of cycles
			CSR=0.15	CSR=0.2	CSR=0.25	CSR=0.3	CSR=0.35	
CUST1	0.97	83	100 (NL)	100 (NL)	22 (L)	-	-	222
CUST2	0.87	83	100(NL)	100 (NL)	145 (L)	-	-	345
CUST3	0.76	83	100(NL)	100 (NL)	100 (NL)	72 (L)	-	372
CUST4	0.6	83	100(NL)	100 (NL)	100 (NL)	100 (NL)	32(L)	432

(NL): *Sample was not liquefied; (L): Sample was liquefied*
CUST: *Cyclic Unsaturated Stepping (CSR) Test*

V.4.1.2. Results

4.1.2.1. Instability and liquefaction evidence

Figure 5.15 shows the change in axial strain and pore water pressure versus the number of cycles for test from 1 to 4. The number of cycles for test CUST1 with B = 0.97 is 222 cycles and the axial strain is 1.7 %. The number of cycles for test CUST2 (with B = 0.87) is 345 cycles and the axial strain of the last cycles is 1.5%. These numbers for test CUST3 (B=0.76) are 372 and 2%; for test CUST4 (B=0.6) are 432 and 1.7%, respectively. Based on these graphs, it can be seen that all the samples were liquefied following the first criterion for the liquefaction assessment presented in chapter 3: The pore water pressure increase to be equal to cell pressure. In these figures, the upper and lower envelopes of pore water pressure were added to show the trend of pore water pressure due to the cyclic loading. The comparison of pore water pressure increment and the deeper study of liquefaction behavior of soil (Ex: the two-peak mechanism, the development of parameters, etc…) will be presented in the next parts where the results of the last load case are shown clearly.

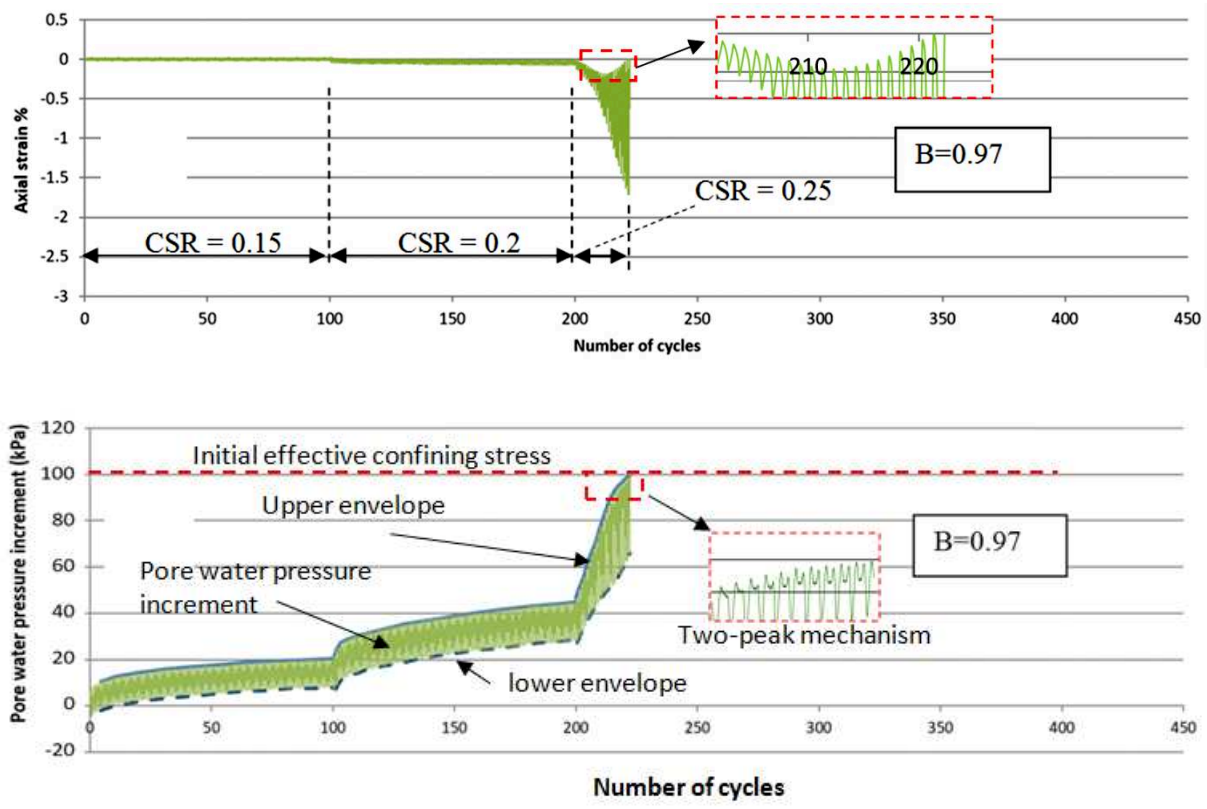

(a) Saturated sample with B = 0.97 (test CUST1)

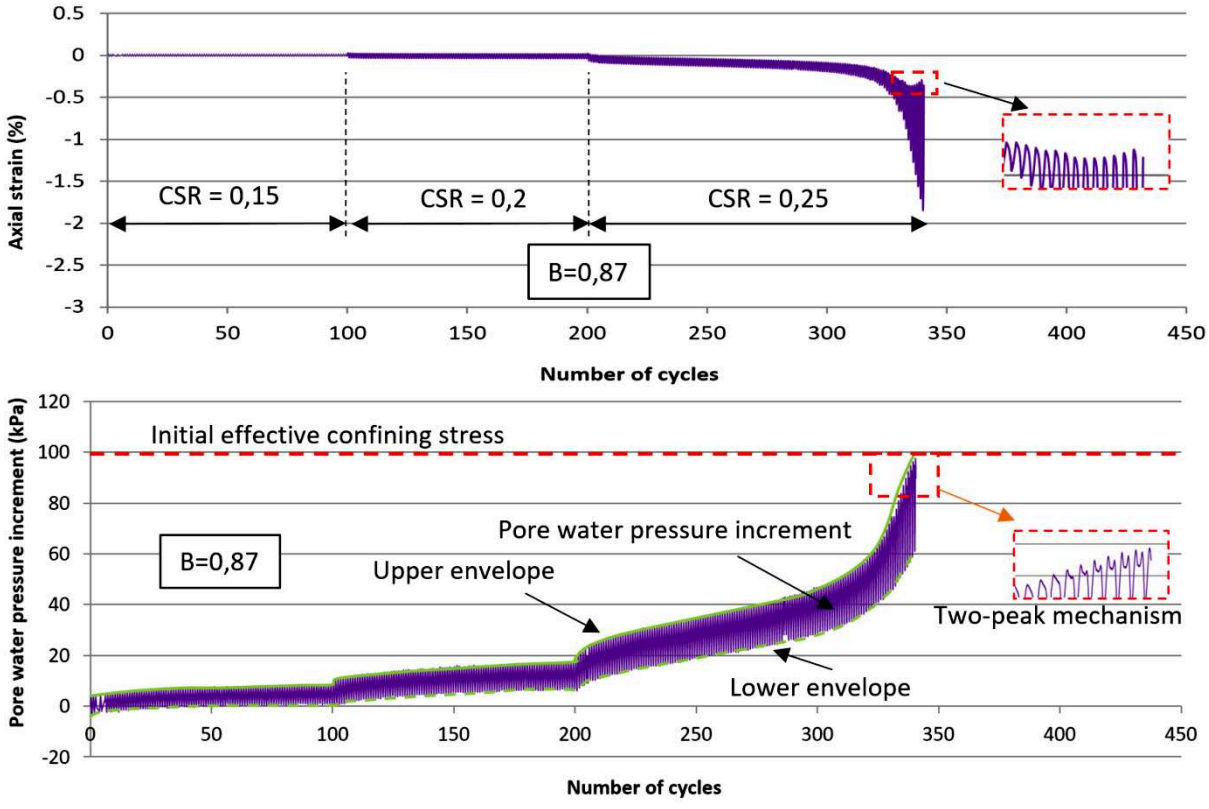

(b) Unsaturated sample with B = 0.87 ((test CUST2)

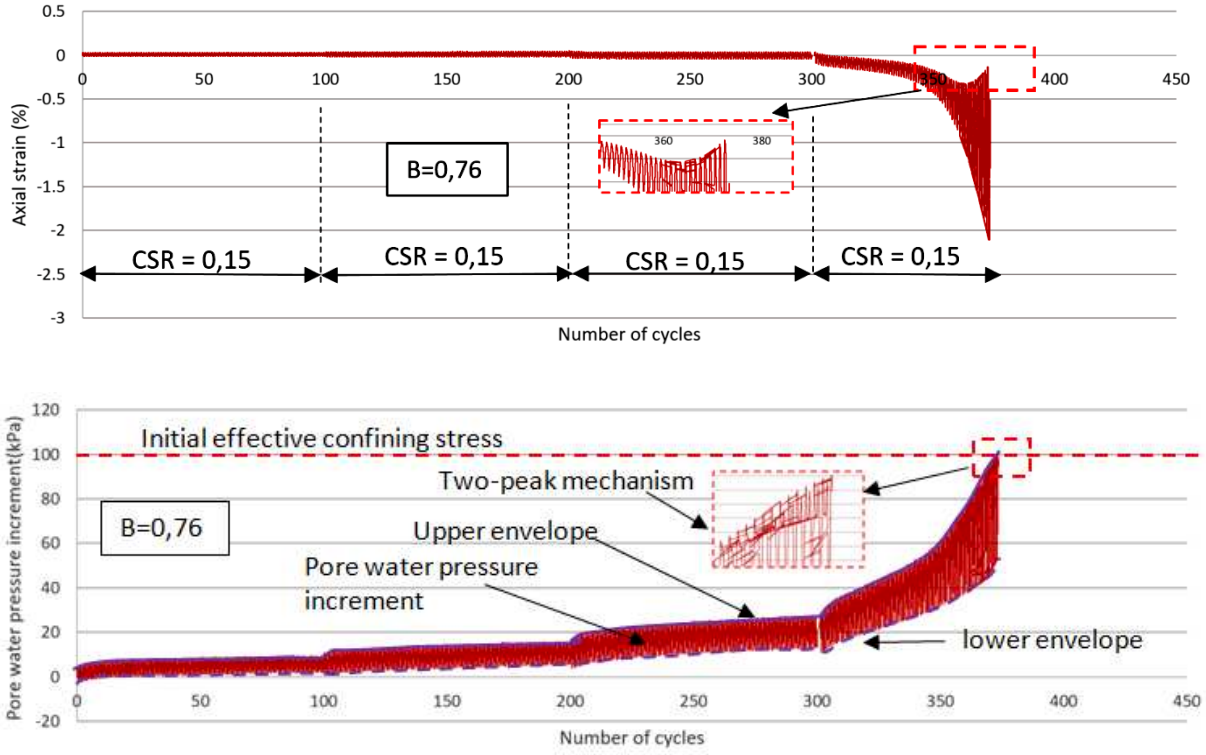

(c) Unsaturated sample with B = 0.76 (test CUST3)

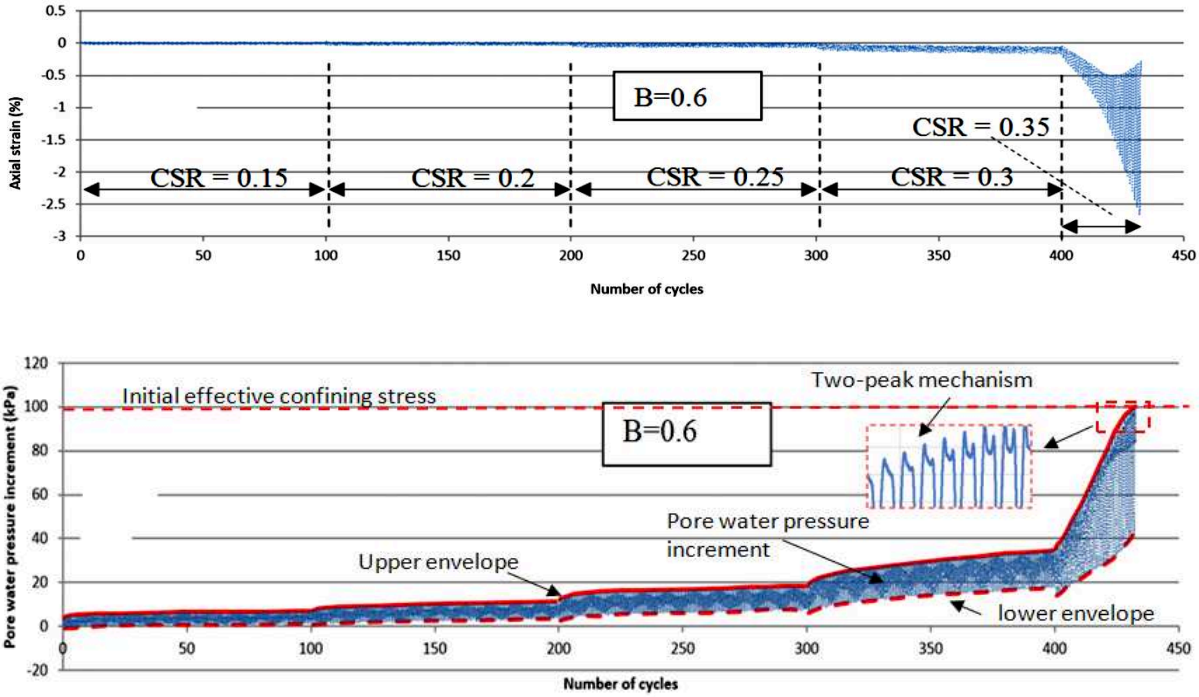

(d) Unsaturated sample with B = 0.6 (test CUST4)

Figure 5.15 Pore water pressure and axial strain in a function of number of cycles for the samples with different saturation degree subjected to stepping CSR cyclic loading

4.1.2.2. The results of the first load case: CSR=0.15

The first load case of all tests has the CSR of 0.15 and the number of cycles is the same at 100 cycles. All the initial parameters are the same except for the saturation degree. Due to this condition, the results of the first load case are useful to study the effect of saturation degree on the behavior of soil. Especially, this load case does not cause the liquefaction on the samples; however, its effect can result in the significant difference of the soil behavior in the next load cases.

The applied deviator stress of all tests is shown in figure 5.16 and the relationship between deviator stress and axial strain is shown in figure 5.17. It can be seen that at this CSR, the axial strain is quite small. So, the apparatus has control very well the deviator stress, the real applied deviator stress is closed to the desired value. In these tests, the effect of the saturation degree on the axial strain development is not clear. The stress – strain path seems to be linear, it suggests that when the axial strain is small, the sample shows an elastic characteristic. Under the symmetrical cyclic loading, the axial strain develops to both negative and positive directions.

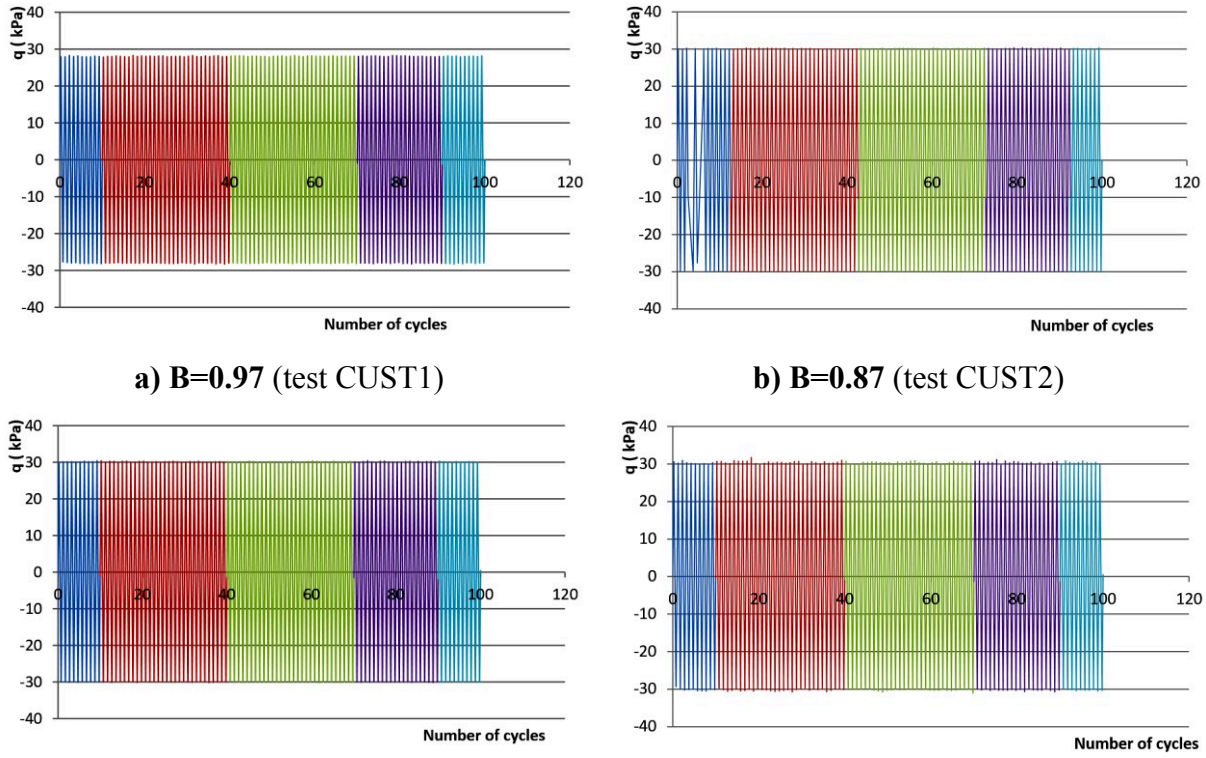

a) B=0.97 (test CUST1) **b) B=0.87** (test CUST2)

c) B=0.76 (test CUST3) **d) B=0.6** (test CUST4)

Figure 5.16. Deviator stress during the first load case of stepping CSR tests

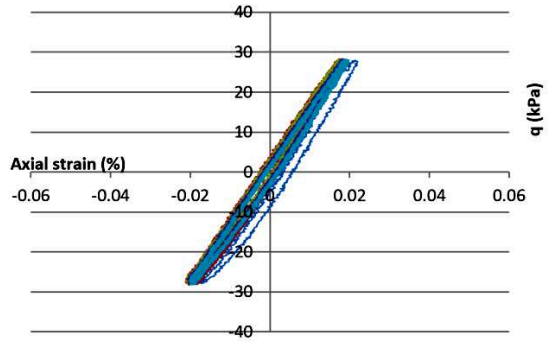

a) B=0.97 (test CUST1)

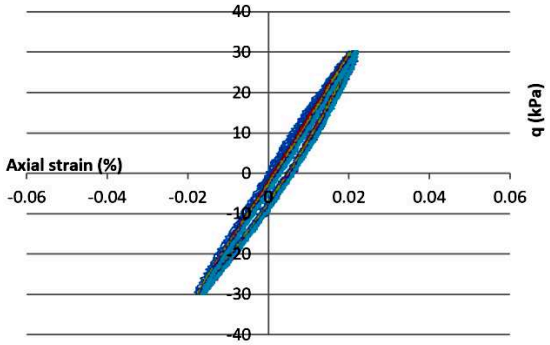

b) B=0.87 (test CUST2)

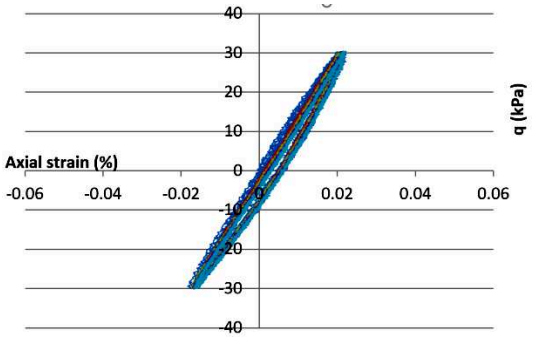

c) B=0.76 (test CUST3)

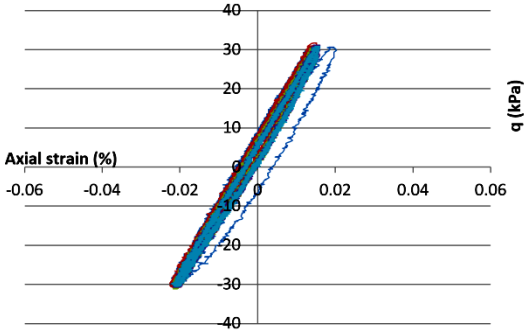

d) B=0.6 (test CUST4)

Figure 5.17 Stress – strain path of the first load case of stepping CSR tests

The development of pore water pressure under the first load case of cyclic loading is shown in figure 5.18. It is clear that the rise of the pore water pressure in the tests is not the same. In figure 5.18a, where B value is 0.97 corresponding to the fully saturated state (test CUST1), the pore water pressure increases nearly 20 kPa after 100 cycles. While in the unsaturated tests, the pore water pressure increment after 100 cycles is 9 kPa, 7 kPa, and 5 kPa corresponding to the B value of 0.87, 0.76, and 0.6, respectively. At the end of load case 1, the pore water pressure increment in all the figures appears to fluctuate around a stable value much smaller than the initial effective stress (100 kPa). All tests stopped without observing any liquefaction. From this data, it can be concluded that although the load case 1 does not cause liquefaction in all samples, it makes the pore water pressure increase, and this increment has been affected by the initial saturation degree.

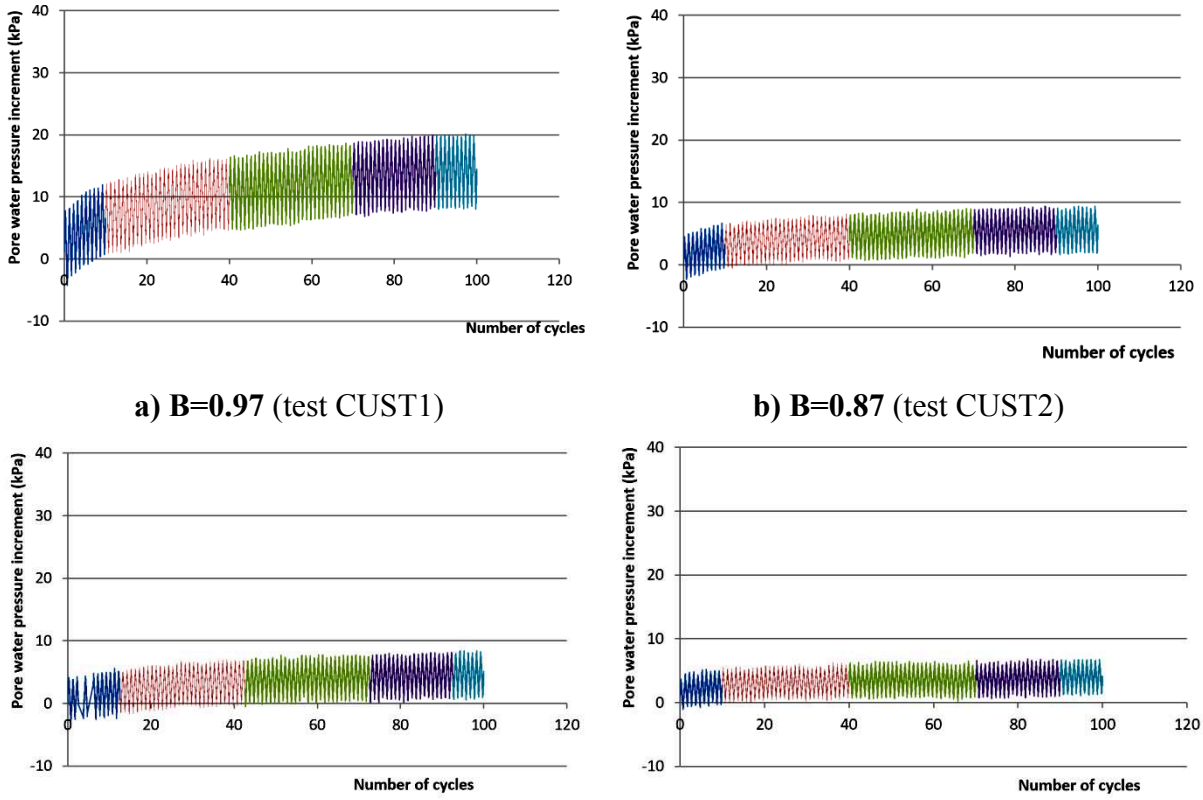

a) B=0.97 (test CUST1)

b) B=0.87 (test CUST2)

c) B=0.76 (test CUST3)

d) B=0.6 (test CUST4)

Figure 5.18 Pore water pressure increment during the first load case of stepping CSR tests

Figure 5.19 shows the relationship between the axial strain and the pore water pressure increment during cyclic loading. The path appears to be linear. The axial strain of different tests seems to have the same value and its development is observed mainly in some first cycles.

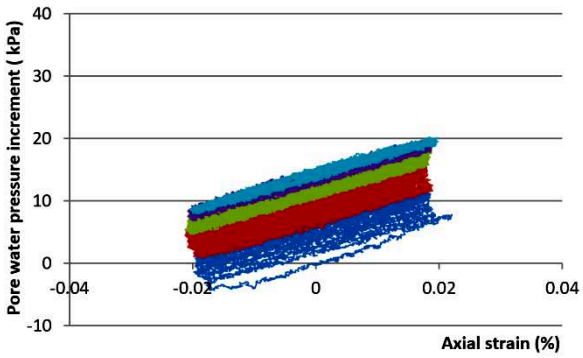

a) B=0.97 (test CUST1)

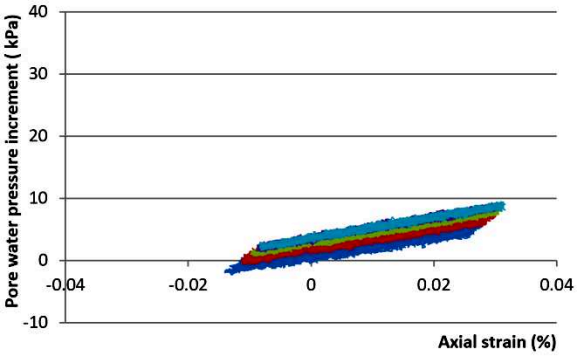

b) B=0.87 (test CUST2)

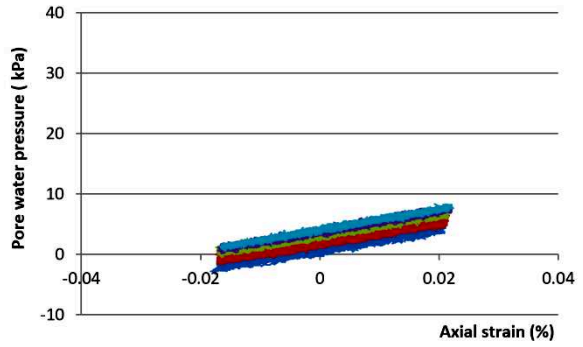

c) B=0.76 (test CUST3)

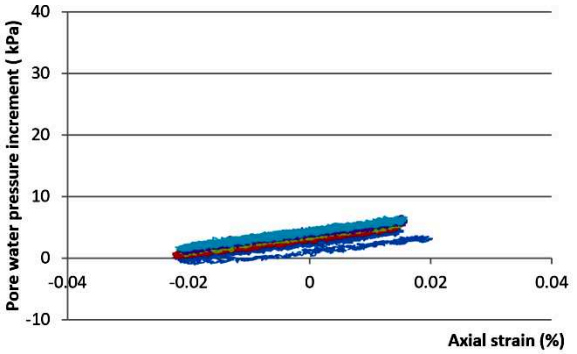

d) B=0.6 (test CUST4)

Figure 5.19 Axial strain versus pore water pressure during the first load case of the stepping CSR tests

The stress path of the tests is presented in figure 5.20. In all tests, the path comes forward to the origin quickly at some first cycles. After that, at the end of the process, the rate of the mean effective stress reduction slows down and the density of the path becomes denser. Although the stress path goes to the left, it is far from the origin and the failure lines. This demonstrates that the samples are completely stable and the liquefaction state is far to reach.

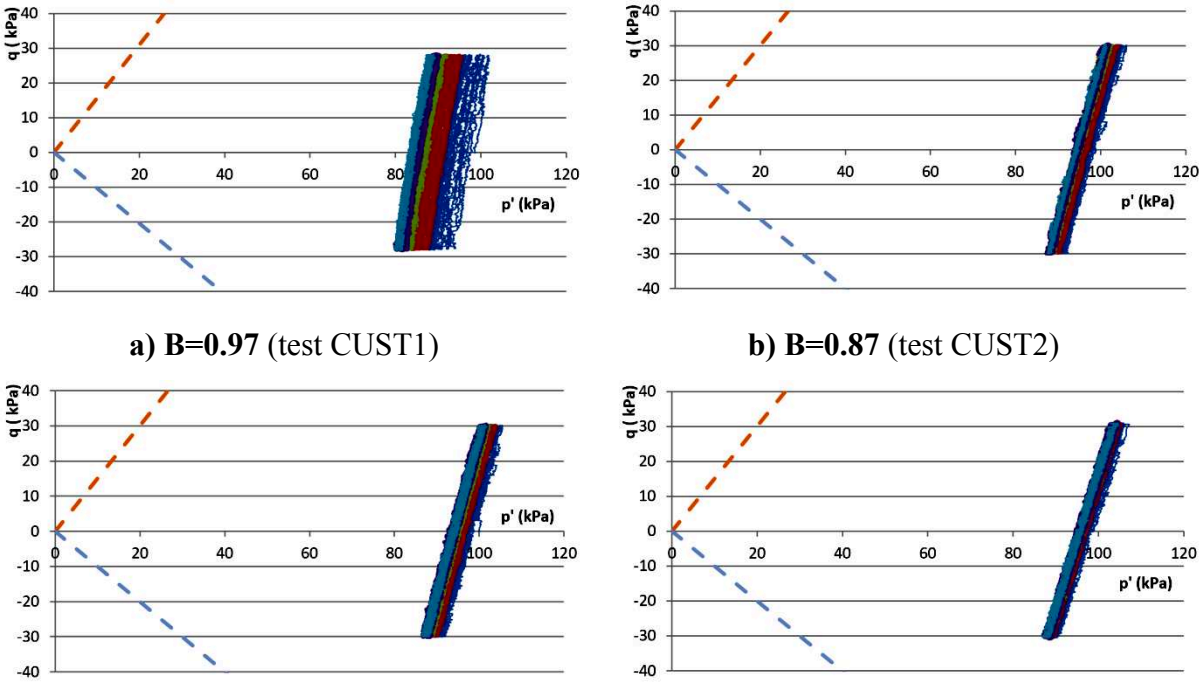

a) B=0.97 (test CUST1)

b) B=0.87 (test CUST2)

c) B=0.76 (test CUST3)

d) B=0.6 (test CUST4)

Figure 5.20 Stress path during the first load case of the stepping CSR tests

4.1.2.3. Behavior of soil under the highest CSR loading (the last load case)

To understand the liquefaction behavior of the samples, in this part, the results of the last load case, when the CSR is at its highest value, is presented. In figure 5.21, the axial strain is put in the relationship with the deviator stress. In figure 5.21a (for saturated test: B=0.97), the sample is liquefied by the load case with CSR of 0.25. The axial strain accumulates after each cycle and reaches -1.7% for the last cycle. The amplitude of the deviator stress is initially equal to 50 kPa, after that it decreases and finally fluctuates between 37 kPa and -26 kPa. In figure 5.21d (for the sample with lowest saturation degree: B = 0.6), the deviator stress firstly fluctuates between 70 and -60 kPa. After 32 cycles, it varies between 56 and -45 kPa. The axial strain of the last cycle changes between 0.3% and 2.7%. The results for the unsaturated tests with B value of 0.87 and 0.76 are exhibited in figure 5.21b and c. It can be seen that the axial strain in all tests is smaller than 5%. It means that the first criterion for liquefaction (double amplitude of the axial strain reaches 5%) has not been observed in these tests

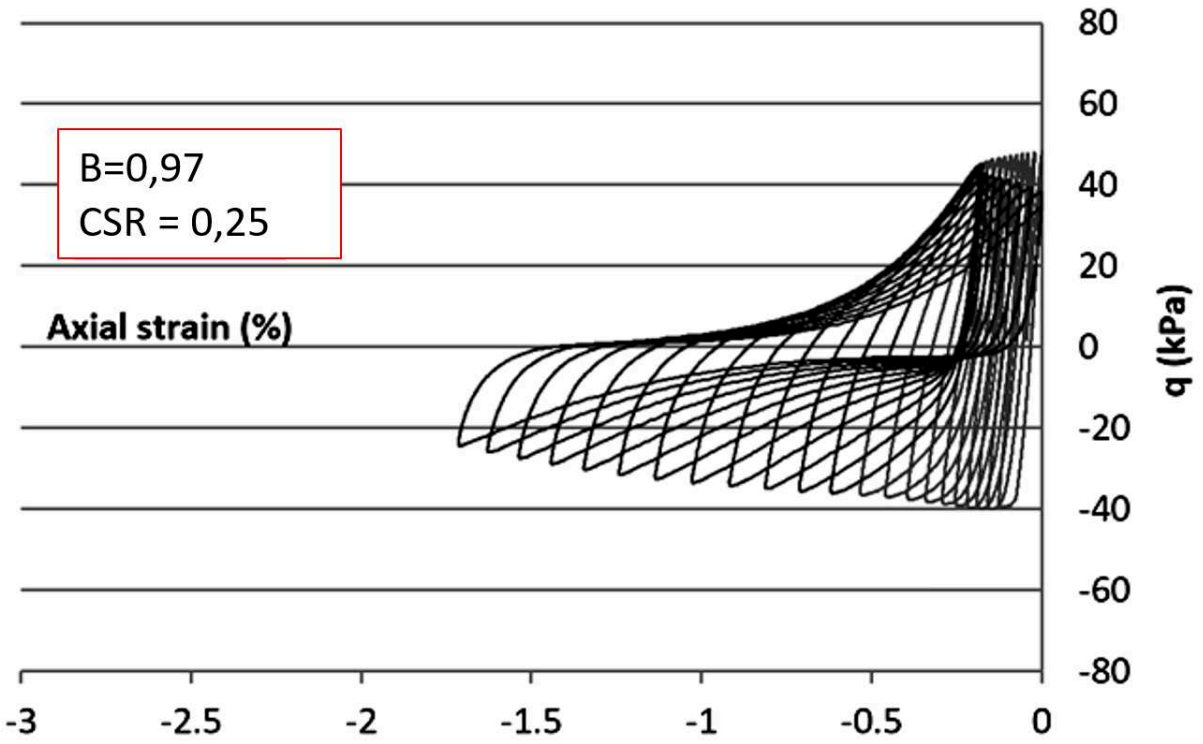

(a) (test CUST1)

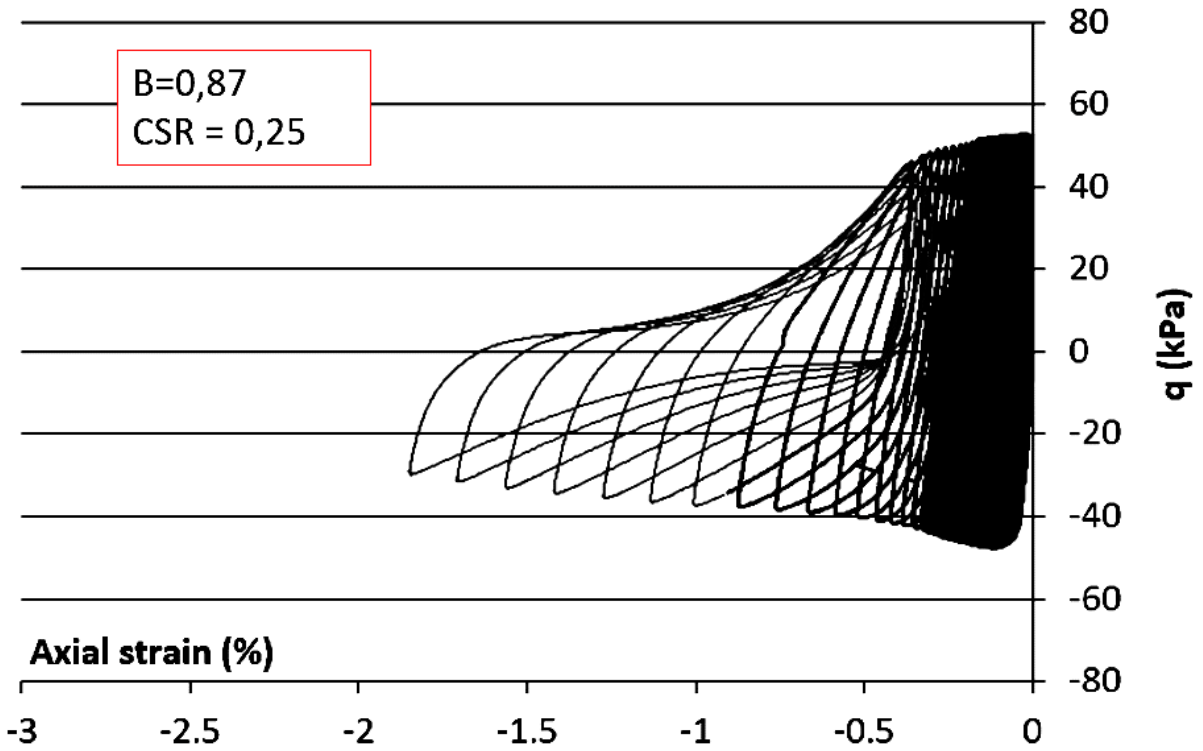

(b) (test CUST2)

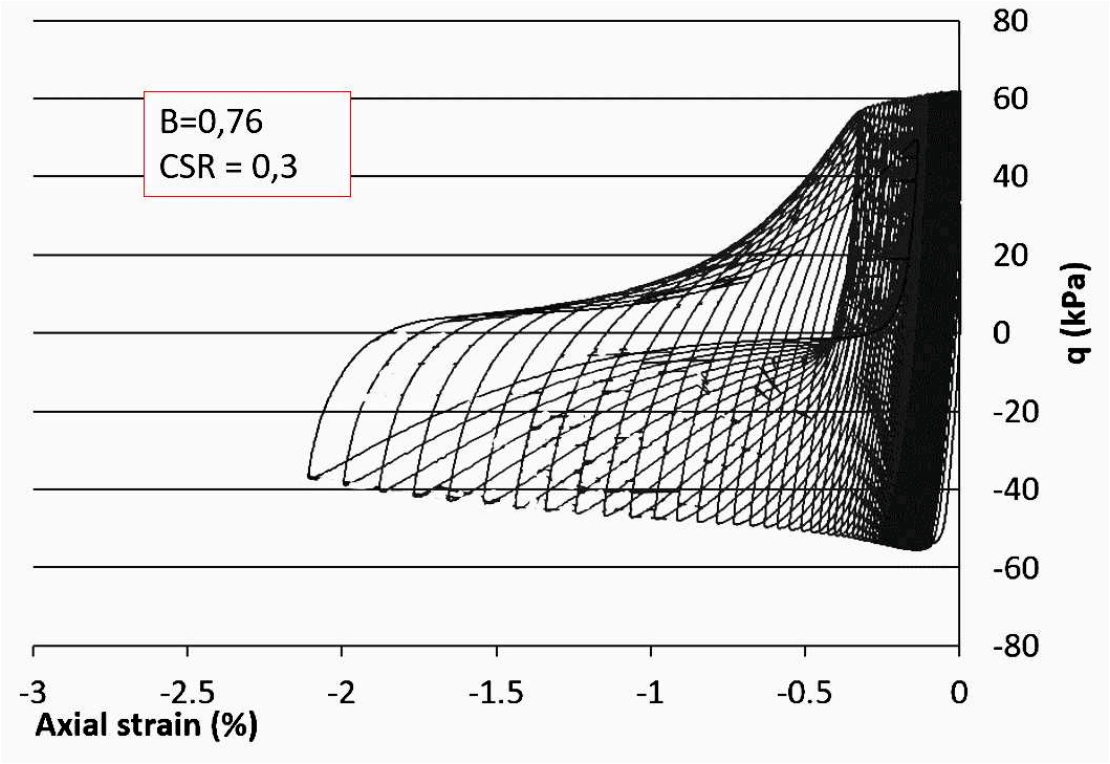

(c) (test CUST3)

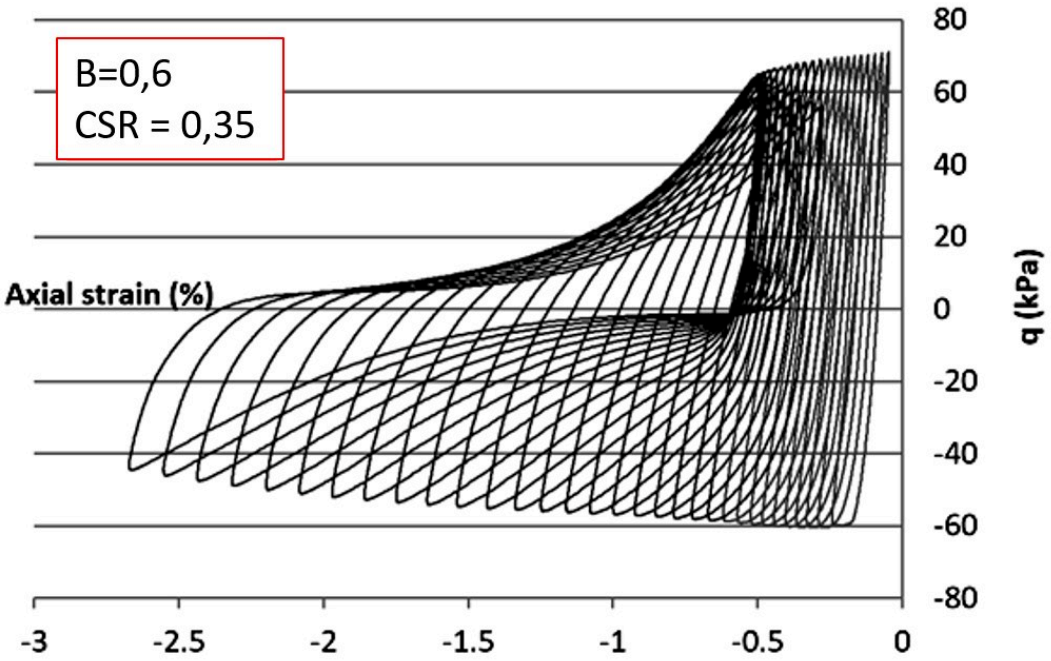

(d) (test CUST4)

Figure 5.21 The axial strain versus deviator stress of the last load case for unsaturated stepping CSR tests.
a) fully saturated sample with B of 0.97. b) unsaturated sample with B = 0.87, c) unsaturated sample with B = 0.76, d) unsaturated sample with B = 0.6

The pore water pressure growth caused by cyclic loading of test CUST1 (B=0.97) is shown in figure 5.22a. The pore water pressure increment rises from 46 kPa to 100 kPa and finally is equal to the initial effective stress after 22 cycles. Meanwhile, in figure 5.22d, the pore water pressure increment of the most unsaturated specimen test CUST4 (B = 0.6) increases from 35 kPa to 100 kPa (the cell pressure) after 32 cycles. The results of the test with B = 0.87 and B = 0.76 are presented in figures 5.22b and 5.22c.

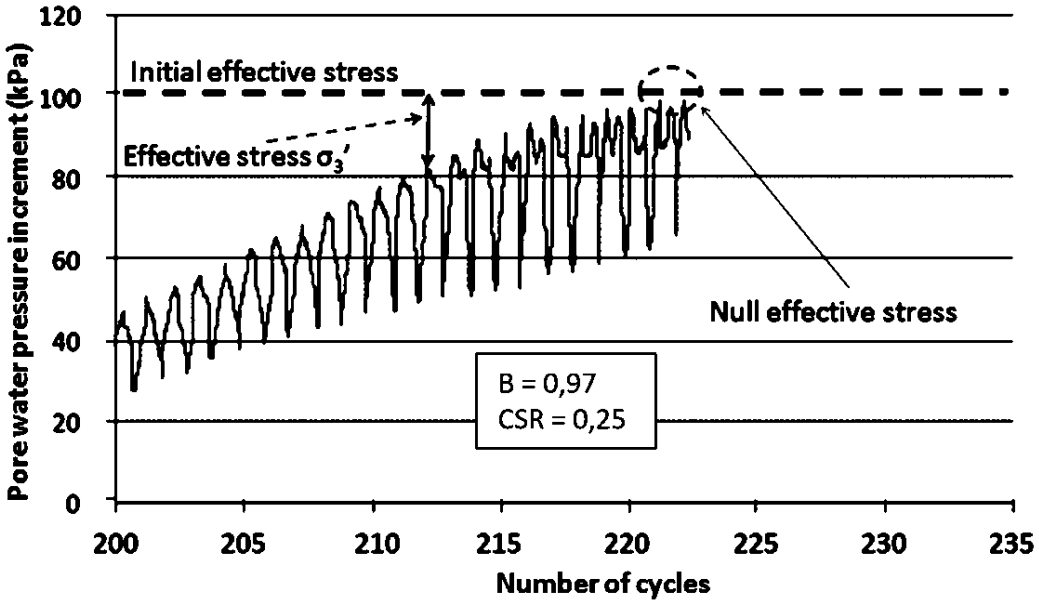

(a) (test CUST1)

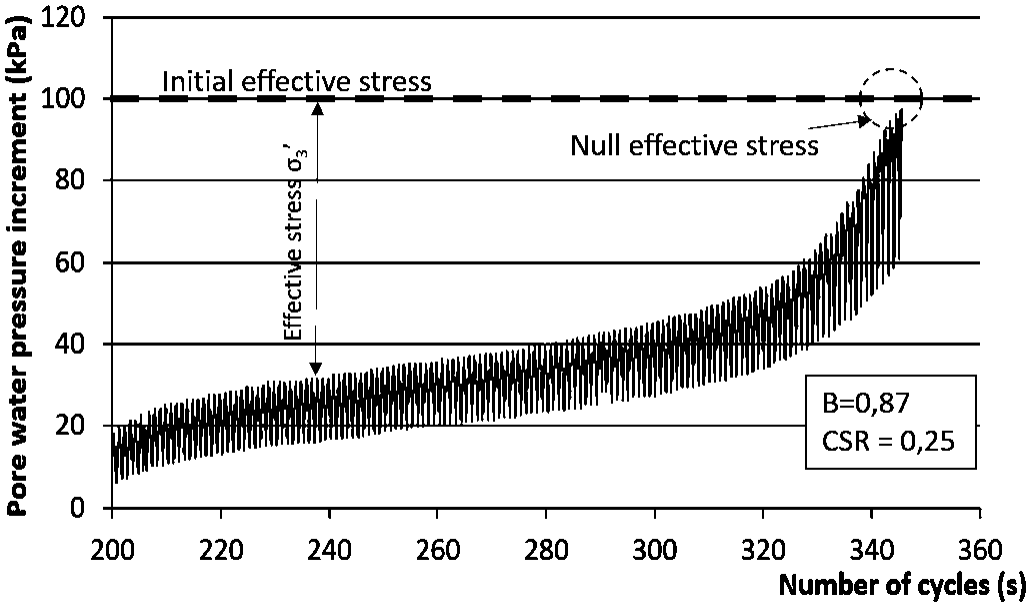

(b) (test CUST2)

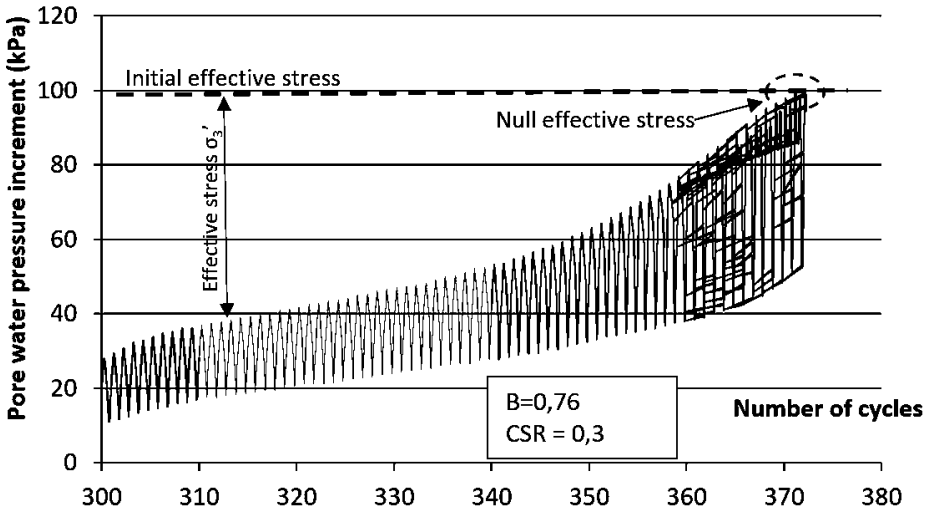

(c) (test CUST3)

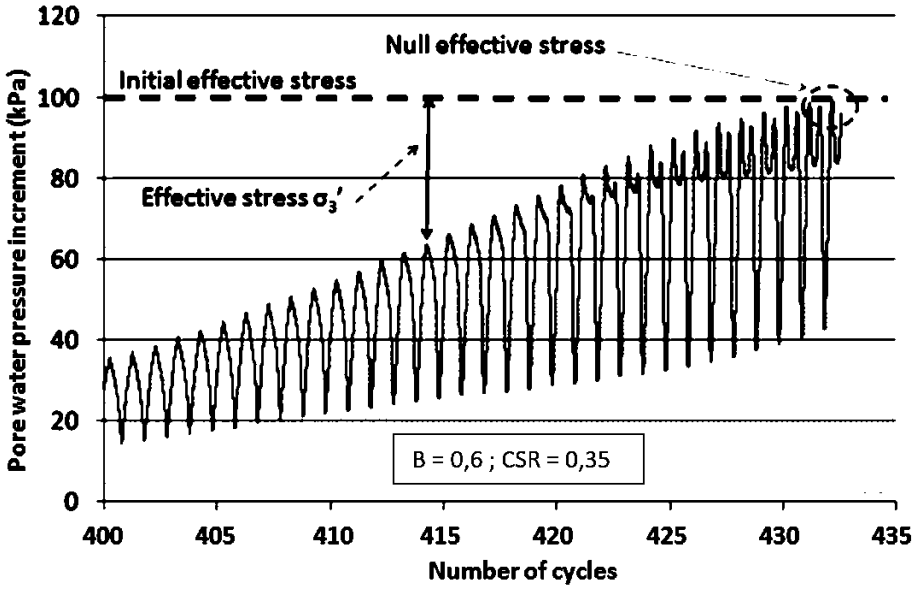

(d) (test CUST4)

Figure 5.22 Pore-water pressure increment of the last load case for stepping CSR test.

a) fully saturated sample with B of 0.97., b) unsaturated sample with B = 0.87, c) unsaturated sample with B = 0.76, d) unsaturated sample with B = 0.6

Figure 5.23 shows the relationship between the pore water pressure increment (Δu) and the axial strain (ε_a) when applying the last load case (the load case corresponding to the CSR_{max}). When Δu increases to the initial effective cell pressure (100 kPa), the axial strain of the saturated test (B = 0.97) in one cycle increases and finally reaches the maximum value of

1.7%. For the unsaturated tests with B = 0.87, 0.76, and 0.6, this value is 1.4%, 2%, and 2.4%, respectively.

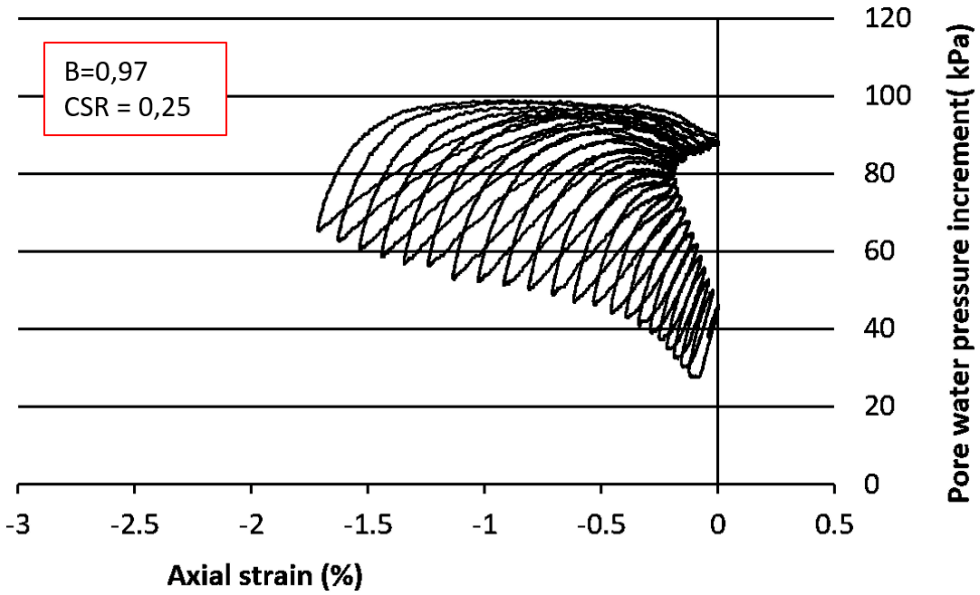

(a) (test CUST1)

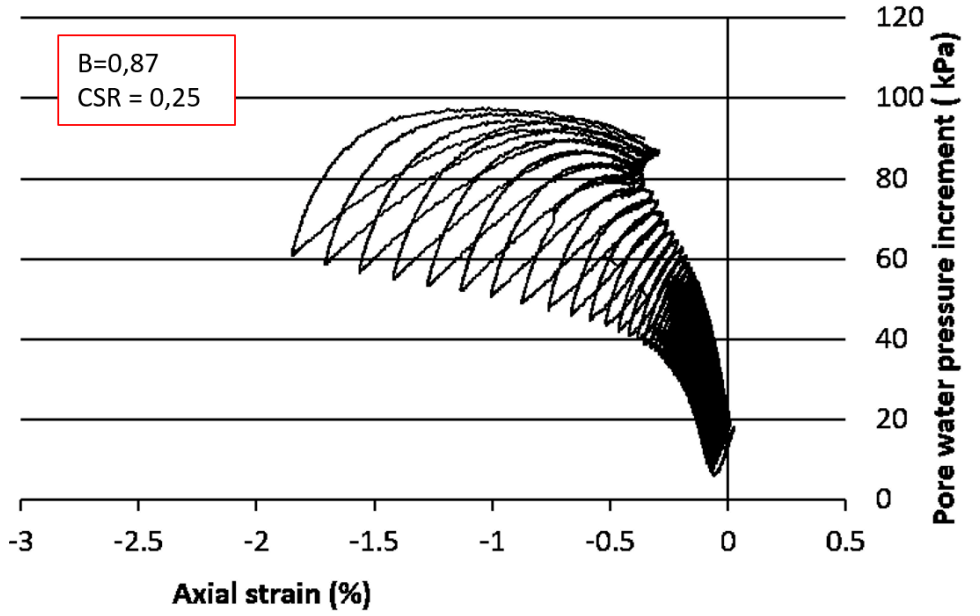

(b) (test CUST2)

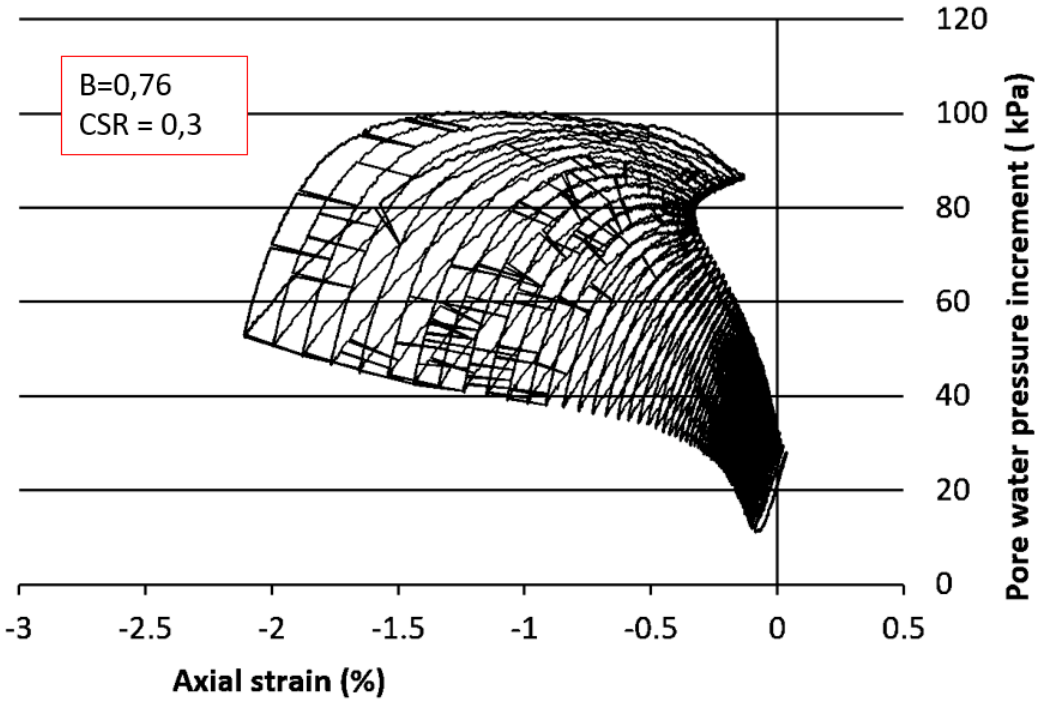

(c) (test CUST3)

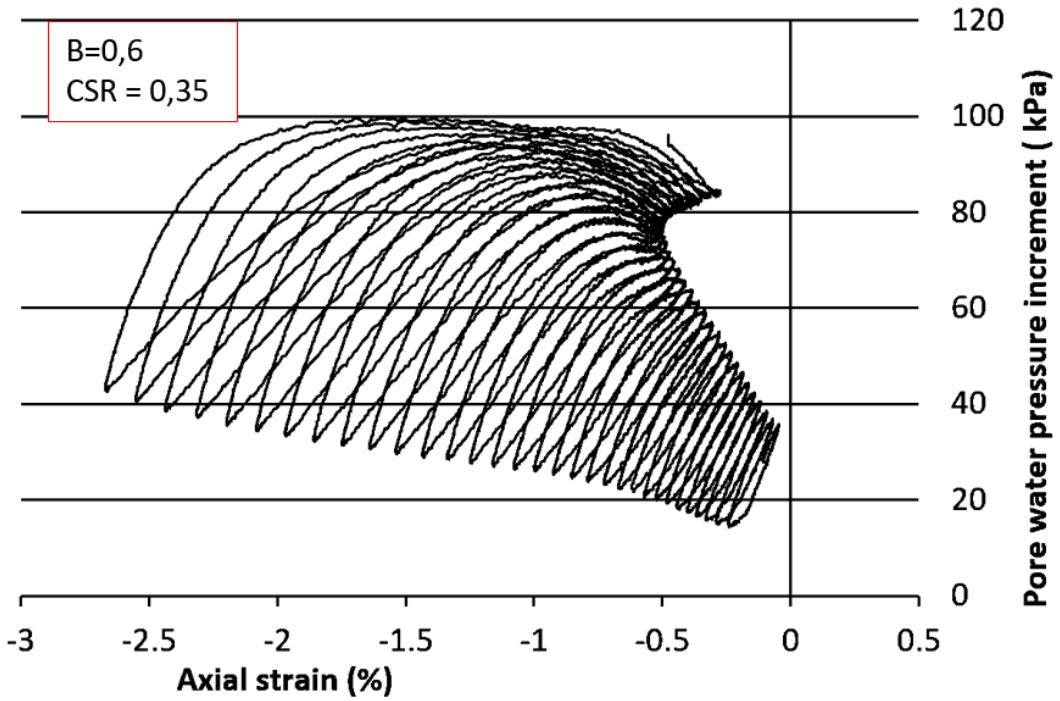

(d) (test CUST4)

Figure 5.23 Pore-water pressure increment during the last load case – stepping CSR tests.

a) for the fully saturated sample with B of 0.97., b) unsaturated sample with B = 0.87, c) unsaturated sample with B = 0.76, d) for the unsaturated sample with B = 0.6.

Figure 5.24 shows the results of the tests in the plane of deviator stress versus effective mean stress. The result of the saturated test is presented in figure 5.24a. In this figure, the stress

path shifts gradually towards the origin. The distinction between the loops is obvious. At the beginning of the loading process, the change of the effective mean stress in one cycle is small; however, from the cycle 210th, the stress path contacts the lower failure line, the change of the effective mean stress value in one cycle increases suddenly. The curve approaches the origin at a higher rate. From the cycles 212th, the stress path contacts both upper and lower failure lines. The curve has the butterfly form. Corresponding to this form of the curve in q-p' is the two - peak mechanism in the plane of pore water pressure versus the number of cycles as presented above (figure 5.22).

The result of test CUST 2 with B value of 0.87 is presented in figure 5.24b. The deviator of the last load case in this test is 50 kPa corresponding to CSR = 0.25. It can be seen that the stress path in this figure includes three phases. In some first cycles the path shifts to the origin quickly and the distinction between loops can be observed clearly. Then the chart becomes denser and the loops overlap. When the curve goes closely to the failure lines, the density of the loops becomes sparser.

It can be commented that there is a difference between the behavior of the samples in tests CUST 1 and CUST2. In figure 5.24a, the path goes rapidly to the origin, the loops are sparse. While, in figure 5.24b, there is an appearance of a stage in which the loops overlap. It is necessary to note that in both tests, the last load case has the same CSR of 0.25, but the effective mean stress at the beginning of the last load case is different.

Figure 5.24c presents the results of test CUST3 with initial B value of 0.76. Figure 5.24d presents the results of test CUST4 with initial B value of 0.6. In all tests from CUST1 to CUST4, two failure lines are added. The slope is 1.5 for the upper line and -1.0 for the lower line. This slope corresponds to the friction angle of 37°. So based on these results, it can be concluded that the friction angle does not depend on the B value. However, it is certain that the saturation degree of these tests is not significantly different.

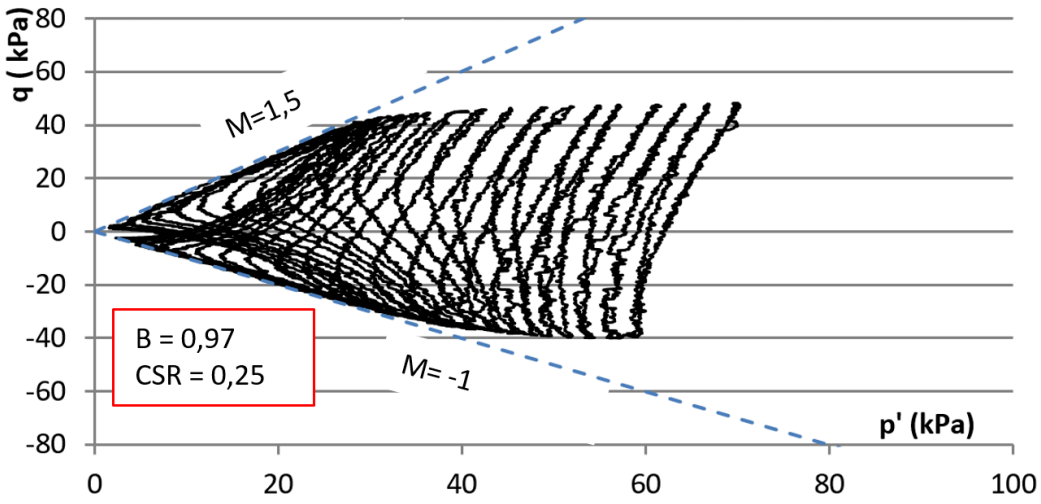

(a) (test CUST1)

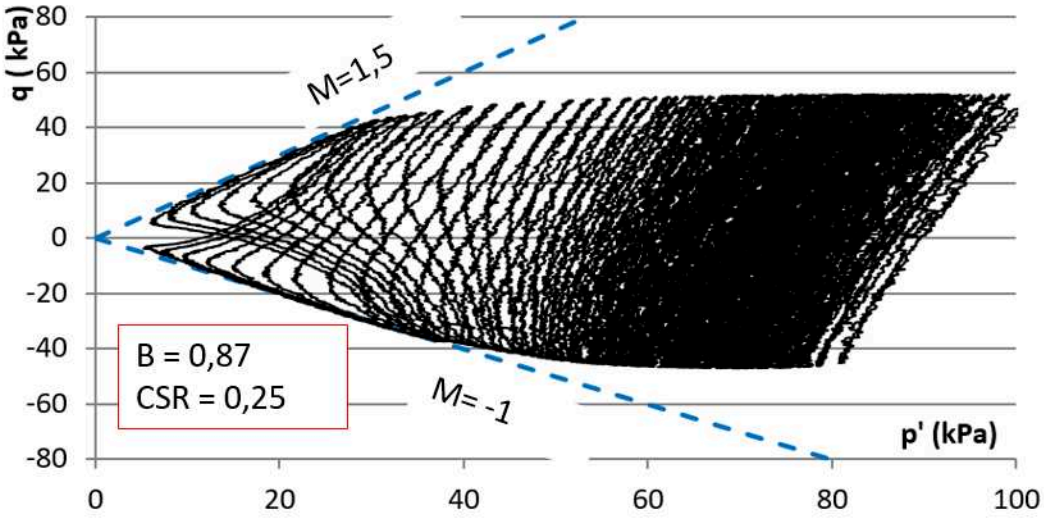

(b) (test CUST2)

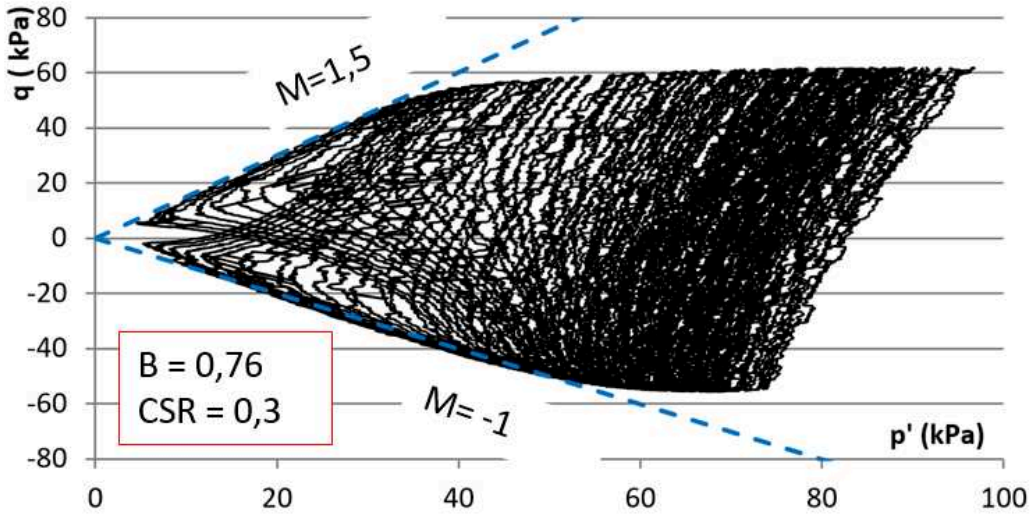

(c) (test CUST3)

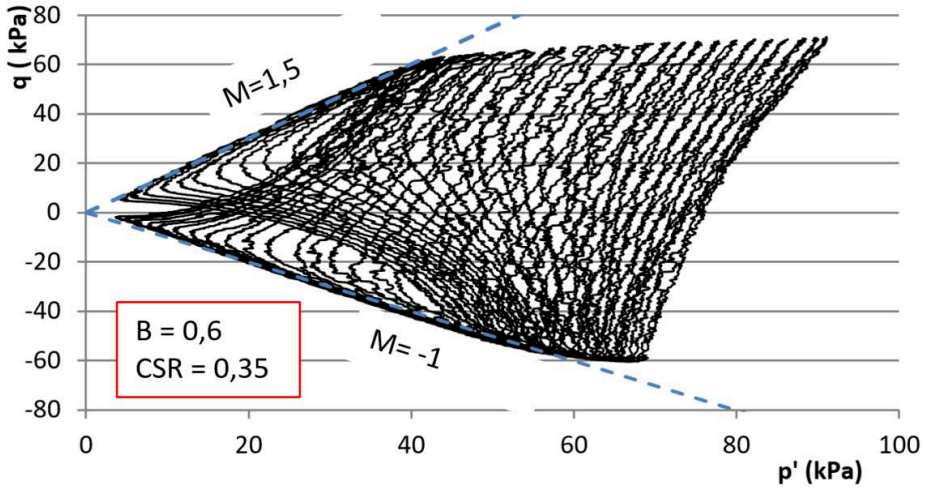

(d) (test CUST4)

Figure 5.24 Relationship between deviator tress and effective mean stress during the last load case – stepping CSR tests.

a) For the fully saturated sample with B of 0.97, b) unsaturated sample with B = 0.87, c) unsaturated sample with B = 0.76, d) for the unsaturated sample with B = 0.6.

V.4.2. Residual strength after liquefaction of unsaturated sand

V.4.2.1. Test program

Similar to the residual strength test after liquefaction (Test CSST-M1), in these unsaturated monotonic tests after liquefaction, the pore water pressure was dissipated. The samples were compressed to reach an axial strain of 5 %, and then, were stretched to -15% of axial strain in drained condition to study the residual strength in extension. The test program is presented in table 5.6

Table 5.6. Monotonic tests after liquefaction

Test name	Preceded cyclic test	CSR of the last load case	Initial B value	Test condition	Axial strain
CUST-M1	CUST1	0.25	0.97	DC	0→5%→ -15%→0%
CUST-M2	CUST2	0.25	0.87	DC	0→5%→ -15%→0%
CUST-M3	CUST3	0.3	0.76	DC	0→5%→ -15%→0%
CUST-M4	CUST4	0.35	0.6	DC	0→5%→ -15%→0%

DC*: Drained Condition*
CUST-M: *Monotonic test after liquefaction test CUST*
CUST*: Cyclic unsaturated stepping (CSR) test*

V.4.2.2. Results

The results of the monotonic tests are shown in figure 5.25 in four plans, deviator stress versus axial strain (Figure 5.25a), deviator stress versus effective mean stress (Figure 5.25b), void ratio versus axial strain (Figure 5.25c), and void ratio versus effective mean stress (Figure 5.25d). The values of B range from 0.6 - 0.97, but the behavior is similar. In the first stage, when the samples are compressed from 0 to 5% of axial strain, the deviator stresses are 391 kPa, 390 kPa and 397 kPa for the tests having B of 0.97, 0.76 and 0.6, respectively (path 1 to 2 in figure 5.25a). This result demonstrates that after dissipation of the pore water pressure due to liquefaction, soil resistance recuperates. In the [p'; q] plan, the maximum values of the deviator stresses are located above the critical state line M=1.5 (point 2 in figure 5.25b), corresponding to a strength peak, characteristic of dense sands, without reaching failure as shown in figure 5.25 a, point 2. This results in a dilatant behavior where the void ratio increases along path 1 to 2 (Figures 5.25 c and d).

In the next stage, the axial strain in extension varies from 5% to -15% (path 2 to 3); the deviator stresses are -52 kPa for the test with B of 0.6, -40 kPa for the test having B of 0.76 and -51 kPa for the last test with B_0 of 0.97. During this stage, the material first exhibits a contracting behavior when the axial strain varies from +5% to 0%, then the material dilates when the axial strain changes from 0 to -15% (figures 5.25c & d), and reaches the extension failure criterion M=-1 (point 3 in figure 5.25b).

In the last stage (path 3 to 4), when the samples are compressed and at the final axial strain of 0%, the deviator stress for tests having B of 0.76 and 0.6 is 330 kPa while that value for the saturated test is 320 kPa. The material shows first a contracting behavior when the axial strain varies from -15% to -7%, then the material dilates up to zero axial strain (paths 3 to 4, figures 5.25c & d). This last point is located on the compression failure criterion M=1.5 (point 4, figure 5.25b).

Biarez and Hicher (1994) have suggested correlations for granular media to position the critical state line (CSL) in the [log p'; e] plan. These correlations depend on the uniformity coefficient $C_u=d_{60}/d_{10}$ of the grain size distribution of the granular soil and the shape of the grains. For Hostun sand, the correlated critical state line is shown in Figure 5.25d. It can be seen that point 4 is located in the vicinity of this line.

However, there is not obvious effect of B on drained behavior of soil after liquefaction, but of course, the saturation degrees of the tests are not significantly different although there are big

differences in B values (Sr varies from 98% to 100% when B value varies from 0.6 to 0.97). It could be explained that when the samples liquefied, all the samples had the effective stress equal to zero and this situation erased the effect of the initial saturation state of the samples. All samples after pore water pressure dissipation had approximately the same state. When the residual strength tests were performed after liquefaction, the samples showed the same behavior as illustrated in figure 5.25.

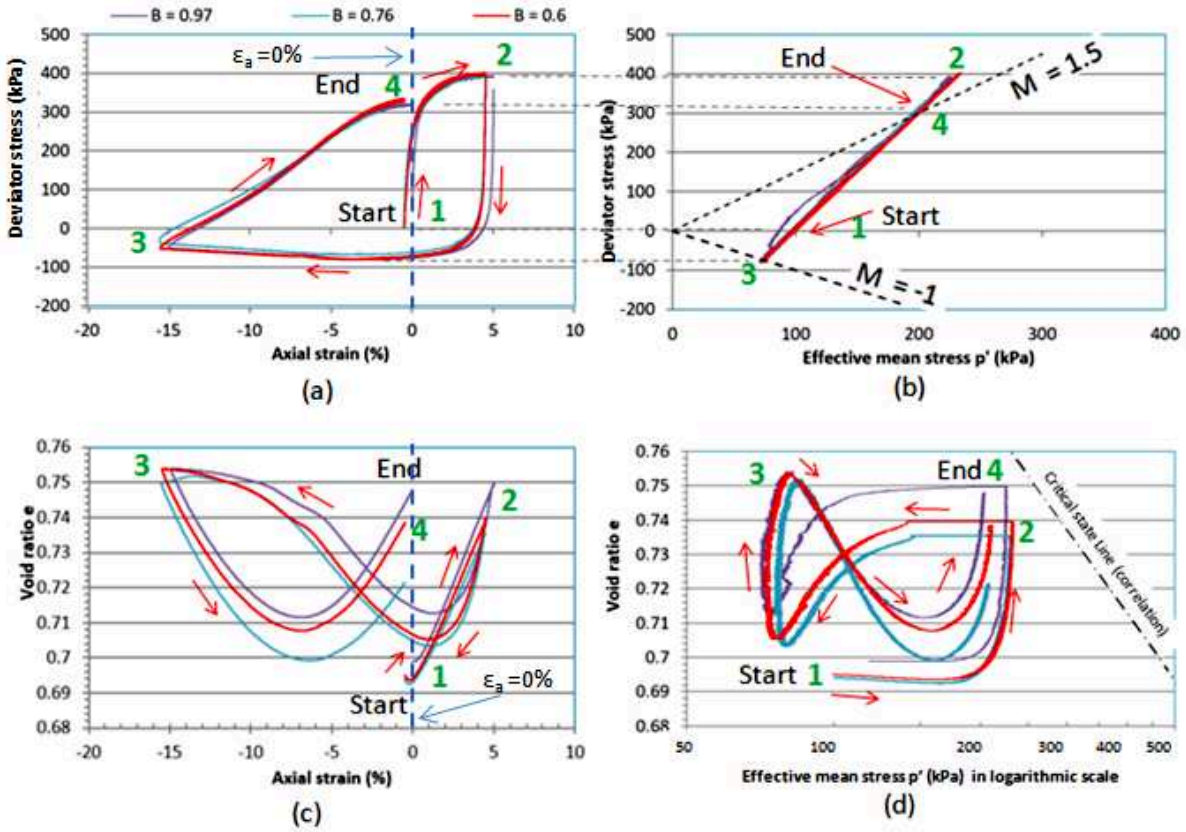

Figure 5.25 Residual behavior after liquefaction

a) deviator stress versus axial strain, b) deviator stress versus effective mean stress, c) void ratio versus axial strain, d) void ratio versus effective mean stress

V.5. Test parameters variation during the tests.

To give an overview of the tests, the parameters of the samples are summarized in table 5.7. With the test protocol presented in chapter 3, the parameters after each stage of the tests can be calculated based on the sample volume change measured by the pressure-volume controller or the balance. Specifically, the change of the void ratio e is calculated according to Equation 5.2.

$$\Delta_e = e_t - e_0 = \varepsilon_v.(1 + e_0) \quad \text{Eq. 5.2}$$

where, e_0 and $e_t$are the void ratio at the beginning and the end of each stage, respectively. ε_v is the volumetric strain of the sample after each stage of tests.

Concerning the unsaturated sand, the values of void ratio, relative density, Skempton's coefficient B, and saturation degree during each test are given in table 5.7. In the vicinity of saturation (Sr >85%), the pore air is considered as the bubbles embedded in pore water (Okamura and Soga 2006; Bian 2007; Fredlund and Rahardjo 1993). Consequently, the pore pressure is due to a homogenized and compressible pore fluid, composed of a mixture of water and occluded air. In this area, Terzaghi's effective stress concept remains valid (Biarez et al. 1991; Fleureau et al. 1992; Fleureau et al. 1993a, b).

From the comment mentioned above it is possible to consider that the volume of air bubbles inside the sample is constant if the pore water pressure is kept stable. With this assumption, the saturation degree during the consolidation process and the monotonic loading process is calculated based on equation 5.3

$$S_r = \frac{V_w}{V_v} = 1 - \frac{V_a}{V_v} = 1 - \frac{V_a/V_s}{V_v/V_s} = 1 - \frac{V_a/V_s}{e_t} \quad \text{Eq.5.3}$$

where, S_r is the saturation degree. V_w, V_a, V_v, and V_s are the volume of water, volume of air bubbles, volume of void, and volume of soil particles, respectively. The ratio V_v/V_s is the void ratio e.

The relation between the initial void ratio e_0 (the void ratio at the beginning of each stage of the test) and the last void ratio e_t (the ratio at the end of each stage of the test) is shown in equation 5.4.

$$e_t = e_0 + \varepsilon_v.(1 + e_0) \quad \text{Eq. 5.4}$$

where ε_v is the volumetric strain of the sample after each stage of the test.

Based on the equations above, the calculation for the test parameters is performed and summarized in the following table and figures. It is noted that in test 2, the data was lost so the saturation degree of the test was not calculated.

Table 5.7. The variations of the parameters during the tests

Test	Stage / Parameters	Before consolidation	Before cyclic loading	After reconsolidation	After monotonic loading
CUST1	e	0.715	0.708	0.699	0.749
	D_r	0.83	0.85	0.87	0.74
	B	0.97	-	-	-
	S_r (%)	100	100	100	100
CUST2	e	0.715	-	-	-
	D_r	0.83	-	-	-
	B	0.87	-	-	-
CUST3	e	0.709	0.705	0.694	0.741
	Dr	0.84	0.86	0.88	0.76
	B	0.76	-	-	-
	S_r (%)	98.73	98.72	98.70	98.78
CUST4	e	0.712	0.707	0.695	0.740
	D_r	0.84	0.85	0.88	0.77
	B	0.60	-	-	-
	S_r (%)	98.06	98.05	98.02	98.14

Figure 5.26 summarizes the change of the void ratio and the saturation degree of test CUST 4 with the lowest B value of 0.6. It can be seen that during the test, the saturation degree reaches its highest value at the liquefaction state.

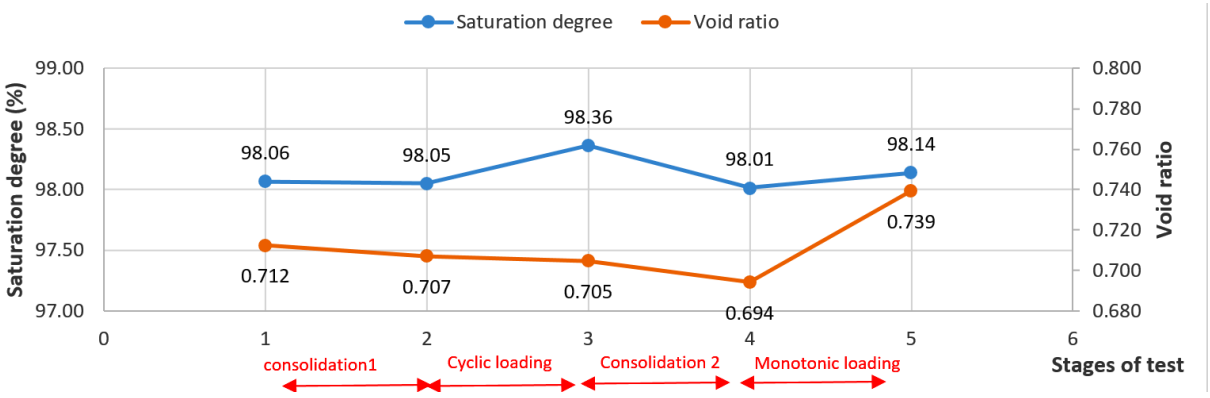

Figure 5.26 Summary of the saturation degree change and void ratio change of test CUST 4 with B of 0.6

Figure 5.27 and figure 5.28 show the sample volume change and the sample volumetric strain of the test measured by two independent methods. The continuous curve shows the results measured by the HAPC and the square points present the results given by the balance. It is noted that during the cyclic loading process, the sample volume change was measured by only one method, using the balance. As mentioned in chapter 3, when using the balance, it is impossible to follow the sample volume change continuously. This method only allows measuring the total change between the start point and the last point of each test stage (the points marked by the squares in figures 5.27 and 5.28). The sample volume change in negative domain corresponds to the dilative behavior of the sample. Conversely, the sample volume change in positive domain shows the contract behavior of the sample volume change. The results show that there is a difference between the results measured by two methods; however, in general, this difference is small and is negligible.

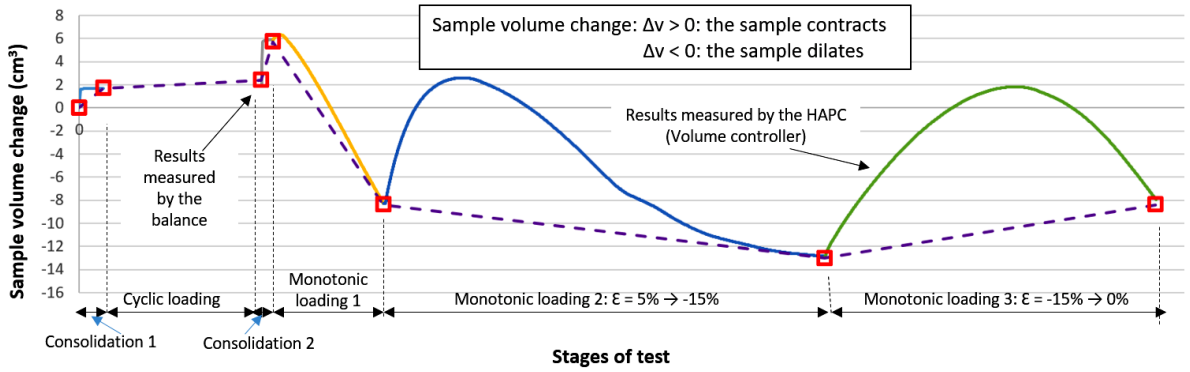

Figure 5.27 Sample volume change measured by two independent methods (test CUST 4)

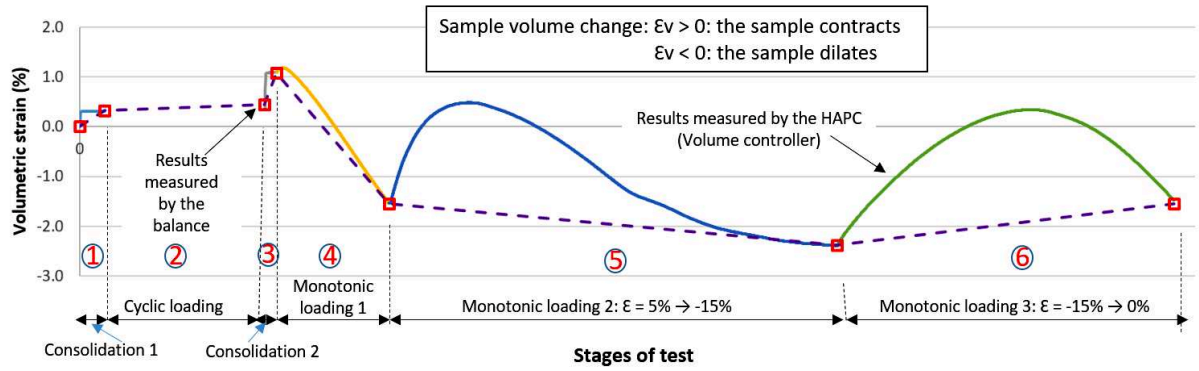

Figure 5.28. Sample volumetric strain during stepping CSR unsaturated test measured by two independent methods (test CUST 4)

Figure 5.29 shows the sample volume change calculated based on the sample volumetric strain measured by the two different methods. It is clear that in the stages from 1 to 3, the sample contracts so the void ratio decreases. In the stages 4th, the sample shows a strong dilative behavior corresponding to the strong increase of the void ratio. In stage 5, when the axial strain varies from 5 to -15%, the void ratio firstly decreases to 0.705, after that it increases to 0.755. In stage 6, when the axial strain increases from -15% to 0%, the void ratio decreases from 0.755 to 0.71 and then increases to 0.74.

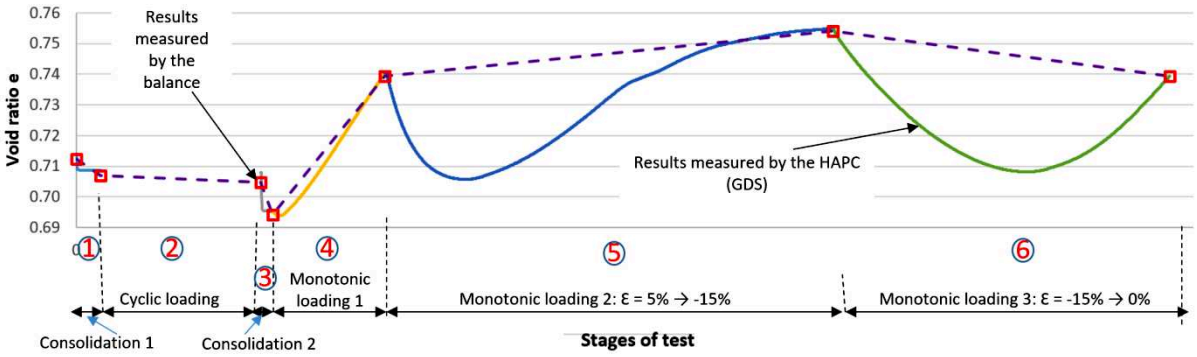

Figure 5.29 Void ratio change during the stepping CSR unsaturated test (test CUST 4)

V.6. Discussion on the effect of saturation degree on the liquefaction and residual strength of unsaturated sand.

Figure 5.30 shows the cyclic deviator stresses and cyclic stress ratios applied to liquefy the sample as a function of B value. The CSR for the first load case of all the tests is 0.15, corresponding to a deviator stress of 30 kPa. It increases of 0.05 after each 100 cycles if the sample is not liquefied. The samples with B of 0.97 and 0.87 are liquefied at the same CSR of 0.25; however, there is a significant difference between the numbers of cycles causing liquefaction. The sample having a lower value of B (0.76) liquefies when the applied CSR is equal to 0.3 and the most unsaturated sample with B = 0.6 is liquefied by the highest value of CSR (0.35). This result demonstrates that the decrease of B value results in the increase of CSR needed to liquefy the sample.

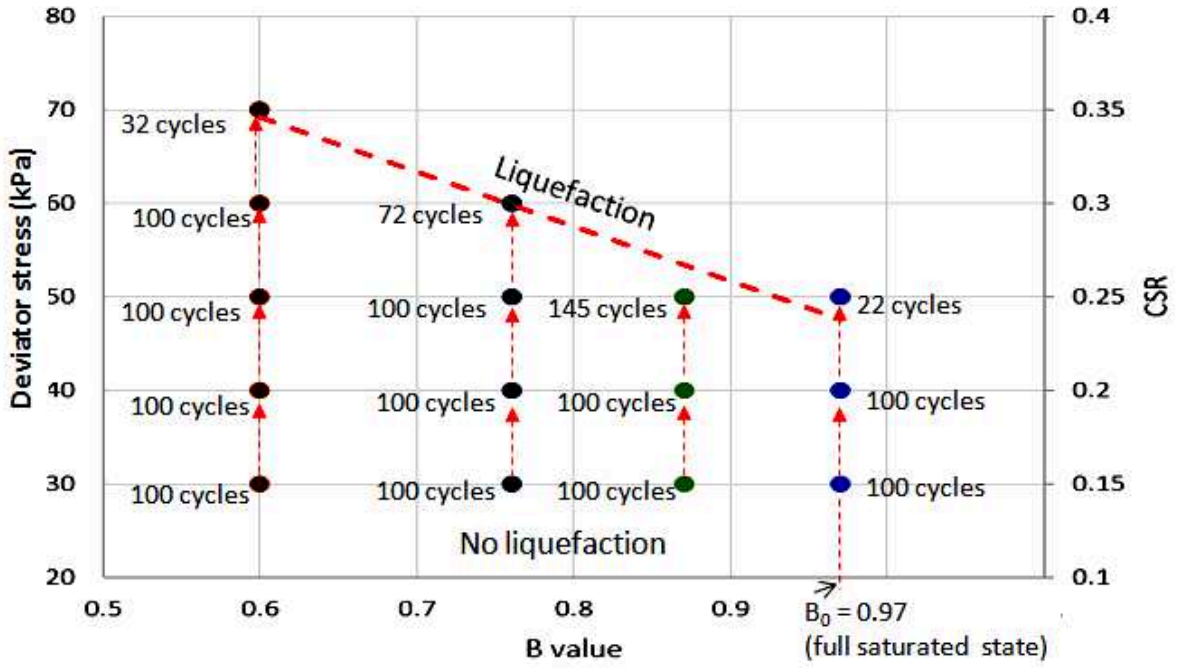

Figure 5.30 Deviator stress and number of cycles in function of B value.

The development of CSR after each given number of cycles is depicted in Figure 5.31. It is obvious to see that samples with higher B values need lower CSR values and lower numbers of cycles to liquefy. All tests start at the same initial state and follow the same path; however, the unsaturated sample with B = 0.6 liquefies at the point where the CSR is 0.35 after 432 cycles while the saturated sample with B_0 = 0.97 liquefies when CSR = 0.25 and the number of cycles is 222. Consequently, according to the protocol followed in these tests, it is noted that the cumulative number of cycles to reach liquefaction increases with the applied CSR value (dashed red line)

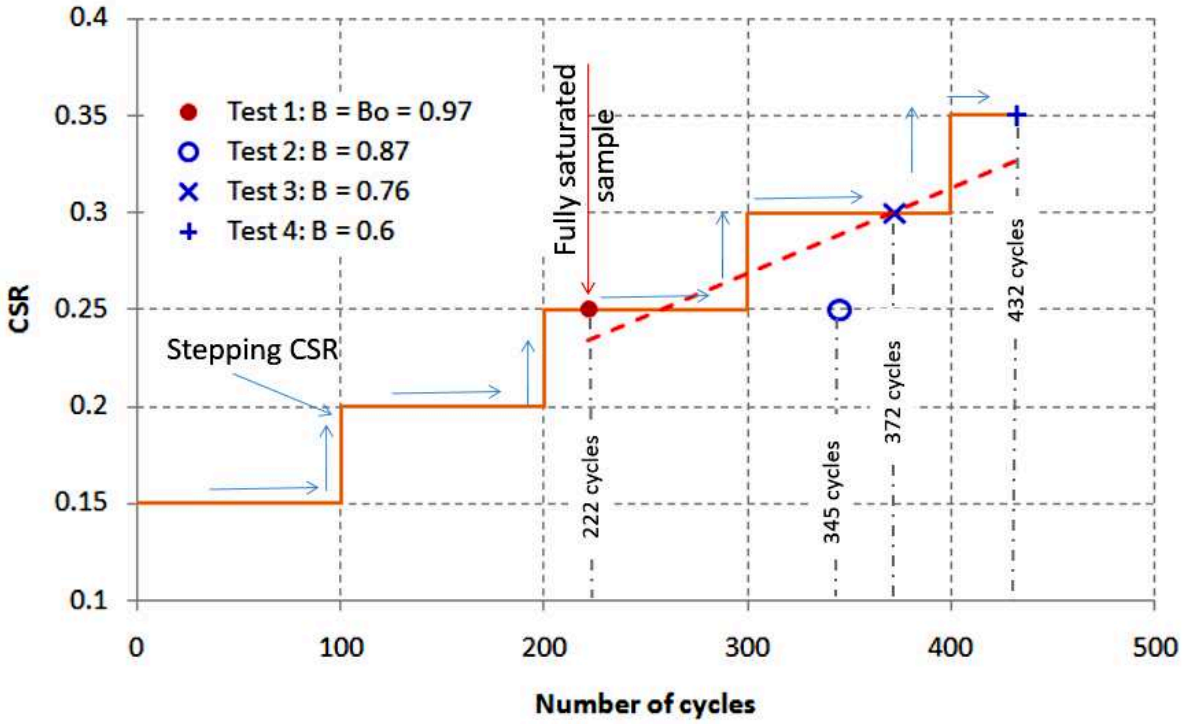

Figure 5.31 Test path in the relationship between CSR and numbers of cycles

Figure 5.32 shows the results in comparison to the results of Arab et al. (2016) carried out on the same material but at a different relative density. As expected, the sample having a relative density of 83% in this study liquefies at a higher number of cycles compared to the sample of Arab et al. (2016) with a relative density of 50%.

These curves in figure 5.32 highlight the possibility of predicting, for each B value, the number of cycles causing liquefaction as a function of the last CSR applied. For example: for curve corresponding to B = 0.97 (red dashed curve), the number of cycles to reach liquefaction is about 320 for a CSR = 0.15 (path K-C); 250 for a CSR = 0.2 (path K-L-B) and about 220 for a CSR = 0.25 (path K-L-A). Similarly, concerning the curve corresponding to B = 0.87 (blue dashed curve), the number of cycles to reach liquefaction is about 350 for a CSR = 0.25 (path K-A-Q-E); about 310 for a CSR = 0.3. However, the lack of experimental data does not allow confirming these predictions with accuracy. Tests are underway to consolidate these claims.

Similarly, the curve 1 corresponding to B =0.97 allows predicting the point C which shows the number of cycles causing liquefaction when the CSR is constant at 0.15 during cyclic loading.

Now, if one compares the Arab et al. (2016) results on the same sand, initially prepared at a relative density D_r = 50% (loose sand) and B = 0.93 with our curve 1 (D_r = 83% and B = 0.97), one notice for a CSR = 0.15, the loose sand liquefies after a number of cycles N = 60 (corresponding to point P in the figure), whereas theoretically, the dense sand (D_r = 83%) would liquefy for a number of cycles N of about 310 corresponding to point C in the figure.

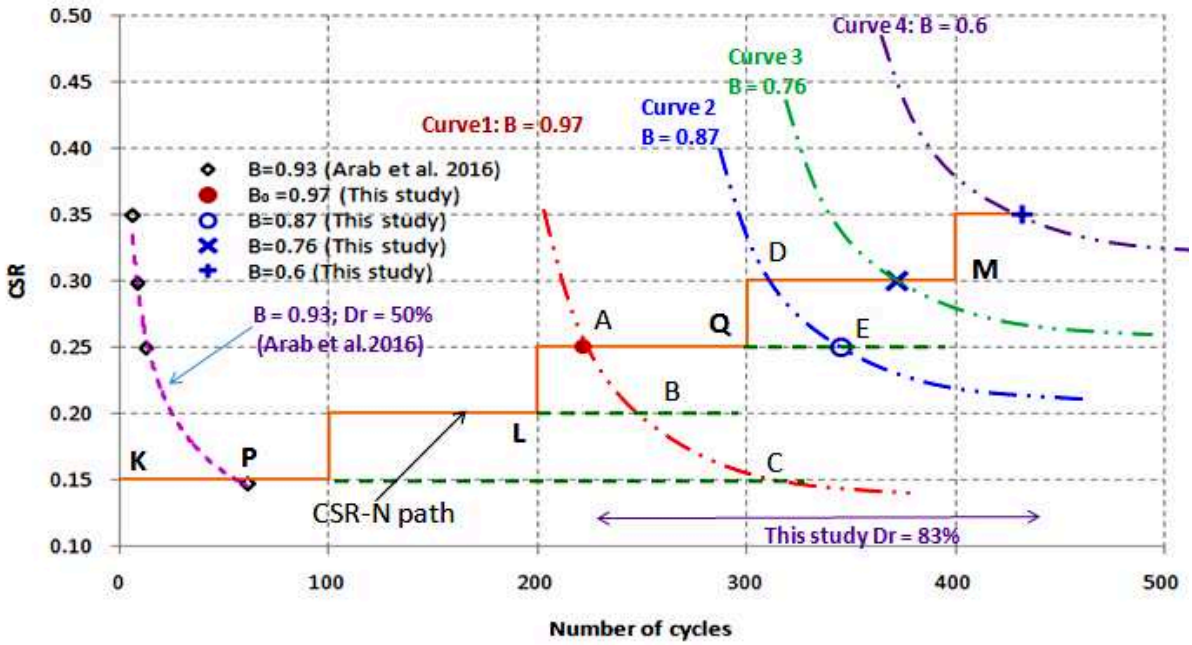

Figure 5.32 Relationship between CSR and numbers of cycles in comparison to the results of Arab et al. (2016)

Figure 5.33 shows the upper and lower envelops of pore water pressure increment in function of number of cycles. The CSR is increased after 100 cycles until liquefaction. From this figure, it is clear that the CSR and the total number of cycles causing liquefaction increase when the B value or saturation degree is reduced. All tests show that, although the samples are liquefied by the last load cases with the maximum CSRs, the load cases with smaller CSRs also contribute to the increase in pore water pressure. In relation to the case of earthquakes mentioned above, this result suggests that the liquefaction is triggered by the main shock but it is also affected by the foreshocks. The pore water increment in foreshocks can affect the triggering time and the duration of liquefaction. When studying the effect of saturation degree on the liquefaction susceptibility of sand, it can be seen from figure 5.33 that the maximum pore water pressure developments of the samples having lower saturation degrees are smaller than that of the samples with higher saturation despite undergoing the

same CSR and after the same number of cycles. This difference is shown most clearly in the first 100 cycles where all tests have the same initial state, CSR and number of cycles. The pore water pressure growth in the saturated test (B_0=0.97) is 20 kPa while these values are 9 kPa and 8 kPa for the tests with B of 0.76 and 0.6 respectively. In the next 100-cycle ranges, the gap in pore water pressure addition between tests is a combination of two elements: the effect of saturation degree and the reduction of effective confining stress due to the accumulated pore water pressure during the previous load cases.

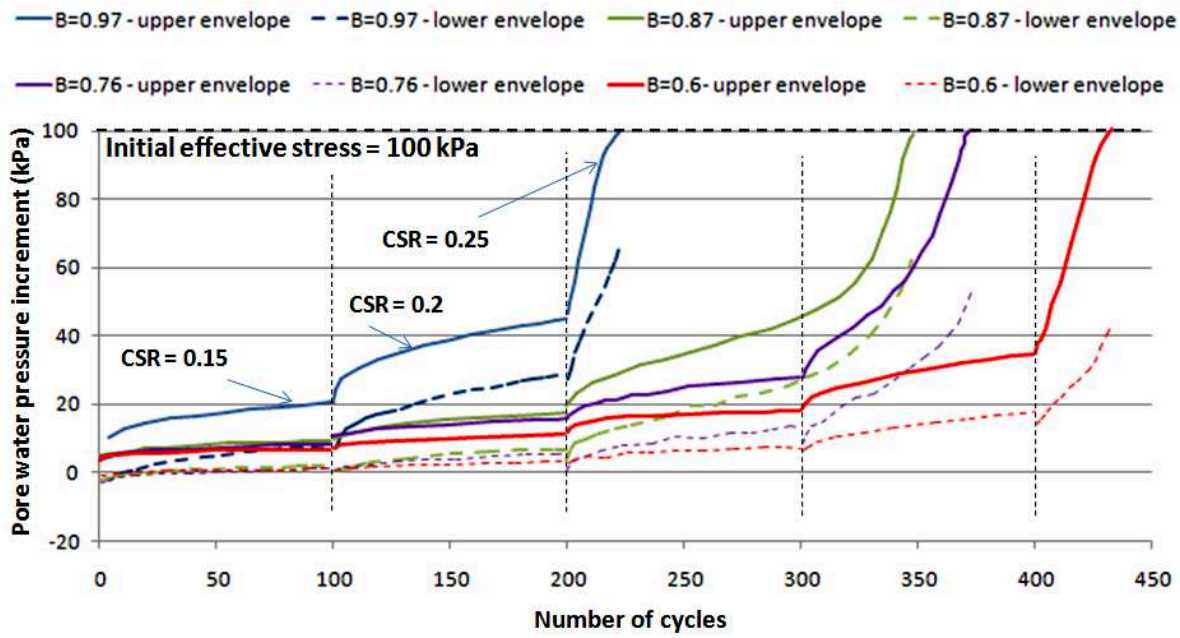

Figure 5.33 Pore-water pressure increments versus the number of cycles

V.7. Conclusions

This chapter presents a laboratory study on the liquefaction behavior of RF Hostun sand in both saturated and unsaturated states. A series of tests was carried out to determine Skempton's coefficient B. The sample with Skempton's parameter B of 0.97 is considered as full saturated sample.

The liquefaction behavior of soil in dense state is studies carefully through these series of tests. The two-peak mechanism was observed in both saturated and unsaturated tests and its relation to the variation of the axial strain was explained. These tests also pointed out the difference in the development of the axial strain caused by the liquefaction and by the excess of deviator stress compared to the extension strength of the sample. When the deviator stress is in the vicinity of the failure lines, the axial strain develops rapidly, however, this

development happens when the pore water pressure equal to the lowest value in a cycle of loading. While the axial strain development caused by the liquefaction happens due to the increase of pore water pressure resulting in the low effective confining stress.

When comparing the friction angle of the test in this chapter with the series of test in chapter 4, it can be seen that the friction angle increases with the rise of the relative density. The friction angle increases from 34° to 37°when the relative density increases from 55% to 83%.

The results show obviously the effect of the saturation degree on the liquefaction susceptibility of soil. When subjected to consecutive increasing cyclic loading cases as mentioned, the lower value of B results in the higher deviator stress of the last load case and the higher number of cycles needed to liquefy the sample. The fully saturated sample (B_0=0.97) is liquefied when CSR is 0.25 while the unsaturated sample with B of 0.6 is liquefied when CSR is 0.35. A 0.37 reduction of Skempton's coefficient B value results in a 0.1 increase of CSR and as well the increase of 210 cycles. The effect of unsaturation on pore water pressure increment can be seen from the beginning of the tests. After a given number of cycles with the same CSR, the sample having a lower value of B shows the lower value of pore water pressure increment compared to that of the higher B value sample. From the second load case, the pore water pressure increment in each load case is the combination of two elements: the effect of saturation degree and the reduction of effective confining stress due to the accumulated pore water pressure in the previous load cases. It can be also seen that although the samples are liquefied by the last load cases which have the highest CSRs, the load cases with smaller CSRs also play a part in the increase of pore water pressures. When applied to real earthquakes, it suggests that the foreshocks with low scale (corresponding to the low values of CSR) can play a role in the liquefaction caused by the main shocks.

The residual strength tests after liquefaction demonstrate that after dissipation of the pore water pressure, soil resistance recuperates. As expected, the soil with the high relative density of 83% shows a strongly dilatant behavior when compressed. However, the effect of Skempton's coefficient B on drained behavior of soil after liquefaction is not obvious. In other words, the liquefaction erases the effect of the initial saturation state of the soil.

GENERAL CONCLUSIONS AND PERSPECTIVES

VI.1. General conclusions

From the literature review performed in this study, it can be seen that the unsaturated soil occupies the majority of the earth's surface and there is a big difference in the behavior of unsaturated soil compared to that of saturated soil. This fact indicates the need to have more researches on the behavior of unsaturated soil.

A large number of studies have been focused on the liquefaction of saturated soil and its mechanism has been clearly understood. However, not many studies have focused on the liquefaction of unsaturated soil. More recent studies have clarified some aspects in the liquefaction mechanism of unsaturated sand; however, most of studies mainly focus on the liquefaction of the unsaturated soil without considering the factors before and after liquefaction. From the context of researches, it can be seen that there are still many issues that need clarification such as:

- The behavior before and after the main shock and their effect on the liquefaction potential.
- The effect of the saturation degree on the CSR (cyclic stress ratio)
- In the case of dense soils, what is the effect of unsaturation on the CSR-number of cycles relationship to reach liquefaction?

In this study, two campaigns of test were carried out to provide some answers to these questions. In the first campaign, the constant CSR cyclic loading was applied to the samples with saturation degree decreasing from 100% to 86%. In the second campaign, the stepping CSR cyclic loading was applied to the samples with saturation degree in the vicinity of full saturation state (from 98% to 100%). All tests were followed by the monotonic loading to study the residual strength after liquefaction.

From the first campaign of experiments, it can be concluded that:

- The liquefaction resistance of the sand increases with the decrease in the initial degree of saturation. The higher the amount of initial air present inside the sample, the lower the liquefaction susceptibility is.
- The effect of saturation degree is more obvious when the saturation degree is at the vicinity of full saturation state. The decrease of saturation degree from 100% to 95%, results in an increase of liquefaction resistance higher than that caused by the decrease

of saturation from 95% to 86%. In other words, the liquefaction resistance of soil is more sensitive to the change of saturation degree in the domain near 100%. Further away from the full saturation state, the influence of saturation degree is lower.

- At a high saturation degree, the two criterions of liquefaction were observed, null effective stress due to the pore water pressure increase and the strain double amplitude of 5%. There is a threshold (between 86% and 95%) that if the saturation degree is lower than, there is only one criterion observed (strain double amplitude) at the liquefaction state. This result is somewhat similar to that of Vernay (2018) and Vernay et al. (2019). In that study, they showed that there is a difference between the cyclic behavior of soil in the zone of saturation higher than 95% and the zone of saturation lower than 95%.
- The sample volume change in the tests with a saturation degree of around 95% is approximately the same. With the saturation degree around 86%, the sample volume change at 5% of axial strain is inverse proportional with the value of CSR applied. The sample volumetric strain of 1.1% corresponds to the CSR of 0.4 while this value is 2% when the CSR is 0.35. A 0.05 increase in CSR results in a 0.9% decrease in sample volumetric strain.
- The monotonic loading after liquefaction demonstrates that after the liquefaction, the pore water pressure dissipates and the soil residual strength recuperates.

From the second campaign of experiments, it can be concluded that:

- The results show obviously the effect of the saturation degree on the liquefaction susceptibility of soil in dense state. When subjected to the stepping CSR loading cases as mentioned, as expected, the lower value of B corresponding to the lower saturation degree results in the higher deviator stress of the last load case and the higher number of cycles needed to liquefy the samples. The fully saturated sample (B_0=0.97) liquefies with CSR of 0.25 while the unsaturated sample with B of 0.6 liquefies when CSR is 0.35. In other words, a reduction of Skempton's coefficient B value from 0.97 to 0.6 results in the increase of 210 cycles and the increase of CSR from 0.25 to 0.35.
- The first load case, although, does not result in liquefaction; however, increases the pore water pressure and this increment in pore water pressure is affected by the value of B.

- In the next load cases of tests, the pore water pressure increment is affected by two elements: the saturation degree of the samples and the reduction of effective confining stress caused by the previous load cases.
- It is clear that although the samples were liquefied by the last load cases; however, the preceded load cases with smaller CSRs also contribute to the increase of pore water pressures. In the relation to real earthquakes, it suggests that the foreshocks with low scale (corresponding to the low values of CSR) can play a role in the liquefaction caused by the main shocks.
- Similar to the first campaign, the residual strength tests after liquefaction demonstrate that soil residual strength recuperates after dissipation of the pore water pressure. Under monotonic loading, the soil with the high relative density of 83% shows a strongly dilatancy, a characteristic of sand in dense state.
- The effect of Skempton's coefficient B on drained behavior of soil after liquefaction is not obvious. In other words, the liquefaction erases the effect of the initial saturation state of the soil.

VI.2. Perspectives.

The experiments have given important information about the behavior of soil in the domain of near saturation, However, it is necessary to have more tests on the same material (RF Hostun sand) or on other materials to build up a database which help to evaluate more exactly the liquefaction phenomenon of granular material, particularly, the studies focusing on the soil behavior which are performed systematically from before to after liquefaction. Due to the complexity as well as the long duration of tests, there is a need for the participation of the community of researchers.

It can be seen that, in the first campaign of tests, the criterion used to determine the liquefaction phenomenon changes with the decrease of saturation. When the saturation degree decreases, in some cases, the sample can failure before reaching the null effective stress state. This observation needs more tests to be understood clearly. Moreover, the aspects like the sample volumetric strain and the effect of sample preparation to the soil liquefaction susceptibility also need more information to understand.

The results of tests with a saturation degree of 86% and 95% suggest an interesting issue. The axial strain at liquefaction state in tests having high saturation degree (95%) is mostly due to the increase of pore water pressure (the axial strain develops at the state when the deviator

stress passes zero) while the axial strain at liquefaction state in tests having a lower saturation degree (86%) is mostly because the deviator stress reaches the extension strength of the material (axial strain develops at the state when the deviator stress reaches its lowest value and contacts the lower failure line). This suggests that there is a value of saturation degree, where the axial strain caused by two reasons (the deviator stress passes zero and the deviator stress reaches the extension strength) is equal.

These second campaigns of experiments also suggest a variety of issues relating to the experimental procedure for unsaturated sand in a dense or very dense state. Accordingly, the stepping CSR cyclic loading procedure needs to be developed. The initial analysis done in chapter 5 shows the flexible variation of the results carried out by this protocol. This protocol also allows studying the liquefaction susceptibility of unsaturated sand in a dense state. Whereas it is difficultly performed by the procedure with constant CSR cyclic loading due to the large number of cycles needed to liquefy the samples.

REFERENCES

Aitchison, G. D., 1965, Moisture Equilibria and Moisture Changes in Soils Beneath Covered Areas. A Symp. in Print, G. D. Aitchison, Ed. Australia: Butterworths, 278 pp.

Alarcon-Guzman, A., Leonards, G. A., Chameau, J. L., 1988, Undrained Monotonic and Cyclic Strength of Sands, Journal of Geotechnical Engineering, ASCE, Vol. 114, No. 10, pp. 1089-1109.

Alonso, E. E., Gens, A. & Josa, A. (1990). A constitutive model for partially saturated soils Geotechnique 40, No. 3, 405-430

Alonso, E. E., Gens, A., High, D. W., 1987, Special problem soils. General report. Proc. 9th European Conf. Soil Mech. Fdn Engng, Dublin, 3, 1087-l 146.

Amini, F., Qi, G., 2000, Liquefaction testing of stratified silty sands. Journal of Geotechnical and Geoenvironmental Engineering, 0208-0217.

Arab, A., Sadek, M., Benkhatir, M. 2016. Saturation Effect on Behavior of Sandy Soil Under Monotonic and Cyclic Loading: A Laboratory Investigation. Geotechnical and Geological Engineering. Geotechnical and Geological Engineering. DOI: 10.1007/s10706-015-9949-6

Been, K., Jefferies, M. G., 1985, A state parameter for sand. Geotechnique, Vol. 35, No. 2, pp. 99–112.

Benahmed, N., 2001, Comportement mécanique d'un sable sous cisaillement monotone et cyclique : application aux phénomènes de liquéfaction et de mobilité cyclique. Thèses doctoral. L'Ecole Nationale des ponts et Chaussées, France.

Benahmed, N., Canou, J., et Jean-Claude D., 2007, Propriétés de liquéfaction et structure des sables lâches. 7ème Colloque National AFPS 2007 – Ecole Centrale Paris. https://www.researchgate.net/profile/J_Dupla/publication/267724708_Proprits_de_liqufaction_et_structure_des_sables_lches/links/54b3a3b10cf28ebe92e2f79f.pdf.

Bian. H., 2007, Modèle numérique pour les sols sableux non saturés en zone sismique: application à la liquéfaction. These pour obtenir le grade de docteur de L'Université des Sciences et Technologies de Lille.

Biarez, J., Fleureau, J.M., Kheirbek-Saoud, S., 1991, Validité de $\sigma' = \sigma - u_w$ dans un sol compacté. Proceedings of the 10th European conference on soil mechanics and foundation engineering. Firenze, Mai, vol. 1, pp. 15-18.

Biarez J., Hicher P.Y., 1994, Elementary mechanics of soils behaviour, saturated remoulded soils, Balkema, Rotterdam.

Biarez, J, Fleureau, J.M., Indarto, Taibi, S. & Zerhouni, M.I, 1989. Influence of water negative pore pressure on the flow of granular materials in silos. Proceedings of the first international conference on Micromechanics of Granular Media, Clermont-Ferrand, 4-8 Septembre 1989. Biarez & Gourvès (eds), A.A. Balkema, Rotterdam

Bishop, A. W., and Blight, G. E., 1963, Some aspects of effective stress in saturated and unsaturated soils, Geotechnical, 13, No. 3, 177–197.

Bishop, A. W., and Donald, I. B. 1961. The experimental study of partly saturated soil in the triaxial apparatus, Proceedings of the Fifth International Conference on Soil Mechanics and Foundation Engineering, Paris, Vol. 1, pp. 13–21.

Bishop, A.W. 1954, The use of pore-pressure coefficients in practice. Géotechnique 4 (4):148- 52

Bishop, A.W. 1959. « The principle of effective stress ». Teknisk Ukeblad 106 (39).

Bishop, A.W., et G.E. Blight. 1963. « Some aspects of effective stress in saturated and partially saturated soils ». Géotechnique 13 (3):177-97.

Blight, G. E., 1965, A study of effective stress for volume change. In Moisture equilibria and moisture changes in soils beneath covered areas, pp. 259-269. Sydney: Butterworths.

Bolt G. H., Miller R. D., 1958, Calculation of Total and Component Potentials of Water in Soil, Amer. Geophys. Union Transportation, vol. 39, pp. 917-928.

Bolzon, G., Schrefler, B.A, Zienkiewicz, O.C, 1996, Elastoplastic soil constitutive laws generalised to partially saturated states, Geotechnique, Vol. 46, pp. 279-89, 1996.

Breul, P., Younes, H., Roland G., 2008, On site characterization and air content evaluation of coastal soils by image analysis to estimate liquefaction risks. Canadian Geotechnical Journal 45 (12):1723-32.

Brule, S., Emmanuel J., 2014, Le traitement contre la liquéfaction des sols en France métropolitaine. In . http://www.cfmr-roches.org/sites/default/files/jngg/139.pdf.

Buckingham E., 1907, Studies of The Movement of Soil Moisture, U.S. D.A. Bur. of Soils, Bulletin No. 38, 1907.

Canou, J., Benahmed, N., Dupla, J.C., Gennaro, V.D., 2002, Instabilités de liquéfaction et phénomène de mobilité cyclique dans les sables. Rev. Fr. Géotech. N° 98, pp. 29–46. https://doi.org/10.1051/geotech/2002098029

Canou, J., Benahmed, N., Jean-Claude D., De Gennaro, V., 2000, Instabilités de liquéfaction et phénomène de mobilité cyclique dans les sables.

Canou, J., 1989, Contribution a l'étude et a l'evaluation des proprietes de liquefaction d'un sable. Paris, France: Thèse de Doctorat de l'Ecole Nationale des Ponts et Chaussées.

Castro, G., Poulos, S. J., 1977, Factors affecting liquefaction and cyclic mobility. Journal of Geotechnical Engineering Division, 103(6).

Castro, G., 1969. Liquefaction of sands. Ph.D. Thesis, Harvard Soil Mechanics Series n°81, Harvard University, Cambridge, MA, 112 p

Chaney, R.C., 1978, Saturation effect on the cyclic strength of sands. In: Proceedings of earthquake engineering and soils dynamics, vol 1, ASCE, New York, 342–359

Chang, W. J., Rathje, E. M., Stokoe, K. H. and Hazirbaba, K., 2007, In Situ Pore-Pressure Generation Behavior of Liquefiable Sand, Journal of Geotechnical and Geoenvironmental Engineering, ASCE, Vol. 133, No. 8, pp. 921-931.

Chu, J., Leong, W. K., Loke, W. L., 2003, Discussion of Defining An Appropriate Steady State Line for Merriespruit Gold Tailings. Can. Geotech. J., Vol. 40, pp. 484–486.

Coleman, J. D., 1962, Stress / strain relations for partly saturated soils, Geotechnical, 12(4), 348–350.

Colliat, J.L., 1986, Comportement des matériaux granulaires sous forte contraintes, influence de la nature minéralogique du matériau étudié, Thèse de doctorat de spécialité, IMG, Grenoble

Corey A. T., Slayter R. 0., Kernper W. D., 1967, Comparative Terminologies for Water in the Soil-Plant-Atmosphere System, in Irrigation in Agricultural Soils, R. M. Hagan et al., Eds., Amer. Soc. Agron., Mono. No. 11, ch. 22.

Coussy O., 2004, Poro mechanics, John-Wiley.

Coussy, O. and Dangla, P., 2002, Approche énergétique du comportement des sols non saturés, in Coussy and Fleureau (eds., Mécanique des Sols non Saturés), Hermès, Paris, pp. 137-174.

Croney, J., Coleman, D., Black W. P. M., 1958, Movement and Distribution of Water in Soil in Relation to Highway Design and Performance, Water and Its Conduction in Soils, Highway Res. Board, Special Report, Washington, DC, no. 40, pp. 226-252, 1958.Croney, J. D. Coleman, and W. P. M. Black, "Movement and Distribution of Water in Soil in Relation to Highway Design and Performance, " Water and Its Conduction in Soils, Highway Res. Board, Special Report, Washington, DC, no. 40, pp. 226-252,12:74

Cubrinovski, M., Aimee, R., Nikolaos N., 2019, System response of liquefiable depsits. Soil Dynamics and Earthquake Engineering. Volume 124, September 2019, Pages 212-229

Dang, Q.H., 2019, Comportement des sols sous liquéfaction artificielle, amélioration des sols à risques liquéfiables. Thèse de doctorat. Université Paris-Est.

Dangla, P., 2002, Plasticité et Hystérésis, in COUSSY and FLEUREAU (eds), Mécanique des Sols non Saturés, Hermès, Paris.

DeGregorio, V.B., 1990, Loading Systems, Sample Preparation, and Liquefaction. J. Geotech. Engrg.,Vol. 116, No. 5, pp. 805–821.

Delage, Pierre, Cui, Y.J., 2000, L'eau dans les sols non saturés. Techniques de l'ingénieur, https://www.techniques-ingenieur.fr/base-documentaire/construction-et-travaux-publics-th3/geotechnique-42238210/l-eau-dans-les-sols-non-satures-c301/

Delage, Pierre, et Yu-Jun Cui. 2001. Comportement mécanique des sols non saturés. Ed. Techniques Ingénieur.

Doanh, T., Ibraim, E., Matiotti, R., 1997, Undrained instability of very loose Hostun sand in triaxial compression and extension. Part 1: Experimental observations. Mechanics of Cohesive-Frictional Materials, 2(1):47-70

Dobry, R., Vasquez-Herrera, A., Mohamad, R. and Vucetic., M., 1985, Liquefaction Flow Failure of Silty Sand by Torsional Cyclic Tests, Advances in the Art of Testing Soils Under Cyclic Conditions, Detroit, Mich., pp. 29-50

Dorsey N. E., Properties of Ordinary Water-Substances, Amer. Chemical Soc., Mono. Series. New Yo&: Reinhold, 1940, 673 pp

Dudley, J. H., 1970, Review of collapsing soils. J. Soil Mech. Fdn Engng, Am. Sot. Civ. Engrs 96, SM3, 925-947.

Dysli, M. 1997. Cours de mécanique des sols. Module B2-2. Cycle postgrade EPFL: Géologie appliquée à l'ingénierie et à l'environnement. Ecole Polytechnique Fédérale de Lausanne.

Eliadorani, A., and Vaid., Y.P., 2003, Discussion of 'effect of undrained creep on the instability behaviour of loose sand. Can. Geotech. J., Vol. 40, pp. 1056–1057.

Erten, D., & Maher, M.H., 1995, Cyclic undrained behaviour of silty sand. Soil Dynamics and Earthquake Engineering 14, pp. 115-123.

Escario, V., Saez, J., 1973, Measurement of the properties of swelling and collapsing soils under controlled suction. Proc. 3rd Int. Conf. Expansive Soils, Haifa, 196200.

Fargeix, D., 1986, Conception et réalisation d'une presse triaxiale dynamique-application à la mesure des propriétés des sols sous sollicitations sismiques. Thèse de doctorat, IRIGM, Grenoble

Finn, W.D.L., Bransby, P.L., & Pickering, D.J., 1970, Effect of strain history on liquefaction of sands. Journal of the Soil Mechanics and Foundation Division, ASCE96 (SM6) pp. 1917-1934

Fleureau, J.M, Indarto, 1993a, Comportement du limon de Jossigny remanié soumis à une pression interstitielle négative Rev. Fr. Geotech., 62 (1993) 59-66. doi: https://doi.org/10.1051/geotech/1993062059.

Fleureau, J.M., Kheirbek-Saoud, S., 1992, Variations de résistance des sols compactés avec la pression interstitielle négative. Rev. Franç. Géotech. n° 59, pp. 57-64.

Fleureau, J.M., Kheirbek-Saoud, S., Soemitro, R., Taibi, S., 1993b, Behavior of clayey soils on drying-wetting paths. Canadian Geotechnical Journal- 30, (2):287-296. doi:10.1139/t93-024|© 1993 NRC

Fourie, A., Hofmann, B., Mikula, R., Lord, E., and Robertson, P., 2001, Partially saturated tailings sand below the phreatic surface. Geotechnique, 51(7), 577–585.

Fredlund D. G., Rahardjo H., Fredlund M. D., 2012, Unsaturated Soil Mechanics in Engineering Practice. John Wiley & Sons, Inc. ISBN 978-1-118-28049-2 (ebk).

Fredlund D.G., Xing, A., 1994, Equations for the soil-water characteristic curve. Can. Geotech. J., 31 (1994), pp. 521-532

Fredlund, D. G. 1996, The emergence of unsaturated soil mechanics. In. Texas.

Fredlund, D. G., and Morgenstern, N. R., 1977, Stress state variables for unsaturated soils, Journal of Geotechnical Engineering Division, 103, 447–466.

Fredlund, D.G., Morgenstern, N.R., and Widger, R.A., 1978, The Shear Strength of Unsaturated Soils. Canadian Geotechnical Journal, 15(3), 313-321.

Fredlund, D.G., Rahardjo H., 1993, Soil mechanics for unsaturated soils. A Wiley-Interscience Publication, New York

Fredlund, D.G., Rahardjo H., 1993, Soil mechanics for unsaturated soils. A Wiley-Interscience Publication, New York

Gallipoli, D., Gens, A., Sharma, R. And Vaunat, J., 2003, An elasto-plastic model for unsaturated soil incorporating the effects of suction and degree of saturation on mechanical behaviour, Geotechnique, Vol. 53, N°1, pp. 123-135, 2003.

Gens, A, 2010, Soil-environment interactions in geotechnical engineering. Géotechnique 60

(1).

GNUEACR (GRID-NAIROBI AND UNIV. OF EAST ANGLIA'S CLIMATE RESEARCH UNIT), 2013, Map courtesy of United Nations Environment Programme. https://www.ialcworld.org/About/aridlands_map.html

Gray, W.G. and Schrefler, B.A., 2001, Thermodynamic approach to effective stress in partially saturated porous media", Eur. J. Mech. A/Solids, Vol. 20. pp. 521-538.

Gudehus, G., 1995, Constitutive relations for granulate-liquid mixtures with a pectic constituent. Mechanics of Materials, Vol. 22, No 2, pp. 93-103.

Halib. P., Luong. M.P., 1978, Sols pulverulent sous chargements cycliques. Ecole polytechnique, plaiseau.

Hassanizadeh, M., Gray, W.G., 1980, General conservation equations for multiphase systems: 3. Constitutive theory for porous media, Advances in Water Resources, Vol. 3,pp.25–40.

He, J., 2013, Mitigation of liquefaction of sand using microbial methods. Doctoral thesis, Nanyang Technological Universty – Singapore.

Hird, C.C., Hassona, F.A.K., 1990, Some factors affecting the liquefaction and flow of saturated sands in laboratory tests. Eng. Geol. (Amsterdam), Vol. 28, pp. 149–170.

Ho, David Y. F., Fredlund D.G., 1982, Strain rates for unsaturated soil shear strength testing. In Proceedings of the Seventh Southeast Asian Geotechnical Conference, 1:787-803. Hong Kong.

Hutter, K., Laloui, L., Vulliet, L., 1999, Thermo-dynamically based mixture models of saturated and unsaturated", J. Coh. Frict. Mat.

Hyodo, M., Yamamoto, Y., Sugiyama, M., 1994, Undrained cyclic shear behaviour normally consolidated clay subjected to initial static shear stress. Soils and Foundations, Vol. 34, No. 4, pp. 1-11.

ICOLD, 2012, Selecting seismic parameters for large dams - Guidelines (revision of Bulletin 72) - Bulletin n° 148.

Idriss, I. M., 1991, Earthquake Ground Motions at Soft Soil Sites, Second International Conference on Recent Advances in Geotechnical Earthquake Engineering and Soil Dynamics, pp. 2265-2272.

Idriss, I. M., Boulanger, R.W., 2008, Soil Liquefaction During Earthquakes, Earthquake Engineering Research Institute (EERI), Oakland, California, USA.

Ishihara, K., & Okada, S., 1978, Yielding of over consolidated sand and liquefaction model under cyclic stresses. Soils and Foundations, Vol. 18, No. 1, pp. 57-72.

Ishihara, K., 1985, Stability of Natural Deposits during Earthquakes. General Rapport 11eme ICSMFE, San Francisco, Vol. 1, pp. 321-376.

Ishihara, K., 1993, Liquefaction and flow failure during earthquakes. Geotechnique 43, 351-415.

Ishihara, K., Tatsuoka, F. and Yasuda, S., 1975, Undrained Deformation and Liquefaction of Sand under Cyclic Stresses, Soils and Foundations, Vol. 15, No. 1, pp. 29-44.

Iwasaki, T., 1986, Soil liquefaction studies in Japan (a state of art). Soil Dynamics and Earthquake Engineering 5(1): 2-68. doi: 10.1016/0267-7261(86)90024-2.

Janssen, D. J., and Dempsey, B. J. 1980. Soil-moisture properties of subgrade soils, paper presented at the Sixtieth Annual Transportation Research Board Meeting, Washington, DC.

Jefferies, M., Been, K., 2016, Soil Liquefaction A Critical State Approach. Taylor & Francis Group. 2016. ISBN-13: 978-1-4822-1367-6

Jennings, J. E., and Burland, J. B., 1962, Limitations to the use of effective stresses in partly saturated soils, Ge´otechnique, 12(2), 125–144.

Jia Y., 2006, Contribution à la modélisation thermo-hydro-mécanuqye des roches partiellement saturées: application au stockage des déchets radioactifs, Thèse de doctorat, Université des Sciences et Technologies de Lille.

Josa, A., Alonso, E. E., Lloret, A., Gens, A., 1987, Stress-strain behavior of partially saturated soils. Proc. 9th European Conz Soil Mech. Fdn Engng, Dublin, 2, 561-564.

Kamata, T., Tsukamoto, Y., Tatsuoka, F., Ishihara, K., 2007, Possibility of undrained flow in suction-developed unsaturated sandy soils in triaxial. http://extras.springer.com/2007/978-1-4020-5893-6/paperpdf/1289_kam.pdf.

Khalili N., Geiser F., Blight GE., 2004, Effective stress in unsaturated soils: A critical review with new evidence, International Journal of Geomechanics. ASCE, Vol. 4,No 2, pp. 115-126.

Khalili N., Loret B., 2001, An elastoplastic model for nonisothermal analysis of flow and deformation in unsaturated soils: Formulation. International Journal of Solids and Structure, Vol. 38, pp. 8305–8330.

Khalili, N., Khabbaz, M.H., 1998, A unique relationship for the determination of the shear strengh of unsaturated soils, Geotechnique, Vol.48, N°5, pp.681-687.

Kohn P. G., 1965, Tables of Some Physical and Chemical Properties of Water," S.E.B. Symp., XIX, The State and Movement of Water in Living Organisms (Cambridge).

Krahn J., Fredlund D. G., 1972, On Total Matric and Osmotic Suction," J. Soil Sci., vol. 114, no. 5, pp. 339-348.

Ladd, R., 1978, Preparing test specimens using undercompaction. Geotechnical Testing Journal.

Lade, P.V., Hernandez, S.B., 1977, Membrane penetration effects in undrained tests. J Geotech Eng Div 103:109–125

Lee, K. L., and Seed, H. B., 1967, Drained strength characteristics of sands, J. Soil Mechanics and Foundations Div., ASCE 93(SM6), 117–41.

Lewis, R.W., Schrefler, B.A., 1987, The Finite Element Method in the Deformation and Consolidation of Porous Media, 1st ed., John Wiley, New York.

Loret B., Khalili N., 2000, A three-Phase model for unsaturated soils, International Journal for Numerical and Analytical Methods in Geomechanics, Vol. 24, pp. 893-927.

Loret, B., Khalili, N., An effective stress elastic-plastic model for unsaturated porous media, Mechanics of Materials, Vol. 34, pp. 97-116, 2002.

Lu. N., Likos W.J., 2004, UNSATURATED SOIL MECHANICS, John Wiley & Sons, Inc., Hoboken, New Jersey. Published simultaneously in Canada.

Luong. M.P., 1978, Etat caractéristique du sol. Mécanique des sols.

Martin, G.R., Finn, W.D.L., Seed, H.D., 1978, Effects of system compliance on liquefaction tests. J Geotech Eng Div 104(4):463–479

Mase, L.Z., Likitlersuang, S., Tobita, T., 2019, Cyclic behaviour and liquefaction resistance of Izumio sands in Osaka, Japan, Journal Marine Georesources & Geotechnology, Volume 37, 2019 - Issue 7, https://doi.org/10.1080/1064119X.2018.1485793

Maswoswe, J., 1985, Stress path for a compacted soil during collapse due to wetting. PhD thesis, Imperial College, London.

Matsushi Y., Matsukura Y., 2006, Cohesion of unsaturated residual soils as a function of volumetric water content, Bull Eng Geol Env, Vol. 65, pp. 449-455.

Matyas, E. L., Radhakrishna, H. S., 1968, Volume change characteristics of partially saturated soils. Geotechnique 18. No. 4.43248.

Michallet, H., Valerie, R., Celine, B., Maxime, B., Barnoud, J.M., Barthelemy, E., 2012. Physical modeling of sand liquefaction under wave breaking on a vertical wall. Coastal Engineering Proceedings 1 (33):78.

Miura, S., Toki, S., & Tatsuoka, F., 1994, Cyclic undrained triaxial behaviour of sand by a cooperative test program in Japan. Dynamic Geotechnical Testing II. A.S.T.M. Philadelphia, pp. 246-260.

Mohkam, M., 1983, Contribution à l'étude expérimentale et théorique du comportement des sables sous chargements cycliques. Thèse de Doctorat de l'Université Scientifique et Médicale, Grenoble, 231 p.

Mory, M, H Michallet, D Bonjean, et I Piedra Cueva, 2007, A field study of momentary liquefaction caused by waves around a coastal structure. Journal of Waterway, Port, Coastal, and OCean Engineering 133 (1).

Mulilis, J., Chan, C.K., Seed, B., 1975, The effects of method of sample preparation on the cyclic stress – strain behavior of sands. Report No. EERC 75-18, Earthquake Engineering Research Center, University of California, Berkley, California.

Mullilis, J.P., Townsend, F.C., Horz, R.C., 1978, Triaxial testing techniques and sand liquefaction. ASTM STP 654 Dyn Geotech Test, pp 265–279

National Research Council's Committee on Earthquake Engineering, 1985, United State of American.

Nazaroff, W., 1992, Radon transport from soil to air . Reviews of geophysics 30 (2).

Ng, Charles W.W., Bruce M., 2007, Advanced Unsaturated Soil Mechanics and Engineering. London; New York: Taylor and Francis.

Nuth, Mathieu, et Lyesse Laloui. 2008. « Effective Stress Concept in Unsaturated Soils: Clarification and Validation of a Unified Framework ». International Journal for Numerical and Analytical Methods in Geomechanics 32 (7):771-801. https://doi.org/10.1002/nag.645.

O-hara, S., Yasunaga, F., Fujii, N., 1974, Dynamic behavior of undisturbed Shirasu. Soils and Foundations, 14(4), 107-114.

Okamura. M., and Soga. Y., 2006, Effect of pore fluid compressibility on liquefaction resistance of partially saturated sand. Soils and Foundations 46 (5):695-700.

Poulos, S.J., 1981, The steady state of deformation. Journal of the Geotechnical Engineering Division, ASCE, 107(5), 553–562.

Ravina, I., 1983, The influence of vegetation on moisture and volume changes. Géotechnique 33 (2):151-57.

Richards, B.G., Peter, P., Emerson, W.W., 1983, The effects of vegetation on the swelling and shrinking of soils in Australia. Géotechnique 33 (2):127-39.

Rico, A., De1 Castillo, H., 1976, La ingenieria de suelos en las vias terrestres. 1, Limusa, Mbxico.

Robertson, P.K., and Fear, C.E., 1996, Soil liquefaction and its evaluation based on SPT and CPT, Liquefaction Workshop, January 1996

Robertson, P.K.,1994, Suggested terminology for liquefaction :An Internal CANLEX Report

Roscoe, K., Schofield, A.N., Wroth, C.P, 1958, On the yielding of soils. Géotechnique, 8(1), 22–53.

Russell A.R., Khalili N., 2006, A unified bounding surface plasticity model for unsaturated soils, Int. J. Num. Analy. Methods in Geomechanics, Vol. 30, No 3, pp. 181- 212.

Seed, B., 1979, Soil liquefaction and cyclic mobility evaluation for level ground during earthquakes. J. Geotech. Engrg. Div. ASCE, Vol. 105, No. GT2, pp. 201-255.

Seed, H. B., Martin, P. P., Lysmer, J., 1975, The Generation and Dissipation of Prore Pressure During Soil Liquefaction, CB/EERC-75/26, Earthquake Engineering Research Center, University of California

Seed, H.B., & Idriss, I.M., 1971, Simplified procedure for evaluation soil liquefaction potential. Journal of Geotechnical Engineering Division, Vol. 97., No. SM9, pp 1249 - 1273.

Seed, H.B., Idriss, I.M., 1982, Ground motion and soil liquefaction during earthquake, Berkeley, University of California.

Seed, H.B., Lee, K.L. 1966. Liquefaction of Saturated Sands During cyclic loading. Journal of the Soil Mechanics and Foundations Division, ASCE 92, 105-134.

Seed, H.B., Mori, K., & Chan, C.K., 1977, Influence of seismic history on liquefaction of sands. Journal of Geotechnical Engineering, ASCE 102 (GT4) pp. 246-270.

Seed, H.B., Peacock, W.H., 1971, Test procedures for measuring soil liquefaction characteristics. Journal of the Soil Mechanics and Foundation Division, ASCE97 (SM8) pp. 1099-1119.

Sheng Z. J., 1999, Theoretical soil mechanics, China Waterpower Press.

Sheng, D., Sloan, S.W., Gens, A., Smith, D.W., 2003, Finite-element formulation and algorithms for unsaturated soils. Part I: Theory", International Journal for Numerical and Analytical Methods in Geomechanics, Vol. 27, No 9, pp. 745-765.

Sherif, M. A., Tsuchiya, C. and Ishibashi, I., 1977, Saturation Effect on Initial Soil Liquefaction, Journal of Geotechnical Engineering, ASCE, Vol. 103, No. 8, pp. 914-917.

Singh, S., 1996, Liquefaction characteristics of silts. Geotechnical and Geological Engineering No. 14, pp. 1-19.

Skempton, A.W., 1954, The pore-pressure coefficients A and B. Géotechnique 4 (4):143-47.

Sladen, J., D'hollander, R., and Krahn, J., 1985, The liquefaction of sands, a collapse surface approach. Canadian Geotechnical Journal 22(4): 564-578. doi: 10.1139/t85-076.

Sladen, J.A., & Handford, G., 1987,A potential systematic error in laboratory testing of very loose sands. Canadian Geotechnical, J. 24, pp. 462-466.

Sun, D.A., Matsuoka, H., Cui, H.B. and Xu,Y.F., 2003, Three-dimensional elastoplastie model for unsaturated compacted soils with different initial densities, International Journal for Numerical and Analytical Methods in Geomechanics, Vol. 27, No 12, pp. 1079-1098.

Taibi S., FleureauJ.-M., HadiwardoyoS., and Kheirbek-Saoud S. (2008) "Small and large strain behaviour of an unsaturated compacted silt", European Journal of Environmental and Civil Engineering, Vol. 12, N° 3, pp. 203-228, 2008.

Taibi, S. ; Fleureau, J.M. ; Hadiwardoyo, Souli, H.; Gomes Correia, (2013) The Concept of Effective Stress in Unsaturated Soils. Chapter 6 in book « Multiscale Geomechanics ; From Soil to Engineering Projects", PP 153–182. P.Y. Hicher Editor- ISTE sci-tech publisher. WILEY. ISBN: 9781848212466 Publication Date: 2013. 416 pp. DOI: 10.1002/9781118601433.ch6

Tamari, Y., Hyodo J., Ichii K., Nakama T., Hosoo A., 2011, Analysis of Liquefaction During 2011 East Japan Earthquake – Part 1: Seismic Ground Behavior in Tokyo Port at the 2011 Off Pacific Coast of Tohoku Earthquake – An Effective Stress Dynamic Analysis Focusing on the Impact of the Aftershock, Part of the Geotechnical, Geological and Earthquake Engineering book series (GGEE, volume 43)

Tatsuoka, F., Goto, S., & Sakamoto, M., 1986, Effects of some factors on strength and deformation characteristics of sand at low pressures. Soils and Foundations, Vol. 26, No. 1, pp. 105-114.

Tatsuoka, F., Toki, S., Miura, S., Kato, H., Okamoto, M., Yamada, S-I., Yasuda, S., & Tanizawa, F., 1986, Some factors affecting cyclic undrained triaxial strength of sand. Soils and Foundations, Vol. 26, No. 3, pp. 99-116.

Thornthwaite C. W., "An Approach Toward a Rational Classification of Climate," Geographical Rev., vol. 38, pp. 55- 94, 1948.

Thornthwaite C. W., 1948, An Approach Toward a Rational Classification of Climate, Geographical Rev., vol. 38, pp. 55- 94.

Toki, S., Tatsuoka, F., Miura, S., Yoshimi, Y., Yasuda, S., & Makihara, Y., 1986, Cyclic undrained triaxial strength of sand by a cooperative test program. Soils and Foundations, Vol. 26, No. 3, pp. 117-128.

Tokimatsu, K., Hosaka, Y., 1986, Effects of sample disturbance on dynamic properties of sand. Soils and Foundations, Vol. 26, No. 1, pp. 53-64.

Tran, K.H., Imanzadeh, S., Taibi, H. Souli, Fleureau, J.L, Hattab M, 2020, Liquefaction behavior of unsaturated fine clean sand subjected to cyclic loading. Journées Nationales Génie Côtier – Génie Civil. Le Havre – France.

Tran, K.H., Imanzadeh, S., Taibi, H. Souli, Fleureau, J.L, Hattab M, Luong N.H.P, 2019a, Effect of Unsaturation on the Liquefaction of Soil: Case study of dense fine clean sand. The 3rd Int. Conf. on Transport Infrastructure & Sustainable Development (TISDIC 2019), Da Nang - Vietnam.

Tran, K.H., Imanzadeh, S., Taibi, S., Dao, D.L, 2019b, Liquefaction behaviour of dense sand relating to the degree of saturation. The 4th International Conference on Geotechnics for Sustainable Infrastructure Development (GEOTEC HANOI), Hanoi - Vietnam.

Tran, K.H., Imanzadeh, S., Taibi, S., Souli, H., Fleufeau, J.M., Bouchemelia, S., Pantet, A, 2018a, Cyclic behavior of unsaturated Hostun sand. The 4th International Conference Unsaturated Soils & Sustainable Construction UNSAT, Oran – Algeria.

Tran, K.H., Imanzadeh, S., Taibi, S., Souli, H., Fleufeau, J.M., Pantet, A., 2018b, Some aspects of the cyclic behavior of quasi-saturated sand. 36èmes Rencontres Universitaires de Génie Civil de l'AUGC. Saint Etienne, France.

Tsukamoto, Y,, Shohei K., Takaji K., 2012, Soil Liquefaction Observed at the Lower Stream of Tonegawa River during the 2011 off the Pacific Coast of Tohoku Earthquake. Soils and Foundations 52 (5):987-99.

Tsukamoto, Y., Shohei K., Jo M., Shotaro H., 2014, Cyclic Resistance of Two Unsaturated Silty Sands against Soil Liquefaction. Soils and Foundations 54 (6):1094-1103. https://doi.org/10.1016/j.sandf.2014.11.005.

Tsukamoto. Y., 2018, Degree of saturation affecting liquefaction resistance and undrained shear strength of silty sands. Soil Dynamics and Earthquake Engineering, https://doi.org/10.1016/j.soildyn.2018.04.041

Unno, T., Kazama, M., Uzuoka, R., 2008, Liquefaction of unsaturated sand considering the pore air pressure and volume compressibility of the soil particle skeleton. Soils and Foundations, Volume 48, Issue 1, February 2008, Pages 87-99. https://doi.org/10.3208/sandf.48.87.

Unno, T., Motoki K., Noriaki S., Ryosuke U., 2006, Cyclic shear behavior of unsaturated volcanic sandy soil under various suction conditions. Unsaturated Soils 2006, 1133-44.

Vaid, Y. P., Sivathayalan S., 2000, Fundamental factors affecting liquefaction susceptibility of sands. Canadian Geotechnical Journal 37 (3):592-606.

Vaid, Y.P., & Finn, W.D.L., 1979, Static shear and liquefaction potential. Journal of the Geotechnical Engineering Division, Vol. 105, No. GT10, pp. 1233-1246.

Vaid, Y.P., Chern, J.C., 1985, Cyclic and monotonic undrained response of saturated sands. Advances in the Art of Testing Soils Under Cyclic Conditions ASCE, Convention, Detroit, Michigan, pp. 120-147.

Vaid, Y.P., Chung, E.K.F., & Kuerbis, R.H., 1989, Preshearing and undrained response of sand. Soils and Foundations, Vol. 29, No. 4, pp. 49-61.

Vaid, Y.P., Sivathayalan, S., Stedman, D., 1999, Influence of specimen-reconstituting method on the undrained response of sand. Geotech. Test. J., Vol. 22, No. 3, pp. 187–195.

Verdugo, R., Ishihara, K., 1996, The steady state of sandy soils. Soils and Foundations, 36(2), 81–91.

Vernay, M., Morvan, M., Breul, P., 2015, Etude du comportement des sols non saturés à la liquéfaction. 33èmes Rencontres de l'AUGC, ISABTP/UPPA, Anglet, 27 au 29

mai 2015

Vernay. M., Morvan. M., Breul. P., 2016, Influence of saturation degree and role of suction in unsaturated soils behaviour: application to liquefaction. 3rd European Conference on Unsaturated Soils – "E-UNSAT 2016". https://doi.org/10.1051/e3sconf/20160914002

Vernay. M., Morvan. M., Breul. P., 2017, Influence of saturation degree on sandy soils behavior: application to liquefaction, 2nd International Conference on Bio-based Building Materials & 1st Conference on ECOlogical valorisation of GRAnular and FIbrous materials.

Vernay, M., Morvan, M., Breul, P., 2019, Experimental study on the influence of saturation degree on unstable behavior within granular material. European Journal of Environmental and Civil Engineering. doi: 10.1080/19648189.2018.1488623.

Vernay, M., 2018, Etude expérimentale de l'influence du degréde saturation sur le comportement instable du sable de Fontainebleau sous sollicitation cyclique:application aux risques de liquéfaction, Thèse de dotoral. Université Clermont Auvergne

Vernay. M., Morvan. M., Breul. P., 2019, Evaluation of the degree of saturation using Skempton coefficient B. Geomechanics and Geoengineering 15(2):1-11. DOI: 10.1080/17486025.2019.1620349

W. K. Wray, "The Principle of Soil Suction and its Geotechnical Engineering Applications," in Proc. 5th Int. Con$ Expansive Soils (Adelaide, South Australia), May 1984, pp. 114- 119

Wheeler, S.L., Sharma, R.L. and Buisson, M.S.R. "Coupling of hydraulic hysteresis and stress-strain behaviour in unsaturated soils". Géotechnique, Vol. 53, N° l, pp. 41-54, 2003.

Wray, W. K., 1984, The Principle of Soil Suction and its Geotechnical Engineering Applications," in Proc. 5th Int. Con$ Expansive Soils (Adelaide, South Australia), pp. 114- 119

Wroth C. P., Houlsby G. T., 1985, Soil mechanics: property characterization and analysis procedure, Proceeding 11th ICSMEF.

Xia, H., Hu, T., 1991, Effects of saturation and back pressure on sand liquefaction. J Geotech Eng 117(9):1347–1362

Yamamuro, J.A., and Lade, P.V., 1997, Static liquefaction of very loose sands. Can. Geotech. J., 34(6), 905–917.

YAMASHITA, S., & TOKI, S., 1993. Effects of fabric anisotropy of sand on cyclic undrained triaxial and torsional strengths. Soils and Foundations, Vol. 33, No. 3, pp. 92-104.

Yang, R. N., Japp, R. D. & How, G., 1971, Shear strength of partially saturated clays. Proc. 4th Asian Reg. Con& Soil Mech. Fdn Engng, Bangkok, 2, 12: 183-187.

Yegian, M. K., Eseller-Bayat, E., Alshawabkeh, A. and Ali, S., 2007, Induced-Partial Saturation for Liquefaction Mitigation: Experimental Investigation, Journal of Geotechnical and Geoenvironmental Engineering, ASCE, Vol. 133, No. 4, pp. 372-380.

Yoshimi Y, Tanaka K, Tokimatsu K.,1989, Liquefaction resistance of partially saturated sand. Soils Found 29(3): 157–162

Yoshimi, Y., Hiroshi O.O., 1975, Influence of degree of shear stress reversal on the liquefaction potential of saturated sand. Soils and Foundations 15 (3).

Yoshimi, Y., Tanaka, K., Tokimatsu, K., 1989, Liquefaction resistance of partially saturated sand. Soils Found 29(3): 157–162.

Youd, T. L., 1972. Compaction of sands by repeated straining, J. Soil Mechanics and Foundations Div., ASCE 98(SM7), 709–25.

Youd, T. L., Idriss, I. M., Andrus, R. D., Arango, I., Castro, G., Christian, J. T., Dobry, R., Finn, W. D. L., Harder, L. F., Hynes, M. E., Ishihara, K., Koester, J. P., Liao, S. S. C., Marcuson, W. F., Martin, G. R., Mitchell, J. K., Moriwaki, Y., Power, M. S., Robertson, P. K., Seed, R. B. and Stokoe, K. H., 2001, Liquefaction Resistance of Soils: Summary Report from the 1996 Nceer and 1998 Nceer/Nsf Workshops on Evaluation of Liquefaction Resistance of Soils, Journal of Geotechnical and Geoenvironmental Engineering, ASCE, Vol. 127, No. 10, pp. 817-833.

Zienkiewicz O. C., Chan A. H. C., Pastor M., Schrefler B. A., Shiomi T., 1999, Computational Geomechanics with special reference to earthquake engineering, John-Wiley.

APPENDIX: VARIATION OF PARAMETERS DURING THE TESTS

-with constant CSR cyclic loading-

TEST CST1					
Parameters	Before consolidation (initial state)	After consolidation 1	After cyclic loading	After consolidation 2	Final state- after monotonic loading
B	0.97				
Sr %	100.00	100.00	100.00	100.00	100
Void volume (cm^3)	240.3	238.2	238.2	234.8	254.6
Water volume (cm^3)	240.3	238.2	238.2	234.8	254.6
Dry weigh of sample (g)	770.1	770.1	770.1	770.1	770.1
Sand particle volume (cm^3)	290.61	290.61	290.61	290.61	290.61
Total sample volume(cm^3)	530.9	528.8	528.8	525.4	545.2
Void ratio: e	0.827	0.820	0.820	0.808	0.876
n	0.453	0.450	0.450	0.447	0.467
Sample volume change (cm^3)	0	2.1	2.1	3.4	-14.3
Volumetric strain (%)	0	0.39	0.39	0.64	-2.70

Note: The sample dilates => volumetric strain is negative. The sample contracts => volumetric strain is positive

TEST CST2

Parameters	Before consolidation (initial state)	After consolidation 1	After cyclic loading	After consolidation 2	Final state- after monotonic loading
B	0.97	-	-	-	-
Sr (%)	100.00	100.00	100.00	100.00	100
Void volume (cm^3)	243.4	241.1	241.1	237.7	249.4
Water volume (cm^3)	243.4	241.1	241.1	237.7	249.4
Dry weigh of sample (g)	773.6	773.6	773.6	773.6	773.6
Sand particle volume (cm^3)	291.91	291.91	291.91	291.91	291.91
Total sample volume(cm^3)	535.3	533.0	533.0	529.6	541.3
Void ratio: e	0.834	0.826	0.826	0.814	0.854
n	0.455	0.452	0.452	0.449	0.461
Sample volume change (cm^3)	0	2.3	2.3	3.4	-6.0
Volumetric strain (%)	0	0.44	0.44	0.64	-1.11

TEST CST3				
Parameters	Before consolidation (initial state)	After consolidation 1	After cyclic loading	Final state
B	0.97			
Sr (%)	100.00	100.00	100.00	100
Void volume (cm^3)	242.2	239.8	239.8	239.8
Water volume (cm^3)	242.2	239.8	239.8	239.8
Dry weigh of sample (g)	775.0	775.0	775.0	775.0
Sand particle volume (cm^3)	292.44	292.44	292.44	292.44
Total sample volume (cm^3)	534.7	532.3	532.3	532.3
Void ratio: e	0.828	0.820	0.820	0.820
n	0.453	0.451	0.451	0.451
Sample volume change (cm^3)	0	2.4	2.4	2.4
Volumetric strain (%)	0	0.45	0.45	0.45

TEST CST4					
Parameters	Before consolidation (initial state)	After consolidation 1	After cyclic loading	After consolidation 2	Final state- after monotonic loading
B	0.97				
Sr (%)	100.00	100.00	100.00	100.00	100
Void volume (cm^3)	243.9	242.0	242.0	234.5	254.7
Water volume (cm^3)	243.9	242.0	242.0	234.5	254.7
Dry weigh of sample (g)	779.0	779.0	779.0	779.0	779.0
Sand particle volume (cm^3)	293.97	293.97	293.97	293.97	293.97
Total sample volume (cm^3)	537.9	535.9	535.9	528.4	548.6
Void ratio: e	0.830	0.823	0.823	0.798	0.866
n	0.453	0.451	0.451	0.444	0.464
Sample volume change (cm^3)	0	1.9	1.9	7.5	-10.8
Volumetric strain (%)	0	0.36	0.36	1.39	-2.00

TEST CUI-1				
Parameters	Before consolidation (Initial state)	After consolidation and before cyclic loading	After cyclic loading and before full saturation	After full saturation and before sample removal (last state)
B	0.21			
Sr (%)	95.98	95.93	98.20	100
Sample volume void(cm^3)	246.7	244.0	238.4	238.4
Dry weigh of sand (g)	776.4	776.4	776.4	776.4
Total sample volume(cm^3)	539.7	537.0	531.4	531.4
Void ratio: e	0.842	0.833	0.814	0.814
n	0.457	0.454	0.449	0.449
Sample volume change (cm^3)	0	-2.7	-5.6	0.0
Volumetric strain (%)	0	-0.50	-1.04	0.00

TEST CUI-4				
Parameters	Before consolidation (Initial state)	After consolidation and before cyclic loading	After cyclic loading and before full saturation	After full saturation and before sample removal (last state)
B	0.21			
Sr (%)	94.31	94.26	95.60	100
Void volume (cm^3)	242.6	240.6	237.3	237.3
Dry weigh of sand (g)	778.1	778.1	778.1	778.1
Total sample volume (cm^3)	536.2	534.2	530.9	530.9
Void ratio: e	0.826	0.820	0.808	0.808
n	0.452	0.450	0.447	0.447
Sample volume change (cm^3)	0	-2.0	-3.4	0.0
Volumetric strain (%)	0	-0.37	-0.63	0.00

TEST CUII-2						
Parameters	Before consolidation (Initial state)	After consolidation 1	After cyclic loading 1	After monotonic loading 2	After re-consolidation	After final full saturation
B	0.056					
Sr (%)	86.26	86.15	86.19	86.91	86.13	100
Void volume (cm^3)	242.0	240.1	240.0	238.0	237.9	237.9
Water volume (cm^3)	208.7	206.8	206.8	206.8	204.9	237.9
Dry weigh of sample (g)	777.7	777.7	777.7	777.7	777.7	777.7
Sand particle volume (cm3)	293.45	293.45	293.45	293.45	293.45	293.45
Total sample volume (cm^3)	535.4	533.5	533.4	531.4	531.3	531.3
Void ratio: e	0.826	0.818	0.818	0.811	0.811	0.811
n	0.452	0.450	0.450	0.448	0.448	0.448
Sample volume change (cm^3)	0	1.9	0.1	2.0	0.1	0.0
Volumetric strain (%)	0	0.35	0.02	0.37	0.02	0.00

TEST CUII-3						
Parameters	Before consolidation (Initial state)	After consolidation 1	After cyclic loading	After monotonic loading	After re-consolidation	After final full saturation
B	0.07					
Sr (%)	87.39	87.26	91.30	84.82	88.33	100
Void volume (cm^3)	243.6	241.2	230.6	248.2	248.5	248.5
Water volume (cm^3)	212.9	210.5	210.5	210.5	219.5	248.5
Dry weigh of sample (g)	772.3	772.3	772.3	772.3	772.3	772.3
Sand particle volume (cm^3)	291.45	291.45	291.45	291.45	291.45	291.45
Total sample volume (cm^3)	535.0	532.7	522.0	539.6	539.9	539.9
Void ratio: e	0.836	0.828	0.791	0.852	0.853	0.853
n	0.455	0.453	0.442	0.460	0.460	0.460
Sample volume change (cm^3)	0	2.4	10.7	-17.6	-0.3	0.0
Volumetric strain (%)	0	0.44	1.99	-3.29	-0.06	0.00